

**Ethylene Activity and Fischer-Tropsch Synthesis: New  
Perspectives in Reaction Mechanisms**

by

**Yusheng Zhang**

submitted in accordance with the requirements for  
the degree of

**DOCTOR OF Philosophy**

in the subject

Thesis: Science, Engineering and Technology

at the

UNIVERSITY OF SOUTH AFRICA

SUPERVISOR: Prof. Yali Yao

CO-SUPERVISOR: Prof. Xinying Liu

Prof. Diane Hildebrandt

January 2021

## DECLARATION

Name: \_\_\_\_\_Yusheng Zhang\_\_\_\_\_

Student number: \_\_\_\_\_54137403\_\_\_\_\_

Degree: \_\_\_\_\_PhD of Philosophy\_\_\_\_\_

Exact wording of the title of the thesis as appearing on the electronic copy submitted for examination:

### **Ethylene Activity and Fischer-Tropsch Synthesis: New Perspectives in Reaction Mechanisms**

---

I declare that the above thesis is my own work and that all the sources that I have used or quoted have been indicated and acknowledged by means of complete references.

I further declare that I submitted the thesis to originality checking software and that it falls within the accepted requirements for originality.

I further declare that I have not previously submitted this work, or part of it, for examination at Unisa for another qualification or at any other higher education institution.



\_\_\_\_\_  
SIGNATURE

\_\_\_\_\_  
19/01/2021  
DATE

**Title of thesis:**

**ETHYLENE ACTIVITY AND FISCHER-TROPSCH SYNTHESIS: NEW PERSPECTIVES IN REACTION MECHANISMS**

**Abstract**

---

With the aim of studying the reactivity of ethylene and consequently understanding and elucidating aspects of the Fischer-Tropsch (FT) reaction mechanism, a large number of experiments were conducted using feed gas mixtures with different proportions of CO/H<sub>2</sub>/C<sub>2</sub>H<sub>4</sub>/inert gas (N<sub>2</sub> or Ar) over a conventional cobalt-based FTS catalyst (15% Co/TiO<sub>2</sub>) at both normal (180-220 °C) and low operating temperatures (100-160 °C). Different kinds of reactions, including C<sub>2</sub>H<sub>4</sub> hydrogenation, C<sub>2</sub>H<sub>4</sub> dimerization, hydroformylation, hydrogenolysis, and the FT chain growth reaction (including the normal FT chain growth and a C<sub>2</sub>H<sub>4</sub> initiated chain growth) were observed. After comparing the experimental results, we concluded that:

1. There are no reactions between C<sub>2</sub>H<sub>4</sub> molecules at any temperature (100-220 °C), based on the results for feed mixtures of C<sub>2</sub>H<sub>4</sub>/N<sub>2</sub>.
2. C<sub>2</sub>H<sub>4</sub> could form both chain growth monomers and initiators with the assistance of H<sub>2</sub>; these, in turn, reacted to produce longer chain hydrocarbons. The products of this reaction (C<sub>3-6</sub>) fitted a typical Anderson–Schulz–Flory (ASF) product distribution.

3. At extremely low reaction temperatures (140-160 °C), CO/H<sub>2</sub> mixtures did not react, indicating that CO could not dissociate in the presence of H<sub>2</sub>. However, CO reacted when co-feeding C<sub>2</sub>H<sub>4</sub> with syngas via the CO insertion mechanism to form long-chain hydrocarbons.
4. Co-feeding a small amount of C<sub>2</sub>H<sub>4</sub> into the syngas promoted the FTS reaction, especially at low reaction temperatures; however, co-feeding CO into the C<sub>2</sub>H<sub>4</sub> hydrogenation system suppressed ethylene reactivity.
5. The paraffin to olefin (P/O) ratio of the products for all the CO/H<sub>2</sub>/ C<sub>2</sub>H<sub>4</sub> experiments fitted the “Yao plot,” which is a linear relationship between P<sub>n+1</sub>/O<sub>n+1</sub> and P<sub>n</sub>/O<sub>n</sub>. A competitive reaction equilibrium was hypothesized to explain this linear relationship.

We concluded that the CO insertion mechanism and the CO dissociation mechanism might exist and compete under normal FTS reaction conditions by investigating the changes in the product distribution and the carbon chain-growth probability for different feed gas mixtures. The CO insertion mechanism is dominant at low reaction temperatures, while the CO dissociation mechanisms dominate at higher reaction temperatures. Furthermore, co-feeding C<sub>2</sub>H<sub>4</sub> could assist the conversion of CO via the CO insertion mechanism.

#### **KEY TERMS:**

Cobalt-catalytic Fischer-Tropsch Synthesis; ethylene and syngas co-reaction system; extra-low temperature Fischer-Tropsch Synthesis; ethylene reactivity; ethylene hydrocracking chain growth mechanism; ethylene-assisted CO insertion mechanism; multi-mechanism reaction system; competitive adsorption; products distribution of co-reaction system; reaction competitive equilibrium

## Okungaqondakali (Abstract in Zulu)

---

Ngenhloso yokutadisha ukwenziwa kabusha kwe-ethylene futhi ngenxa yalokho ukuqonda nokucacisa izici zendlela yokuphendula ye Fischer-Tropsch (FT), inani elikhulu lokuhlolwa lenziwe kusetshenziswa izingxube zegesi yokuphakela ngezilinganiso ezahlukahlukene zegesi ye-CO/H<sub>2</sub>/C<sub>2</sub>H<sub>4</sub>/inert (I-N<sub>2</sub> noma i-Ar) ngaphezulu kwe-cobalt-based based FTS catalyst (15%Co/TiO<sub>2</sub>) kokujwayelekile (180-220 °C) kanye namazinga okushisa aphantsi okusebenza (100-160 °C). Izinhlobo ezahlukahlukene zokuphendula, kufaka phakathi i-C<sub>2</sub>H<sub>4</sub> hydrogenation, i-C<sub>2</sub>H<sub>4</sub> dimerization, i-hydroformylation, i-hydrogenolysis, kanye ne-FT chain reaction reaction (kufaka phakathi ukukhula okujwayelekile kwe-FT chain kanye ne-C<sub>2</sub>H<sub>4</sub> eqalwe ukukhula kwamaketanga). Ngemuva kokuqhathanisa imiphumela yokuhlola, siphethe ngokuthi:

1. Akukho kusabela phakathi kwama-molecule e-C<sub>2</sub>H<sub>4</sub> kunoma yikuphi ukushisa (100-220 °C), ngokuya ngemiphumela yezingxube ze-feed ze-C<sub>2</sub>H<sub>4</sub> / N<sub>2</sub>.
2. I-C<sub>2</sub>H<sub>4</sub> ingakha womabili ama-monomers kanye nabaqalayo ngosizo lwe-H<sub>2</sub>; laba, nabo, baphendula ngokukhiqiza ama-hydrocarbon amakhebuli amade. Imikhiqizo yalokhu kusabela (i-C<sub>3-6</sub>) ifake ukusatshalaliswa komkhiqizo okujwayelekile kwe-Anderson-Schulz-Flory (ASF).
3. Emazingeni okushisa aphantsi ngokweqile (140-160 °C), izingxube ze-CO / H<sub>2</sub> azizange zisabele, okukhombisa ukuthi i-CO ayikwazanga ukuhlukanisa phambi kwe-H<sub>2</sub>.

Kodwa-ke, i-CO isabele lapho iphakela ngokubambisana i-C<sub>2</sub>H<sub>4</sub> ngama-syngas ngendlela ye-CO yokufaka ukuze yakhe ama-hydrocarbon amaketanga amade.

4. Ukondla inani elincane le-C<sub>2</sub>H<sub>4</sub> kuma-syngas kukhuthaze ukusabela kwe-FTS, ikakhulukazi emazingeni okushisa aphansi okusabela; kodwa-ke, ukondla i-CO kuhlelo lwe-C<sub>2</sub>H<sub>4</sub> hydrogenation kucindezele ukwenziwa kabusha kwe-ethylene.
5. Isilinganiso sikapharafini ku-olefin (P/O) semikhiqizo yazo zonke izivivinyo ze-CO/H<sub>2</sub>/C<sub>2</sub>H<sub>4</sub> sifake i- "Yao plot," okuwubudlelwano obumugqa phakathi kwe- $P_{n+1}/O_{n+1}$  ne- $P_n/O_n$ . Ukulingana kokuphendula ngokuncintisana kwafakwa ekuchazeni lobu budlelwane obuqondile.

Siphethe ngokuthi indlela yokufaka i-CO kanye nendlela yokuhlukanisa i-CO ingahle ibe khona futhi incintisane ngaphansi kwezimo ezijwayelekile zokuphendula kwe-FTS ngokuphenya ushintsho ekusabalalisweni komkhiqizo kanye nethuba lokukhula kwekhabhoni yezinhlanganisela zegesi yokuphakelayo ehluke. Indlela yokufaka ye-CO ibaluleke kakhulu emazingeni okushisa aphansi okusabela, kuyilapho izindlela zokuhlukanisa ze-CO zibusa emazingeni okushisa aphezulu okusabela. Ngaphezu kwalokho, ukondla ngokubambisana i-C<sub>2</sub>H<sub>4</sub> kungasiza ekuguqulweni kwe-CO ngendlela ye-CO yokufaka.

## ACKNOWLEDGEMENT

I would like to express my sincere gratitude to the following people and institutions for assisting me and making this thesis possible.

- My supervisor Professor Yali Yao and co-supervisors, Professor Xinying Liu and Professor Diane Hildebrandt, for their invaluable inspiration, guidance and support. When I was feeling that there was no doorway of escape out of the black research box, they always opened a window for me.
- Dr. Joshua Gorimbo, Dr. Mahluli Moyo and Prof. Xiaojun Lu, for their guidance, assistance and co-supervision.
- The editor, Mrs. Juliet Gillies and Mrs. Philippa Lange, for their great help in editing my thesis.
- Other members of Institute for the Development of Energy for African Sustainability (IDEAS) for providing a stimulating and fun environment in which to learn and grow.
- The University of South Africa (UNISA), and National Research Foundation (NRF) for their financial support; the Nuclear Energy Company of South Africa (Necsa) and Synfuel China (Pty) Ltd, for their supplying for the experiment.

Finally, I would like to express the utmost thanks to my family (my parents, my wife and my daughter) for their love and support throughout the entire period of my studies. My father passed away during my PhD, but he provided me with all the courage and strength I needed. Here I need to give special thanks to my wife and daughter, even though they are thousands of miles apart; they are like angels, giving me infinite power. To all of them, I extend my gratitude and thanks.

## LIST OF PUBLICATIONS AND PRESENTATIONS

### Publications:

---

1. Zhang, Y., Tshwaku, M., Yao, Y., Chang, J., Lu, X., Liu, X., & Hildebrandt D. (2020). **Reaction of Ethylene over a typical Fischer-Tropsch Synthesis Co/TiO<sub>2</sub> Catalyst.** Engineering Reports. 2(9), e12232.  
DOI: 10.1002/eng2.12232
2. Zhang, Y., Yao, Y., Chang, J., Lu, X., Liu, X., & Hildebrandt, D. (2020). **Fischer-Tropsch synthesis with ethene co-feeding: experimental evidence of the CO-insertion mechanism at low temperature.** AIChE J. e17029.  
DOI: 10.1002/aic.17029
3. Zhang Y., Yao, Y., Chang, J., Gorimbo J., Liu, X., & Hildebrandt, D. (2021). **The interaction of CO, H<sub>2</sub> and ethylene over a typical Cobalt-based Fischer-Tropsch Synthesis catalyst.** Appl. Catal. A; 118024.  
DOI: 10.1016/j.apcata.2021.118024
4. Zhang, Y., Yao, Y., Shen, J., Chang, J., Gorimbo, J., Liu, X., & Hildebrandt, D. (2021). **Effect of ethylene co-feeding in Fischer-Tropsch synthesis: A study of reaction equilibrium and competition.** Fuel, 302, 121146.  
DOI: 10.1016/j.fuel.2021.121146

5. Chang, J., Zhang, Y., Lu, X., Yao, Y., Liu, X., & Hildebrandt, D. (2021). **Insight into the role of Co<sub>2</sub>C supported on reduced graphene oxide in Fischer-Tropsch synthesis and ethene hydroformylation.** *Appl. Catal. A*, 614, 118050.

DOI: 10.1016/j.apcata.2021.118050

## International conference:

---

### 1. AICHE 2016:

Oral presentation: **A Study of Fischer-Tropsch Synthesis: Does the product distribution approach Quasi-Thermodynamic equilibrium?**

### 2. Syngas conversion 2018:

Poster presentation: **Reaction of C<sub>2</sub>H<sub>4</sub> under Low Temperature Fischer-Tropsch Conditions on a TiO<sub>2</sub> Supported Cobalt Catalyst with Co-feeding of H<sub>2</sub> and Syngas**

## National conference:

---

### 1. Catalysis Society of South Africa (CATSA) 2015:

Poster presentation: **Effect of ceria doping in different impregnation steps on Ni-based catalysts loading on TiO<sub>2</sub>-SiC for CO Methanation**

### 2. CATSA 2016:

Poster presentation: **The performance of  $\alpha$ -olefins on Co-based catalysts in typical Fischer-Tropsch synthesis reaction condition**

### 3. CATSA 2017:

Oral presentation: **Ethylene reactions on Co/TiO<sub>2</sub> under typical FTS operation condition**

### 4. CATSA 2018:

Oral presentation: **Ethylene partial pressure effects on typical Co catalytic Fischer-Tropsch Synthesis**

# TABLE OF CONTENTS

DECLARATION .....	I
Abstract.....	II
KEY TERMS: .....	III
Okungaqondakali .....	IV
ACKNOWLEDGEMENT.....	VI
LIST OF PUBLICATIONS AND PRESENTATIONS.....	VII
TABLE OF CONTENTS.....	X
LIST OF FIGURES.....	XIV
LIST OF TABLES.....	XX
LIST OF SCHEMES .....	XXII
ABBREVIATIONS AND ACRONYMS.....	XXIII
Chapter 1.....	1
Introduction .....	1
1.1. Motivation and rationale .....	1
1.2. Aim and objectives.....	3
1.3. Outline of this thesis .....	3
REFERENCES:.....	6
Chapter 2.....	9
Literature review.....	9
2.1. The history of Fischer-Tropsch Synthesis.....	9
2.2. Types of reactors used for FTS.....	12
2.3. Catalysts used in Fischer-Tropsch Synthesis.....	18
2.2.1. Iron-based catalysts .....	18
2.2.2. Cobalt-based catalysts .....	20
2.4. Chemistry and mechanism of Fischer Tropsch Synthesis (FTS) .....	22
2.4.1. Chemistry in FTS.....	22
2.4.2. Mechanism of FTS.....	23
2.5. Product distribution in FTS.....	28
2.5.1. Ideal ASF distribution .....	29
2.5.2. Deviation from the ideal ASF distribution.....	31
2.6. Secondary reaction of $\alpha$ -olefins in FTS .....	32
2.7. Ethylene chemistry in FTS.....	36

2.8. Potential equilibrium in FTS.....	37
REFERENCES:.....	42
Chapter 3.....	61
Experiment.....	61
3.1. Introduction .....	61
3.2. Materials and chemicals .....	62
3.2.1. Gases .....	62
3.2.2. Chemicals used in catalyst preparations.....	64
3.3. Experimental set-up and reactor .....	64
3.3.1 Experimental set-up.....	64
3.3.2 Reactor .....	68
3.4. Preparation and characteristics of Cobalt-based catalysts.....	70
3.4.1. Preparation of the catalyst .....	70
3.4.2. Characteristics of the catalysts .....	71
3.5. Product analysis .....	78
3.5.1. Online GC in Necsa.....	78
3.5.2. Online GC at Synfuels China.....	84
3.6. Components of feed gas used in this study .....	89
3.7. Data calculation and analysis.....	90
REFERENCES:.....	97
Chapter 4.....	99
Reaction of Ethylene over a typical Fischer-Tropsch Synthesis Co/TiO <sub>2</sub> Catalyst.....	99
ABSTRACT.....	99
4.1. Introduction .....	100
4.2. Experimental Methods.....	102
4.2.1. Catalyst preparation.....	102
4.2.2. Reaction procedure and product analysis .....	104
4.2.3. Catalyst Characterisation .....	106
4.3. Experiment results .....	108
4.3.1. Catalyst Characterization .....	108
4.3.2. Confirming FTS Reactivity of the Co catalyst .....	110
4.3.3. Feeding C <sub>2</sub> H <sub>4</sub> /N <sub>2</sub> to the reactor .....	113
4.3.4. Feeding C <sub>2</sub> H <sub>4</sub> /H <sub>2</sub> to the reactor .....	113
4.4. Discussion.....	126
4.4.1. Carbon chain growth.....	126
4.4.2. Possible C <sub>2</sub> H <sub>4</sub> reactions .....	131

4.5. Conclusion.....	136
REFERENCES:.....	138
Chapter 5.....	143
Fischer-Tropsch synthesis with ethylene co-feeding: experimental evidence of the CO-insertion mechanism at low temperature .....	143
ABSTRACT.....	143
5.1. Introduction .....	144
5.2. Experimental.....	149
5.2.1. Preparation and characterization of catalysts .....	149
5.2.2. Experimental design.....	149
5.3. Results and discussion .....	153
5.3.1. Set 1: H <sub>2</sub> rich conditions .....	153
5.3.2. Set 2: Constant Partial Pressure of H <sub>2</sub> and CO and Varying Partial Pressure C <sub>2</sub> H <sub>4</sub> .....	162
5.4. Conclusion.....	170
REFERENCES:.....	171
Supplementary Material for Chapter 5.....	176
Chapter 6.....	180
Effect of co-feeding ethylene on the light hydrocarbon product distribution during cobalt catalysed Fischer Tropsch synthesis .....	180
ABSTRACT.....	180
6.1. Introduction .....	181
6.2. Experiments .....	184
6.3. Results.....	187
6.3.1. CO conversion X <sub>CO</sub> .....	187
6.3.2. Ethylene reactivity .....	189
6.3.3. Side reactions.....	193
6.3.4. Product distribution .....	204
6.4. Discussion.....	209
6.5. Conclusions .....	213
REFERENCES:.....	215
Chapter 7.....	221
The influence of CO partial pressure on the ethylene reaction with hydrogen under typical Co-based Fischer-Tropsch Synthesis catalysts.....	221
ABSTRACT.....	221
7.1. Introduction .....	222
7.2. Experiment.....	225

7.3.	Results.....	230
7.3.1.	Ethylene reactivity .....	230
7.3.2.	CO reactivity.....	232
7.3.3.	Ethylene hydrogenation.....	235
7.3.4.	Ethylene hydroformylation .....	238
7.3.5.	Ethylene dimerization .....	241
7.3.6.	Odd carbon number products.....	245
7.4.	Discussion.....	249
7.4.1.	The inhibiting effect of CO .....	249
7.4.2.	Effect of CO on product distribution.....	251
7.5.	Conclusion.....	255
	REFERENCES:.....	256
	Chapter 8.....	262
	Effect of ethylene co-feeding in Fischer-Tropsch synthesis: A study of reaction equilibrium and competition.....	262
	ABSTRACT.....	262
8.1.	Introduction .....	263
8.2.	Experiment.....	266
8.3.	Results and discussion .....	269
8.3.1.	Reactant conversion .....	269
8.3.2.	Paraffins/Olefin (P/O) ratio.....	272
8.3.3.	Quasi-equilibrium: Yao plot .....	277
8.4.	Discussion.....	286
	Competition equilibrium between hydrogenation and chain growth.....	287
8.5.	Conclusion.....	291
	REFERENCES:.....	293
	Chapter 9.....	298
	Conclusive remark and perspectives .....	298
9.1.	Conclusion remarks.....	299
9.1.1.	Reactant activity and product selectivity.....	299
9.1.2.	Product distribution .....	300
9.1.3.	Reaction paths and mechanisms .....	301
9.2.	Perspectives .....	303

## LIST OF FIGURES

### Chapter 2

**Figure 2. 1:** (a) Ideal ASF distribution of all products and (b) Hydrocarbon weight fraction selectivity as a function of  $\alpha$  value [77, 106] ..... 30

**Figure 2. 2:** Normalized mole fraction for  $O_n$ ,  $P_n$  and  $O_{n+1}$  ..... 39

**Figure 2. 3:** The molar ratio of  $P(n+1)/O(n+1)$  as a function of the molar ratio of  $P(n)/O(n)$  for FTS: (a) using a fixed bed reactor over a cobalt-based catalyst; (b) using a fixed bed reactor over an iron based catalyst; (c) using a spinning basket reactor over an iron based catalyst (data from literature) [167]; (d) using a slurry reactor over an iron based catalyst (data from literature) [167]. ..... 41

### Chapter 3

**Figure 3. 1:** Schematic diagram of the experimental setup in the lab at Necsa..... 65

**Figure 3. 2:** Schematic diagram of the experimental setup in the lab at Synfuels China. .... 66

**Figure 3. 3:** Photo of the TFBR used in the current experimental study. (a) is used at Necsa; (b) is used at Synfuels China..... 69

**Figure 3. 4:** XRD patterns for 15%Co/TiO<sub>2</sub> before and after reduction ..... 75

**Figure 3. 5:** TPR results of 15%Co/TiO<sub>2</sub>. (a) H<sub>2</sub>-TPR profiles with the reduction temperature rising from room temperature to 700 °C at a rate of 10 °C /min). (b) H<sub>2</sub>-TPR profiles with the reduction temperature increasing from room temperature to 350 °C (10 °C /min) and then being maintained at 350 °C for 1 hour..... 76

**Figure 3. 6:** TEM images of 15%Co/TiO<sub>2</sub> before reduction..... 77

**Figure 3. 7:** The sampling flow scheme of the online GC Agilent 7890B at Necsa. In this figure: a is the delay part; b and f are the Molsieve 13X column; c is the Heyasep Q column; d is split part; e is the LTM system with a CP-Sil 5 CB column; g is a Plot Q column; h, i, and j are sampling loops. .... 80

**Figure 3.8:** Chromatogram of the reaction of ethylene and hydrogen in Necsa..... 83

**Figure 3.9:** Sampling flow scheme of online GC Agilent 7890A at Synfuels China. .... 85

**Figure 3.10:** Chromatogram of the reaction of ethylene co-fed FTS in Synfuels China ..... 88

## Chapter 4

**Figure 4.1:** Characterization results for: (a) H<sub>2</sub>-TPR profiles with the reduction temperature increasing from room temperature to 700 °C at a rate of 10 °C/min); (b) H<sub>2</sub>-TPR profiles with the reduction temperature increasing from room temperature to 350 °C (10 °C/min) and then being maintained at 350 °C for 1 hour; (c) XRD patterns for 15% Co/TiO<sub>2</sub> before and after reduction; (d) TEM images of the catalyst ..... 109

**Figure 4.2:** CO conversion and CH<sub>4</sub> selectivity under typical FTS conditions, at 30 ml/min, 200 °C and 20 bar (on gauge). ..... 112

**Figure 4.3:** The effect of C<sub>2</sub>H<sub>4</sub> : H<sub>2</sub> molar ratio on the C<sub>2</sub>H<sub>4</sub> reaction at 180 °C and 20 bar gauge): (a) conversion of reactants and the selectivity of C<sub>2</sub>H<sub>6</sub>; (b) selectivity of CH<sub>4</sub> and C<sub>3</sub> products; (c) selectivity of C<sub>4</sub> products..... 115

**Figure 4.4:** Effect of temperature on C<sub>2</sub>H<sub>4</sub> reaction when H<sub>2</sub> is in excess (C<sub>2</sub>H<sub>4</sub>/H<sub>2</sub> = 0.8, total flow rate: 52.5 ml/min; reaction pressure: 20 bars). (a) Conversion of reactants and selectivity of C<sub>2</sub>H<sub>6</sub>. (b) Selectivity of CH<sub>4</sub> and C<sub>3</sub>. (c) Selectivity of C<sub>4</sub>..... 117

**Figure 4.5:** Effect of reaction temperature on CH<sub>4</sub> yield, total C<sub>3</sub> and total C<sub>4</sub>, when H<sub>2</sub> is in excess. 119

**Figure 4.6:** Effect of temperature on the C<sub>2</sub>H<sub>4</sub> reaction when H<sub>2</sub> is limiting (C<sub>2</sub>H<sub>4</sub>/H<sub>2</sub> = 4.8, total flow rate: 50 ml/min; reaction pressure: 20 bar gauge). (a) Conversion of reactants and the selectivity of C<sub>2</sub>H<sub>6</sub>. (b) Selectivity of CH<sub>4</sub> and C<sub>3</sub>. (c) Selectivity of C<sub>4</sub>. ..... 123

**Figure 4.7:** Effect of reaction temperature on the CH<sub>4</sub> yield, total C<sub>3</sub> and total C<sub>4</sub>, for a H<sub>2</sub> limited feed. .... 125

**Figure 4.8:** Logarithmic product distribution ( $\alpha$ -olefins + n-paraffins), as a function of the carbon number (ASF plot). (a) Normal FTS feed (H<sub>2</sub>/CO/N<sub>2</sub> = 6:3:1, total flow rate: 30 ml/min; reaction pressure: 20 bar (on gauge)). (b) H<sub>2</sub> rich feed (C<sub>2</sub>H<sub>4</sub>/H<sub>2</sub> = 0.8, total flow rate: 60 ml/min; reaction pressure: 20 bar (on gauge)). (c) H<sub>2</sub> limited feed (C<sub>2</sub>H<sub>4</sub>/H<sub>2</sub> = 4.8, total flow rate: 60 ml/min; reaction pressure: 20 bar (on gauge)). ..... 129

## Chapter 5

**Figure 5.1:** Examples of the possible CO activation pathways: (a) CO-dissociation mechanism, [7, 10-14]; (b) CO-insertion mechanism [18]..... 148

**Figure 5.2:** Conversion of reactants for reaction temperatures between 100 and 220 °C, over a catalyst of 15% Co/TiO<sub>2</sub>: (a) CO and H<sub>2</sub> conversion; (b) C<sub>2</sub>H<sub>4</sub> conversion. (Reaction conditions: 20 bar: (i) feed with C<sub>2</sub>H<sub>4</sub>: 80 ml/min with molar composition 52.5% H<sub>2</sub>/ 7.5% CO/ 37.5% C<sub>2</sub>H<sub>4</sub>/ 2.5% N<sub>2</sub>; and (ii) feed without C<sub>2</sub>H<sub>4</sub> 50 ml/min with composition 84% H<sub>2</sub>/ 12% CO / 4% N<sub>2</sub>. ..... 156

**Figure 5.3:** An ASF plot of the light hydrocarbon products formed over a 15% Co/TiO<sub>2</sub> catalyst: (a) with co-feeding ethylene; and (b) without co-feeding ethylene. Reaction conditions: (a) 20 bar, 140 – 220 °C, 80ml/min, feed gas composition: 52.5% H<sub>2</sub> / 7.5% CO / 37.5% C<sub>2</sub>H<sub>4</sub> / 2.5% N<sub>2</sub>; and (b) 20 bar, 200 – 220 °C, 50 ml/min, feed gas composition: 84% H<sub>2</sub> / 12% CO / 4% N<sub>2</sub>. ..... 160

**Figure 5.4:** CO conversion at different reaction temperatures, with different percentages of C<sub>2</sub>H<sub>4</sub> in the syngas feed, over a 15% Co/TiO<sub>2</sub> catalyst. (Reaction conditions: total reaction pressure: 20 bar; total flow rate: 50 ml/min; feed gas composition: 40% H<sub>2</sub>/ 20% CO / X% C<sub>2</sub>H<sub>4</sub>/ (40-X) % Ar, X=0%, 10%, 20% or 30%). ..... 164

**Figure 5.5:** ASF plot of the experimental hydrocarbon data with varying proportions of C<sub>2</sub>H<sub>4</sub> in the feed: (a) at 160 °C; (b) at 180 °C. (Reaction conditions: total reaction pressure: 20 bars; total flow rate: 50 ml/min; and feed gas composition: 40% H<sub>2</sub>/ 20% CO / X% C<sub>2</sub>H<sub>4</sub>/ (40-X) % Ar, X=0%, 10%, 20% or 30%). ..... 165

**Figure 5.6:** Ratio of CO conversion with syngas to the CO conversion with X % C<sub>2</sub>H<sub>4</sub> co-feeding (X=10%, 20% or 30%). (Reaction conditions: total reaction pressure: 20 bars; total flow rate: 50 ml (NTP)/min; and feed gas composition: 40% H<sub>2</sub>/ 20% CO / X% C<sub>2</sub>H<sub>4</sub>/ (40-X)% Ar, X=0%, 10%, 20% or 30%). ..... 169

### Supplementary Material for Chapter 5

**Figure 5.S1:** Product selectivity under different reaction temperatures over a 15% Co/TiO<sub>2</sub> catalyst: (a) methane selectivity; (b) ethane selectivity. Reaction conditions: 20 bar, 80 ml/min for the feed of syngas with ethylene (52.5% H<sub>2</sub>/ 7.5% CO/ 37.5% C<sub>2</sub>H<sub>4</sub>/ 2.5% N<sub>2</sub>), and 50 ml/min for the feed of syngas without ethylene (84% H<sub>2</sub>/ 12% CO / 4% N<sub>2</sub>). ..... 177

**Figure 5.S2:** Product selectivity under different reaction temperatures over a 15% Co/TiO<sub>2</sub> catalyst: (a) 1-olefin + n-paraffin selectivity of (C<sub>3</sub> + C<sub>4</sub>); (b) 2-butene (including cis- and trans-) selectivity. Reaction conditions: 20 bar, 80 ml/min for the feed of syngas with ethylene (52.5% H<sub>2</sub>/ 7.5% CO/ 37.5% C<sub>2</sub>H<sub>4</sub>/ 2.5% N<sub>2</sub>); and 50 ml/min for the feed of syngas without ethylene (84% H<sub>2</sub>/ 12% CO / 4% N<sub>2</sub>). ..... 178

**Figure 5.S3:** Oxygenate product selectivity at different reaction temperatures over a 15% Co/TiO<sub>2</sub> catalyst. Reaction conditions: 20 bar, 80 ml/min for a feed of syngas with ethylene (52.5% H<sub>2</sub>/ 7.5% CO/ 37.5% C<sub>2</sub>H<sub>4</sub>/ 2.5% N<sub>2</sub>). ..... 179

## Chapter 6

**Figure 6.1:** CO conversion  $X_{CO}$  at different reaction temperatures and different ethylene partial pressure over 15% Co/TiO<sub>2</sub>. (Reaction conditions: total reaction pressure - 21 bars; total flow rate - 50 ml (NTP)/min; feed gas composition – (40% H<sub>2</sub>; 20% CO ; X% C<sub>2</sub>H<sub>4</sub>; (40-X)% Ar) where X=0%, 10%, 20% or 30%. ..... 188

**Figure 6.2:** Ethylene conversion  $X_{C_2H_4}$  (a) and ethylene reaction rate (b) under different reaction temperatures and different ethylene partial pressure, over 15% Co/TiO<sub>2</sub> ( Reaction conditions: total reaction pressure - 21 bars; total flow rate - 50 ml (NTP)/min; feed gas composition – (40% H<sub>2</sub>; 20% CO; X% C<sub>2</sub>H<sub>4</sub>; (40-X)% Ar) , for X=0%, 10%, 20% or 30%). ..... 191

**Figure 6.3:** CH<sub>4</sub> selectivity based on total carbon source (a), CH<sub>4</sub> formation rate (b) and CH<sub>4</sub> selectivity based on CO (c) at different reaction temperatures, with different ethylene partial pressures in the feed over a 15% Co/TiO<sub>2</sub> catalyst. (Reaction conditions: total reaction pressure - 21 bars; total flow rate - 50 ml (NTP)/min; feed gas composition - 40% H<sub>2</sub>/ 20% CO / X% C<sub>2</sub>H<sub>4</sub>/ (40-X)% Ar, X=0%, 10%, 20% or 30%). ..... 194

**Figure 6.4:** C<sub>2</sub>H<sub>6</sub> selectivity based on total carbon source (a), C<sub>2</sub>H<sub>6</sub> formation rate (b) and C<sub>2</sub>H<sub>6</sub> selectivity, based on C<sub>2</sub>H<sub>4</sub> (c) at different reaction temperatures, with different ethylene partial pressure levels over 15% Co/TiO<sub>2</sub>. (Reaction conditions: total reaction pressure - 21 bars; total flow rate - 50 ml (NTP)/min; feed gas composition (40% H<sub>2</sub>; 20% CO ; X% C<sub>2</sub>H<sub>4</sub>; (40-X)% Ar) where X=0%, 10%, 20% or 30%). ..... 198

**Figure 6.5:** Propanal selectivity  $S_{C_2H_5CHO}$  (a), the formation rate of propanal (b), propanal selectivity based on CO consumption  $S_{C_2H_5CHO\_CO}$  (c) and propanal selectivity based on C<sub>2</sub>H<sub>4</sub> consumption  $S_{C_2H_5CHO\_C_2H_4}$  (d), under different reaction temperatures with different ethylene partial pressure levels over 15% Co/TiO<sub>2</sub>. (Reaction conditions: total reaction pressure - 21 bars; total flow rate - 50 ml (NTP)/min; feed gas composition - 40% H<sub>2</sub>/ 20% CO / X% C<sub>2</sub>H<sub>4</sub>/ (40-X)% Ar, X=0%, 10%, 20% or 30%). ..... 201

**Figure 6.6:** The selectivity and formation rate of C<sub>4</sub> products, i.e. the selectivity of 1-butene (a), n-butane (b), trans-2-butene (c), cis-2-butene (d) and the formation rate of 1-butene (e), n-butane (f),

trans-2butene (g), cis-2-butene (h) under different reaction temperatures, with different ethylene partial pressure levels, over 15% Co/TiO<sub>2</sub>. (Reaction conditions: total reaction pressure - 21 bars; total flow rate - 50 ml (NTP)/min; feed gas composition - 40% H<sub>2</sub>/ 20% CO / X% C<sub>2</sub>H<sub>4</sub>/ (40-X)% Ar, X=0%, 10%, 20% or 30%). ..... 203

**Figure 6.7:** Examples of the experimental data fitted to an ASF plot: (a) 160 °C; (b) 180 °C; (c) 220 °C. .... 208

## Chapter 7

**Figure 7.1:** C<sub>2</sub>H<sub>4</sub> conversion. (Reaction conditions: 20 bar (gauge), total flow rate of 50 ml/min, 40% H<sub>2</sub> / 40% C<sub>2</sub>H<sub>4</sub> / x % CO/ (20-x) % Ar) ..... 231

**Figure 7.2:** Rate of CO: (a) conversion; (b) reaction rate. (Reaction conditions: 20 bar (gauge), total flow rate of 50 ml/min, 40% H<sub>2</sub> / 40% C<sub>2</sub>H<sub>4</sub> / x % CO/ (20-x) % Ar) ..... 233

**Figure 7.3:** Selectivity and formation rate of C<sub>2</sub>H<sub>6</sub>. (a) Selectivity based on all carbon sources; (b) selectivity based on ethylene; (c) formation rate. (Reaction conditions: 20 bar (gauge), total flow rate of 50 ml/min, 40% H<sub>2</sub> / 40% C<sub>2</sub>H<sub>4</sub> / x % CO/ (20-x) % Ar)..... 236

**Figure 7.4:** Selectivity and formation rate of propanal: (a) propanal selectivity based on total carbon consumption; (b) propanal selectivity based on CO consumption; (c) propanal selectivity based on ethylene consumption; (d) propanal formation rate. (Reaction conditions: 20 bar (gauge), total flow rate of 50 ml/min, 40% H<sub>2</sub> / 40% C<sub>2</sub>H<sub>4</sub> / x % CO/ (20-x) % Ar) ..... 240

**Figure 7.5:** Selectivity and formation rate of various C<sub>4</sub> products: (a) selectivity, and; (b) formation rate. (Reaction conditions: 20 bar (gauge), total flow rate of 50 ml/min, 40% H<sub>2</sub> / 40% C<sub>2</sub>H<sub>4</sub> / x % CO/ (20-x) % Ar)..... 244

**Figure 7.6:** Selectivity of: (a) methane; (b) C<sub>3</sub> products, and; (c) C<sub>5</sub> products. (Reaction conditions: 20 bar (gauge), total flow rate of 50 ml/min, 40% H<sub>2</sub> / 40% C<sub>2</sub>H<sub>4</sub> / x % CO/ (20-x) % Ar). ..... 248

**Figure 7.7:** Product distribution spectrum of: (a) CO, and; (b) ethylene under different reaction temperatures at different CO partial pressure levels. (Reaction conditions: 20 bar (gauge), total flow rate of 50 ml/min, 40% H<sub>2</sub> / 40% C<sub>2</sub>H<sub>4</sub> / x % CO/ (20-x) % Ar) In this figure, hydrocarbons represent all the C<sub>x</sub>H<sub>y</sub>, except C<sub>2</sub>H<sub>6</sub> and 2-butene.) ..... 250

**Figure 7.8:** Experimental results plotted into an ASF product distribution model of the results seen when using different feed gas compositions. .... 253

## Chapter 8

**Figure 8.1:** Mole paraffins to olefins ( $P_n/O_n$ ) ratio as a function of reaction temperature, with different amounts of ethylene in the feed gas: (a)  $n=2$ ; (b)  $n=3$ ; (c)  $n=4$ ; (d)  $n=5$ ; (e)  $n=6$ . ..... 273

**Figure 8.2:** Mole paraffins to olefins ( $P_2/O_2$ ) ratio as a function of the reaction temperature, with different quantities of CO in the ethylene hydrogenation feed gas: (a)  $n=2$ ; (b)  $n=3$ ; (c)  $n=4$ ; (d)  $n=5$ ; (e)  $n=6$ . ..... 275

**Figure 8.3:** The Yao plot - paraffin (P) to olefin (O) ratio  $P_3/O_3$  as a function of  $P_2/O_2$  for: (a) normal FTS (S1); (b) ethylene co-feeding FTS (S2 to S4); (c) CO co-feeding ethylene hydrogenation (S6 and S7); (d) ethylene hydrogenation in ethylene rich environment; (e) summary of all the results together. .... 279

**Figure 8.4:** The Yao plot - paraffin (P) to olefin (O) ratio  $P_4/O_4$  as a function of  $P_3/O_3$  for: (a) normal FTS (S1); (b) ethylene co-feeding FTS (S2 to S4); (c) CO co-feeding ethylene hydrogenation (S6 and S7); (d) ethylene hydrogenation in an ethylene rich environment; (e) summary of all the results together. 281

**Figure 8.5:** The Yao plot - paraffin (P) to olefin (O) ratio  $P_5/O_5$  as a function of  $P_4/O_4$  for: (a) normal FTS (S1); (b) ethylene co-feeding FTS (S2 to S4); (c) CO co-feeding ethylene hydrogenation (S6 and S7); (d) summary of all the results together. .... 282

**Figure 8.6:** The Yao plot - paraffin (P) to olefin (O) ratio  $P_6/O_6$  as a function of  $P_5/O_5$  for: (a) normal FTS (S1); (b) ethylene co-feeding FTS (S2 to S4); (c) CO co-feeding ethylene hydrogenation (S6 and S7); (d) summary of all the results together. .... 283

**Figure 8.7:** The Yao plot -  $P_{n+1}/O_{n+1}$  ratio as a function of  $P_n/O_n$  ratio ( $n = 3, 4$  and  $5$ ). (Summary of the data in Figures 8.4 to 8.6.) ..... 285

## LIST OF TABLES

### Chapter 2

<b>Table 2.1:</b> Advantages and disadvantages of TFB [22-26].....	14
<b>Table 2.2:</b> Advantages and disadvantages of CFB [6, 21, 27-28].....	15
<b>Table 2.3:</b> Advantages and disadvantages of the SCBR [31-34] .....	16
<b>Table 2.4:</b> Characteristics of Sasol's commercial FT processes [35].....	17

### Chapter 3

<b>Table 3.1:</b> Properties of the catalysts (15% Co/TiO <sub>2</sub> ) used in this work. ....	74
<b>Table 3.2:</b> Operational information of the Agilent 7890B used in this experimental study .....	81
<b>Table 3.3:</b> Order of peaks in different detectors on Agilent 7890B .....	82
<b>Table 3.4:</b> Specific operational information of the Agilent 7890A in this experiment.....	86
<b>Table 3.5:</b> Order of peaks in different detectors on Agilent 7890B .....	87
<b>Table 3.6:</b> Molar RF for hydrocarbons .....	93

### Chapter 4

<b>Table 4.1:</b> Properties of the catalyst (15% Co/TiO <sub>2</sub> ) used in this work.....	103
<b>Table 4.2:</b> Reaction conditions for all 11 runs. ....	107
<b>Table 4.3:</b> Conversion of reactants and carbon based selectivity of products under typical FTS conditions, at 30 ml/min, 200 °C and 20 bar (on gauge). ....	111
<b>Table 4.4:</b> $\alpha$ -value of normal FTS result and C <sub>2</sub> H <sub>4</sub> reacted with H <sub>2</sub> . ....	130
<b>Table 4.5:</b> The selectivity of products C <sub>1</sub> to C <sub>4</sub> on ethylene hydrogenation condition. ....	133

### Chapter 5

<b>Table 5.1:</b> Reaction condition for the various experiments .....	152
<b>Table 5.2:</b> Reactant activity, product selectivity and formation rate over a FT catalyst of 15% Co/TiO <sub>2</sub> during low temperature reaction. ....	157

### Chapter 6

<b>Table 6.1:</b> Feed conditions for the various experiments. The feed composition is denoted (40% H <sub>2</sub> ; 20% CO; X% C <sub>2</sub> H <sub>4</sub> ; (40-X)% Ar) where X= (0, 10, 20, 30). .....	185
<b>Table 6.2:</b> The conversion of ethylene in X <sub>C<sub>2</sub>H<sub>4</sub></sub> when using a feed of ethylene and H <sub>2</sub> , (C <sub>2</sub> H <sub>4</sub> :H <sub>2</sub> = 55.5:45.5) at low temperatures over the Co-based FTS catalyst.....	192
<b>Table 6.3:</b> The α-values of olefins, paraffins and hydrocarbons (paraffins + olefins) at different reaction temperatures and with different ethylene partial pressure levels over 15% Co/TiO <sub>2</sub> (Reaction conditions: total reaction pressure - 20 bars; total flow rate - 50 ml (NTP)/min; feed gas composition - 40% H <sub>2</sub> / 20% CO / X% C <sub>2</sub> H <sub>4</sub> / (40-X)% Ar= X).....	207
<b>Table 6.4:</b> Reactant activity and product selectivity over FTS catalyst of 15% Co/TiO <sub>2</sub> for low temperature reaction. ....	210
<b>Chapter 7</b>	
<b>Table 7.1:</b> Various α-olefins secondary reactions in FTS .....	224
<b>Table 7.2:</b> Physical properties of 15 % Co/TiO <sub>2</sub> .....	227
<b>Table 7.3:</b> The components of the feed gas used for this experiment.....	229
<b>Table 7.4:</b> The a-value of total hydrocarbons, α-olefins and n-paraffins under different reaction temperatures with CO partial pressure over 15% Co/TiO <sub>2</sub> . (Pressure: 20 bars; Total flow rate: 50 ml/min, H <sub>2</sub> : 40%, C <sub>2</sub> H <sub>4</sub> : 40%.).....	254
<b>Chapter 8</b>	
<b>Table 8.1:</b> The different operating conditions during FTS .....	268
<b>Table 8.2:</b> Reactant conversion using different reaction temperatures with different ethylene/CO partial pressure over 15% Co/TiO <sub>2</sub> . (Reaction pressure: 20 bars (gauge); for S1 to S4, H <sub>2</sub> : 40%; CO: 20%; C <sub>2</sub> H <sub>4</sub> : x%; Ar: 40-x%. x= 0, 10, 20 and 30; for S5 to S7, H <sub>2</sub> : 40%; C <sub>2</sub> H <sub>4</sub> : 40%; CO: x%; Ar: 20-x%. x= 0, 6 and 14; for S8, H <sub>2</sub> : 17%; C <sub>2</sub> H <sub>4</sub> : 83%). .....	271

## LIST OF SCHEMES

### Chapter 2

**Scheme 2.1:** Pathways of the CO insertion mechanism ..... 27

### Chapter 6

**Scheme 6.1:** Pathways of the CO dissociation-type mechanism [43] and CO insertion mechanism [44]. ..... 212

### Chapter 8

**Scheme 8.1:** Carbon chain growth and termination in FTS. .... 289

## ABBREVIATIONS AND ACRONYMS

ASF	Anderson, Schultz and Flory
P <sub>n</sub>	Paraffin with carbon number n
α	Chain growth probability
O <sub>n</sub>	Olefin with carbon number n
FTS	Fischer-Tropsch Synthesis
BASF	Badische Anilin und Soda Fabrik
SASOL	South African Coal Oil and Gas Cooperation
GTL	Gas to liquid
LTFT	Low-temperature FT technology
HTFT	High-temperature FT technology
TFB	Tubular fixed bed reactor
CFB	Circulating fluidized bed reactor
FFB	Fixed fluidized bed reactor
SBCR	Slurry bubble column reactor
BLT	Biomass to liquid
FT-IR	Fourier Transform infrared spectroscopy

DRIFTS	Diffuse Reflectance Infrared Fourier Transform Spectroscopy
WGS	Water gas shift reaction
$W_n$	Weight fraction of hydrocarbon product containing $n$ atoms
$r_p$	Carbon chain growth rate
$r_t$	Carbon chain termination rate
VLE	Vapour–liquid equilibrium
$P_n/O_n$	The paraffin to olefin ratio with carbon number $n$
NECSA	Nuclear Energy Company of South Africa
UHP	ultra-high purity
TCD	Thermal Conductivity Detector
FID	Flame ionization detector
GC	Gas chromatograph
ID	Internal diameter
XRD	X-ray diffraction
TPR	Temperature programmed reduction
$H_2$ -TPR	Hydrogen temperature programmed reduction
NTP	Normal Temperature and Pressure
BET	Brunauer–Emmett–Teller

TEM	Transmission electron microscope
g	Gram
g·cat	Per gram catalyst
$\%I_{\text{gas}}$	Molar percentage of gas I in feed gas or tailgas
$A_{I,\text{gas}}$	Integrate area of GC peak corresponding the gas I in analysing gas
$A_{I,\text{calibration}}$	Integrate area of GC in calibration gas
$\%I_{\text{calibration}}$	Molar percentage of gas I in calibration gas
$RF_{J,I}$	Relative response factor of gas J with respect to the reference gas I
$F_{\text{in}}$	Molar flow rate of total feed gas
$F_{\text{out}}$	Molar flow rate of total tailgas
$\theta$	Reactant
$F_{\theta,\text{in}}$	Molar flow rate of reactant $\theta$ in feed gas
$F_{\theta,\text{out}}$	Molar flow rate of reactant $\theta$ in tailgas
$\%\theta_{\text{conv}}$	Conversion of reactant $\theta$
$r_{\theta}$	Reaction rate of reactant $\theta$
$S_J$	Selectivity of product J
T	Temperature
P	Pressure

FR	Flow rate
JCPDS	Joint Committee on Powder Diffraction Standards
CTL	Coal to liquid
P/O	Paraffins to olefins ratio
$\alpha_o$	Chain growth probability of $\alpha$ -olefins
$\alpha_p$	Chain growth probability of paraffins
Eq.	Equation

# Chapter 1

## Introduction

---

### 1.1. Motivation and rationale

Liquid fuels are currently widely used in many aspects of life. The primary source of these fuels is crude oil. As crude oil resources are being exhausted globally, more and more researchers are seeking alternative ways to produce liquid fuels. Among these alternatives, the Fischer Tropsch (FT) reaction has a long history, and is currently used to produce transport fuels from syngas derived from carbon-based materials, such as natural gas and coal. The use of syngas derived from alternative carbon sources, such as biomass and municipal waste, as a feed for FTS, is a promising new, green alternative technology for producing liquid fuels. In addition, there has been increasing interest recently in using FTS to produce value-added hydrocarbons, including higher alcohols, light olefins and hard waxes [1-4].

The product distribution of FTS is complex due to the large number of products that are produced as well as the fact that the products are in the gaseous, solid and liquid states [5]. The main products of FTS are linear alkanes and alkenes, but certain oxygenated organics, such as aldehydes, alcohols, ketones, and acids, are also formed. In an effort to increase the production of desired products, many researchers have focused on the reaction mechanism [6-7], the performance of the catalyst [8-9] and optimization of industrial FTS processes [10].

The carbon chain growth that occurs in FTS is seen as a process of monomer polymerization, in which methylene (which is considered to be a monomer) is formed by CO dissociation and partial hydrogenation [1, 11]. The most widely used model for describing the distribution of FTS products was proposed by Anderson, Schulz, and Flory (referred to as the ASF distribution) [11-13]. However, more and more experimental results show that, in actual operation, the product distribution of FTS does not follow the ASF model completely and that there are significant deviations in the light hydrocarbons [14-17]. The ASF distribution is not accurate enough to meet the requirements of laboratories and industry for modelling the FTS product distribution. In recent decades, various theories and models have been proposed to explain the deviation of the actual product distribution from the ASF model. As of yet, no theory as yet can fully explain it [18].

It is generally accepted that the primary products of FTS include linear paraffins and  $\alpha$ -olefins. Unlike paraffins, which are not reactive under FTS conditions,  $\alpha$ -olefins can re-adsorb and participate in secondary reactions. Therefore, it is necessary to do further research on the mechanisms and reaction rates of the secondary reactions of these  $\alpha$ -olefins, which might help develop better models of the overall product distribution in FTS. In addition,  $\alpha$ -olefins are high-value products that are widely used in industry; the uses include polymer production, additives, and specialty chemicals. Ethylene has two  $\alpha$ -carbons and has a symmetry not found in the other  $\alpha$ -olefins; it also exhibits a negative deviation from the ASF distribution. Therefore, it is worthwhile doing more research to understand the behaviour of ethylene in FTS.

The FTS product distribution must also satisfy thermodynamic considerations, such as increasing (or maximizing in the limit) entropy or equivalently reducing/ minimizing the Gibbs

Free Energy of the system. Several researchers have indicated that FTS does not achieve the global thermodynamic equilibrium; however, partial thermodynamic equilibrium may be approached, limiting both the olefin and paraffin product distribution during FTS [19-20]. However, how the reactions of the olefins occur to approach the partial reaction equilibrium is still not clear. Therefore, it is suggested that more experimental work needs to be done to investigate the effect of olefins, and in particular ethylene, on the product distribution of FTS.

## **1.2. Aim and objectives**

This thesis aims to investigate the role of ethylene and its effect on the performance of a cobalt-based catalyst during FTS. This research intends to provide valuable information to understand the reaction pathways and mechanisms of the olefins in FTS. The research objectives were:

- To study the reactivity of ethylene using firstly feed mixtures of ethylene/H<sub>2</sub> and thereafter co-feeding CO into the feed, to determine how the reactivity of ethylene is impacted by CO under typical FTS conditions.
- To investigate the effect of co-feeding ethylene into mixtures of CO/H<sub>2</sub> on the catalyst activity and product selectivity during FTS.
- To investigate the impact of co-feeding ethylene on the paraffin to olefin ratio in order to investigate the potential competitive equilibria between the products of FTS.
- To study the FTS reaction mechanism.

## **1.3. Outline of this thesis**

This chapter introduces the structure of the thesis. The thesis consists of nine chapters. Five of these chapters have either been published, submitted for publication, or are ready for submission; therefore, there is a certain amount of repetition in the content. The reaction system used throughout is similar, and the experimental methods are almost the same.

**Chapter 2** provides a literature review on this subject, including how FTS has developed; the catalysts and reactors used in FTS; the reactions in FTS and the reaction mechanisms; the product distribution of FTS; the secondary reactions of the  $\alpha$ -olefins in FTS, and the potential approach to thermodynamic equilibrium in FTS.

**Chapter 3** describes the equipment, the instruments, and the materials used in the experiments done in this study, the operating parameters, and the analytical equipment. The calculations and analysis used for all test results are also provided in this chapter.

**Chapter 4** deals with the reactivity of ethylene (i.e no CO in the feed) over a cobalt-based FTS catalyst. This chapter describes the experimental results obtained when using different feed gases, including ethylene only, ethylene/ N<sub>2</sub> mixtures, and ethylene /H<sub>2</sub> mixtures. The proportions of the feed gases were varied, and a range of reaction temperatures was tested. This work has been published in *Engineering Reports*, 2(9), e12232. [21]

**Chapter 5** discusses the mechanisms (carbide type mechanism and CO insertion mechanism) and describes the chain growth reactions in FTS. Experimental results are analyzed, and the role of ethylene and CO as chain-growth initiators and/or monomers are explored, leading to proposed reaction mechanisms. This work has been published in *AIChE Journal*, 66(11), e17029. [22]

**Chapter 6** deals with the reactivity of ethylene when co-fed with syngas over a cobalt-based FT catalyst. The results of the experiments done using syngas (i.e., no ethylene) and with different proportions of ethylene in the syngas are given. Comparisons of the conversion of reactants, the selectivity of products, and chain-growth probability are shown. Part of this work has been published in *Applied Catalysis A: General*, 614, 118024, combined with Chapter 7. [23]

**Chapter 7** reports on the effect of co-fed CO on ethylene hydrogenation over a typical FT Co-based catalyst. The results show the impact of CO on ethylene hydrogenation and CO reactivity. The conversion of the reactants, the selectivity of products, and chain-growth probability are compared. Part of this work has been published in *Applied Catalysis A: General*, 614, 118024, combined with Chapter 6. [23]

**Chapter 8** details the effect of feeding ethylene on the paraffin to olefin ratio of the product; and the approach to equilibrium of the olefins and paraffin distributions. In this regard, quasi-reaction equilibrium models (Yao Plot) are applied.

**Chapter 9** is a brief conclusion of this thesis.

## REFERENCES:

1. Fischer, F., & Tropsch, H. (1923). The Preparation of Synthetic Oil Mixtures (Synthol) from Carbon Monoxide and Hydrogen. *Brennstoff-Chem*, 4, 276-285.
2. Dry, M. E. (1981). The Fischer-Tropsch Synthesis in *Catalysis Sciences and Technology*, Anderson, J. R. and Boudart, M.,(Eds.) 1.
3. Sasol. (2000). 50 Years of Innovation.
4. Leckel, D. (2009). Diesel Production from Fischer– Tropsch: the Past, the Present, and New Concepts. *Energy & Fuels*,23(5), 2342-2358.
5. Anderson, R. B., Kölbl, H., & Ralek, M. (1984). *The Fischer-Tropsch Synthesis (Vol. 16)*. New York: Academic Press.
6. Mousavi, S. , Zamaniyan, A. , Irani, M. , & Rashidzadeh, M. . (2015). Generalized kinetic model for iron and cobalt based fischer–tropsch synthesis catalysts: review and model evaluation. *Applied Catalysis A General*, *Applied Catalysis A: General*(506), 57-66.
7. Branislav Todić, Wenping Ma, Gary Jacobs, Burtron H. Davis, & Dragomir B. Bukur. (2014). Corrigendum to: co-insertion mechanism based kinetic model of the fischer–tropsch synthesis reaction over re-promoted co catalyst. *Catalysis Today*, 228(3), 32-39.
8. Suo, H. , Wang, S. , Zhang, C. , Xu, J. , Wu, B. , & Yang, Y. , et al. (2012). Chemical and structural effects of silica in iron-based fischer–tropsch synthesis catalysts. *Journal of Catalysis*, 286(none), 111-123.
9. Hong, J. , Du, J. , Wang, B. , Zhang, Y. , Liu, C. , & Xiong, H. , et al. (2018). Plasma-assisted preparation of highly dispersed cobalt catalysts for enhanced fischer-tropsch synthesis performance. *Acs Catalysis*, acscatal.8b00960.

10. Moazami, N. , Wyszynski, M. L. , Rahbar, K. , & Tsolakis, A. . (2017). Parametric study and multiobjective optimization of fixed-bed fischer–tropsch (ft) reactor: the improvement of ft synthesis product formation and synthetic conversion. *Industrial & Engineering Chemistry Research*, 56(34), 9446-9466.Schulz, H. (1999). Short History and Present Trends of Fischer–Tropsch Synthesis. *Applied Catalysis A: General*, 186(1-2), 3-12.
11. Pichler, V. H., & Schulz, H. (1970). Neuere Erkenntnisse Auf Dem Gebiet Der Synthese Von Kohlenwasserstoffen Aus CO Und H<sub>2</sub>. *Chemie Ingenieur Technik*, 42(18), 1162-1174.
12. Friedel, R. A., & Anderson, R. B. (1950). Composition of Synthetic Liquid Fuels. I. Product Distribution and Analysis of C<sub>5</sub>—C<sub>8</sub> Paraffin Isomers from Cobalt Catalyst<sup>1</sup>. *Journal of the American Chemical Society*, 72(3), 1212-1215.
13. Flory, P. J. (1936). Molecular Size Distribution in Linear Condensation Polymers<sup>1</sup>. *Journal of the American Chemical Society*, 58(10), 1877-1885.
14. Iglesia, E., Vroman, H., Soled, S., Baumgartner, J., & Fiato, R. A. (1991). U.S. Patent No. 5,036,032. Washington, DC: U.S. Patent and Trademark Office.
15. Jordan, D. S., & Bell, A. T. (1986). Influence of Ethylene on the Hydrogenation of Carbon Monoxide Over Ruthenium. *The Journal of Physical Chemistry*, 90(20), 4797-4805.
16. Schulz, H., Van Steen, E., & Claeys, M. (1993). Olefin Formation, Hydrogenation and Isomerization in the Kinetic Regime of Fischer-Tropsch Synthesis. *Selective Hydrogenation and Dehydrogenation*.
17. James, O. O., Chowdhury, B., Mesubi, M. A., & Maity, S. (2012). Reflections on The Chemistry of The Fischer–Tropsch Synthesis. *Rsc Advances*, 2(19), 7347-7366.

18. Lu, X., Hildebrandt, D., Liu, X., & Glasser, D. (2012). A Thermodynamic Approach to Olefin Product Distribution in Fischer–Tropsch Synthesis. *Industrial & Engineering Chemistry Research*, 51(51), 16544-16551.
19. Masuku, C. M., Ma, W., Hildebrandt, D., Glasser, D., & Davis, B. H. (2012). A Vapor–Liquid Equilibrium Thermodynamic Model for a Fischer–Tropsch Reactor. *Fluid Phase Equilibria*, 314, 38-45.
20. Yao, Y., Liu, X., Hildebrandt, D., & Glasser, D. (2012). Fischer–Tropsch Synthesis Using H<sub>2</sub>/CO/CO<sub>2</sub> Syngas Mixtures: A Comparison of Paraffin to Olefin Ratios for Iron and Cobalt Based Catalysts. *Applied Catalysis A: General*, 433, 58-68.
21. Zhang, Y., Tshwaku, M., Yao, Y., Chang, J., Lu, X., Liu, X., & Hildebrandt, D. (2020). Reaction of ethylene over a typical Fischer-Tropsch synthesis Co/TiO<sub>2</sub> catalyst. *Engineering Reports*, 2(9), e12232.
22. Zhang, Y., Yao, Y., Chang, J., Lu, X., Liu, X., & Hildebrandt, D. (2020). Fischer–Tropsch synthesis with ethene co-feeding: Experimental evidence of the CO-insertion mechanism at low temperature. *AIChE Journal*, 66(11), e17029.
23. Zhang, Y., Yao, Y., Chang, J., Gorimbo, J., Liu, X., & Hildebrandt, D. (2021). The interaction of CO, H<sub>2</sub> and ethylene over a typical cobalt-based Fischer-Tropsch synthesis catalyst. *Applied Catalysis A: General*, 614, 118024.

## Chapter 2

### Literature review

---

In this section, some of the fundamental knowledge of Fischer-Tropsch synthesis (FTS) and the research process are reviewed, which includes the history of FTS, the catalysts used in FTS, the chemistry and mechanism of FTS and the product distribution of FTS. Since this thesis investigate the effect of olefins co-feeding on FTS, this chapter gives a detailed review on the influence of co-feeding olefins with different reaction conditions on the catalytic performance of FTS.

#### **2.1. The history of Fischer-Tropsch Synthesis**

With crude oil resource being depleted all around the world, many researchers are focussing on finding other ways to produce liquid fuels that can replace crude oil. Indirect liquefaction processes generally involve: gasification of solid carbon resources (coal/ biomass/ waste/ natural gas) to a mixture of carbon monoxide and hydrogen (called synthesis gas or syngas in short); then using a process called FTS to convert syngas into liquid hydrocarbon products. This has become a promising route to meet the continuously increasing demand for liquid fuels and chemical feedstock, and it is attracting a great deal of attention from scientists and engineers.

As early as the end of the 19th century, synthesis gas was converted into a liquid product by means of electrical discharge, as reported by Losanitsch and Jovitschitsch [1]. At the beginning

of the 20th century (1902), Paul Sabatier and Jean Baptiste Senderens reported that methane could be formed when carbon monoxide and hydrogen pass through dispersed nickel or cobalt at atmospheric pressure and 200 to 300 °C [2]. German scientists systematically studied the subject for more than a decade, and by 1913, Badische Anilin und Soda Fabrik (BASF) proposed a patent for the hydrogenation of carbon, ketones, acids and hydrocarbons from carbon monoxide, at an elevated temperature, using cobalt catalysts [3]. At that time, BASF's research focused on hydrogenation of carbon monoxide to produce methanol. In the 1920s, FTS was officially born. In 1923, two German researchers, Franz Fischer and Hans Tropsch, of the Kaiser Wilhelm Institute for Coal Research, proved that CO hydrogenation over Fe, Co or Ni catalysts at 180–250°C and atmospheric pressure produced a mixture of linear hydrocarbons [4-9].

The industrial history of FTS can be roughly separated into two stages that are separated by World War II: (1) Germany's industrialization of Fischer-Tropsch (FT) processes from 1935 to 1945; and (2) global transfer of the German technology to Britain, France, Japan, Canada, the United States, South Africa, China and other nations after the end of World War II [10].

Between 1935 and 1939, Germany built nine plants that delivered a total annual output of 700,000 tons of synthesized hydrocarbons using cobalt-based catalysts [10-14]. At that time, Germany produced a large amount of synthetic fuel, most of which was used as engine fuel. The catalyst used was mainly Co-based (Co: ThO<sub>2</sub>: MgO: Kiesselguhr) [5-6, 15]. Since 1944, 40% of FT product has been used as chemical feedstock, and the original cobalt-based catalysts have been gradually replaced by iron-based catalysts [11]. FT production was estimated to have accounted for 9% of Germany's war production fuels and 25% of its automotive fuels.

After World War II, the South African Coal Oil and Gas Cooperation (SASOL) built SASOL-I in Sasolburg in 1955, 80 km from its headquarters in Johannesburg [12]. This was the first indirect fuel oil from coal liquefaction plant in South Africa [12]. After the Middle East oil crisis in the 1970s, the company established the larger SASOL-II and SASOL-III plants in 1980 and 1982. At present, the total amount of coal processed in the three plants is 45.9 million tons [16]. The annual processing volume of SASOL-I is 6.5 million tons, and the total annual processing capacity of SASOL-II and III is 39.4 million tons [16]. SASOL is the world's largest producer of synthetic oils and chemicals from coal. Except for the successful commercial operations of South Africa's SASOL, the viability of coal-based FT fuel routes has varied with fluctuations in crude oil prices since the 1950s. By the end of the 1980s, interest in using FTS to convert natural gas into liquid fuels strengthened, due to the discovery of natural gas reserves all over the world.

The birth of the modern-day gas to liquid (GTL) industry began in 1993, with the commissioning of two new plants [17]. The first was a wax-cracking plant built by Shell in Bintulu, Malaysia, with a capacity of 10,000 bbl/day using Co-based catalysts. The other was a natural gas to gasoline plant built in Mossel Bay, South Africa, by PetroSA [17]. The plant uses Fe-based catalysts and has a capacity of 25,000 bbl/day. In 2006, China established Synfuels China who developed a high-temperature slurry bed coal-to-liquids process and catalyst technology in 2008 [18]. At present, the technology is being implemented at the various indirect coal liquefaction commercial plants constructed throughout China, which has a capacity of nearly 13.5 million tons/year [18-19].

## 2.2. Types of reactors used for FTS

In the ninety years since the first development of FTS, many types of commercial reactors have been designed and built for FTS. Most of them can be classified as falling within two categories: low-temperature Fischer-Tropsch (LTFT) technology and high-temperature Fischer-Tropsch (HTFT) technology [9, 20-21]. HTFT synthesis can produce gasoline, diesel fuel, solvent oil and olefin by means of FTS operated at a high temperature (300–350 °C, 20 bars) [9, 20-21]. LTFT synthesis, on the other hand, takes place at a relatively low temperature (200–240°C) [9, 20-21]. Its main product is paraffin that can be processed into a special wax or hydrocracked/isomerized to produce high-quality diesel [9, 20-21].

Currently, four types of FTS reactors are generally used in the industry, as follows: tubular fixed bed (TFB) reactor, circulating fluidized bed (CFB) reactor, fixed fluidized bed (FFB) reactor, and slurry bubble column (SBCR) reactor.

1. **TFB:** The first TFB reactor was developed by Ruhrchemir and Lurge, and was referred to as the ARGE reactor. This type is currently operating at SASOL I, in Sasolburg, South Africa. Another representative sample of TFB was designed by Shell, which is currently used in Bintulu, Malaysia and in the Pearl Project in Qatar as well [6, 9, 20]. The advantages and disadvantages of TFB are listed in Table 2.1.
2. **CFB:** With the CFB, the catalyst is entrained in the fast-moving stream. A representative CFB is the SASOL Synthol Reactor, which is used at SASOL-II, SASOL-III and Petro SA. Table 2.2 shows the advantages and disadvantages of CFB.
3. **FFB:** With an FFB reactor, the catalyst bed remains stationary, and gas passes upwards through it. The first FFBs were developed by Hydrocarbon Research Inc. and Standard

Oil Company in the USA [6, 29]. Compared to CFB, FFB has the advantages of being relatively simple, low in cost, easy to operate, and low in catalyst consumption.

4. **SBCR:** SBCR is a reactor in which solid particles of catalyst are suspended in a liquid medium. The liquid medium is generally inert and only acts as a suspension catalyst that facilitates heat and mass transfer. The most representative SBCR is the SASOL Chevron slurry reactor in Qatar (Oryx Project), which uses cobalt catalysts [30]. In addition, three demonstration plants in Shenhua, Yitai and Luan in China use SBCRs and Fe-based catalysts [18-19]. The advantages and disadvantages of SCBR are listed in Table 2.3.

When the reaction temperature is used as the differentiator: TFB and SBCR belong to the LTFT category; the other two belong to the HTFT category. The parameters for the TFB, CFB and SBCR reactors used by SASOL in its commercial FT processes are listed in Table 2.4 [35].

**Table 2.1:** Advantages and disadvantages of TFB [22-26].

<b>ADVANTAGES</b>	<b>DISADVANTAGES</b>
<b>HIGHER CONVERSION</b>	Low heat transfer
<b>NO CATALYST LOSS</b>	Limited productivity
<b>LONGER CATALYST LIFE</b>	More complex construction
<b>OPERATIONAL FLEXIBILITY</b>	Greater pressure drop
<b>EASY CATALYST-PRODUCT SEPARATION</b>	Difficult to change catalysts

**Table 2.2:** Advantages and disadvantages of CFB [6, 21, 27-28]

<b>ADVANTAGES</b>	<b>DISADVANTAGES</b>
<b>Excellent temperature control</b>	Requirement of a gas pass-by
<b>Free from diffusion limitation</b>	Difficult to separate the products and catalysts
<b>Easy catalyst loading</b>	Not easy to scale-up
<b>Easy catalysts replacing in operation</b>	Requires catalysts that can resist attrition
<b>Low differential pressure</b>	Poor operational flexibility
	Easy to completely deactivate the catalyst by trace H <sub>2</sub> S

**Table 2.3:** Advantages and disadvantages of the SCBR [31-34]

<b>ADVANTAGES</b>	<b>DISADVANTAGES</b>
<b>Excellent temperature control</b>	Narrow gas velocity range
<b>Wild range ratio of H<sub>2</sub>/CO</b>	Difficult to scale up
<b>Adaptable to various operating conditions</b>	Not easy to determine the true residence time
<b>Replace catalysts during run</b>	Design parameters are not readily available
<b>Low differential pressure</b>	Difficult to separate the products and catalysts
<b>Small amount of catalyst</b>	
<b>Simplest structure</b>	

**Table 2.4:** Characteristics of Sasol's commercial FT processes [35]

Characteristics	SBCR	CFB	TFB
Reaction temperature(°C)	250~300	300~350	220~250
Reaction pressure (MPa)	2.4	2.0~2.3	2.3~2.5
(H <sub>2</sub> + CO) conversion (%)	90	77~85	50
C <sub>3+</sub> yield (g·m <sup>-3</sup> H <sub>2</sub> + CO)	166	110	104
Space velocity [(m <sup>-3</sup> H <sub>2</sub> + CO)/ (m <sup>-3</sup> ·h)]	5000	700	500~700
Catalyst productivity [t C <sub>3+</sub> /(t·d <sup>-1</sup> )]	10.6	1.85	1.35
Reactor productivity [t C <sub>3+</sub> /( m <sup>3</sup> ·d <sup>-1</sup> )]	1.86	2.1	1.25

### **2.3. Catalysts used in Fischer-Tropsch Synthesis**

Since the birth of the FTS technology, researchers have conducted extensive research on the type of catalyst that can be used. Many experimental studies have shown that the most active metal for FTS is Group VIII metal, such as Fe, Co, Ni, Ru etc. [36]. Under typical FTS, these elements are generally present in the form of metals, oxides or carbides, and they can adsorb the reactants physically or chemically. Ni has a high hydrogenation ability and can make CO easy to dissociate; it is most suitable for synthesising methane, but not used as a catalyst to synthesize long-chain hydrocarbons [2, 12, 37-39]. The noble metal Ru exhibits the highest catalytic activity and the best selectivity to long chain hydrocarbons [40-41]. Moreover, during the last ten years, research has shown that a Ru-based catalyst can maintain high activity in a higher water pressure and oxide-containing atmosphere; therefore, it may play a role in future in the biomass to liquid (BLT) process [42-44]. However, it is too expensive and scarce [45] to use as an industrial catalyst. Therefore, cobalt (Co) [15, 40, 46-48] and iron (Fe) [48-49] are the preferred metals for FTS, which are used currently in the industrial processes.

#### **2.2.1. Iron-based catalysts**

As the most abundant transition metal element in the earth, iron is relatively inexpensive. In addition, Fe-based catalysts have high reactivity and water gas shift reaction (WGS) activity, and the applicable H<sub>2</sub>/CO ratio range is wide. These characteristics mean that Fe-based catalysts have been widely studied and applied in FTS. Fe-based catalysts are usually used in both HTFT and LTFT. Used in fixed or slurry beds below 280 °C, where the Fe-based catalyst is completely submerged in the wax phase; above 320 °C in a fluidized bed, the temperature will be used to maximum the short carbon chain olefinic products as the boundary [6, 15, 20].

In the iron-based FTS catalyst system,  $\text{Fe}_2\text{O}_3$  is used as a precursor of the catalyst, and is gradually converted into metastable  $\text{Fe}_3\text{O}_4$  in a syngas atmosphere, and then converted into iron carbide compounds [50-52]. Li et al. systematically studied the existence and experimental regulation of various phases of iron carbide, and based on these studies, developed series of commercial iron-based FTS catalysts [50, 53-60]. Their experimental study found that pre-treatment, reaction conditions and promoters affect the composition of iron carbide phases in the catalyst. The difference in the phase composition of the iron-based catalyst also has a significant effect on the activity and selectivity of the FTS reaction [58-60].

The addition of promoters plays a crucial role in regulating the activity and selectivity of Fe-based catalysts. Ngantsoue et al. [61] studied the effect of different alkali metals on the catalytic performance of Fe/SiO<sub>2</sub> catalysts. The experimental results show that the addition of K not only increases the FTS synthesis activity, but also increases the WGS reactivity. It is generally accepted that the alkali metals, as electronic promoters, can change the electronic properties of Fe-based catalysts, then affect the adsorption of H<sub>2</sub> and CO on the active sites on the surface of the catalysts [62]. Li et al. found the addition of sodium in Fe-based catalyst made carburization easy by XRD and MES results, and obtained maximum in CO conversion and light olefin selectivity in 2.8 mol. % Na/Fe catalyst. [63] Similarly, as reported by Ribeiro et al., alkali promoters improved the carburization of iron oxide (activated by CO), and the order of the rate of carburization is unpromoted < Li < Na < K [64]. Furthermore, the addition of all alkali metals reduced the selectivity of CH<sub>4</sub>, and the addition of Na gave the best C<sub>5-11</sub> hydrocarbon selectivity (about 35%) [61]. Zhang et al. showed that the addition of Cu to Fe-Mn/SiO<sub>2</sub> catalyst could improve the reduction performance of the catalyst, promote the adsorption of H<sub>2</sub>. Copper, to some extent, increase the activity of FTSs reaction, shortening

the reaction induction. However, the effect on the distribution of hydrocarbon products is not obvious [65].

In fact, the active phase of iron-based catalysts, and the role of various phases in the iron-based FT catalysis process are still controversial. With the advancement of science and technology, in situ characterization techniques and the application of quantum chemical computation, will have a deeper understanding of the basic problems in the FT process.

### **2.2.2. Cobalt-based catalysts**

Compared with Fe-based catalysts, Co-based catalysts have higher chain growth ability and are not sensitive to water-gas shift reactions [5-6, 15]. Due to the higher FTS activity, the Co-catalytic FTS operation temperature is lower than that at Iron-based catalytic condition. Moreover, most of FTS Co-based catalysts are supported catalysts. It is stable during the reaction process (lower temperature), is not easy to deposit carbon and poison, and contains less oxygen compounds in the product [6, 15, 66]. For the above reasons, although Co is more expensive than Fe, Co-based catalysts are still one of the research hotspots of FTS catalysts in recent years.

The active phase of the Co-based catalyst on FTS is the metal phase, and the active sites composed of metal cobalt atoms determine the activity and selectivity of the catalyst. Sometimes, syngas or CO may change the  $\text{Co}^*$  to  $\text{Co}_x\text{C}$ , which is not active with chain growth reaction. However, it shows high activity for oxygenates. Pei et al reported the Co- $\text{Co}_2\text{C}$  exhibited excellent activity and selectivity for alcohol formation under FTS reaction condition [67].

Particle size and pore size are key factors that affect the performance of the catalyst. Bezemer et al. [67] used inert carbon nanotubes as support to prepare a series of catalysts with metallic Co particle size of 2.6 to 27 nm. The experimental results show that the minimum cobalt particle size suitable for FTS is 6-8 nm [68]. Similar results also reported by Borg et al [69]. They synthesised more than 20 different Co-based catalyst supported on  $\alpha$ -Al<sub>2</sub>O<sub>3</sub> or  $\gamma$ -Al<sub>2</sub>O<sub>3</sub>, with which the Co particle sizes were ranged from 3-18 nm. Based on the experiment results, they found products selectivity is depend on Co particle size, when it less than 7 nm (the selectivity of C<sub>5+</sub> increased with particle size increasing). However, when the Co particle size was bigger than 9 nm, the selectivity of C<sub>5+</sub> was not affected by it [69].

Promoters on cobalt based catalysts play a significant role during FTS. The addition of a small amount of noble metals (promoters) can improve the reducibility of the catalyst; in consequence, promote the catalytic performance of the catalyst. Zhang et al. investigated the effect of noble metals on the catalytic performance of Co-based catalysts [70]. They found that the addition of precious metal auxiliaries reduced the reduction temperature of the Co-based catalyst, increased the active site, and exhibited excellent CO hydrogenation activity and higher C<sub>5+</sub> long-chain hydrocarbon selectivity in the FTS [70]. More research work improves such La, Ru and CeO<sub>2</sub> has positive effect on CO conversion and product selectivity [71-73].

The support effect on Co-based catalyst is obvious. In the 1980s, Reuel et al. investigated the effects of some supports on the activity of FT Co-based catalysts and found the catalyst activity was in the order of TiO<sub>2</sub> < SiO<sub>2</sub> < Al<sub>2</sub>O<sub>3</sub> < C < MgO under 1 bar and 225°C [74]. The results obtained by Price is slightly different to them, of which the order of catalysts activity was SiO<sub>2</sub> < TiO<sub>2</sub> < Al<sub>2</sub>O<sub>3</sub> under 8 bars and 220°C [75]. This difference can be attributed to a

slight difference in operating conditions. In general, the order of influence of the catalyst support on the cobalt-based catalyst is  $\text{Al}_2\text{O}_3 > \text{TiO}_2 > \text{SiO}_2$  [30]. Mesoporous molecular sieves have ordered mesoporous, large specific surface areas and pore volumes. As support of Co-based catalyst, it can obtain a high-dispersion cobalt-based catalyst to enhance the catalytic activity of FTS [76].

## 2.4. Chemistry and mechanism of Fischer Tropsch Synthesis (FTS)

### 2.4.1. Chemistry in FTS

FTS is a very complex reaction system yielding a wide variety of products. The reactions in FTS process occur differently depending on the catalyst and operating conditions applied. The major overall reactions in FTS are as follow equations [77-79]:

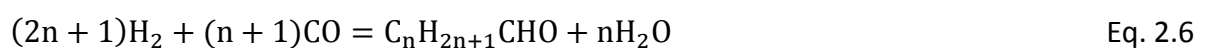
(1) Linear paraffins generation



(2) Olefins generation



(3) Alcohols and aldehydes generation:



(4) Water gas shift (WGS) reaction:



(5) Methanation reaction and Boudouard reaction (main side reaction):



#### 2.4.2. Mechanism of FTS

As has been mentioned, it is assumed that the formation of hydrocarbons in FTS is based on three stages: (i) the initiation of the carbon chain, (ii) the growth of the carbon chain, and (iii) the termination/desorption of the carbon chain [80]. To better understand FTS, various reaction mechanisms have been proposed by scientists [4-5, 49, 81-82]. Among them, the most important and widely cited mechanisms have three types: directly CO dissociation mechanism [4, 49], ENOL mechanism (H-assisted CO dissociation) [78-79] and CO insertion mechanism [80].

##### (1) Directly CO dissociation mechanism

When Fischer and Tropsch first proposed the surface carbide mechanism [4], they believed that CO first adsorbs on the surface of the catalyst and then dissociates into active metal carbide species, which then react with H<sub>2</sub> to form a methylene (CH<sub>2</sub>) intermediate. This intermediate is further polymerized to form paraffins and olefins. This mechanism well describes the linear hydrocarbon product formation, but it does not explain the formation of branched products and organic oxygenates.

The carbide mechanism can be explained as follows:

Initiation:



Chain growth:



Chain termination:



Based on carbide mechanism, scientists developed several different chain growth mechanisms with different chain initiators and monomers in next few decades. Brady and Pettit considered that the chain growth monomer was still  $\text{CH}_2^*$ , but the carbon chain initiator was  $\text{CH}_3^*$  rather than of  $\text{CH}_2^*$  [83]. Maitlis et al proposed another mechanism named Alkenyl mechanism and considered an adsorbed vinyl ( $\text{CH}_2=\text{CH}^*$ ) was the initiator of carbon chain growth, while  $\text{CH}_2^*$  was monomer [84]. Moreover, Alkylidene–hydride–methylidyne mechanism, which developed by Ciobîcă et al, described that iso-vinyl ( $^* \text{CH}_2\text{-CH}^{**}$ ) was the chain growth initiator, the monomer was  $\text{CH}^* + \text{H}^*$  rather than  $\text{CH}_2^*$  [85].

## (2) H-assisted CO dissociation mechanism

Difference from the direct CO dissociation mechanism, H-assisted CO dissociation mechanism believed that the formation rate of monomer was suppressed by the high activation barrier

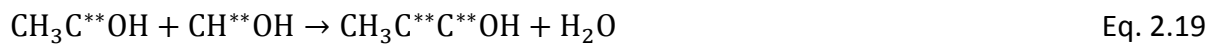
of CO direct dissociation on typical FTS catalysts. Storch et al. [86] and Eidus [87] proposed the ENOL mechanism. It is believed that CO\* and H\* react to produce surface ENOL intermediate species, and that two CH\*\*OH species condense to form CH\*\*C\*\*OH intermediates, which are further hydrogenated to form hydrocarbons and organic oxygenates. However, the enol intermediate has not been observed.

The ENOL mechanism can be explained as follows:

Initiation:



Chain growth:



Chain termination:



In recent years, the computation work showed that when H\* atoms existed on the flat facet of Co (0001), the CO was easier to dissociation. This is the theoretical basis for H-assisted CO-dissociation mechanism [88].

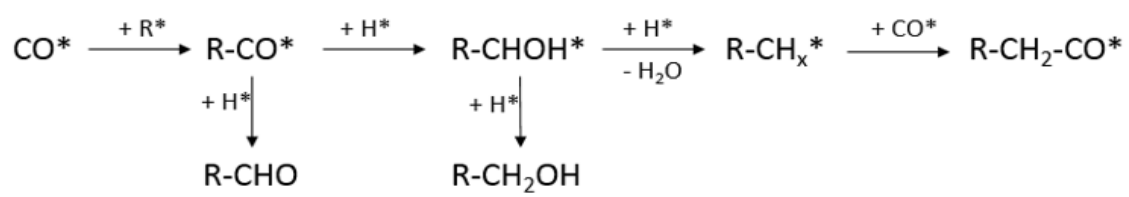
Moreover, another computational work indicated that directly CO dissociation and H-assisted CO dissociation mechanisms were preferred to Co-fcc phase and hcp phase, respectively [89].

### (3) CO insertion mechanism

In both cases (H-assisted CO dissociation or direct CO dissociation), the C-O bond cleavage was prior than C-C bond coupling, while Pichler et al. [90] proposed a CO insertion mechanism considered C-C bond coupling was before the C-O bond breaking. Here, it was believed that the surface species was formed by hydrogenation of the surface-adsorbed CO, and further hydrogenated to form a bridged oxymethylene species. This species is hydrogenated and dehydrated to form carbene and methyl groups. The chain is grown by repeated insertion and hydrogenation of CO in metal-hydrogen bonds and metal-alkyl bonds to form C-C bonds. Although, Zhuo et al [91-92] conducted DFT calculations and concluded that CO insertion mechanism was preferable over other mechanisms on Co-based FTS catalysts, this mechanism was still lacking solid experimental evidence.

The CO insertion mechanism is shown in Scheme 2.1:

It is generally believed that the complex FTS reaction system may not be controlled by a single reaction mechanism. The diversity and distribution characteristics of FTS products are the result of the combined effects of several reaction mechanisms. With the FTS reaction mechanism, it is a mechanism for multiple parallel paths. In other words, it has infinite scientific space and artistic charm for the precise regulation of C-H-O reaction network system.



**Scheme 2.1:** Pathways of the CO insertion mechanism

In-situ Fourier Transform infrared spectroscopy (FT-IR), which can provide time-resolved observations about the reaction mechanisms, is an ideal technology to investigate the adsorption and dissociation of reactants, as well formation and transformation of intermediates. This characterization can provide direct evidence for FTS mechanism [93-94]. Jiang et al. [95-96] observed no adsorbed CO on both Co- and Fe-based catalysts, result of the dissociation of CO occurred on very fine metallic particles, when they applied Diffuse Reflectance Infrared Fourier Transform Spectroscopy (DRIFTS) to study the manganese promoted cobalt and iron catalysts. However, other research groups monitoring the evidence of CO adsorption on supported Co-based catalysts by using in-situ FT-IR exist [97-99]. King et al., employed in-situ FT-IR on supported Fe- and Ru-based catalysts on FTS condition, [100] and also Schanke et al. [101] found the relative intensity of bands shifted towards lower CH<sub>2</sub>:CH<sub>3</sub> intensities with increasing temperature, which implied short chain products preferred to high temperature. It was consistent with typical FTS result. For Co-based catalyst, researcher considered the bands present for CH<sub>2</sub> species to be related with accumulated long chain products in pores [102].

## **2.5. Product distribution in FTS**

Since many congeners of hydrocarbons (linear alkanes and linear  $\alpha$ -alkenes) were produced in Fischer-Tropsch synthesis, Herington summarized FTS as a complex catalytic polymerization system as early as 1946 [103]. The kinetic model currently widely used to predict the distribution of Fischer-Tropsch synthesis products was proposed by Anderson, Schultz and Flory and is referred to as the ASF kinetic model [90, 104-105]. In this model, the carbon chain growth and carbon chain termination of the hydrocarbon product are independent of the

length of the carbon chain. Based on the ASF theory, a variable independent of the carbon number  $n$  of the product is defined as the probability of carbon chain growth, which is indicated as  $\alpha$  value. The following equations are used to calculate the value of  $\alpha$ :

$$\frac{W_n}{n} = (1 - \alpha)^2 \alpha^{n-1} \quad \text{Eq. 2.23}$$

$$\text{Ln}\left(\frac{W_n}{n}\right) = 2\text{Ln}(1 - \alpha) + (n - 1)\text{Ln}\alpha \quad \text{Eq. 2.24}$$

$$\alpha = \frac{r_p}{r_p + r_t} \quad \text{Eq. 2.25}$$

Where:  $W_n$  is the weight fraction of the hydrocarbon product containing  $n$  atoms;  $n$  is the carbon number. In the last equation,  $r_p$  and  $r_t$  refer to the carbon chain growth rate and carbon chain termination rate, respectively. By plotting  $\text{Ln}(W_n/n)$  and the carbon number  $n$ , the slope is indicated as  $\text{Ln}\alpha$ .

### 2.5.1. Ideal ASF distribution

The ideal distribution of ASF products is shown in Figure 2.1 (a). When calculated by the ideal state ASF, the hydrocarbon product selectivity for different carbon chain lengths based on weight fraction is shown in Figure 2.1 (b) [77, 106]. As can be seen in Figure 2.1 (b), when  $\alpha$  value is less than 0.2, almost no  $C_{5+}$  product is formed. The maximum mass fraction selectivity of the gas phase hydrocarbon  $C_2$ - $C_4$  occurs in the range of  $\alpha$  value from 0.4-0.5. When  $\alpha$  value exceeds 0.8, the main product is the long chain product  $C_{5+}$ .

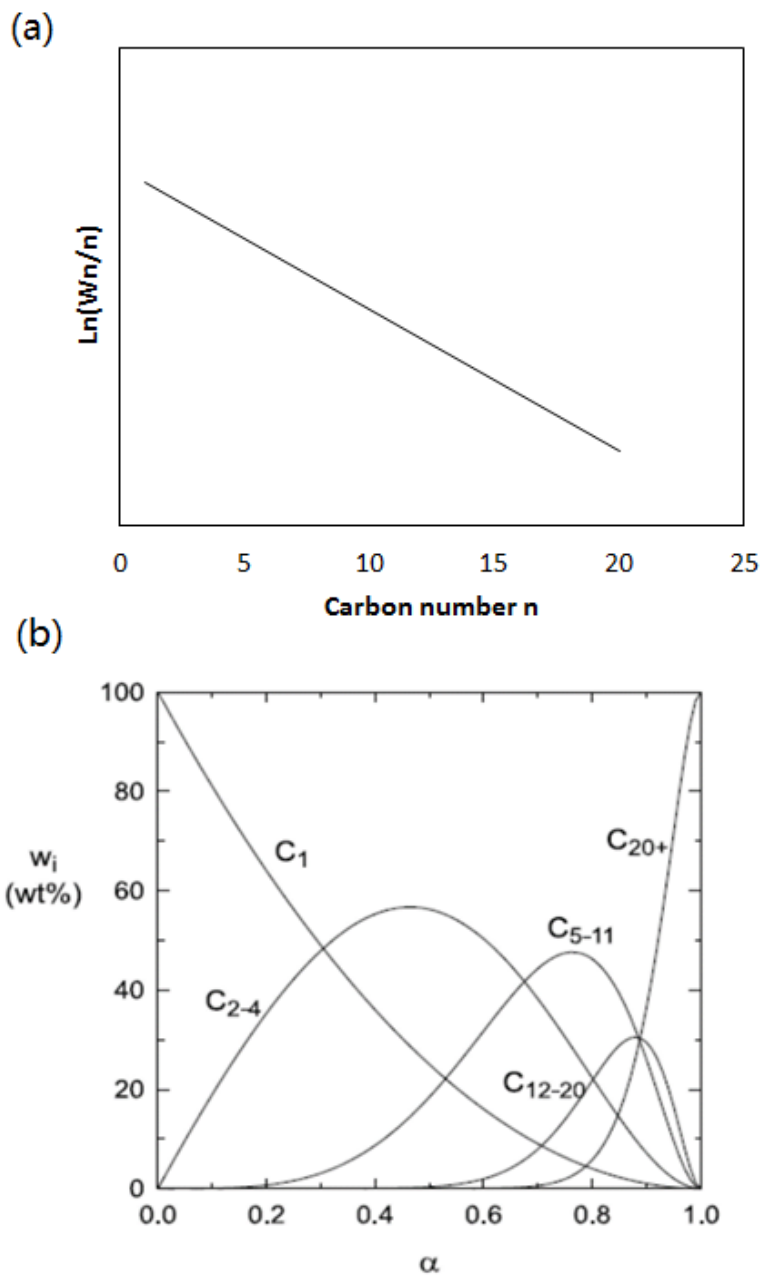


**Figure 2. 1:** (a) Ideal ASF distribution of all products and (b) Hydrocarbon weight fraction selectivity as a function of  $\alpha$  value [77, 106]

### 2.5.2. Deviation from the ideal ASF distribution

Under actual reaction conditions, many experimental results deviate from the ideal ASF product distribution model, including positive and negative deviations. In earlier studies, this deviation was considered as an operational error or an experimental error, with the earliest report appearing in 1943 [107]. However, since the 1980s, researchers have reported the product distribution deviates from the ideal ASF model, which mainly includes the following cases:

- (1) Extremely high C<sub>1</sub> (methane) selectivity [15, 108-110].
- (2) Extremely low C<sub>2</sub> selectivity [111-114].
- (3) The curve distribution of long-chain hydrocarbons deviates from the ASF model. As the carbon chain grows, the  $\alpha$ -value reaches asymptotic values [115-119].

To explain the deviation of this experimental result from the distribution of ASF products, some researchers developed a variety of theories and mechanisms, which were summarised by Lu et al. as follows [120]:

- (1) Assume two different carbon chain growth active sites on the catalysts (double  $\alpha$  model).
- (2) There is an accumulation of long chain hydrocarbon products (passive deviation of carbon number  $n > 10$  from ideal ASF products distribution).
- (3) There is a vapour-liquid equilibrium on the surface of catalysts (liquid layer formed by long chain Hydrocarbons products).

- (4) The secondary reaction of  $\alpha$ -olefins is:  $\alpha$ -olefins re-adsorb and reinserts into carbon chains, which enhances generation of long chain hydrocarbons.

Besides the explanations listed above, there are several others developed to explain the deviation from ideal ASF product distribution, especially high methane selectivity [17, 108-109]: 1. Hot spots formed in the catalyst bed, which cause the uneven temperature in catalyst bed. 2. More rapid diffusion of  $H_2$  than CO within liquid filled pores, which drives up termination for sites deeply embedded within the catalyst. 3. Methanation occurring on promoter sites, which leads to the risen of methane selectivity. 4. The presence of cobalt oxides in reduced catalyst can drive up WGS, which can cause the increase of methane selectivity due to localized  $H_2$  forming from WGS. 5. The presence of promoter promotes the oxidation of the metal phase, thereby further enhancing WGS and promoting the generation of hydrogen and methane.

## **2.6. Secondary reaction of $\alpha$ -olefins in FTS**

In the previous section, the secondary reaction of olefins is mentioned as a reasonable explanation for why the distribution of FTS products deviated from the ideal ASF kinetic model. Many reports indicate that the primary products of FTS include linear paraffins and  $\alpha$ -olefins [21, 121-122]. Unlike paraffins, which do not show reactivity under FTS conditions, it is a well-established fact that  $\alpha$ -olefins resorb under experimental conditions and continue to participate in the reaction [113, 123-126].

In earlier studies, the researchers studied the secondary reaction of  $\alpha$ -olefins by investigating FTS reactant residence time in the catalyst bed [126-127]. In 1967, Pichler et al. showed that by changing the residence time of the reactant, the  $\alpha$ -olefins are resorbed on the catalyst

surface and isomerized to internal olefins or hydrogenated to form corresponding paraffins [127]. Later, Schulz reported that the secondary reaction of  $\alpha$ -olefins was limited due to the short residence time of the reaction gas in the bed [126].

However, it is more intuitive to study the secondary reaction of  $\alpha$ -olefins by means of  $\alpha$ -olefin co-feed into syngas. Many experiments involving co-feeding  $\alpha$ -olefins into the FTS reaction system were conducted by scientists using Fe-based [128-132], Co-based [87,93-94, 133-142] and Ru-based catalysts [129, 141, 143-144]. Based on the researchers' conclusions, the types of secondary reactions of  $\alpha$ -olefins include the following:

### **(1) Hydrogenation**

Hydrogenation of  $\alpha$ -olefin to form linear paraffin with their corresponding carbon numbers is the fastest reaction among all the olefin secondary reactions. Schulz et al. [133] studied the reactivity of olefins by adding a very small amount (0.1-0.3 vol.%) of  $\alpha$ -olefins with different carbon numbers (ethylene, propene,  $\alpha$ -butene and  $\alpha$ -hexadecene) to the feed gas of iron-based catalytic FTS (Fe/K) and cobalt-based catalysed FTS (Co/ThO<sub>2</sub>/SiO<sub>2</sub>). They found that, under all reaction conditions, hydrogenation of olefins was the main reaction [133]. Other researchers have reported that when they co-feed 1-octene and 1-dodecene into a cobalt-based catalytic FTS system, more than 60% of the olefins were hydrogenated to form paraffins [145]. The hydrogenation reaction after  $\alpha$ -olefins resorption only changes the paraffins to olefins ratio but has no effect on the probability of carbon chain growth.

### **(2) Isomerization**

Isomerization, or the double bond shift reaction, can only take place when the carbon number of  $\alpha$ -olefins is greater than 3, and it would generate internal olefins with corresponding

carbon numbers. However, the further isomerization products (3-olefins) were observed [146]. Similar as the hydrogenation reaction, this reaction shows no carbon number change, so that it does not affect the probability of carbon chain growth. The kinetic scheme of  $\alpha$ -olefin isomerization was described by Schulz et al. [146], and it is shown in the following equation:



### **(3) Hydrogenolysis**

The  $\alpha$ -olefin undergoes a hydrogenolysis reaction with the assistance of hydrogen to form a short-chain hydrocarbon product and surface  $\text{C}_1$  species. This reaction shortens the carbon chain and has a negative effect on the probability of carbon chain growth. At the same time, the  $\text{C}_1$  surface species as a precursor is prone to hydrogenation to form methane, which may result in the high selectivity of methane in FTS to some extent. Liu et al. [147] investigated the reactions of 1-dodecene in the presence of  $\text{H}_2$  (not syngas) and found that products are generated from  $\text{C}_1$  to  $\text{C}_{25}$  under this condition. As per their report, two explanations are proposed: the oligomerization (dimerization) of added 1-olefin and its successive cracking; or the addition of methylene species, which is formed via the demethylation reaction [147]. Since the methane yield is much higher than the product of the adjacent carbon number, hydrogenolysis of olefin is the main cause of this phenomenon. Chen et al. [142] obtained similar results when they co-fed propylene to hydrogen under FTS Co-based catalysts and FTS operation conditions.

### **(4) Reinsertion**

The re-adsorption and re-insertion reactions of  $\alpha$ -olefins have been recognized by researchers as secondary reactions of olefins that mainly increase the length of the carbon chains. The reinsertion of such olefins mainly has two manifestations: first, the olefin is inserted as a monomer into the carbon chain (mainly ethylene) [148]; second, the surface species formed by the olefin resorption works as a carbon chain initiator continues to polymerize the monomer. As reported by Zhang et al. [148], the co-feeding of labelled acetylene ( $^{13}\text{C}_2\text{H}_2$ ) results in an increase in hydrocarbon products, especially olefins. They believed that both ethylene and acetylene can participate in carbon chain growth, but ethylene works as a monomer, while acetylene works as a chain growth initiator.

It is worth noting that some experimental data shows that there are two  $\alpha$  values obtained when the product distribution is plotted via ASF model, the light hydrocarbon products have a lower  $\alpha$  value, while the long chain hydrocarbon products ( $n>8$ ) hold a higher  $\alpha$  value. Iglasia and his colleagues believe that: long-chain olefins can more easily re-adsorb and reinsert into carbon chains to increase the probability of carbon chain growth; the number of short-chain olefins adsorbed is relatively negligible [123, 149-151]. Therefore, the distribution of hydrocarbon products with a high carbon number is significantly positive deviation from that predicted by the ASF model.

### **(5) Hydroformylation**

In modern catalysis, the hydroformylation reaction, which is independent of FTS, is the reaction of syngas with olefins, but the earliest hydroformylation was found under FTS conditions [152]. In fact, FTS primary product  $\alpha$ -olefin is adsorbed on the surface of the catalyst as an initiator of carbon chain growth and reacts with the surface-adsorbed CO in accordance with the CO insertion mechanism, which is the hydroformylation reaction.

Therefore many oxygenated products, such as aldehydes and alcohols, are reported as being produced in many FTS reactions when co-feeding  $\alpha$ -olefins [126, 147].

As reported in the literature, the order of activity of transition metals for hydroformylation is  $Rh > Co > Ru > Fe > Ni$  [153]. It is not difficult to see that catalysts possessing hydroformylation activity generally have FTS activity, and cobalt is very active against both hydroformylation and Fischer-Tropsch Synthesis. With cobalt-based catalysts, the cobalt-based catalytic olefin hydroformylation activity is not high, because the activity of olefin hydrogenation is much higher than that of olefin hydroformylation [154]. Some researchers introduced activated carbon as a support into a heterogeneous cobalt-based catalytic hydroformylation reaction system and found that the hydroformylation activity is good [155]. This may be because activated carbon can limit hydrogen dissociation in the adsorbed state, and enhance the adsorption of CO, which results in surface dissociation of CO and hydrogenation [156-157].

In addition, the researchers reported that co-feeding olefin inhibited the formation of methane. As reported by Snel and Espinoza, the selectivity of methane was reduced by half, when 10% ethylene was co-fed into the reaction system [129]. They speculated that, in the presence of large amounts of ethylene, ethylene was rapidly adsorbed on the surface of the catalyst; it reacted with the adsorbed hydrogen and the methane precursor  $C_1$  species [129]. Similar results were obtained by other researchers [93-94, 114, 131-132, 158-159].

## **2.7. Ethylene chemistry in FTS**

Ethylene with two  $\alpha$ -carbon is the most common  $\alpha$ -olefin produced during FTS. Comparing with the ideal products distribution, the FTS  $C_2$  product obtained under actual operation condition is obviously lower than the ASF model in the actual FTS results. In addition, ethylene

has symmetry that other  $\alpha$ -olefins do not have. For these reasons, many ethylene co-fed FTS experiments have been conducted by scientists.

Starting in the 1940s, Russian scientist Eidus and his colleagues conducted a series of experiments on ethylene co-fed synthesis gas [87, 135-139, 160-161]. In some of the experiments, the CO content in the feed gas was very low (less than 0.4 vol.%), and they found that when no CO is present, ethylene hydrogenation is the dominant reaction [87]. When CO is introduced, the reaction (dimerization) of ethylene to form a long-chain product is promoted [160-161]. During the same period, Kokes conducted an experiment by feeding ethylene and hydrogen mixture into a reactor loaded unsupported cobalt catalyst at room temperature and found that about 8% of the dimerization product  $C_4$  was formed when ethylene was excessive [162]. Furthermore, they proposed that the precursor of the ethylene dimerization reaction was ethylidene.

Cant et al. [163] conducted a series of experiments by introducing trace CO into an ethylene hydrogenation system. Three different types of ethylene-based reactions were reported, i.e. ethylene hydrogenation, ethylene dimerization, and further surface reactions. More recently, Yang et al reported co-feeding ethylene promoted the chain growth probability and increased the olefin to paraffin ratio of  $C_{3+}$  products [164]. They concluded this phenomenon was attributed by H-scavenging effect of added ethylene.

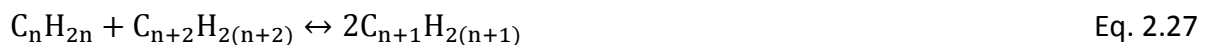
## **2.8. Potential equilibrium in FTS**

Thermodynamic equilibrium analysis is a very important research tool for reaction systems, and is widely used in various chemical engineering processes, including FTS. Some researchers have calculated that if there is a global thermodynamic equilibrium in FTS, then methane is

the only thermodynamically stable product [165]. As is well known, the products of the FTS reaction are diverse, and the global thermodynamic equilibrium does not exist in FTS. However, FT products could be the result of a system at partial equilibrium, in which some, but not all, species equilibrate, as reported by Masuku [165-166]. Their results show that the olefin product distribution is determined by equilibrium, and that paraffins are formed by secondary reactions that are kinetically determined [165-166].

Lu et al. conducted a series of FTS experiments on cobalt-based catalysts with different temperatures and different flow rates, in both a fixed bed and a continuously stirred tank reactor [120]. When they substituted the experimental data into a triangular chart commonly used for analytical distillation, they found that the olefin mole fraction ratio of adjacent carbon numbers was constant, when the carbon number is greater than 2 [120]. These results are shown in Figure 2.2. The researchers proposed that: the product distribution of  $\alpha$ -olefins may follow a thermodynamic equilibrium approach during FTS with carbon number  $n$  higher than 2; moreover, the equilibrium constant is not sensitive to the reaction temperature [120].

The olefins equilibrium can be explained using the following equation:



In addition, some researchers have obtained several stable points by introducing their experimental data (which is produced by switching between co-feeding and stop co-feeding inert gas into the reactor system, and the experiments were run continuously for more than 3,000 hours) into the olefin equilibrium model [167].

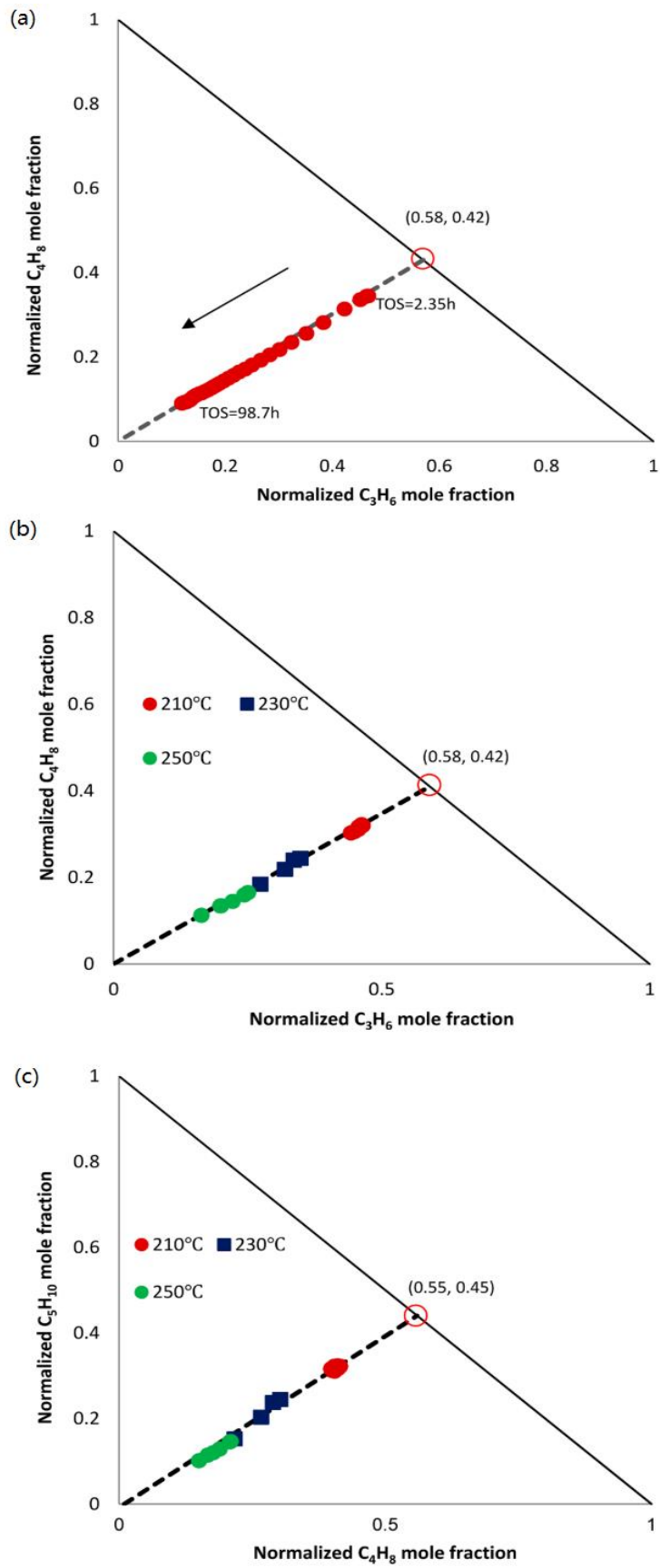
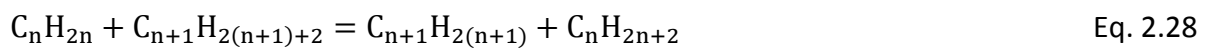


Figure 2. 2: Normalized mole fraction for On, Pn and On+1

Moreover, Yao et al. [168] showed that, based on experimental evidence, there is a linear relationship between the paraffin to olefin ratio with carbon number  $n+1$  and the paraffin to olefin ratio with carbon number  $n$  and this relationship holds for a large group of experiments with different kinds of catalysts, different types of reactors and a wide range of experimental conditions. The results are shown in Figure 2.3. Similar straight lines were also obtained by Muleja et al. [167].

Yao and co-workers developed two models based on vapour-liquid equilibrium and quasi-reaction equilibrium. The experimental results are quite close to the equilibrium calculations, and postulated that the product distribution might be determined by considering reaction equilibrium and vapour-liquid equilibrium. For example, in the model, based on quasi-reaction equilibrium, they assume that the following mass balance reaches quasi-equilibrium:



Similar straight lines were obtained when they substituted the experimental results into the quasi-reaction equilibrium model. This indicates that this potential balance is widespread in the FTS reaction system.

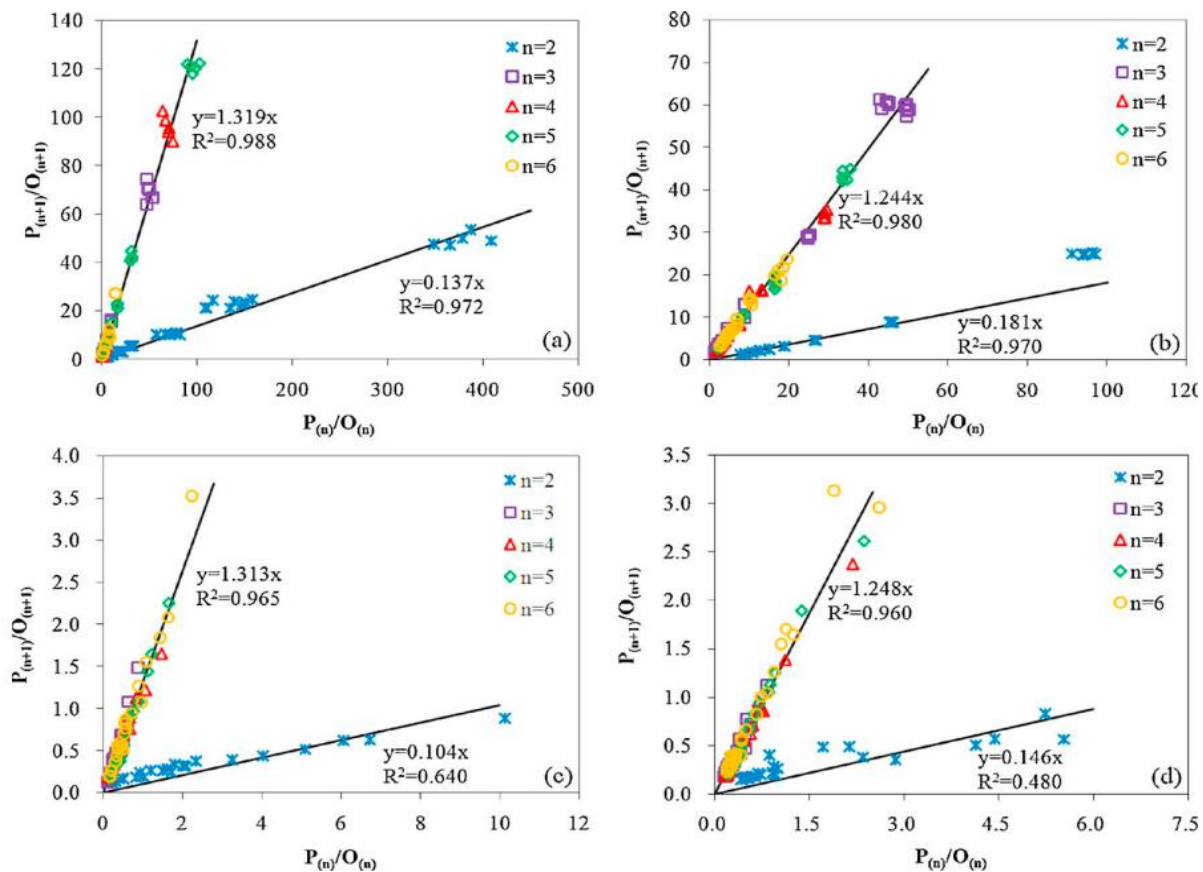


**Figure 2. 3:** The molar ratio of  $P_{(n+1)}/O_{(n+1)}$  as a function of the molar ratio of  $P_{(n)}/O_{(n)}$  for different FTS: (a) using a fixed bed reactor over a cobalt-based catalyst; (b) using a fixed bed reactor over an iron based catalyst; (c) using a spinning basket reactor over an iron based catalyst (data from literature) [167]; (d) using a slurry reactor over an iron based catalyst (data from literature) [167].

## REFERENCES:

1. Losanitsch, S. M., & Jovitschitsch, M. Z. (1897). Ueber chemische synthesen mittels der dunklen elektrischen entladung. *Berichte Der Deutschen Chemischen Gesellschaft*, 30(1), 135-139.
2. Sabatier, P., & Senderens, J. B. (1902). Direct hydrogenation of oxides of carbon in the presence of various finely divided metals. *CR Acad Sci*, 134, 689-691.
3. Hinrichsen, K. O., & Strunk, J. (2006). Basischemikalie methanol. *Nachrichten Aus Der Chemie*, 54(11), 1080-1084.
4. Fischer, F., & Tropsch, H. (1923). The preparation of synthetic oil mixtures (Synthol) from carbon monoxide and hydrogen. *Brennstoff-Chem*, 4, 276-285.
5. Anderson, R. B., Kölbl, H., & Ralek, M. (1984). *The Fischer-Tropsch Synthesis (Vol. 16)*. New York: Academic Press.
6. Dry, M. E. (1981). The Fischer-Tropsch Synthesis in Catalysis Sciences and Technology, Anderson, JR and Boudart, M.,(Eds.) 1.
7. Pichler, H. (1952). Twenty-five years of synthesis of gasoline by catalytic conversion of carbon monoxide and hydrogen. In *Advances in Catalysis* (Vol. 4, pp. 271-341). Academic Press.
8. Sasol. (2000). 50 Years of Innovation.
9. Dry, M. E., & Steynberg, A. P. (2004). Commercial FT process applications. In *Studies in Surface Science and Catalysis* (Vol. 152, pp. 406-481). Elsevier.
10. Stranges, A. N. (2007). A History of the Fischer-Tropsch Synthesis in Germany 1926-45. *Studies in Surface Science and Catalysis*, 1-27.
11. Leckel, D. (2009). Diesel production from Fischer-Tropsch: The past, the present, and new concepts. *Energy & Fuels*, 23(5), 2342-2358.

12. Dry, M. E. (2002). The Fischer–Tropsch Process: 1950–2000. *Catalysis Today*, 71(3-4), 227-241.
13. Van der Laan, G. P., & Beenackers, A. A. C. M. (1999). Kinetics and selectivity of the Fischer–Tropsch Synthesis: A literature review. *Catalysis Reviews*, 41(3-4), 255-318.
14. Anderson, R. B. (1956). Hydrocarbon synthesis, hydrogenation and cyclization. *Catalysis*, 4, 29-255.
15. Dry, M. E. (1982). Catalytic aspects of industrial Fischer-Tropsch Synthesis. *Journal of Molecular Catalysis*, 17(2-3), 133-144.
16. Chunlai, W. (2003). Sasol synfuels-indirect coal liquefaction technology in South Africa. *Coal Chemical Industry*, 2, 3-6.
17. Lu, X. (2012). Fischer-Tropsch Synthesis: Towards Understanding. (Doctoral Dissertation, University of the Witwatersrand).
18. Xiaodong, W., Yong, Y., Hongwei, X., Haijun, J., & Yongwang, L. (2017). The design principle of iron-based catalysts for Fischer-Tropsch Synthesis: From theory to practice. *Scientia Sinica Chimica*, 47(11), 1298-1311.
19. Xiang, H., Yang, Y., & Li, Y. (2014). Indirect coal-to-liquids technology from fundamental research to commercialization. *Scientia Sinica Chimica*, 44(12), 1876-1892.
20. Chronis, T. (1999). A Fischer-Tropsch study of Co. (Doctoral Dissertation, University of the Witwatersrand).
21. Cornaro, U., Rossini, S., Montanari, T., Finocchio, E., & Busca, G. (2012). K-doping of Co/Al<sub>2</sub>O<sub>3</sub> low temperature Fischer–Tropsch catalysts. *Catalysis today*, 197(1), 101-108.
22. Atwood, H. E., & Bennett, C. O. (1979). Kinetics of the Fischer-Tropsch reaction over iron. *Industrial & Engineering Chemistry Process Design and Development*, 18(1), 163-170.

23. Bub, G., Baerns, M., Büssemeier, B., & Frohning, C. (1980). Prediction of the performance of catalytic fixed bed reactors for Fischer-Tropsch Synthesis. *Chemical Engineering Science*, 35(1-2), 348-355.
24. Jess, A., Popp, R., & Hedden, K. (1999). Fischer–Tropsch Synthesis with nitrogen-rich syngas: Fundamentals and reactor design aspects. *Applied Catalysis A: General*, 186 (1-2), 321-342.
25. Wang, Y. N., Xu, Y. Y., Li, Y. W., Zhao, Y. L., & Zhang, B. J. (2003). Heterogeneous modeling for fixed-bed Fischer–Tropsch Synthesis: Reactor model and its applications. *Chemical Engineering Science*, 58(3-6), 867-875.
26. Guettel, R., & Turek, T. (2009). Comparison of different reactor types for low temperature Fischer–Tropsch Synthesis: A simulation study. *Chemical Engineering Science*, 64(5), 955-964.
27. Bartholomew, C. H. (1991). Recent developments in Fischer-Tropsch catalysis. In *Studies in Surface Science and Catalysis* (Vol. 64, Pp. 158-224). Elsevier.
28. Espinoza, R. L., Steynberg, A. P., Jager, B., & Vosloo, A. C. (1999). Low temperature Fischer–Tropsch Synthesis from a Sasol perspective. *Applied Catalysis A: General*, 186 (1-2), 13-26.
29. Keith, P. C. (1946). Gasoline from natural gas. *The Oil and Gas Journal*.
30. Mukenz, T. M. (2010). Graphical methods for the representation of the Fischer-Tropsch reaction: Towards understanding the mixed iron-cobalt catalyst systems (Doctoral Dissertation, University of the Witwatersrand).
31. Dry, M. E. (1983). The Sasol Fischer-Tropsch processes. *Applied Industrial Catalysis*, 2, 167-213.

32. Jager, B., Kelfkens, R. C., & Steynberg, A. P. (1994). A slurry bed reactor for low temperature Fischer-Tropsch. In *Studies in Surface Science and Catalysis* (Vol. 81, pp. 419-425). Elsevier.
33. Maretto, C., & Krishna, R. (1999). Modelling of a bubble column slurry reactor for Fischer-Tropsch Synthesis. *Catalysis Today*, 52(2-3), 279-289.
34. Saxena, S. C. (1995). Bubble column reactors and Fischer-Tropsch Synthesis. *Catalysis Reviews*, 37(2), 227-309.
35. Chunlai, W. (2003). Indirect coal liquefaction technology and its industrialized prospect in China. *Coal Conversion*, 2.
36. Biloen, P., & Sachtler, W. M. H. (1981). Mechanism of hydrocarbon synthesis over Fischer-Tropsch catalysts. In *Advances in Catalysis* (Vol. 30, Pp. 165-216). Academic Press.
37. Chai, G. Y., & Falconer, J. L. (1985). Alkali promoters on supported nickel: Effect of support, preparation, and alkali concentration. *Journal of Catalysis*, 93(1), 152-160.
38. Vannice, M. A. (1977). The catalytic synthesis of hydrocarbons from H<sub>2</sub>/CO mixtures over the group VIII metals. *J. Catal.*, 50, 228-236.
39. Vannice, M. A. (1975). The catalytic synthesis of hydrocarbons from H<sub>2</sub>CO mixtures over the group VIII metals: I. The specific activities and product distributions of supported metals. *Journal of Catalysis*, 37(3), 449-461.
40. Rao, V. U. S., Stiegel, G. J., Cinquegrane, G. J., & Srivastava, R. D. (1992). Iron-based catalysts for slurry-phase Fischer-Tropsch process: Technology review. *Fuel Processing Technology*, 30(1), 83-107.
41. Niemelä, M. K., Backman, L., Krause, A. O. I., & Vaara, T. (1997). The activity of the Co<sub>2</sub> catalyst in relation to pretreatment. *Applied Catalysis A: General*, 156(2), 319-334.

42. Simonetti, D. A., Rass-Hansen, J., Kunkes, E. L., Soares, R. R., & Dumesic, J. A. (2007). Coupling of glycerol processing with Fischer–Tropsch Synthesis for production of liquid fuels. *Green Chemistry*, 9(10), 1073-1083.
43. Okabe, K., Murata, K., Nakanishi, M., Ogi, T., Nurunnabi, M., & Liu, Y. (2009). Fischer–Tropsch Synthesis over Ru catalysts by using syngas derived from woody biomass. *Catalysis Letters*, 128(1-2), 171-176.
44. Murata, K., Okabe, K., Inaba, M., Takahara, I., & Liu, Y. (2009). Zr- and Li-Modified Ru/SiO<sub>2</sub> catalysts for Fischer–Tropsch Synthesis. *Catalysis Letters*, 128(3-4), 343-348.
45. Vannice, M. A., & Garten, R. L. (1980). Influence of the support on the catalytic behavior of ruthenium in CO/H<sub>2</sub>/Synthesis reactions. *J. Catal.*, (United States), 63(1).
46. Caesar, P. D., Brennan, J. A., Garwood, W. E., & Ciric, J. (1979). Advances in Fischer–Tropsch chemistry. *Journal of Catalysis*, 56(2), 274-278.
47. Dry, M. E., & Erasmus, H. D. W. (1987). Update of the Sasol synfuels process. *Annual Review of Energy*, 12(1), 1-46.
48. Janardana Rao, M. (1990). Direct catalytic conversion of synthesis gas to lower olefins. *Industrial & Engineering Chemistry Research*, 29(9), 1735-1753.
49. Schulz, H. (1999). Short history and present trends of Fischer–Tropsch Synthesis. *Applied Catalysis A: General*, 186(1-2), 3-12.
50. Qing, M., Yang, Y., Wu, B., Xu, J., Zhang, C., Gao, P., & Li, Y. (2011). Modification of Fe–SiO<sub>2</sub> interaction with zirconia for iron-based Fischer–Tropsch catalysts. *Journal of Catalysis*, 279(1), 111-122.
51. Wang, B., Yu, X., Huo, C., Wang, J., & Li, Y. (2014). Density Functional Theory study of the adsorption and reaction of C<sub>2</sub>H<sub>4</sub> on Fe<sub>3</sub>C (100). *Chinese Journal of Catalysis*, 35(1), 28-37.

52. Petersen, M. A., Cariem, M. J., Claeys, M., & Van Steen, E. (2015). A DFT perspective of potassium promotion of X-Fe<sub>5</sub>C<sub>2</sub> (1 0 0). *Applied Catalysis A: General*, 496, 64-72.
53. Ding, M., Yang, Y., Wu, B., Xu, J., Zhang, C., Xiang, H., & Li, Y. (2009). Study of phase transformation and catalytic performance on precipitated iron-based catalyst for Fischer–Tropsch synthesis. *Journal of Molecular Catalysis A: Chemical*, 303(1-2), 65-71.
54. Hou, W., Wu, B., Yang, Y., Hao, Q., Tian, L., Xiang, H., & Li, Y. (2008). Effect of SiO<sub>2</sub> content on iron-based catalysts for slurry Fischer–Tropsch synthesis. *Fuel Processing Technology*, 89(3), 284-291.
55. Wang, H., Yang, Y., Wu, B. S., Xu, J., Ding, M. Y., Wang, H. L. ... & Li, Y. W. (2009). Hydrogen reduction kinetics modeling of a precipitated iron Fischer–Tropsch catalyst. *Journal of Molecular Catalysis A: Chemical*, 308(1-2), 96-107.
56. Meng, Y., Liu, X. W., Huo, C. F., Guo, W. P., Cao, D. B., Peng, Q. ... & Jiao, H. (2016). When density functional approximations meet iron oxides. *Journal of Chemical Theory and Computation*, 12(10), 5132-5144.
57. Niu, L., Liu, X., Liu, X., Lv, Z., Zhang, C., Wen, X. ... & Xu, J. (2017). In situ XRD study on promotional effect of potassium on carburization of spray-dried precipitated Fe<sub>2</sub>O<sub>3</sub> catalysts. *Chemcatchem*, 9(9), 1691-1700.
58. Liu, X. W., Zhao, S., Meng, Y., Peng, Q., Dearden, A. K., Huo, C. F. ... & Wen, X. D. (2016). Mössbauer spectroscopy of iron carbides: From prediction to experimental confirmation. *Scientific Reports*, 6, 26184.
59. Zhao, S., Liu, X. W., Huo, C. F., Li, Y. W., Wang, J., & Jiao, H. (2015). Determining surface structure and stability Of E-Fe<sub>2</sub>C, X-Fe<sub>5</sub>C<sub>2</sub>, Θ-Fe<sub>3</sub>C and Fe<sub>4</sub>C phases under carburization environment from combined DFT and atomistic thermodynamic studies. *Catalysis, Structure & Reactivity*, 1(1), 44-60.

60. He, Y., Zhao, P., Guo, W., Yang, Y., Huo, C. F., Li, Y. W., & Wen, X. D. (2016). Hägg carbide surfaces induced Pt morphological changes: A theoretical insight. *Catalysis Science & Technology*, 6(17), 6726-6738.
61. Ngantsoue-Hoc, W., Zhang, Y., O'Brien, R. J., Luo, M., & Davis, B. H. (2002). Fischer–Tropsch Synthesis: Activity and selectivity for Group I alkali promoted iron-based catalysts. *Applied Catalysis A: General*, 236(1-2), 77-89.
62. Jin, E., Zhang, Y., He, L., Harris, H. G., Teng, B., & Fan, M. (2014). Indirect coal to liquid technologies. *Applied Catalysis A: General*, 476, 158-174.
63. Li, J. B., Ma, H. F., Zhang, H. T., Sun, Q. W., Ying, W. Y., & Fang, D. Y. (2014). Sodium promoter on iron-based catalyst for direct catalytic synthesis of light alkenes from syngas. *Fuel processing technology*, 125, 119-124.
64. Ribeiro, M. C., Jacobs, G., Davis, B. H., Cronauer, D. C., Kropf, A. J., & Marshall, C. L. (2010). Fischer–Tropsch synthesis: an in-situ TPR-EXAFS/XANES investigation of the influence of Group I alkali promoters on the local atomic and electronic structure of carburized iron/silica catalysts. *The Journal of Physical Chemistry C*, 114(17), 7895-7903.
65. Zhang, C., Yang, Y., Tao, Z., Li, T., Wan, H., Xiang, H., & Li, Y. (2006). Effects of Cu and K on Co-precipitated Fe<sub>m</sub>n/SiO<sub>2</sub> catalysts for Fischer-Tropsch Synthesis. *Acta Physico-Chimica Sinica*, 22(11), 1310-1316.
66. Anderson, R. B. (1984). *The Fischer-Tropsch Synthesis*. Academic Press. New York.
67. Pei, Y., Liu, J., Zhao, Y., Ding, Y., Liu, T., ... & Li, W. (2015). High Alcohols Synthesis via Fischer–Tropsch Reaction at Cobalt Metal/Carbide Interface. *Acs Catalysis*, 5(6), 3620-3624.
68. Bezemer, G. L., Bitter, J. H., Kuipers, H. P., Oosterbeek, H., Holewijn, J. E., Xu, X. ... & De Jong, K. P. (2006). Cobalt particle size effects in The Fischer–Tropsch reaction studied with

- carbon nanofiber supported catalysts. *Journal of The American Chemical Society*, 128(12), 3956-3964.
69. Borg, Ø., Dietzel, P. D., Spjelkavik, A. I., Tveten, E. Z., Walmsley, J. C., Diplas, S., ... & Rytter, E. (2008). Fischer–Tropsch synthesis: Cobalt particle size and support effects on intrinsic activity and product distribution. *Journal of Catalysis*, 259(2), 161-164.
70. Zhang, H., Wei, C. (2009). Effects of noble metal promoters on supported cobalt-based Fischer-Tropsch catalysts. *Progress in Chemistry*, 21(4), 622-628.
71. Zhao, Z., Lu, W., Zhu, H., Dong, W., Lyu, Y., Liu, T., ... & Ding, Y. (2018). Tuning the Fischer–Tropsch reaction over Co<sub>x</sub>Mn<sub>y</sub>La/AC catalysts toward alcohols: Effects of La promotion. *Journal of Catalysis*, 361, 156-167.
72. Zhang, R., Liu, H., Li, Q., Wang, B., Ling, L., & Li, D. (2018). Insight into the role of the promoters Pt, Ru and B in inhibiting the deactivation of Co catalysts in Fischer-Tropsch synthesis. *Applied Surface Science*, 453, 309-319.
73. Khalaf, A. L., Al-Zuhairi, F. K., Kadhim, W. A., & Ab Rahim, M. H. (2020). The Effects of Cerium Promoter on the Performance of Cobalt-Based Catalysts in Fischer Tropsch Synthesis for Liquid Fuel Production. *IJUM Engineering Journal*, 21(2), 1-11.
74. Reuel, R. C., & Bartholomew, C. H. (1984). Effects of Support and dispersion on the CO hydrogenation activity/ selectivity properties of cobalt. *Journal of Catalysis*, 85(1), 78-88.
75. Price, J. G. (1994). An investigation into novel bimetallic catalysts for use in the Fischer-Tropsch reaction. (Doctoral Dissertation, University of The Witwatersrand)
76. Jia, L. H., Jia, L. T., Li, D. B., Hou, B., Wang, J. G., & Sun, Y. H. (2010). Effect of silylation of SBA-15 supported cobalt catalysts on their performances in Fischer-Tropsch Synthesis. *Natural Gas Chemical Industry*, 4.

77. Bartholomew, C. H., & Guzzi, L. (1991). New trends in CO activation. *Stud. Surf. Sci. Catal.*, 64, 158.
78. Stoop, F., & Van der Wiele, K. (1986). Formation of Olefins from synthesis gas over silica-supported rufe bimetallic catalysts. *Applied Catalysis*, 23(1), 35-47.
79. Su, H. Q., Zhang, X. H., Ding, N., Du, Y., Ma, Y., Bai, F. H. ... & Yu, S. Y. (2009). Research progress of Fischer-Tropsch synthesis Catalysts. *Journal of Inner Mongolia University*, 4.
80. Dry, M. E. (2004). Chemical concepts used for engineering purposes. In *Studies in Surface Science and Catalysis*. 152, 196-257.
81. Dry, M., & Steynberg, A. (Eds.). (2004). Fischer-Tropsch technology. *Studies in Surface Science and Catalysis*. Elsevier Science & Technology.
82. Lee, W. H., & Bartholomew, C. H. (1989). Multiple reaction states in CO hydrogenation on alumina-supported cobalt catalysts. *Journal of Catalysis*, 120(1), 256-271.
83. Brady III, R. C., & Pettit, R. (1980). Reactions of diazomethane on transition-metal surfaces and their relationship to the mechanism of the Fischer-Tropsch reaction. *Journal of the American Chemical Society*, 102(19), 6181-6182.
84. Maitlis, P. M. (2004). Fischer-Tropsch, organometallics, and other friends. *Journal of organometallic chemistry*, 689(24), 4366-4374.
85. Ciobîcă, I. M., Kramer, G. J., Ge, Q., Neurock, M., & Van Santen, R. A. (2002). Mechanisms for chain growth in Fischer-Tropsch synthesis over Ru (0001). *Journal of Catalysis*, 212(2), 136-144.
86. Storch, H. H. (1951). The Fischer-Tropsch and related syntheses: Including a summary of theoretical and applied contact catalysis. Wiley.

87. Eidus, Y. T. (1967). The mechanism of the Fischer–Tropsch reaction and the initiated hydropolymerisation of alkenes, from radiochemical and kinetic data. *Russian Chemical Reviews*, 36(5), 338.
88. Ojeda, M., Nabar, R., Nilekar, A. U., Ishikawa, A., Mavrikakis, M., & Iglesia, E. (2010). CO activation pathways and the mechanism of Fischer–Tropsch synthesis. *Journal of Catalysis*, 272(2), 287-297.
89. Weststrate, C. J., Gericke, H. J., Verhoeven, M. W., Ciobica, I. M., Saib, A. M., & Niemantsverdriet, J. W. (2010). Ethanol decomposition on Co (0001): C–O bond scission on a close-packed cobalt surface. *The Journal of Physical Chemistry Letters*, 1(12), 1767-1770.
90. Pichler, V. H., & Schulz, H. (1970). Neuere Erkenntnisse Auf Dem Gebiet Der Synthese Von Kohlenwasserstoffen Aus CO Und H<sub>2</sub>. *Chemie Ingenieur Technik*, 42(18), 1162-1174.
91. Zhuo, M., Tan, K. F., Borgna, A., & Saeys, M. (2009). Density functional theory study of the CO insertion mechanism for Fischer–Tropsch synthesis over Co catalysts. *The Journal of Physical Chemistry C*, 113(19), 8357-8365.
92. Zhuo, M., Borgna, A., & Saeys, M. (2013). Effect of the CO coverage on the Fischer–Tropsch synthesis mechanism on cobalt catalysts. *Journal of catalysis*, 297, 217-226.
93. McNab, A. I., Mccue, A. J., Dionisi, D., & Anderson, J. A. (2017). Quantification and qualification by in-situ FTIR of species formed on supported-cobalt catalysts during the Fischer-Tropsch reaction. *Journal of Catalysis*, 353, 286-294.
94. McNab, A. I., Mccue, A. J., Dionisi, D., & Anderson, J. A. (2018). Combined quantitative FTIR and online GC study of Fischer-Tropsch synthesis involving co-fed ethylene. *Journal of Catalysis*, 362, 10-17.

95. Jiang, M., Koizumi, N., Ozaki, T., & Yamada, M. (2001). Adsorption properties of cobalt and cobalt-manganese catalysts studied by in situ diffuse reflectance FTIR using CO and CO+ H<sub>2</sub> as probes. *Applied Catalysis A: General*, 209(1-2), 59-70.
96. Jiang, M., Koizumi, N., & Yamada, M. (2000). Adsorption properties of Iron and Iron-manganese catalysts investigated by in-situ diffuse reflectance FTIR spectroscopy. *The Journal of Physical Chemistry B*, 104(32), 7636-7643.
97. McCue, A. J., Aponaviciute, J., Wells, R. P., & Anderson, J. A. (2013). Gold modified cobalt-based Fischer-Tropsch catalysts for conversion of synthesis gas to liquid fuels. *Frontiers of Chemical Science and Engineering*, 7(3), 262-269.
98. Couble, J., & Bianchi, D. (2013). Experimental microkinetic approach of the surface reconstruction of cobalt particles in relationship with the CO/H<sub>2</sub> reaction on a reduced 10% Co/Al<sub>2</sub>O<sub>3</sub> catalyst. *The Journal of Physical Chemistry C*, 117(28), 14544-14557.
99. Paredes-Nunez, A., Lorito, D., Guilhaume, N., Mirodatos, C., Schuurman, Y., & Meunier, F. C. (2015). Nature and reactivity of the surface species observed over a supported cobalt catalyst under CO/H<sub>2</sub> mixtures. *Catalysis Today*, 242, 178-183.
100. King, D. L. (1980). An in situ infrared study of CO hydrogenation over silica and alumina-supported ruthenium and silica-supported iron. *Journal of Catalysis*, 61(1), 77-86.
101. Schanke, D., Fredriksen, G. R., Blekkan, E. A., & Holmen, A. (1991). CO hydrogenation on SiO<sub>2</sub>-supported Fe and Ru catalysts studied by in situ IR spectroscopy. *Catalysis Today*, 9(1-2), 69-76.
102. Lorito, D., Paredes-Nunez, A., Mirodatos, C., Schuurman, Y., & Meunier, F. C. (2016). Determination of formate decomposition rates and relation to product formation during CO hydrogenation over supported cobalt. *Catalysis Today*, 259, 192-196.

103. Herington, E. F. G. (1946). Fischer-Tropsch Synthesis considered as a polymerization reaction. *Chem. Ind.* (London).
104. Friedel, R. A., & Anderson, R. B. (1950). Composition of synthetic liquid fuels. I. product distribution and analysis of C5—C8 paraffin isomers from cobalt catalyst 1. *Journal of The American Chemical Society*, 72(3), 1212-1215.
105. Flory, P. J. (1936). Molecular size distribution in linear condensation polymers1. *Journal of the American Chemical Society*, 58(10), 1877-1885.
106. Dry, M. E. (1990). The Fischer-Tropsch process-commercial aspects. *Catalysis Today*, 6(3), 183-206.
107. Ji, Y. Y., Xiang, H. W., Yang, J. L., Xu, Y. Y., Li, Y. W., & Zhong, B. (2001). Effect of reaction conditions on the product distribution during Fischer–Tropsch synthesis over an industrial Fe-Mn catalyst. *Applied Catalysis A: General*, 214(1), 77-86.
108. Dictor, R. A., & Bell, A. T. (1986). Fischer-Tropsch Synthesis over reduced and unreduced iron oxide catalysts. *Journal of Catalysis*, 97(1), 121-136.
109. Wojciechowski, B. W. (1988). The kinetics of the Fischer-Tropsch Synthesis. *Catalysis Reviews Science and Engineering*, 30(4), 629-702.
110. Chen, W., Pestman, R., Zijlstra, B., Filot, I. A., & Hensen, E. J. (2017). Mechanism of cobalt-catalyzed CO hydrogenation: 1. Methanation. *ACS Catalysis*, 7(12), 8050-8060.
111. Novak, S., Madon, R. J., & Suhl, H. (1981). Models of hydrocarbon product distributions in Fischer–Tropsch Synthesis. I. *The Journal of Chemical Physics*, 74(11), 6083-6091.
112. Schulz, H., Beck, K., & Erich, E. (1988). DM Bibby, CD Chang, RF Howe and S. Yurchak (Eds.), Methane Conversion 457. *Methane Conversion*, 36, 457.

113. Schulz, H., Van Steen, E., & Claeys, M. (1993). Olefin formation, hydrogenation and isomerization in the kinetic regime of Fischer-Tropsch Synthesis. Selective hydrogenation and dehydrogenation.
114. Jordan, D. S., & Bell, A. T. (1986). Influence of ethylene on the hydrogenation of carbon monoxide over ruthenium. *The Journal of Physical Chemistry*, 90(20), 4797-4805.
115. Huff Jr, G. A., & Satterfield, C. N. (1984). Intrinsic kinetics of the Fischer-Tropsch Synthesis on a reduced fused-magnetite catalyst. *Industrial & Engineering Chemistry Process Design and Development*, 23(4), 696-705.
116. Egiebor, N. O., Cooper, W. C., & Wojciechowski, B. W. (1985). Carbon number distribution of Fischer–Tropsch CO-hydrogenation products from precipitated iron catalysts. *The Canadian Journal of Chemical Engineering*, 63(5), 826-834.
117. Yates, I. C., & Satterfield, C. N. (1992). Hydrocarbon selectivity from cobalt Fischer-Tropsch catalysts. *Energy & Fuels*, 6(3), 308-314.
118. Iglesia, E., Vroman, H., Soled, S., Baumgartner, J., & Fiato, R. A. (1991). U.S. Patent No. 5,036,032. Washington, DC: U.S. Patent And Trademark Office.
119. James, O. O., Chowdhury, B., Mesubi, M. A., & Maity, S. (2012). Reflections on the chemistry of the Fischer–Tropsch Synthesis. *RSC Advances*, 2(19), 7347-7366.
120. Lu, X., Hildebrandt, D., Liu, X., & Glasser, D. (2012). A thermodynamic approach to olefin product distribution in Fischer–Tropsch Synthesis. *Industrial & Engineering Chemistry Research*, 51(51), 16544-16551.
121. Duyckaerts, N., Trotoş, I. T., Swertz, A. C., SchüTh, F., & Prieto, G. (2016). In situ hydrocracking of Fischer–Tropsch hydrocarbons: CO-prompted diverging reaction pathways for paraffin and A-olefin primary products. *ACS Catalysis*, 6(7), 4229-4238.

122. Steynberg, A. P. (2004). Introduction to Fischer-Tropsch technology. In *Studies in Surface Science and Catalysis* (Vol. 152, pp. 1-63). Elsevier.
123. Novak, S., Madon, R. J., & Suhl, H. (1982). Secondary effects in the Fischer-Tropsch Synthesis. *Journal of Catalysis*, 77(1), 141-151.
124. Iglesia, E., Reyes, S. C., & Madon, R. J. (1991). Transport-enhanced A-olefin readsorption pathways in Ru-catalyzed hydrocarbon synthesis. *Journal of Catalysis*, 129(1), 238-256.
125. Linghu, W., Liu, X., Li, X., & Fujimoto, K. (2006). Selective synthesis of higher linear A-olefins over cobalt Fischer-Tropsch catalyst. *Catalysis Letters*, 108(1-2), 11-13.
126. Schulz, H., & Claeys, M. (1999). Reactions of A-olefins of different chain length added during Fischer-Tropsch Synthesis on a cobalt catalyst in a slurry reactor. *Applied Catalysis A: General*, 186(1-2), 71-90.
127. Pichler, H., Schulz, H., & Elstner, M. (1967). Gesetzmässigkeiten Bei Der Synthese Von Kohlenwasserstoffen Aus Kohlenoxid Und Wasserstoff. *Brennstoff-Chemie*, 48(3), 78.
128. Kummer, J. T., & Emmett, P. H. (1953). Fischer-Tropsch Synthesis mechanism studies. The addition of radioactive alcohols to the synthesis gas. *Journal of the American Chemical Society*, 75(21), 5177-5183.
129. Snel, R., & Espinoza, R. L. (1987). Secondary reactions of primary products of the Fischer-Tropsch Synthesis: Part 1. The role of ethene. *Journal of Molecular Catalysis*, 43(2), 237-247.
130. Botes, F. G. (2007). Proposal of a new product characterization model for the iron-based low-temperature Fischer-Tropsch Synthesis. *Energy & Fuels*, 21(3), 1379-1389.

131. Boelee, J. H., Cüsters, J. M. G., & Van der Wiele, K. (1989). Influence of reaction conditions on the effect of co-feeding ethene in the Fischer-Tropsch Synthesis on a fused-iron catalyst in the liquid phase. *Applied Catalysis*, 53(1), 1-13.
132. Hanlon, R. T., & Satterfield, C. N. (1988). Reactions of selected 1-olefins and ethanol added during the Fischer-Tropsch Synthesis. *Energy & Fuels*, 2(2), 196-204.
133. Schulz, H., Ramananda, R., & Elstner, M. (1970). Carbon-14 studies for the evaluation of the reaction mechanism of the Fischer-Tropsch Synthesis. *Erdoel Kohle, Erdgas, Petrochem. Brennst.-Chem.*, 23(10).
134. Smith, D. F., Hawk, C. O., & Golden, P. L. (1930). The mechanism of the formation of higher hydrocarbons from water gas 1. *Journal of the American Chemical Society*, 52(8), 3221-3232.
135. Eidus, Y. T., Zelinskii, N. D., & Ershov, N. I. (1948). O kondensiruyushchem deistvii metilenovykh radikalov na etilen. *Doklady Akademii Nauk SSSR*, 60(4), 599-601.
136. Eidus, Y. T. (1950). ND 7. Elinskii, And KV Puzitskii. *Izvest. Akad. Nauk SSSR, Otdel. Khim, Nauk*, 98.
137. Eidus, Y. T., Zelinskii, N. D., Puzitskii, K. V., & Ershov, N. I. (1952). \* O kataliticheskoi gidrokondensatsii okisi ugleroda s olefinami. 7. Vliyanie kontsentratsii okisi ugleroda na protsess ee gidrokondensatsii s propilenom i n-butilenom. *Izvestiya Akademii Nauk Sssr-Seriya Khimicheskaya*, (1), 145-151.
138. Eidus, Y. T., & Ordyan, M. B. (1957). Methylation of cyclopentene by methylene radicals that form when carbon monoxide is reduced by contact with hydrogen. In *Doklady Akademii Nauk* (Vol. 116, No. 1, pp. 101-104). Russian Academy of Sciences.

139. Puzitskii, K. V. E., Eidus, Y. T., & Ryabova, K. G. (1961). Production of carboxylic acids and their esters by acid catalysis from carbon monoxide and alcohols. In *Doklady Akademii Nauk* (Vol. 141, No. 3, pp. 636-637). Russian Academy of Sciences.
140. Schulz, H., & Achtsnit, H. D. (1977). Olefin reactions during the Fischer-Tropsch Synthesis. *Revista Portuguesa De Quimica, Lisboa*, 19(1-4), 317-322.
141. Iglesia, E., Soled, S. L., Fiato, R. A., & Via, G. H. (1993). Bimetallic synergy in cobalt ruthenium Fischer-Tropsch Synthesis catalysts. *Journal of Catalysis*, 143(2), 345-368.
142. Chen, W., Filot, I. A., Pestman, R., & Hensen, E. J. (2017). Mechanism of cobalt-catalyzed CO hydrogenation: 2. Fischer-Tropsch Synthesis. *ACS Catalysis*, 7(12), 8061-8071.
143. Jordan, D. S., & Bell, A. T. (1987). The influence of propylene on CO hydrogenation over silica-supported ruthenium. *Journal of Catalysis*, 107(2), 338-350.
144. Jordan, D. S., & Bell, A. T. (1987). The influence of butene on CO hydrogenation over ruthenium. *Journal of Catalysis*, 108(1), 63-76.
145. Liu, X., Li, X., & Fujimoto, K. (2007). Effective control of carbon number distribution during Fischer-Tropsch Synthesis over supported cobalt catalyst. *Catalysis Communications*, 8(9), 1329-1335.
146. Schulz, H. (1977). Molecular formation in FT (Fischer-Tropsch) Synthesis reaction steps in molecular formation by catalytic reaction of carbon monoxide and hydrogen. *Erdöl, Kohle, Erdgas Petrochem*, 30, 123-31.
147. Liu, X., Li, X., Suehiro, Y., & Fujimoto, K. (2007). Elucidation of reaction network and effective control of carbon number distribution in the three phase Fischer-Tropsch Synthesis. *Applied Catalysis A: General*, 333(2), 211-218.

148. Zhang, R., Hao, X., & Li, Y. (2011). Investigation of acetylene addition to Fischer–Tropsch Synthesis. *Catalysis Communications*, 12(12), 1146-1148.
149. Madon, R. J., Reyes, S. C., & Iglesia, E. (1991). Primary and secondary reaction pathways in ruthenium-catalyzed hydrocarbon synthesis. *The Journal of Physical Chemistry*, 95(20), 7795-7804.
150. Madon, R. J., & Iglesia, E. (1993). The importance of olefin readsorption and H<sub>2</sub>/CO reactant ratio for hydrocarbon chain growth on ruthenium catalysts. *Journal of Catalysis*, 139(2), 576-590.
151. Iglesia, E., Reyes, S. C., Madon, R. J., & Soled, S. L. (1993). Selectivity control and catalyst design in the Fischer-Tropsch Synthesis: Sites, pellets, and reactors. In *Advances in Catalysis* (Vol. 39, pp. 221-302). Academic Press.
152. Falbe, J., & Bahrmann, H. (Eds.). (1980). *New syntheses with carbon monoxide* (Vol. 11). Springer.
153. Cornils, B., Herrmann, W. A., Beller, M., & Paciello, R. (Eds.). (2017). *Applied homogeneous catalysis with organometallic compounds: A comprehensive handbook in four volumes* (Vol. 4). John Wiley & Sons.
154. Arakawa, H., Takahashi, N., Hanaoka, T., Takeuchi, K., Matsuzaki, T., & Sugi, Y. (1988). Effect of Rh dispersion on vapor phase and pressurized hydroformylation of ethylene over Rh/SiO<sub>2</sub> catalyst. *Chemistry Letters*, 17(11), 1917-1918.
155. Zhang, Y., Shinoda, M., Shiki, Y., & Tsubaki, N. (2006). Hydroformylation of 1-hexene for oxygenate fuels via promoted cobalt/ active carbon catalysts at low-pressure. *Fuel*, 85(9), 1194-1200.
156. Omata, K., Fujimoto, K., Shikada, T., & Tominaga, H. (1988). Vapor-phase carbonylation of organic compounds over supported transition metal catalyst. 6. On the

- character of nickel/ active carbon as methanol carbonylation catalyst. *Industrial & Engineering Chemistry Research*, 27(12), 2211-2213.
157. Zhang, H., Qiu, J., Liang, C., Li, Z., Wang, X., Wang, Y. & Li, C. (2005). A novel approach to Co/Cnts catalyst via chemical vapor deposition of organometallic compounds. *Catalysis Letters*, 101(3-4), 211-214.
158. Zhang, Y., Zhang, H. B., Lin, G. D., Chen, P., Yuan, Y. Z., & Tsai, K. R. (1999). Preparation, characterization and catalytic hydroformylation properties of carbon nanotubes-supported Rh–phosphine catalyst. *Applied Catalysis A: General*, 187(2), 213-224.
159. Kibby, C. L., Pannell, R. B., & Kobylinski, T. P. (1984). Hydrogenation of olefins in the presence of carbon monoxide on supported cobalt catalysts. *Preprints-American Chemical Society. Division of Petroleum Chemistry*, 29(4), 1113-1119.
160. Ershov, N. I., Éidus, Y. T., & Erokhina, V. R. (1967). Heterogeneous-catalytic hydropolymerization of ethylene initiated by carbon monoxide at a temperature below 100 degrees C. *Doklady Akademii Nauk SSSR*, 177(6), 1345.
161. Ershov, N., Iem, K., & Eidus, Y. (1974). Hydropolymerization of ethylene initiated by carbon-monoxide in presence of Co-zeolite catalysts at temperatures below 100 degrees C. *Izvestiya Akademii Nauk Sssr-Seriya Khimicheskaya*, (4), 894-896.
162. Kokes, R. J. (1969). Formation of dimeric products during steady state hydrogenation of ethylene over cobalt. *Journal of Catalysis*, 14(1), 83-92.
163. Cant, N. W., Liu, I. O., & Scott, J. A. (2013). Ethylene oligomerisation over Co/SiO<sub>2</sub> in the presence of trace carbon monoxide: The Eidus reaction revisited. *Catalysis Today*, 215, 267-275.

164. Yang, J., Rodriguez, C. L., Qi, Y., Ma, H., Holmen, A., & Chen, D. (2020). The effect of Co-feeding ethene on Fischer Tropsch Synthesis to Olefins over Co-based catalysts. *Applied Catalysis A: General*, 117564.
165. Masuku, C. M., Hildebrandt, D., & Glasser, D. (2011). The role of vapour–liquid equilibrium in Fischer–Tropsch product distribution. *Chemical Engineering Science*, 66(23), 6254-6263.
166. Masuku, C. M., Ma, W., Hildebrandt, D., Glasser, D., & Davis, B. H. (2012). A vapor–liquid equilibrium thermodynamic model for a Fischer–Tropsch reactor. *Fluid Phase Equilibria*, 314, 38-45.
167. Muleja, A. A., Yao, Y., Glasser, D., & Hildebrandt, D. (2016). A study of Fischer-Tropsch Synthesis: Product distribution of the light hydrocarbons. *Applied Catalysis A: General*, 517, 217-226.
168. Yao, Y., Liu, X., Hildebrandt, D., & Glasser, D. (2012). Fischer–Tropsch Synthesis using H<sub>2</sub>/CO/CO<sub>2</sub> syngas mixtures: A comparison of paraffin to olefin ratios for iron and cobalt based catalysts. *Applied Catalysis A: General*, 433, 58-68.

## Chapter 3

### Experiment

#### 3.1. Introduction

To investigate the reactivity of co-fed ethylene under Fischer-Tropsch synthesis (FTS) conditions, many related experiments were conducted. These experiments were performed at various reaction temperatures over a typical FTS Co-based catalyst with wide range of inlet gases including: normal syngas ( $H_2/CO=2:1$ ); ethylene feedstock after FTS synthesis; ethylene plus nitrogen; ethylene plus hydrogen; different amounts of ethylene co-feed with syngas; different amount of CO co-feed ethylene hydrogenation system. The experimental results provided us with sufficient experimental data to evaluate the role of ethylene in FTS conditions and contribute to an in-depth understanding of FTS and other syngas reactions.

As mentioned in the literature review, the products of FTS are diverse with mainly linear paraffins and  $\alpha$ -olefins products [1-3]. However, by co-feeding ethylene into the reaction system the product spectrum comparatively becomes more complicated than the conventional FTS [4-8]. Laboratory-level reaction conditions are more demanding, because a small amount of catalyst is more critical to the reaction conditions, and any small changes can result in very different experimental results. Therefore, more attention needs to be paid to the experimental process, to avoid operational errors and reduce the impact of systematic errors in the experimental results.

Since our experiments were conducted in two different laboratories (one at the Nuclear Energy Company of South Africa (Necsa), the other at Synfuel China), the equipment used and the source of the reactive gases differ. Full details are provided later in this chapter.

In this chapter, we briefly describe the experimental process and experimental equipment. Additional experimental details are provided in the following chapters. Since chapters 4 to 7 are prepared as forthcoming papers or have been published in the peer reviewed journals, there is, inevitably, a certain degree of repetition in describing the experimental portion.

## 3.2. Materials and chemicals

### 3.2.1. Gases

All the gases used in the lab at Necsa were supplied by AFROX (Africa Oxygen) Ltd, while Beijing ZG Special Gases Science & Technology Co., Ltd supplied all the gases used in the lab at Synfuel China. The gas composition in each gas cylinder was indicated on the gas certificate hanging on the cylinder. All pure gases used were ultra-high purity (UHP) gases (purity > 99.99 percentage).

All experiments and the chromatography used the following gases:

- 1) The syngas used in normal FTS is a mixture of hydrogen, CO and nitrogen with the ratio of H<sub>2</sub>/CO/N<sub>2</sub> is 6:3:1.
- 2) The feed gas in the ethylene reaction is UHP ethylene, UHP N<sub>2</sub>, UHP H<sub>2</sub>, UHP CO, UHP Ar.
- 3) Calibration gas
  - Calibration gas used at Necsa had the following composition:  
H<sub>2</sub>/CO/CO<sub>2</sub>/N<sub>2</sub>/CH<sub>4</sub>/C<sub>2</sub>H<sub>4</sub>/C<sub>2</sub>H<sub>6</sub> = 51.24/29/5/10.6/3.3/0.2/0.46

➤ Calibration gas used at Synfuels China was as follows:

a) With the thermal conductivity detector (TCD):

$$\text{H}_2/\text{CO}/\text{Ar} = 48/48/4$$

$$\text{H}_2/\text{CO}/\text{Ar}/\text{N}_2 = 24/5.01/6.03/64.96$$

$$\text{CO}/\text{He} = 4.99/95.01$$

$$\text{H}_2/\text{CO}/\text{CO}_2/\text{N}_2/\text{CH}_4/\text{C}_2\text{H}_4 = 64.32/29.32/1.95/0.99/2.94/0.49$$

$$\text{H}_2/\text{CO}/\text{Ar} = 4/1.99/94.01$$

$$\text{H}_2/\text{He} = 10/90$$

b) With the flame ionization detector (FID):

$$\text{N}_2/\text{CH}_4/\text{C}_2\text{H}_4/\text{C}_2\text{H}_6/\text{C}_3\text{H}_6/\text{C}_3\text{H}_8/\text{C}_4\text{H}_8/\text{C}_4\text{H}_{10}/\text{C}_5\text{H}_{10}/\text{C}_5\text{H}_{12}/\text{C}_6\text{H}_{12}/\text{C}_6\text{H}_{14}$$

$$= 93.353/3.02/0.3/0.502/0.608/0.401/0.504/0.301/0.404/0.205/0.204/0.198$$

$$\text{N}_2/\text{CH}_4/\text{C}_2\text{H}_6/\text{C}_3\text{H}_8/\text{C}_4\text{H}_{10}/\text{C}_5\text{H}_{12} = 92.261/5.99/1/0.5/0.149/0.1$$

4) UHP N<sub>2</sub> was used as flushing gas at Necca, while UHP Ar was used at Synfuels China.

5) The carrier gases used by GC were:

a) Two kinds of carrier gases were used with the TCD at Necca: UHP He, UHP Ar

b) Two kinds of carrier gases used for TCD at Synfuels China: UHP He, UHP N<sub>2</sub>

c) The flame gas air, UHP H<sub>2</sub> and the carrier gas UHP Ar for the FID are used at Necca.

d) The flame gas air, UHP H<sub>2</sub> and the carrier gas UHP N<sub>2</sub> for the FID are used at Synfuels China.

### **3.2.2. Chemicals used in catalyst preparations**

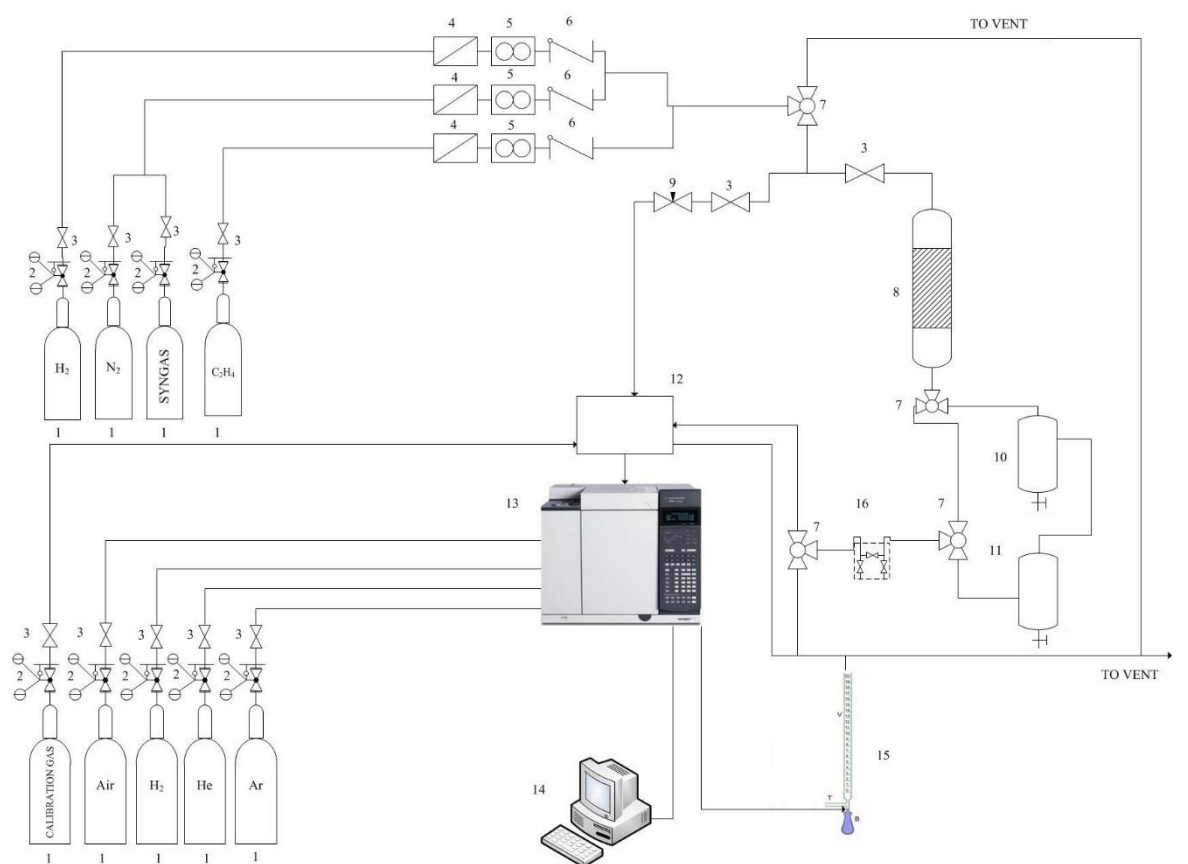
The cobalt source  $[\text{Co}(\text{NO}_3)_2 \cdot 6\text{H}_2\text{O}]$  was supplied by Sigma-Aldrich, and the precursor of support P25  $\text{TiO}_2$  was supplied by Degussa.

### **3.3. Experimental set-up and reactor**

#### **3.3.1 Experimental set-up**

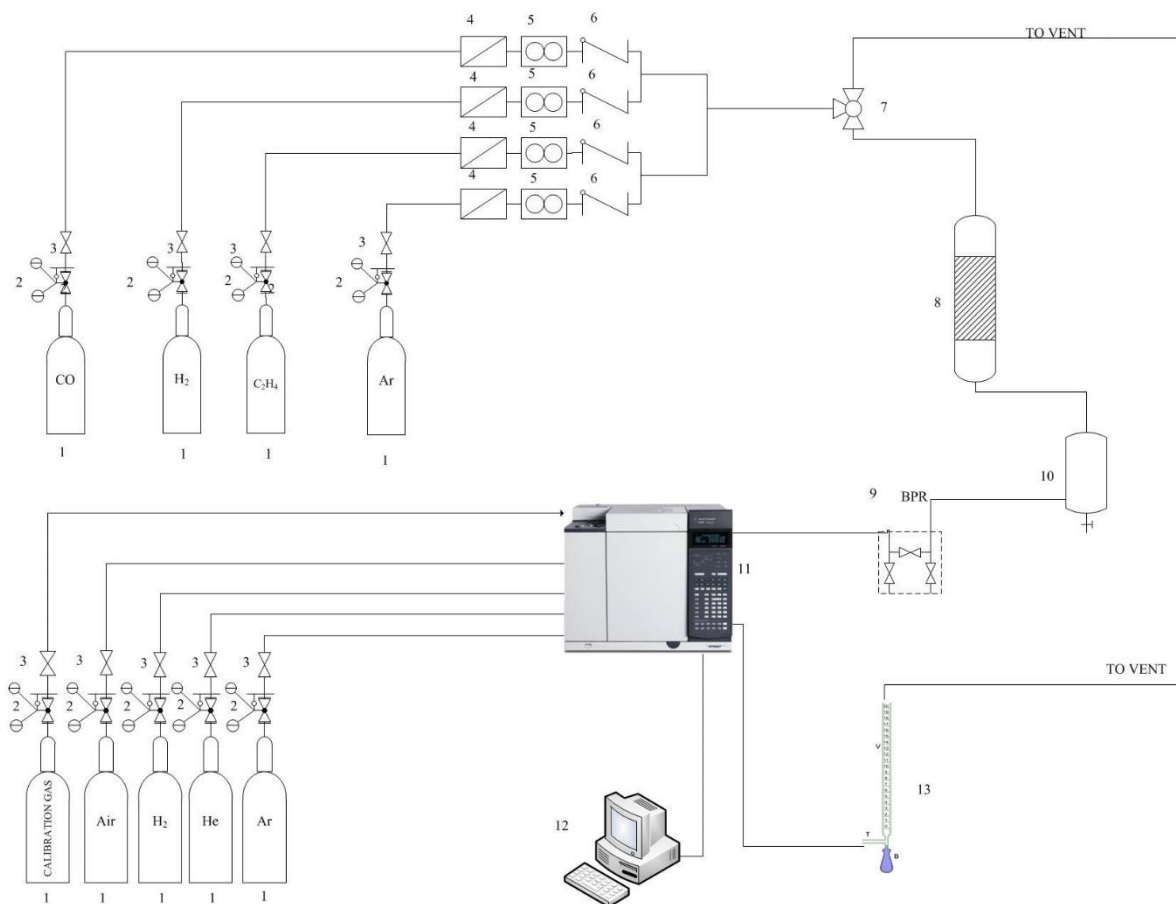
All experiments were carried out using a stainless-steel tubular fixed bed reactor (TFBR). The equipment used at Necsa and at Synfuels China were similar, except for the quantity of gas paths and product separators. Details of equipment used in this study are provided below.

Figure 3.1 and 3.2 show the equipment used at Necsa and Synfuels China, respectively. As can be seen, the difference between the two pieces of equipment is that the unit at Necsa has three inlets and two product separators, while the unit at Synfuels China has four inlets and one product separator. In addition, with the equipment at Necsa, there is a three-way valve at the outlet of the reactor, which can be switched to the bypass pathway that is connected directly to the back pressure valve without passing through the product separator.



**Figure 3. 1:** Schematic diagram of the experimental setup in the lab at Necsa.

1. Gas cylinder; 2. Pressure regulator; 3. Shut-off valves; 4. Filter; 5. Mass flow controller; 6. One-way valve; 7. Three-way valve; 8. Reactor; 9. Needle valve; 10. Hot trap; 11. Cold trap; 12. Multiple sampling valve; 13. Agilent GC 7890B; 14. Computer; 15. Bubble flow meter; 16. Back pressure regulator.



**Figure 3. 2:** Schematic diagram of the experimental setup in the lab at Synfuels China.

1. Gas cylinder; 2. Pressure regulator; 3. Shut-off valves; 4. Filter; 5. Mass flow controller; 6. One-way valve; 7. Three-way valve; 8. Reactor; 9. Back pressure regulator; 10. Liquid products separator; 11. Agilent GC 7890A; 12. Computer; 13. Bubble flow meter.

Mass flow controllers (Brooks) were used to control the flow rate of the gases. All the reaction gas and diluent gases were pre-mixed before they were introduced into the reactor. The gas compositions designed for the experiments were controlled by adjusting the flow rates of the gases required. In case, a filter was in place between the gas cylinder and the mass flow controller to filter the very small amount of solid impurities that may be present in the cylinder. A check valve was connected after the mass flow controller to prevent backflow. The gases used in the experiments are detailed in section 3.2.1.

1 g of 15% Co/TiO<sub>2</sub> catalyst was packed in the constant temperature zone of the reactor, and the other idle positions in the reactor were filled with ceramic balls. The catalyst and ceramic balls were separated using glass wool, as the ceramic balls on the upper part of the catalyst can also play a role in pre-heating the feed gas.

- In the lab at Necsa, see Figure 3.1

The reaction tail-gas, including the gas phase products, unreacted reactant gases and the diluent gas, passed through the bottom of the reactor to the three-way valve. This three-way valve switched the tailgas freely either to pass two product condensers (hot trap and cold trap, see Figure 3.1) or to pass a bypass, thereafter these two gas paths joined another three-way valve and then pass through the back-pressure valve. The former condenser is a hot trap that was heated to 200 °C; the latter condenser is a cold trap that was kept at room temperature.

- In the lab at Synfuels China, see Figure 3.2
- The exhaust gas passed through a product condenser to the back-pressure valve. The condenser in this equipment was heated to 120 °C to collect the long-chain hydrocarbons.

All steel pipes, fittings and valves between the reactor and the gas chromatograph were heated to 200 °C, to prevent the condensation of the high boiling products for both labs. After the back pressure regulators, tail gases were introduced into the sampling loops of online GCs (Agilent 7890B at Necsa; Agilent 7890A at Synfuels China). After GC analysis, the tailgas is introduced into a bubble flow meter, to measure the flow rate of the tailgas. Finally, the gas passes through the vent line to the vent.

### **3.3.2 Reactor**

In the experiment, both TFBRs were used at relatively low temperatures (less than 250°C), in alignment with low temperature FTS. The gas stream was blown from the top of the fixed bed reactor to the bottom, which approximated as a plug flow. Figure 3.3 shows the reactor used at Necsa (Figure 3.3(a)) and the one used at Synfuels China (Figure 3.3(b)).

Both the stainless TFBR at Necsa (with a length of 203.8 mm and an ID of 8 mm) and the one at Synfuels China (with the length of 230 mm and an ID of 8 mm) were heated by a long heating zone to make sure there were constant temperature zones for FTS reaction. The difference was that a heating jacket fitted with a thermocouple heated the reactor at Necsa, while the reactor at Synfuels China was heated by an external heating furnace, with a separate thermocouple contacting the outer wall of the reactor, which cooperated to control the heating temperature. The catalyst was loaded in a constant temperature zone of each reactor. As mentioned in section 3.3.1, the ceramic pellets were used to fill up the gaps in each of the reactor with two main functions: one was to pre-heat the feed gas; the other was to support and hold the catalyst. Quartz cotton was placed on the upper and lower portions of the catalyst to separate the ceramic pellets and the catalyst.



**Figure 3. 3:** Photo of the TFBR used in the current experimental study. (a) is used at Necsa; (b) is used at Synfuels China.

### 3.4. Preparation and characteristics of Cobalt-based catalysts

#### 3.4.1. Preparation of the catalyst

In this project, 15% Co supported on TiO<sub>2</sub> was used as the catalyst: Co(NO<sub>3</sub>)<sub>2</sub>·6H<sub>2</sub>O was used as the cobalt source; P25 TiO<sub>2</sub> was used as the precursor of the support. The catalyst was prepared using the incipient wetness method [8-10]:

(1) Pre-treatment of TiO<sub>2</sub> was as follows:

- a. Mixing TiO<sub>2</sub> and distilled water at a mass ratio of 1:1 to form a paste.
- b. The paste was dried in a constant temperature vacuum oven at 120 °C for 2 hours.
- c. The dried TiO<sub>2</sub> was sent to a muffle furnace for calcining. The calcination temperature was raised from room temperature to 400 °C at a rate of 5° C/min, and then maintained for 6 hours.
- d. The calcined support was crushed and sieved to particles size of 0.5 to 1 mm.

(2) The support bulk porosity volume test was done as follows:

1 g of the supporter was selected, and distilled water was gradually dropped onto the supporter until the surface moist.

(3) The steps followed in preparing the catalysts were as follows:

- a. Dissolve designed amount of [Co(NO<sub>3</sub>)<sub>2</sub>·6H<sub>2</sub>O] (Sigma-Aldrich) into the calculated amount of distilled water. The volume of the water was calculated based on the support pore volume.
- b. Mix the support and the cobalt solution thoroughly.
- c. Dry in a vacuum oven at 120C for 2 hours.
- d. Calcination in a muffle furnace. The calcination conditions were consistent with step C of the support pre-treatment steps. (The calcination temperature was

raised from room temperature to 400 °C at a rate of 5° C/min, and then maintained for 6 hours.)

### **3.4.2. Characteristics of the catalysts**

Characterization is the best way to understand the physical and chemical properties of a catalyst. Through analysis of the characterization results, we can explain the performance of the catalyst in the reaction to some extent and provide effective information regarding improving and upgrading of the catalyst. The characterization of the catalyst was conducted by following methods.

#### **X-ray diffraction (XRD)**

X-ray diffraction (XRD) analysis was performed using a Rigaku D/max-2500 diffractometer, with Cu K $\alpha$  radiation at 40 kV and 100 mA, in a scanning range of 3-80° (2 $\theta$ ). The diffraction peaks of the crystalline phase were compared with those of standard compounds reported in the JCPDS Date File. Figure 3.4 shows the XRD results of the catalysts before and after reduction. Average crystallite sizes of Co<sub>3</sub>O<sub>4</sub> in the sample before reduction is around 18.9 nm, which was evaluated from X-ray line broadening analysis (XLBA) by the Scherrer equation. Although the peaks of metallic Co in the sample after reduction is difficult to identify from noise, it can be estimated as 14.2 nm by correcting using a contraction of 0.75.

## **H<sub>2</sub>-Temperature programmed reduction (TPR) and Temperature programmed desorption (TPD)**

The reducibility of the catalysts was measured by hydrogen temperature programmed reduction (H<sub>2</sub>-TPR). Two experiments were conducted for the measurement. (1) Experiment one, with 50mg of catalyst loaded into the quartz reactor. 5% H<sub>2</sub>/N<sub>2</sub> reducing mixture was flowed into the reactor at a flowrate of 30 (NPT) mL/min, and the temperature of the reactor was programmed from room temperature to 700 °C at a heating rate of 10 °C /min. (2) Experiment two followed the same experimental procedure as experiment one; the difference was that the reaction temperature was increased from room temperature to 350 °C at a rate of 10 °C /min and then maintained at 350 °C for 50 minutes. The H<sub>2</sub> concentration during the reduction was measured using a thermal conductivity detector (TCD). Figure 3.5 shows the TPR results based on different testing condition.

In H<sub>2</sub>-TPD experiment, 20 mg calcined catalysts were first reduced with flowing hydrogen (5 ml H<sub>2</sub>/ g-cat-s) for 16 hours at 350 °C, and then evacuated to less than 10 μmm Hg to remove all chemisorbed hydrogen. The catalysts were then cooled to 100 °C and isotherms measured at nine to eleven hydrogen pressures between 100 and 800 mm Hg. Adsorption isotherms were extrapolated to zero pressure to obtain chemisorption uptake. The equation given below was used to calculate the dispersion values:

$$D\% = [(V_m/V_{mol})/(W\%/W_a)] \times F_s$$

Where V<sub>m</sub> is the total volume of hydrogen chemisorbed, V<sub>mol</sub> the hydrogen molar volume, W% the percent of cobalt by weight, W<sub>a</sub> is the cobalt atomic weight, and F<sub>s</sub> is the stoichiometry factor (F<sub>s</sub> = 2 for H<sub>2</sub>).

### **Nitrogen adsorption–desorption experiment**

The nitrogen adsorption–desorption experiment was measured on a Quantachrome Autosorb-1MP sorption analyzer at  $-196^{\circ}\text{C}$ . Before measurement, samples were degassed at  $200^{\circ}\text{C}$  for at least 6 h. The specific surface area (SBET) was calculated as per the Brunauer–Emmett–Teller (BET) method ( $P/P_0 < 0.1$ ). The physical characteristics of the catalysts are listed in Table 3.1.

### **Transmission electron microscope (TEM)**

TEM images were performed using a Keol JEM 2100F at 200kV. Figure 3.6 is an image of 15%Co/TiO<sub>2</sub> before the reduction.

**Table 3.1:** Properties of the catalysts (15% Co/TiO<sub>2</sub>) used in this work.

<b>CATALYST</b>	<b>15% CO/TIO<sub>2</sub></b>
<b>PARTICLE SIZE (MM)</b>	0.5-1
<b>SURFACE AREA (M<sup>2</sup>/G)</b>	42.92
<b>PORE VOLUME (CM<sup>3</sup>/G)</b>	0.24
<b>AVERAGE PORE DIAMETER (NM)</b>	16.7
<b>DISPERSION (%)</b>	1.66

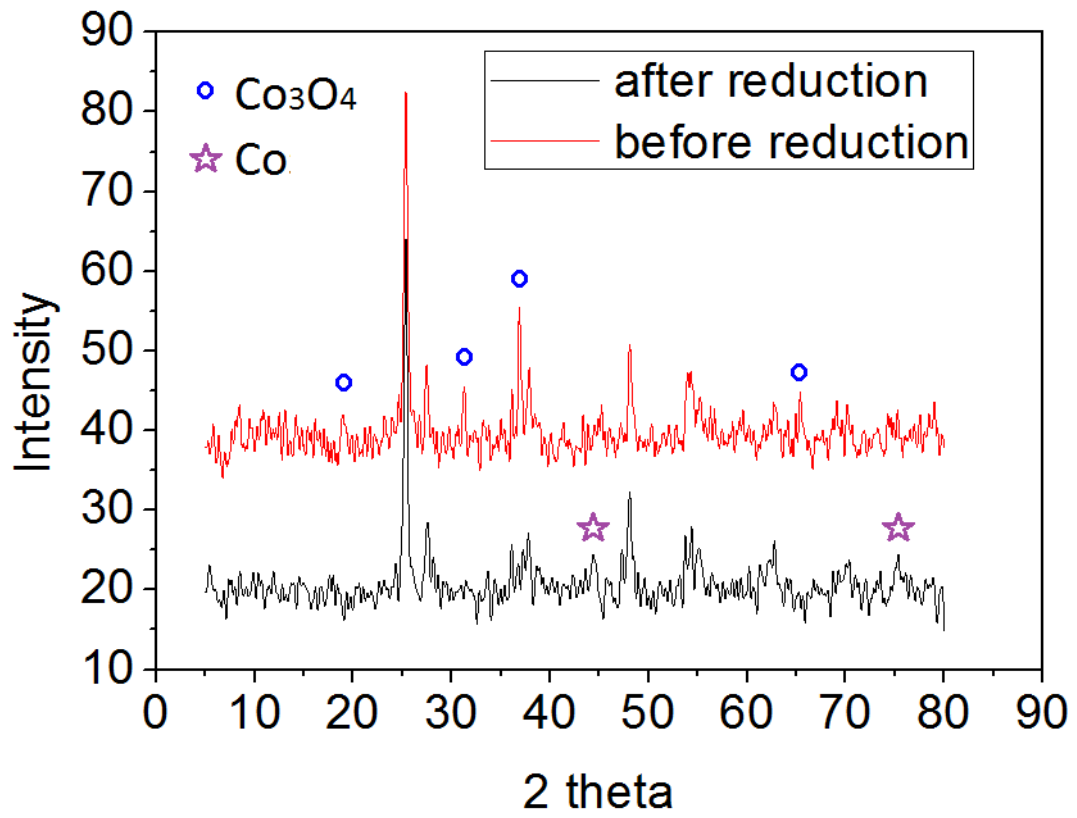
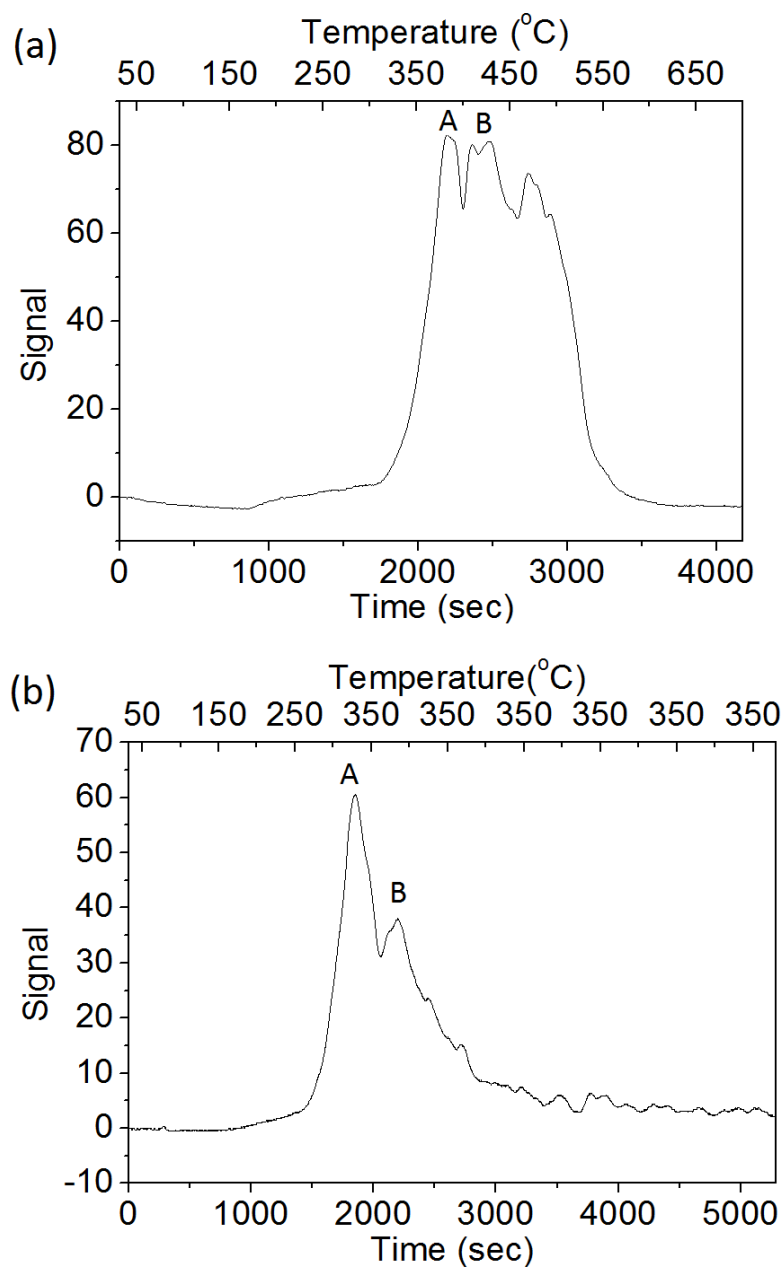
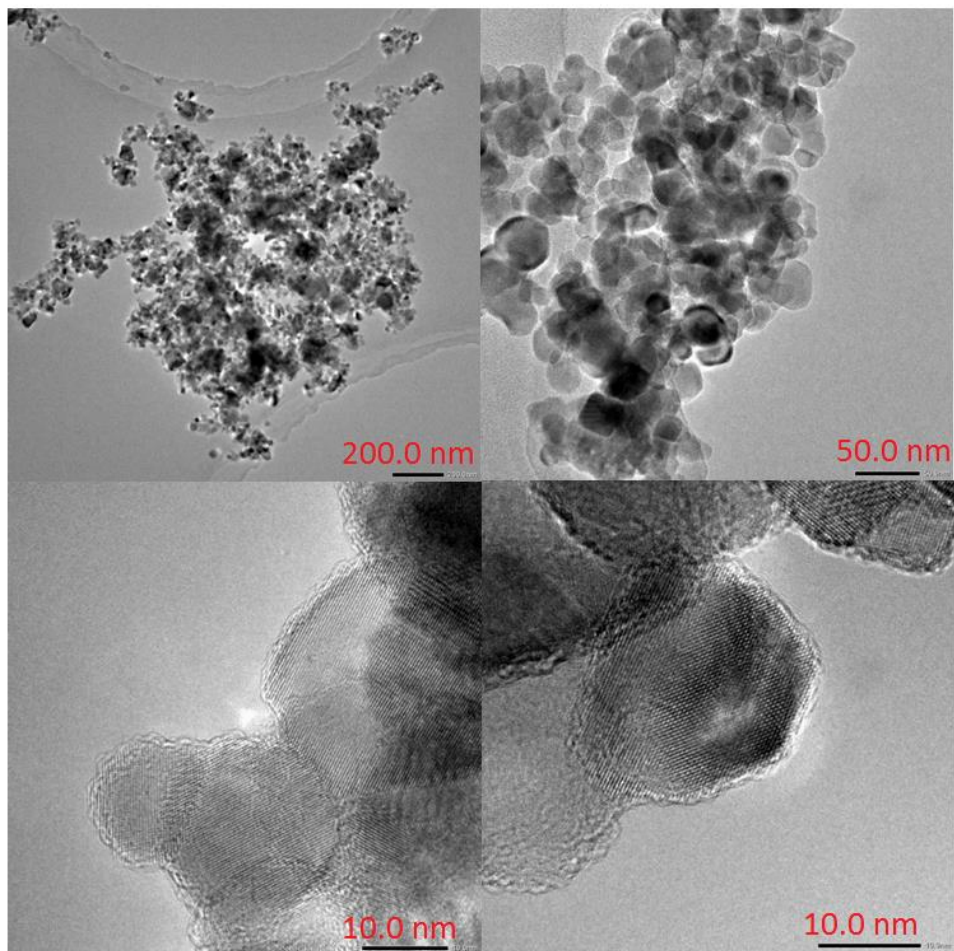


Figure 3. 4: XRD patterns for 15%Co/TiO<sub>2</sub> before and after reduction



**Figure 3. 5:** TPR results of 15%Co/TiO<sub>2</sub>. (a) H<sub>2</sub>-TPR profiles with the reduction temperature rising from room temperature to 700 °C at a rate of 10 °C /min). (b) H<sub>2</sub>-TPR profiles with the reduction temperature increasing from room temperature to 350 °C (10 °C /min) and then being maintained at 350 °C for 1 hour.



**Figure 3. 6:** TEM images of 15%Co/TiO<sub>2</sub> before reduction.

### **3.5. Product analysis**

As discussed earlier, organic products formed from FTS are diverse, coupled with inorganic by-product water and carbon dioxide, as well as unreacted reaction gases, H<sub>2</sub> and CO, which are highly demanding for product analysis. When ethylene is introduced into the reaction system, the product distribution becomes more complicated, which requires the analysis system to more effectively separate various products and accurately quantify them.

On-line analysis of tailgas was done using Agilent Chromatography 7890B with two TCD detectors and one FID detector (at Necsa), as well as a TCD detector and two FID detectors Agilent Chromatography 7890A (at Synfuels China). TCD detectors are used to characterize and quantify inorganic products, while FID detectors are used to analyse a variety of organic products, including alkanes, alkenes and oxygenated organics.

#### **3.5.1. Online GC in Necsa**

The reacted off-gas was sent to the sampling loop through a stainless-steel tube that was heated to 200 °C. The 200 °C gas enters the chromatographic analysis system through two six-way valves and two ten-way valves and the temperature of all detectors were maintained at 250 °C. The flow chart of the gas in the chromatograph is shown in Figure 3.7. It is worth noting that in this figure 3.7, all six-way valves and ten-way valves are in the off state. The analysis time of the entire tailgas was 25 minutes. Details of all the columns, carrier gases and testing procedures are provided in Table 3.2.

In this chromatogram, one TCD detector is dedicated to detecting hydrogen and the other is used to detect other inorganic gases, such as CO, CO<sub>2</sub>, N<sub>2</sub>, water and methane. The FID detector is capable of separating and quantifying hydrocarbon products with carbon numbers

1 to 13 under the conditions used in this study. The peak order of all the detectors is listed in Table 3.3.

Figure 3.8. shows a chromatogram of typical ethylene and hydrogen reactions.

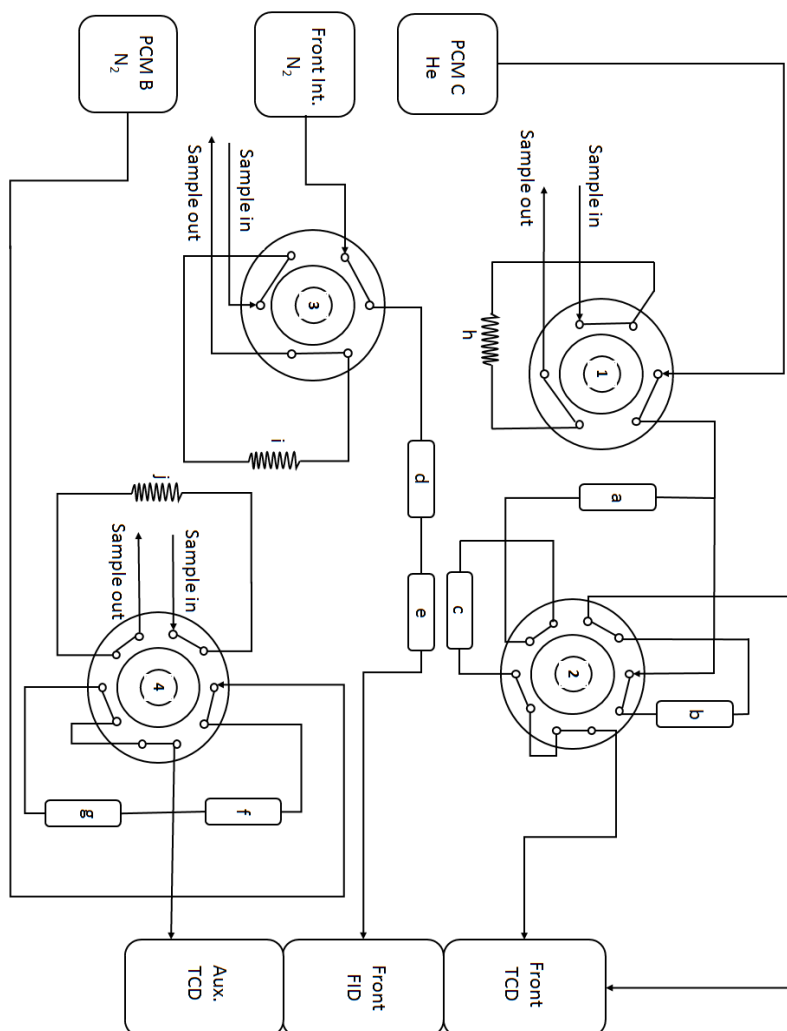


**Figure 3. 7:** The sampling flow scheme of the online GC Agilent 7890B at Necsca. In this figure: a is the delay part; b and f are the Molsieve 13X column; c is the Heyasep Q column; d is split part; e is the LTM system with a CP-Sil 5 CB column; g is a Plot Q column; h, i, and j are sampling loops.

**Table 3.2:** Operational information of the Agilent 7890B used in this experimental study

<i>Agilent 7890B</i>	
<i>Detector</i>	<b>Front TCD, T=250 °C</b>
<i>Column 1</i>	RESTEK, Molesieve 13X, 80/100 mush, 1.00mm * 2.00m * 1/16", max temperature: 350°C
<i>Column 2</i>	RESTEK, Hayesep Q, 100/120 mush, 0.75mm * 1m * 0.95mm, max temperature 275°C
<i>Six-way valve</i>	200°C
<i>Ten-way valve</i>	200°C
<i>Carrier gas</i>	UHP He with the flow rate of 30 ml(NTP)/min
<i>Oven temperature program</i>	Hold at 50 °C for 5 min, heat to 80 °C at 10 °C /min, hold at 80 °C for 17 min
<i>Products analysing</i>	N <sub>2</sub> , CO, CO <sub>2</sub> , H <sub>2</sub> O and methane
<i>Detector</i>	<b>AUX TCD, T=250°C</b>
<i>Column 3</i>	RESTEK, Molesieve 13X, 80/100 mush, 1.00mm * 2.00m * 1/16", max temperature: 350°C
<i>Column 4</i>	RESTEK, Hayesep Q, 100/120 mush, 0.75mm * 1m * 0.95mm, max temperature 275 °C
<i>Ten-way valve</i>	200 °C
<i>Carrier gas</i>	UHP N <sub>2</sub> with the flow rate of 30 ml(NTP)/min
<i>Temperature program</i>	Hold at 50 °C for 5 min, heat to 80 °C at 10 °C /min, hold at 80 °C for 17 min
<i>Products analysing</i>	H <sub>2</sub>
<i>Detector</i>	<b>Front FID, T=250 °C</b>
<i>Column 5</i>	CP-Sil 5 CB, 25m * 150µm * 2µm, max temperature: 350 °C
<i>Six-way valve</i>	200 °C
<i>Carrier gas</i>	UHP N <sub>2</sub> with the flow rate of 30 ml(NTP)/min
<i>Temperature program</i>	Hold at 50 °C for 5 min, heat to 200 °C at 25 °C /min, hold at 200 °C for 12.2 min
<i>Products analysing</i>	C <sub>1</sub> to C <sub>13</sub>

**Table 3.3:** Order of peaks in different detectors on Agilent 7890B

Peak number	Front TCD	AUX TCD	Front FID
1	N <sub>2</sub>	H <sub>2</sub>	C <sub>1</sub>
2	CH <sub>4</sub>		O <sub>2</sub>
3	CO		P <sub>2</sub>
4	CO <sub>2</sub>		O <sub>3</sub>
5	H <sub>2</sub> O		P <sub>3</sub>
6			O <sub>4</sub>
7			P <sub>4</sub>
8			Trans-2-O <sub>4</sub>
9			Cis-2-O <sub>4</sub>
10			O <sub>5</sub>
11			P <sub>5</sub>
12			O <sub>6</sub>
13			P <sub>6</sub>

In this table, C<sub>1</sub> is methane, O<sub>n</sub> and P<sub>n</sub> are  $\alpha$ -olefin and n-paraffin with carbon number n, respectively. Trans- and Cis-2-O<sub>4</sub> are Trans- and Cis-2-butene.

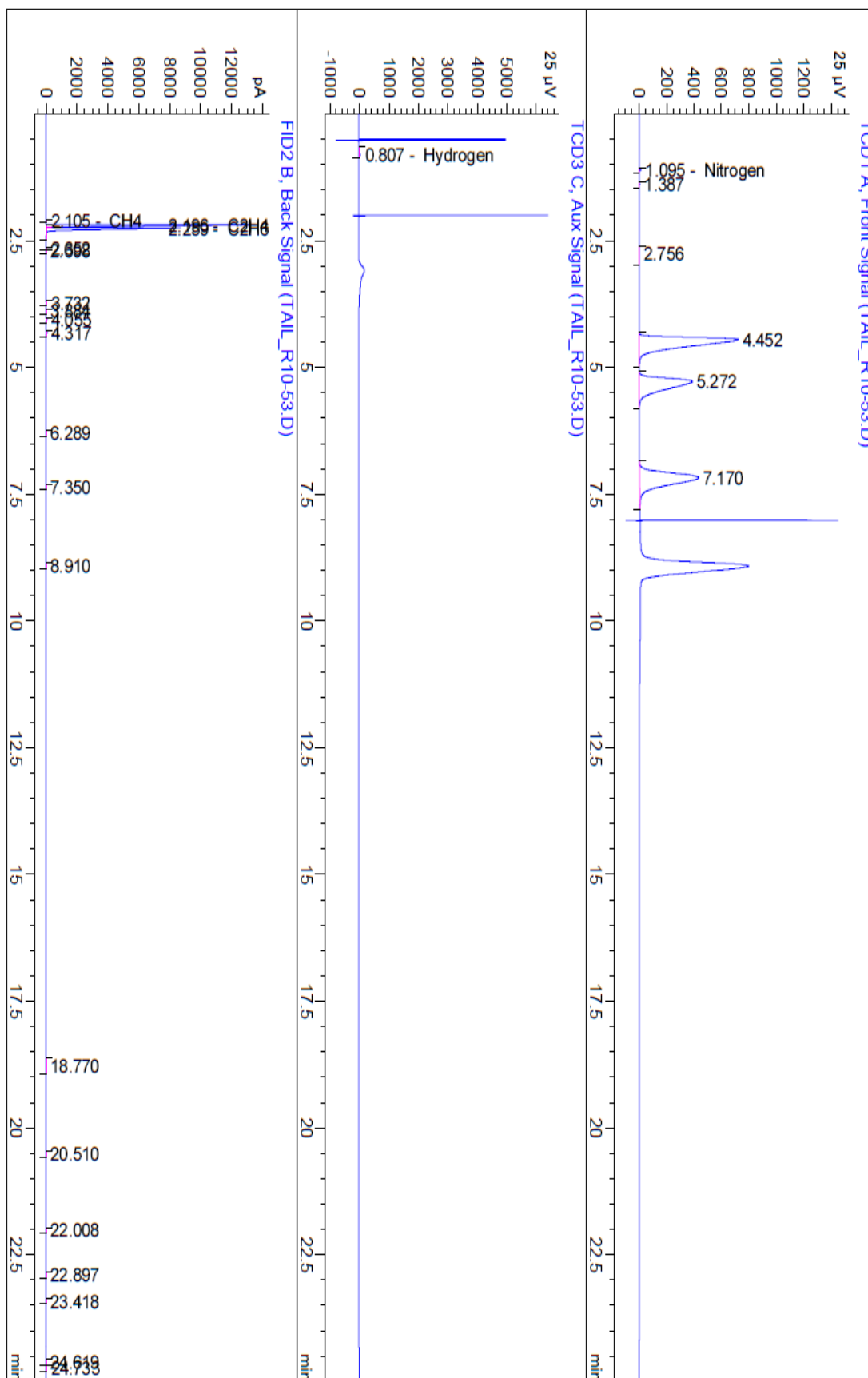


**Figure 3.8:** Chromatogram of the reaction of ethylene and hydrogen in Neca

### **3.5.2. Online GC at Synfuels China**

The operating parameters of this GC are different from the 7890B used in Necsca mentioned previously. Because of the two FID detectors and the one TCD detector in this GC, the flow path of the gas in the chromatogram is not the same as the GC Agilent 7890B. The flow chart for the gas in the chromatograph is shown in Figure 3.9. In this figure, all the multi-port valves are in the off state.

The analysis time of the tailgas on this gas chromatograph was 100 minutes. The TCD detector is used to detect inorganic gases and methane, while the two FID detectors detect C<sub>1</sub>-C<sub>4</sub> and all the organic products. Detailed information on columns, carrier gas and procedures are listed in Table 3.4. The peak order of each detector is shown in Table 3.5.

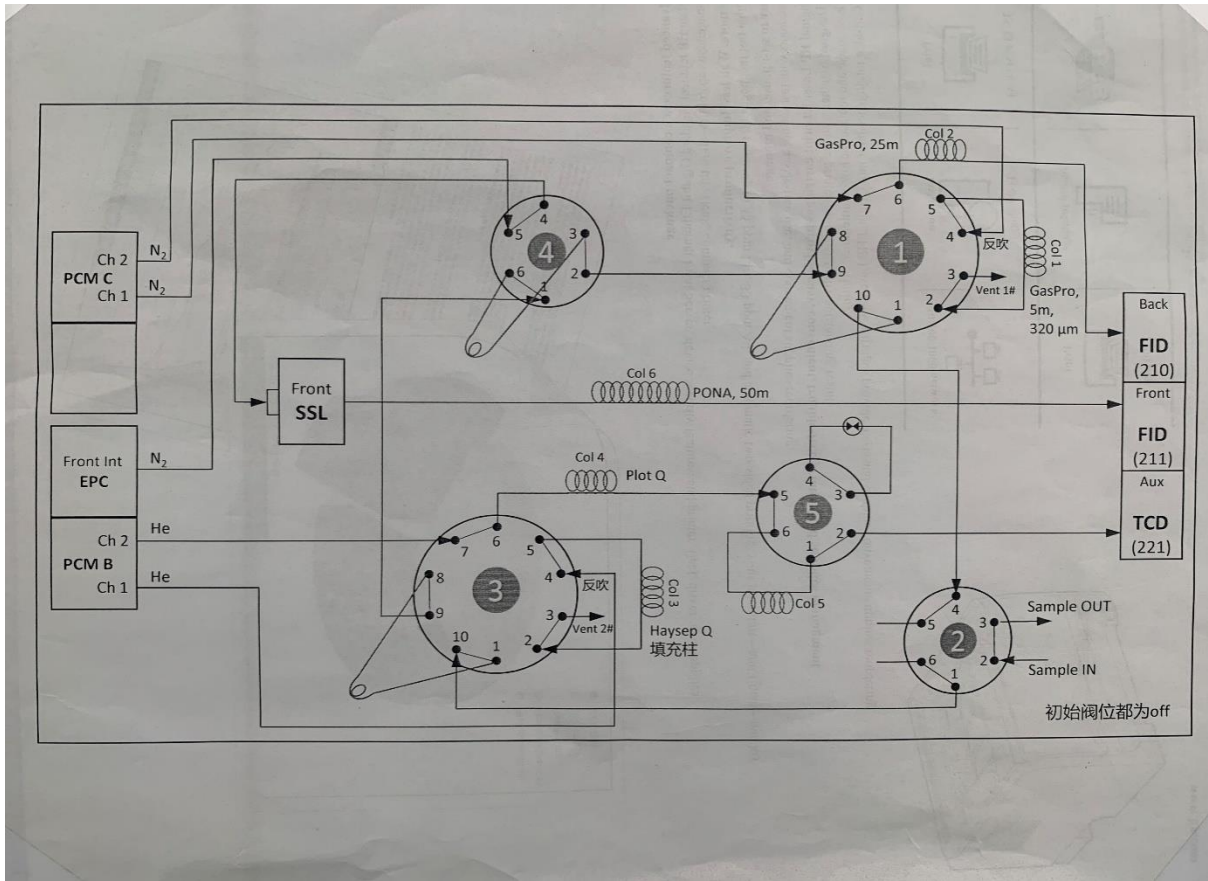


Figure 3.9: Sampling flow scheme of online GC Agilent 7890A at Synfuels China.

**Table 3.4:** Specific operational information of the Agilent 7890A in this experiment

<i>Agilent 7890B</i>	
<i>Detector</i>	<b>BACK FID, T=250 °C</b>
<i>Column 1</i>	Agilent, GS-GasPro, 320µm * 5.00m, max temperature: 340 °C
<i>Column 2</i>	Agilent, GS-GasPro, 320µm * 25.00m, max temperature: 340 °C
<i>Multiple-way valve</i>	180°C
<i>Carrier gas</i>	UHP N <sub>2</sub> with the flow rate of 30 mL(NTP)/min
<i>Oven temperature program</i>	Hold at 40 °C for 13 min, heat to 230 °C at 3 °C /min, hold at 230 °C for 23 min
<i>Products analysing</i>	C <sub>1</sub> to C <sub>4</sub>
<i>Detector</i>	<b>AUX TCD, T=250 °C</b>
<i>Column 3</i>	Agilent, Hayesep Q, 80/100 mush, 2 mm * 2 m * 1/8', max temperature 275 °C
<i>Column 4</i>	Agilent, HP-Plot Q, 320 µm*30 m, max temperature: 270 °C
<i>Column 5</i>	Molsieve 5A, 80/100 mush, 1.5 m * 1/8', max temperature: 400 °C
<i>Multiple-way valve</i>	180 °C
<i>Carrier gas</i>	UHP He with the flow rate of 30 mL(NTP)/min
<i>Temperature program</i>	Hold at 40 °C for 13 min, heat to 230 °C at 3 °C /min, hold at 230 °C for 23 min
<i>Products analysing</i>	H <sub>2</sub> , N <sub>2</sub> , CO, CO <sub>2</sub> , Ar and methane
<i>Detector</i>	<b>Front FID, T=250 °C</b>
<i>Column 6</i>	Agilent, HP-PONA, 200 µm * 50 m * 0.5 µm, max temperature: 350 °C
<i>Multiple-way valve</i>	180 °C
<i>Carrier gas</i>	UHP N <sub>2</sub> with the flow rate of 30 mL(NTP)/min
<i>Temperature program</i>	Hold at 40 °C for 13 min, heat to 230 °C at 3°C /min, hold at 230 °C for 23 min
<i>Products analysing</i>	C <sub>1</sub> to longer chain hydrocarbons

**Table 3.5:** Order of peaks in different detectors on Agilent 7890B

Peak number	AUX TCD	BACK TCD	Front FID
1	CO <sub>2</sub>	C <sub>1</sub>	C <sub>1</sub>
2	H <sub>2</sub>	P <sub>2</sub>	O <sub>2</sub>
3	Ar	O <sub>2</sub>	P <sub>2</sub>
4	N <sub>2</sub>	P <sub>3</sub>	O <sub>3</sub>
5	CH <sub>4</sub>	O <sub>3</sub>	P <sub>3</sub>
6	CO	P <sub>4</sub>	O <sub>4</sub>
7		O <sub>4</sub>	P <sub>4</sub>
8			Trans-2-O <sub>4</sub>
9			Cis-2-O <sub>4</sub>
10			O <sub>5</sub>
11			P <sub>5</sub>
12			O <sub>6</sub>
13			P <sub>6</sub>

In this table, C<sub>1</sub> is methane, O<sub>n</sub> and P<sub>n</sub> are  $\alpha$ -olefin and n-paraffin with carbon number n, respectively. Trans- and Cis-2-O<sub>4</sub> are Trans- and Cis-2-butene.

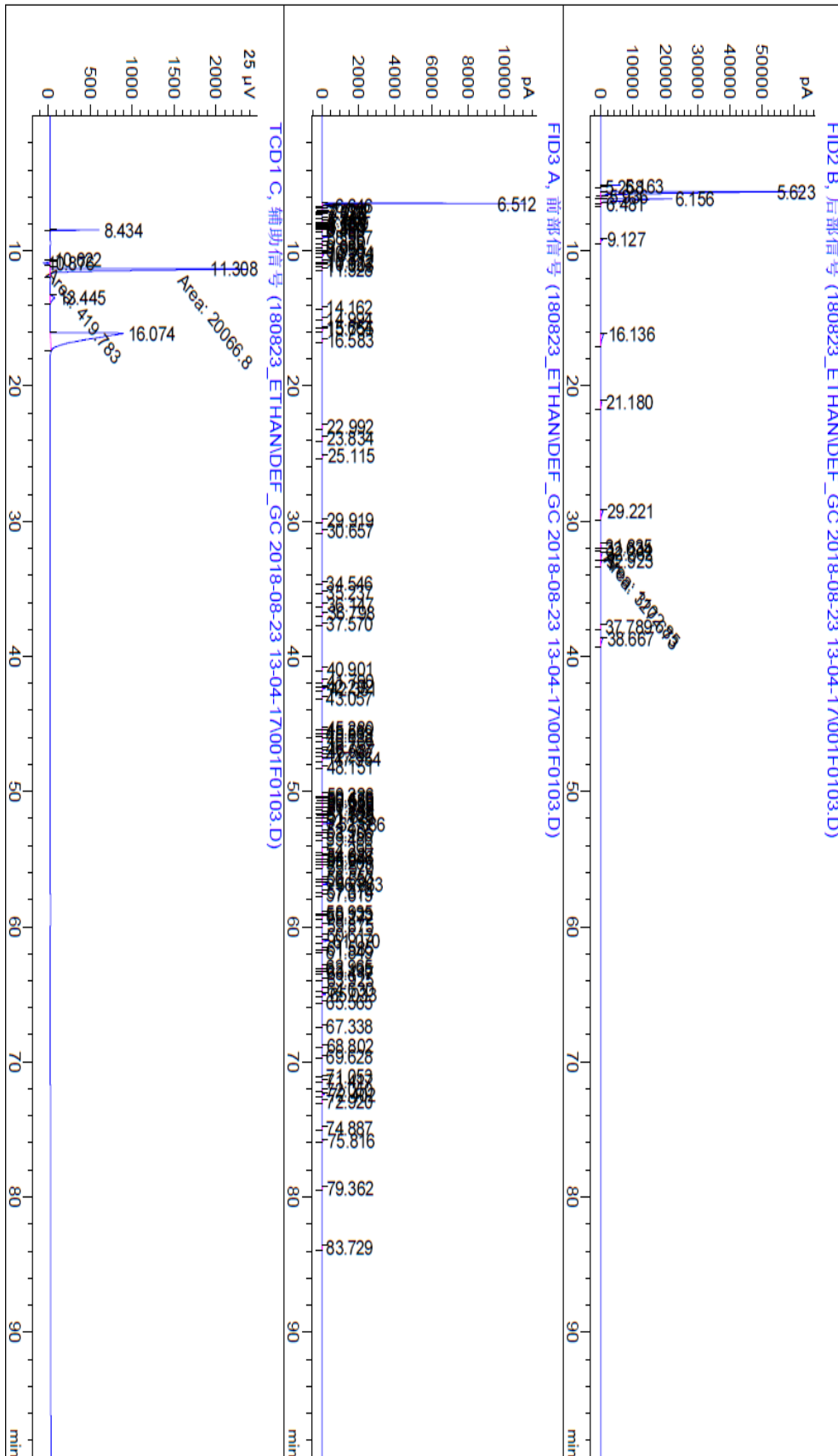


Figure 3.10: Chromatogram of the reaction of ethylene co-fed FTS in Synfuels China

### 3.6. Components of feed gas used in this study

As indicated earlier, to study the performance of ethylene in cobalt-based catalytic FTS reactions, many experiments were conducted using different feed gases. These experiments can be divided into seven groups, depending on the composition of the feed gas. All original data obtained by gas chromatography were analysed, calculated, compared and simulated. The feed gas composition and reaction conditions of each group of experiments were as follows.

- Group 1: To detect the Fischer-Tropsch reactivity of the catalyst, a typical FT feed gas (syngas:  $H_2/CO/N_2 = 6:3:1$ ) was introduced into the TFBR at Necsa. The reaction temperature was  $200^\circ C$ , and the pressure 20 bar gauge. The flow rate of syngas was  $30 \text{ mL(NTP)/(min} \cdot \text{g} \cdot \text{cat)}$ .
- Group 2: After running a typical FT, ethylene, as the only feed gas, was introduced in TFBR at Necsa. The reaction temperature range was 180 to  $220^\circ C$  and the pressure was 20 bar gauge. The flow rate of ethylene was  $50 \text{ ml (NTP)/(min} \cdot \text{g} \cdot \text{cat)}$ .
- Group 3:  $N_2$  works as a dilute gas and was co-fed with ethylene to modify the partial pressure (at Necsa). The reaction temperature range was 180 to  $220^\circ C$ , and pressure was 20 bar gauge. The flow rate of total feed gas was  $50 \text{ ml (NTP)/(min} \cdot \text{g} \cdot \text{cat)}$ .
- Group 4: Different ratios of hydrogen and ethylene mixed gas were fed to the TFBR at Necsa, to investigate the performance of the ethylene reaction with hydrogen. The reaction temperature was  $180^\circ C$ , and pressure was 20 bar gauge. The range of  $C_2H_4/H_2$  ratio was 0.5 to 4.6.

- Group 5: To investigate the effect of reaction temperature, in this group experiment, the ratio of  $C_2H_4/H_2$  in feed gas was fixed at 0.8 and 4.8 (at Necsa). The reaction temperature range was 100 to 250 °C, and the pressure was 20 bar gauge.
- Group 6: To investigate the effect of co-fed ethylene in FTS, feed gases with different ethylene content was introduced in TFBR at Synfuels China. The total flow rate of feed gas was maintained at 50 mL (NTP)/(min · g · cat), and partial pressure of  $H_2$  and CO was fixed. The co-fed ethylene content range was 0 to 30 vol. %. The reaction temperature range was 160 to 220 °C, and the pressure was 20 bar gauge.
- Group 7: In order to investigate the effect of co-fed CO in ethylene hydrogenation system, feed gases with different CO content was introduced in TFBR at Synfuels China. The total flow rate of feed gas was maintained at 50 ml (NTP)/(min · g · cat), and partial pressure of  $H_2$  and ethylene were fixed. The co-fed CO content range was 0 to 7 vol. %. The reaction temperature range was 140 to 220°C, and the pressure was 20 bar gauge.

### 3.7. Data calculation and analysis

Feed mixtures,  $CO/H_2/N_2$ ,  $C_2H_4/N_2$ ,  $C_2H_4/H_2$ ,  $C_2H_4/H_2/Ar$  and  $CO/H_2/C_2H_4/Ar$ , were used as feeds for the experiments.  $N_2$  or Ar was introduced into the feed gases as a diluent gas, which was used to calculate the flow rate of the tail gas. An online gas chromatogram (GC) with one FID and two TCD was used to analyse the components of both feed gas and tailgas. To convert the peak area obtained from the GC to mole composition of each of the components, a calibration gas with a mixture of  $CO/H_2/CO_2/N_2/CH_4/C_2H_4/C_2H_6$  was used as an external standard.

Under the reaction conditions we conducted, the molar percentage of each gas in the mixed gas was proportional to the peak area of each component obtained by GC analysis. . Through analysis of the calibration gas, we can obtain the corresponding relationship between the peak area and gas molar percentage. Thus, for any product, reactant or diluent gas “I” in the feed gas or tailgas, which was also present in the calibration mixture, its molar percentage can be obtained from the following equation:

$$\%I_{gas} = \left( \frac{A_{I,gas}}{A_{I,calibration}} \right) \times \%I_{calibration} \quad \text{Eq. 3.2}$$

Where:  $\%I_{gas}$  is the molar percentage of gas I in feed gas or tailgas;  $A_{I,gas}$  is the integrated peak area of I in the online GC;  $A_{I,calibration}$  is the integrated peak area of I in the online GC, when analysing the calibration gas;  $\%I_{calibration}$  is the molar percentage of gas I in calibration gas.

For both paraffin and olefin products with a carbon number higher than 2, which is not present in calibration gas, its mole percentage was calculated using the following equation:

$$\%J_{gas} = \left( \frac{A_{J,gas}}{A_{h,calibration}} \right) \times \%I_{calibration} \times RF_{J,h} \quad \text{Eq. 3.3}$$

Where:  $\%J_{gas}$  is the molar percentage of gas J in feed gas or tailgas;  $A_{J,gas}$  is the integrated peak area of J in GC;  $RF_{J,h}$  is the relative response factor of gas J corresponding to the reference gas h (h=ethylene for olefin product calculation; and h = ethane for paraffin

product calculation)Based on the references [11-12], the RF used in this paper is listed in Table

3.6.

**Table 3.6:** Molar RF for hydrocarbons

<b>Carbon number</b>	<b>RF (olefins)</b>	<b>RF (paraffins)</b>
2	1	1
3	0.7	0.74
4	0.55	0.55
5	0.47	0.47
6	0.4	0.4
7	0.35	0.35
8	0.32	0.32
9	0.28	0.28

In the feed gas and tailgas, the amount of the unreacted inert gas N<sub>2</sub> or Ar does not change. Therefore, the relationship between the standard molar flow rate of the feed gas and the exhaust gas can be shown as the following equation:

$$F_{in} \times \%N2_{gas,in} = F_{out} \times \%N2_{gas,out} \quad \text{Eq. 3.4}$$

Where:  $F_{in}$  and  $F_{out}$  represent the molar flow rate (mol/min) of total feed gas and tailgas, respectively.  $\%N2_{gas,in}$  and  $\%N2_{gas,out}$  represent the molar percentage (%) of N<sub>2</sub> in feed gas and tailgas, respectively.

The molar flow rate of the reactant  $\theta$  in the feed gas and tailgas can be obtained from the following equations:

$$F_{\theta,in} = F_{in} \times \% \theta_{gas,in} \quad \text{Eq. 3.5}$$

$$F_{\theta,out} = F_{out} \times \% \theta_{gas,out} \quad \text{Eq. 3.6}$$

Where:  $F_{\theta,in}$  and  $F_{\theta,out}$  represents the molar flow rate of reactant  $\theta$  in feed gas and tailgas, respectively. While,  $\% \theta_{gas,in}$  and  $\% \theta_{gas,out}$  represent the molar percentage of reactant  $\theta$  in feed gas and tailgas, respectively. In this paper,  $\theta$  is CO, H<sub>2</sub> and C<sub>2</sub>H<sub>4</sub>.

Therefore, the conversion ( $\% \theta_{conv}$ ) and reaction rate (mol/min/g cat) of reactant  $\theta$  can be calculated as follows:

$$\% \theta_{conv} = (F_{\theta,in} - F_{\theta,out}) / F_{\theta,in} \quad \text{Eq. 3.7}$$

$$-r_{\theta} = (F_{\theta,in} - F_{\theta,out}) / m_{cat} \quad \text{Eq. 3.8}$$

Where:  $m_{cat}$  is the weight of the catalysts.

For reactions with only CO and no ethylene participation, the selectivity of product  $J_n$  with carbon number  $n$  ( $S_J$ ) is calculated using the following equation:

$$S_J = (n \times F_{out} \times \%J_{n,gas}) / (F_{CO,in} - F_{CO,out}) \quad \text{Eq. 3.9}$$

Where:  $\%J_{n,gas}$  is the molar percentage of product  $J_n$  in tailgas.

For reactions with only ethylene and no CO participation, the selectivity of product  $J_n$  with carbon number  $n$  ( $S_J$ ) is calculated using the following equation:

$$S_J = (n \times F_{out} \times \%J_{n,gas}) / [2 \times (F_{C_2H_4,in} - F_{C_2H_4,out})] \quad \text{Eq. 3.10}$$

For experiments in which both CO and ethylene participate in the reaction, the selectivity of product  $J_n$  is calculated using the following equation:

$$S_J = (n \times F_{out} \times \%J_{n,gas}) / [(F_{CO,in} - F_{CO,out}) + 2 \times (F_{C_2H_4,in} - F_{C_2H_4,out})] \quad \text{Eq. 3.11}$$

For the hydroformylation of ethylene, we know that CO and ethylene react 1:1 to form propanal. Therefore, the selectivity of propanal based on CO consumption  $S_{C_2H_5CHO,CO}$  and selectivity based on ethylene consumption  $S_{C_2H_5CHO,C_2H_4}$  can be obtained using the following equations:

$$S_{C_2H_5CHO,CO} = (F_{out} \times \%C_2H_5CHO_{gas,out}) / (F_{CO,in} - F_{CO,out}) \quad \text{Eq. 3.12}$$

$$S_{C_2H_5CHO,C_2H_4} = (F_{out} \times \%C_2H_5CHO_{gas,out}) / (F_{C_2H_4,in} - F_{C_2H_4,out}) \quad \text{Eq. 3.13}$$

Where:  $\%C_2H_5CHO_{gas,out}$  is the molar percentage of propanal in tailgas.

## REFERENCES:

1. Bartholomew, C. H., & Guzzi, L. (1991). New Trends in CO Activation. *Stud. Surf. Sci. Catal*, 64, 158.
2. Stoop, F., & Van der Wiele, K. (1986). Formation of Olefins from Synthesis Gas over Silica-Supported Rufe Bimetallic Catalysts. *Applied Catalysis*, 23(1), 35-47.
3. Su, H. Q., Zhang, X. H., Ding, N., Du, Y., Ma, Y., Bai, F. H., ... & Yu, S. Y. (2009). Research Progress of Fischer-Tropsch Synthesis Catalysts [J]. *Journal of Inner Mongolia University*, 4.
4. Kokes, R. J. (1969). Formation of Dimeric Products During Steady State Hydrogenation of Ethylene over Cobalt. *Journal of Catalysis*, 14(1), 83-92.
5. Schulz, H., & Claeys, M. (1999). Reactions of A-Olefins of Different Chain Length Added During Fischer-Tropsch Synthesis on a Cobalt Catalyst in a Slurry Reactor. *Applied Catalysis A: General*, 186(1-2), 71-90.
6. Liu, X., Li, X., Suehiro, Y., & Fujimoto, K. (2007). Elucidation of Reaction Network and Effective Control of Carbon Number Distribution in the Three Phase Fischer-Tropsch Synthesis. *Applied Catalysis A: General*, 333(2), 211-218.
7. Cant, N. W., Liu, I. O., & Scott, J. A. (2013). Ethylene Oligomerisation over Co/SiO<sub>2</sub> in the Presence of Trace Carbon Monoxide: The Eidus Reaction Revisited. *Catalysis Today*, 215, 267-275.
8. Bartholomew, C. H. (1991). Recent Developments in Fischer-Tropsch Catalysis. In *Studies in Surface Science and Catalysis* (Vol. 64, pp. 158-224). Elsevier.
9. Chronis, T. (1999). A Fischer-Tropsch Study of Co/Ru Catalysts (Doctoral dissertation, University of the Witwatersrand).

10. Lu, X., Hildebrandt, D., Liu, X., & Glasser, D. (2012). A Thermodynamic Approach to Olefin Product Distribution in Fischer–Tropsch Synthesis. *Industrial & Engineering Chemistry Research*, 51(51), 16544-16551.
11. Scanlon, J. T., & Willis, D. E. (1985). Calculation of Flame Ionization Detector Relative Response Factors Using the Effective Carbon Number Concept. *Journal of Chromatographic Science*, 23(8), 333-340.
12. Lu, X. (2012). Fischer-Tropsch Synthesis: Towards Understanding (Doctoral Dissertation, University of the Witwatersrand).

## Chapter 4

### Reaction of Ethylene over a typical Fischer-Tropsch Synthesis Co/TiO<sub>2</sub> Catalyst

This work had been published in the *Engineering Reports*, 2020, 2(9), e12232. Part of this work was presented at CATSA 2017.

---

#### ABSTRACT

In order to identify the potential reaction paths of C<sub>2</sub>H<sub>4</sub> and their product distribution in Fischer-Tropsch synthesis (FTS), a series of experiments were designed over a Co/TiO<sub>2</sub> catalyst in the absence of CO. C<sub>2</sub>H<sub>4</sub> did quickly react with H<sub>2</sub> to produce C<sub>1-6</sub> products under Fischer-Tropsch (FT) reaction conditions. Although the dominant reaction is C<sub>2</sub>H<sub>4</sub> hydrogenation to ethane, changing the reaction conditions (temperature and partial pressure of reactants) can lead to the other reaction pathways being enhanced, resulting in varying product selectivity to both linear and branch olefins and paraffins. Possible reaction pathways had been summarized and discussed, which including C<sub>2</sub>H<sub>4</sub> reaction to ethylidene followed by dimerization; C<sub>2</sub>H<sub>4</sub> insertion into C<sub>2</sub> surface species and dimerization and C<sub>4</sub> decomposition and/or direct C<sub>2</sub> hydrogenolysis. Furthermore, the products obtained from C<sub>2</sub>H<sub>4</sub> reactions were fit to a typical FTS product distribution, which indicate that both the chain growth initiators and monomers are not necessarily only derived from hydrogenation of CO but also from the secondary reactions of olefins.

#### 4.1. Introduction

Fischer-Tropsch synthesis (FTS) is an important technology used to convert syngas derived from coal/ gas/ biomass into clean transport fuels or other valuable organics [1-8]. FTS is generally regarded as a polymerization-like reaction. The products of FTS are a wide range of hydrocarbons, consisting of mainly olefins and paraffins, with a small amount of oxygenates. The Anderson-Schulz-Flory (ASF) equation is used to describe the FT product distribution; however, deviations from the ideal ASF distribution, such as a higher yield of C<sub>1</sub>, and a lower yield of C<sub>2</sub>, have been observed [9-10]. Many theories have been proposed to explain the deviation, and secondary reactions of olefins is considered as a reasonable explanation [11-14]. Therefore, it is interesting to investigate the reaction of C<sub>2</sub>H<sub>4</sub> under typical FTS operating conditions (similar space velocity, temperatures and pressures).

The olefin product produced by the FTS may re-adsorb on the catalyst surface and undergo secondary reactions. The effect of co-feeding low concentrations of C<sub>2</sub>H<sub>4</sub> to the Fischer-Tropsch synthesis (FTS) reaction system has been studied previously, in order to investigate the reactivity of the olefins in the FTS reaction [14-20]. Different secondary reactions of olefins have been reported, and in particular hydrogenation, [14-15] isomerization (bond shift reaction), [16] hydrogenolysis, [17] reinsertion into chain growth as monomers, [18] initiation of hydrocarbon chain [19] and hydroformylation [20] have been observed.

The reactivity of C<sub>2</sub>H<sub>4</sub> under FTS conditions has been reported for both Fe-based and Co-based catalysts [21-23]. Schulz et al. [24] found that the conversion of C<sub>2</sub>H<sub>4</sub> was less than 80% for iron-based catalysts, while almost all the C<sub>2</sub>H<sub>4</sub> was converted (conversions over 90%) when using cobalt-based catalysts. In addition, hydrogenation of C<sub>2</sub>H<sub>4</sub> is the dominant reaction under all reaction conditions [21-23]. Later, reabsorption and insertion of C<sub>2</sub>H<sub>4</sub> to form longer carbon chain products on Co-based catalysts was reported [14, 25-27].

Furthermore, a decrease in CH<sub>4</sub> selectivity was found when C<sub>2</sub>H<sub>4</sub> was co-fed, which was considered due to the competitive reaction between CO methanation and C<sub>2</sub>H<sub>4</sub> incorporation with the C<sub>1</sub> species [26].

Some studies focused on the hydro-polymerisation of C<sub>2</sub>H<sub>4</sub> at very low partial pressures of CO over supported Co-based catalysts [28-32]. It is reported that the C<sub>2</sub>H<sub>4</sub> in the feed was completely consumed, and the CO partially hydrogenated to generate longer chain hydrocarbons. Kokes et al. [31] found that a large number of C<sub>2</sub>H<sub>4</sub> dimerization products (C<sub>4</sub>), especially olefins, were formed when hydrogen was deficient. They [31] proposed that an adsorbed intermediate of 1, 1-σ-ethylidene, converted by 1, 2-diadsorbed C<sub>2</sub>H<sub>4</sub> with hydrogen assistance, could polymerise to form C<sub>2</sub>H<sub>4</sub> dimers. However, most of the studies reported were carried out under typical FTS reaction conditions, such as low conversion and/or a typical pressure. More recently, some studies on co-feeding C<sub>2</sub>H<sub>4</sub> to a FTS reaction system were carried out using a combined quantitative in-situ FTIR and online gas chromatography [33-34]. The researchers [33-34] found that co-feeding C<sub>2</sub>H<sub>4</sub> did not alter the selectivity of the product, but changed the chain length of the adsorbate on the catalyst surface.

In summary, the types of FTS catalyst, and the operating conditions (temperature, residence time and partial pressure of the reactants and products) had a significant impact on the secondary reactions of C<sub>2</sub>H<sub>4</sub> [12]. Researchers have found that it was difficult to investigate certain aspects independently due to the system complexity and number of the reactions occurring in FTS. In addition, some reaction pathways may be obscured when many reactions are occurring simultaneously. In order to fully understand the reaction pathways of the olefin, we suggest simplifying the complex system and investigating one aspect at a time.

In this work, several groups of experiments were carried out over a FTS Co-based catalyst, in the absence of CO, under typical S reaction conditions. Firstly, mixtures of C<sub>2</sub>H<sub>4</sub> and N<sub>2</sub> were fed to the reactor and later the feed was changed to mixtures of C<sub>2</sub>H<sub>4</sub> and H<sub>2</sub>. The effect of the feed gas ratio (C<sub>2</sub>H<sub>4</sub>/H<sub>2</sub>) and the reaction temperatures on the reactivity of C<sub>2</sub>H<sub>4</sub> and resulting product selectivity could be investigated without either the reactant CO or the FT by-products influencing the system.

## **4.2. Experimental Methods**

### **4.2.1. Catalyst preparation**

The catalysts used in this study (15 wt.% Co supported on TiO<sub>2</sub>) were prepared using the incipient wetness method. Co(NO<sub>3</sub>)<sub>3</sub>·6H<sub>2</sub>O (Sigma Aldrich) was used as the metal precursor salt, and TiO<sub>2</sub> (Degussa P-25) was used as the catalyst support precursor. The TiO<sub>2</sub> paste was made by mixing TiO<sub>2</sub> with distilled water at a mass ratio of 1:1. After being dried at 120 °C for two hours, the paste was calcined in a Muffle oven that was heated from room temperature to 400 °C at a rate of 5 °C/min and then maintained at 400 °C for 6 hours. The support was crushed and sieved after calcination, and particles of which between 0.5 mm and 1 mm were selected for the impregnation step [35]. 1 g of the support was measured out, and distilled water (0.8 ml) was gradually dropped onto the support until the surface was infiltrated. The pre-treated and selected TiO<sub>2</sub> support was impregnated with a Co(NO<sub>3</sub>)<sub>3</sub> aqueous solution, with a Co metal loading of 15% by mass. Thereafter, the wet catalyst was dried at 120 °C for two hours, and then calcined at 400 °C for six hours. Catalyst information is summarised in Table 4.1.

**Table 4.1:** Properties of the catalyst (15% Co/TiO<sub>2</sub>) used in this work.

Catalyst	15% Co/TiO <sub>2</sub>
Particle Size (mm)	0.5-1
Surface area (m <sup>2</sup> /g)	42.92
Pore volume (cm <sup>3</sup> /g)	0.24
Average pore diameter (nm)	16.7

#### 4.2.2. Reaction procedure and product analysis

The fixed bed reactor used in this study had a 203.8 mm long stainless tube with an inner diameter of 8 mm. 1 g of catalyst was loaded into the reactor, and the catalyst was reduced at 350 °C in pure H<sub>2</sub> (AFROX (African Oxygen) Ltd., 99.999%), for 4 h at 30 ml/min and 1 bar gauge. After catalyst reduction, the reactor was cooled to a temperature below 100 °C. Thereafter, three groups of experiments were conducted, as follows:

➤ Group 1 (Run 1)

A normal FTS reaction was conducted with a feed gas of H<sub>2</sub>/CO/N<sub>2</sub> (H<sub>2</sub>/CO=2:1), at 30 ml/min, 200 °C and 20 bar (on gauge). This was used to test the catalyst performance during FTS. Thereafter, the reactor was purged with inert gas N<sub>2</sub>.

➤ Group 2 (Runs 2-4)

Firstly, a feed of pure C<sub>2</sub>H<sub>4</sub> was introduced into the reactor at 20 bar and the temperature was varied between 180 to 220 °C, while the total flow rate was maintained at 50 ml/min. Then, N<sub>2</sub> was co-fed into the reactor using various C<sub>2</sub>H<sub>4</sub>/N<sub>2</sub> ratios. The operating temperature was also varied from 180 to 220 °C while keeping the total pressure at 20 bar.

➤ Group 3 (Runs 5-11)

H<sub>2</sub> was co-fed with C<sub>2</sub>H<sub>4</sub> into the reactor at 20 bar and 180 °C, 60 ml/min. The ratio of C<sub>2</sub>H<sub>4</sub> to hydrogen was changed from 0.5 to 4.6. Thereafter, experiments were run at 2 different C<sub>2</sub>H<sub>4</sub>/H<sub>2</sub> ratios, namely 0.8 (which we denote "Excess H<sub>2</sub>") followed by 4.8 (denoted "H<sub>2</sub> limiting"), and the operating temperature in the reactor was varied between 100 to 250 °C, to investigate the effect of the C<sub>2</sub>H<sub>4</sub>/H<sub>2</sub> ratio and temperature on C<sub>2</sub>H<sub>4</sub> reactivity.

The reaction conditions are summarised in Table 4.2. The feed and tail gas were analysed using an online Gas Chromatograph (GC, Agilent 7890B). A flame ionization detector (FID) was used to analyse the hydrocarbons, and two thermal conductivity detectors (TCD) were used to analyse H<sub>2</sub>/N<sub>2</sub>. The experimental results monitored by the GC indicated that the normal FTS reaction (Run 1) stabilized after 13 h (see in Figure 2); and the C<sub>2</sub>H<sub>4</sub> hydrogenation reaction reached a steady state less than 2 h for each run. The experimental results reported in the current work were the average values obtained between 17 to 23 h for all the runs.

In the FTS experiment (Run 1), the feed gas flow rate was controlled by a mass flow controller (Brooks) and N<sub>2</sub> was used as an internal standard for the calculation of the results. The CO conversion ((%)CO) and hydrocarbon selectivity ( $S_{Cn-1}$ ) were calculated using the following equations:

$$(\%)CO = (F_{CO,in} - F_{CO,out})/F_{CO,in} \times 100\% \quad \text{Eq. 4.1}$$

$$S_{Cn-1} = n \times F_{Cn,out}/(F_{CO,in} - F_{CO,out}) \times 100\% \quad \text{Eq. 4.2}$$

During the reaction of ethylene (Runs 5-11), the flow rate of feed gas was controlled by a mass flow controller (Brooks) and the flow rate of the tailgas was measured using a bubble flow meter. The C<sub>2</sub>H<sub>4</sub> conversion ((%)C<sub>2</sub>H<sub>4</sub>) and hydrocarbons selectivity ( $S_{Cn-2}$ ) were estimated using the following equations:

$$(\%)C_2H_4 = (F_{C_2H_4,in} - F_{C_2H_4,out})/F_{C_2H_4,in} \times 100\% \quad \text{Eq. 4.3}$$

$$S_{Cn-2} = n \times F_{Cn,out}/[2 \times (F_{C_2H_4,in} - F_{C_2H_4,out})] \times 100\% \quad \text{Eq. 4.4}$$

Where:  $F_{CO,in}$  and  $F_{CO,out}$  are the CO molar flow rates of the feed gas and the tailgas, respectively (mmol/min),  $F_{C_2H_4,in}$  and  $F_{C_2H_4,out}$  are the ethylene molar flow rates of the feed gas and the tailgas, respectively (mmol/min),  $n$  is the carbon number of product C<sub>n</sub> and

$F_{Cn,out}$  is the molar flow rate of hydrocarbon product with carbon number  $n$  in tailgas (mmol/min).

#### 4.2.3. Catalyst Characterisation

The reducibility of the catalyst was measured by hydrogen temperature programmed reduction ( $H_2$ -TPR). Two experiments were conducted:

(1) Experiment 1: 50 mg of catalyst was loaded into the quartz reactor. A 5%  $H_2/N_2$  reducing mixture, at a flow rate of 30 ml/min, was passed through the reactor. The temperature of the reactor was programmed to increase from room temperature to 700 °C at a heating rate of 10 °C/min.

(2) Experiment 2: the same experimental procedure was followed as with experiment 1, the difference being that the reaction temperature increased from room temperature to 350 °C at a rate of 10 °C/min, and it was then maintained at 350 °C for 1 hour. The  $H_2$  concentration during the reduction was measured using a thermal conductivity detector (TCD).

X-ray diffraction (XRD) analysis was performed on a Rigaku D/max-2500 diffractometer, with Cu  $K\alpha$  radiation at 40 kV and 100 mA in a scanning range of 3-80 ° ( $2\theta$ ). The diffraction peaks of the crystalline phase were compared with those of standard compounds reported in the JCPDS Date File.

The nitrogen adsorption–desorption experiment was measured using a Quantachrome Autosorb-1MP sorption analyzer at -196 °C. Before measurement, the samples were degassed at 200 °C for at least 6 h. The specific surface area (SBET) was calculated using the Brunauer–Emmett–Teller (BET) method ( $P/P_0 < 0.1$ ).

**Table 4.2:** Reaction conditions for all 11 runs.

Experiment	Feed	Temperature	Total Pressure	Total Flow	Feed Partial pressure (bar)			
		°C	Bar (on gauge)	ml/min	C <sub>2</sub> H <sub>4</sub>	H <sub>2</sub>	N <sub>2</sub>	C <sub>2</sub> H <sub>4</sub> /H <sub>2</sub>
Run 1	H <sub>2</sub> /CO/N <sub>2</sub>	200	20	30	H <sub>2</sub> /CO/N <sub>2</sub> =6:3:1 with no C <sub>2</sub> H <sub>4</sub>			
Run 2	C <sub>2</sub> H <sub>4</sub> /N <sub>2</sub>	180 to 220	20	50	21.0	0.0	0.0	N/A
Run 3	C <sub>2</sub> H <sub>4</sub> /N <sub>2</sub>	180 to 220	20	50	16.8	0.0	4.2	N/A
Run 4	C <sub>2</sub> H <sub>4</sub> /N <sub>2</sub>	180 to 220	20	50	10.5	0.0	10.5	N/A
Run 5	C <sub>2</sub> H <sub>4</sub> /H <sub>2</sub>	180	20	45	7.0	14.0	0.0	0.5
Run 6	C <sub>2</sub> H <sub>4</sub> /H <sub>2</sub>	180	20	52.5	9.0	12.0	0.0	0.8
Run 7	C <sub>2</sub> H <sub>4</sub> /H <sub>2</sub>	180	20	60	10.5	10.5	0.0	1.0
Run 8	C <sub>2</sub> H <sub>4</sub> /H <sub>2</sub>	180	20	45	14.8	6.2	0.0	2.4
Run 9	C <sub>2</sub> H <sub>4</sub> /H <sub>2</sub>	180	20	50	17.2	3.8	0.0	4.6
Run 10	C <sub>2</sub> H <sub>4</sub> /H <sub>2</sub>	100 to 250	20	52.5	9.3	11.7	0.0	0.8
Run 11	C <sub>2</sub> H <sub>4</sub> /H <sub>2</sub>	110 to 250	20	50	17.4	3.6	0.0	4.8

### 4.3. Experiment results

#### 4.3.1. Catalyst Characterization

The characteristic results of TPR and XRD are shown in Figure 4.1 (a-c). Figure 4.1 (a) indicates that the catalyst starts to reduce at temperatures above 320 °C. Figure 4.1 (b) shows that the catalyst can be activated at 350 °C. Based on the literature, there are two steps during the cobalt catalyst reduction process: (1) from  $\text{Co}_3\text{O}_4$  to  $\text{CoO}$ , around 300 °C; (2) from  $\text{CoO}$  to metallic  $\text{Co}$ , around 500 °C [36]. As shown in Figure 4.1 (a) and (b), A and B represent these two reduction steps. It indicates at 350 °C, at least part of  $\text{Co}_3\text{O}_4$  reduce to metallic  $\text{Co}$ . The comparison of the XRD results for the fresh catalyst, before reduction and after reduction, at 350 °C, is shown in Figure 4.1 (c). The pattern produced by the catalyst before reduction, shows some sharp peaks, which may be due to the cubic  $\text{Co}_3\text{O}_4$  (JCPDS65-3103). However, after reduction, the intensity of the  $\text{Co}_3\text{O}_4$  peaks either disappears or is reduced. At the same time, certain  $\text{Co}$  (JCPDS15-0806) peaks appear. Although the signal of metallic  $\text{Co}$  is weak and difficult to distinguish from the noise, combined with the TPR result, it confirms that metallic  $\text{Co}$  exists in reduced catalysts. According to the BET results, the catalyst surface area is about  $43 \text{ m}^2/\text{g}$ , the pore volume is  $0.24 \text{ cm}^3/\text{g}$  and the average pore diameter is 16.7 nm. (See Table 2.) All the characterization results show that the catalyst used in this experiment is a typical  $\text{Co}$ -based FTS catalyst. Figure 4.1 (d) shows the TEM images of catalysts.

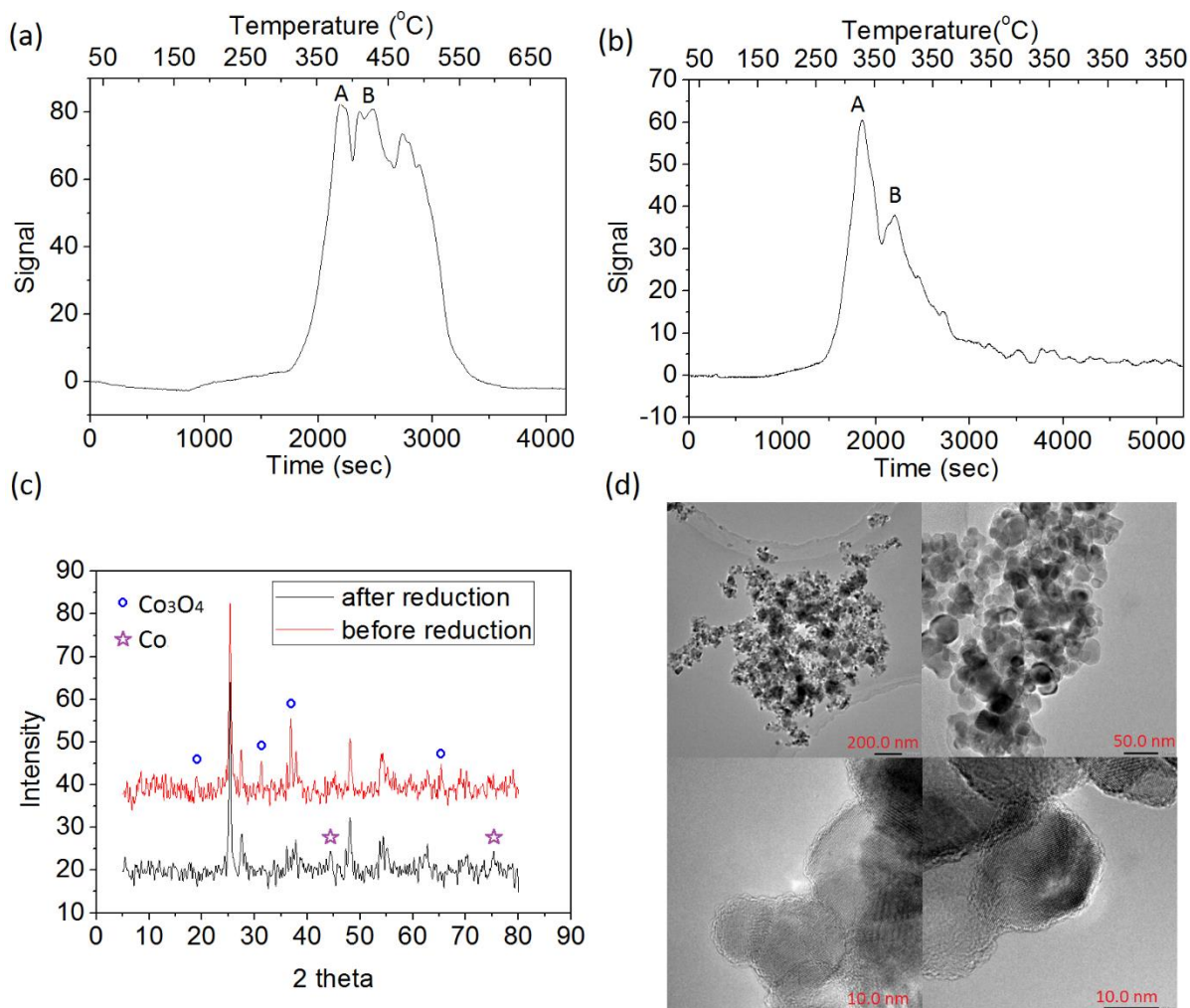


**Figure 4.1:** Characterization results for: (a) H<sub>2</sub>-TPR profiles with the reduction temperature increasing from room temperature to 700 °C at a rate of 10 °C/min); (b) H<sub>2</sub>-TPR profiles with the reduction temperature increasing from room temperature to 350 °C (10 °C/min) and then being maintained at 350 °C for 1 hour; (c) XRD patterns for 15% Co/TiO<sub>2</sub> before and after reduction; (d) TEM images of the catalyst

### 4.3.2. Confirming FTS Reactivity of the Co catalyst

When the syngas ( $H_2/CO = 2:1$ ) is introduced into the reactor, a typical product distribution of a Co-based FT catalyst [13] is obtained (See Table 4.3 and Figure 4.8 (a)). The  $CH_4$  selectivity is high (16%), while the  $C_2$  product selectivity is lower than that expected from an ideal ASF distribution. In addition, the  $C_{3+}$  product distribution is consistent with an ASF distribution, with  $\alpha$ -value = 0.82 (Figure 4.8 (a)). Moreover, the total  $C_{5+}$  selectivity is 65.03%. Figure 4.2 shows the CO conversion and methane selectivity with respect to time on stream (TOS). As can be seen, FTS stabilized at around 13 hours TOS. To avoid errors, the average value of results obtained between 17 to 23 hours after the experimental conditions are changed are used in Table 4.3 and Figure 4.8 (a). The experimental results clearly confirm that the catalyst used in this experiment is a typical FTS Co-based catalyst [37].

**Table 4.3:** Conversion of reactants and carbon based selectivity of products under typical FTS conditions, at 30 ml/min, 200 °C and 20 bar (on gauge).

<b>Conversion (%)</b>										
<b>CO</b>					<b>H<sub>2</sub></b>					
11.93					12.98					
<b>Carbon based Selectivity (mol %)</b>										
<b>CH<sub>4</sub></b>	<b>C<sub>2</sub>H<sub>4</sub></b>	<b>C<sub>2</sub>H<sub>6</sub></b>	<b>C<sub>3</sub>H<sub>6</sub></b>	<b>C<sub>3</sub>H<sub>8</sub></b>	<b>C<sub>4</sub>H<sub>8</sub></b>	<b>C<sub>4</sub>H<sub>10</sub></b>	<b>C<sub>5</sub>H<sub>10</sub></b>	<b>C<sub>5</sub>H<sub>12</sub></b>	<b>C<sub>6</sub>H<sub>12</sub></b>	<b>C<sub>6</sub>H<sub>14</sub></b>
16.0	0.86	1.90	5.48	2.32	5.44	2.97	5.37	2.83	4.78	2.74

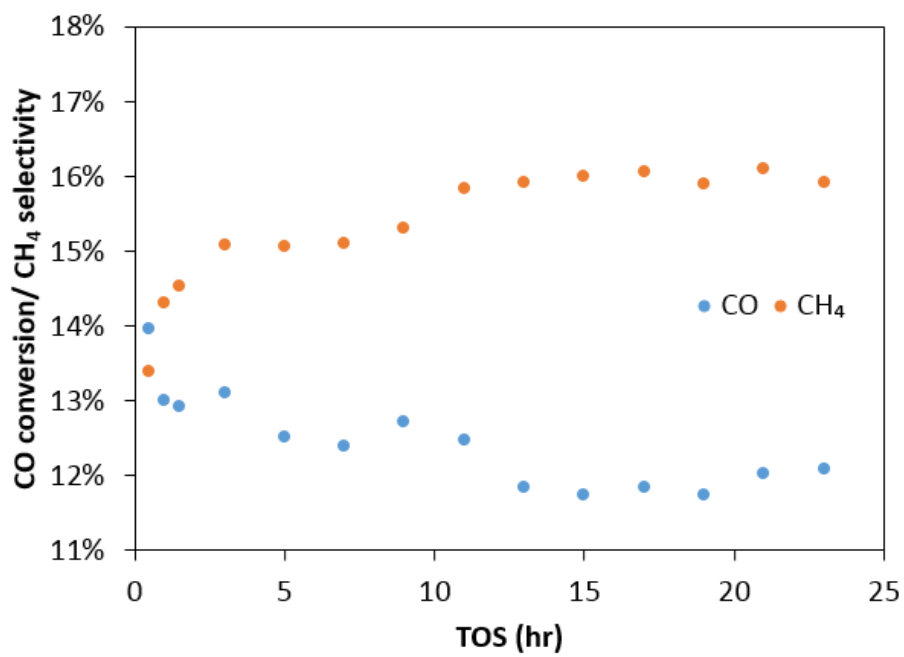


**Figure 4.2:** CO conversion and CH<sub>4</sub> selectivity under typical FTS conditions, at 30 ml/min, 200 °C and 20 bar (on gauge).

### 4.3.3. Feeding C<sub>2</sub>H<sub>4</sub>/N<sub>2</sub> to the reactor

In order to test if pure C<sub>2</sub>H<sub>4</sub> could react under normal FT operating conditions, gas mixtures of C<sub>2</sub>H<sub>4</sub>/N<sub>2</sub> were fed to the reactor. N<sub>2</sub> is an inert gas with the function of adjusting the partial pressure of C<sub>2</sub>H<sub>4</sub> to the reactor system. When the reactor was operated at 20 bars (on gauge) and 180 °C, no product was detected by the online GC. The reaction temperature was then increased from 180 °C to 220 °C, but product was still not detected. Adjusting the partial pressure of C<sub>2</sub>H<sub>4</sub>, by changing the molar ratio of C<sub>2</sub>H<sub>4</sub>/N<sub>2</sub> in the feed mixture (Table 4.2), did not result in the C<sub>2</sub>H<sub>4</sub> reacting. These results indicate that the C=C double bond of C<sub>2</sub>H<sub>4</sub> could not open or break when only C<sub>2</sub>H<sub>4</sub> (with or without an inert gas N<sub>2</sub>) is fed to the reactor. In other words, C<sub>2</sub>H<sub>4</sub> itself does not easily react as a monomer to polymerize to form long chain hydrocarbons, without the assistance of other gases, such as H<sub>2</sub>.

### 4.3.4. Feeding C<sub>2</sub>H<sub>4</sub>/H<sub>2</sub> to the reactor

#### 4.3.4.1. Effect of C<sub>2</sub>H<sub>4</sub>/H<sub>2</sub> molar feed ratio

The feed gas was switched to a mixture of C<sub>2</sub>H<sub>4</sub>/H<sub>2</sub> with the reactor operating at 180 °C and 20 bars gauge and the GC detected some short chain hydrocarbon products. The feed ratio was varied and the conversion of C<sub>2</sub>H<sub>4</sub> and H<sub>2</sub> and the product selectivity are plotted in Figure 4.3. Figure 4.3 (a) shows that when C<sub>2</sub>H<sub>4</sub>/H<sub>2</sub> < 1, C<sub>2</sub>H<sub>4</sub> is completely converted. However, the conversion of H<sub>2</sub> reaches more than 98% when C<sub>2</sub>H<sub>4</sub>/H<sub>2</sub> ≥ 1, but the C<sub>2</sub>H<sub>4</sub> conversion drops from 91% to 22%. (See Figure 4.3 (a)) The ethane selectivity decreases from 98.98% to 95.75%, when the C<sub>2</sub>H<sub>4</sub>/H<sub>2</sub> ratio is increased from 0.5 to 1; thereafter the ethane selectivity does not change much as the C<sub>2</sub>H<sub>4</sub>/H<sub>2</sub> ratio is increased above 1. In all cases hydrogenation of

C<sub>2</sub>H<sub>4</sub> to ethane is the main reaction and this contributes to the high ethane selectivity (>95%).

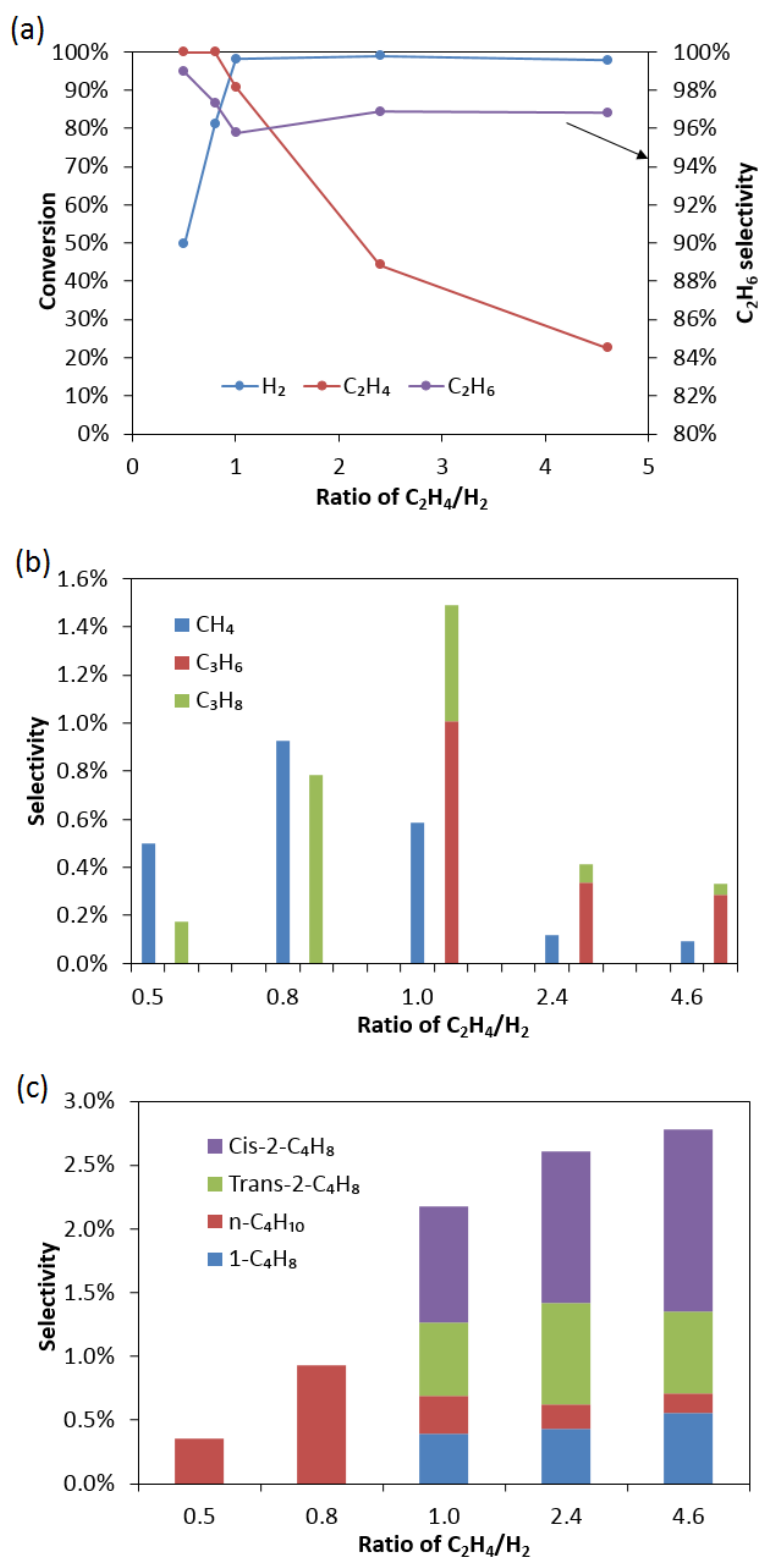
This is in line with published reports [6].

Figure 4.3 (b) and (c) shows:

- (1) When the C<sub>2</sub>H<sub>4</sub>/H<sub>2</sub> ratio increases from 0.5 to 4.6, the paraffin product selectivity for C<sub>1</sub>, C<sub>3</sub> and C<sub>4</sub> increases, reaching a maximum at ratio of 0.8 and then decreases.
- (2) When C<sub>2</sub>H<sub>4</sub>/H<sub>2</sub> ≥ 1, both C<sub>3</sub> and C<sub>4</sub> olefins (including the corresponding isomers) are produced, and the total yield of olefins is much higher than that of paraffins.
- (3) When the C<sub>2</sub>H<sub>4</sub>/H<sub>2</sub> ratio is increased from 1 to 4.6: the selectivity of total C<sub>4</sub> product increases from 2.2% to 2.8%; the selectivity of CH<sub>4</sub> and total C<sub>3</sub> product decreases from 0.5% to 0.1% and 1.5% to 0.3%, respectively.

Because C<sub>2</sub>H<sub>4</sub> was the only carbon source in these experiments, the production of C<sub>1</sub> and C<sub>3</sub> indicates that the C-C bond ruptures to form odd carbon number products when co-feeding H<sub>2</sub>. The selectivity of both CH<sub>4</sub> and C<sub>3</sub> decreases with increasing partial pressure of C<sub>2</sub>H<sub>4</sub> (C<sub>2</sub>H<sub>4</sub>/H<sub>2</sub> > 1). This implies that few carbon chain products formed from the hydrocracking or demethylation reaction.

The major C<sub>4</sub> olefin under these reaction conditions was 2-butene. This phenomenon indicates that the production of 2-butene in FTS may come from the C<sub>2</sub>H<sub>4</sub> dimerization reaction. In addition, with an increase in the partial pressure of C<sub>2</sub>H<sub>4</sub>, the selectivity of cis-2-butene increased, while the trans-2-butene yield decreased.



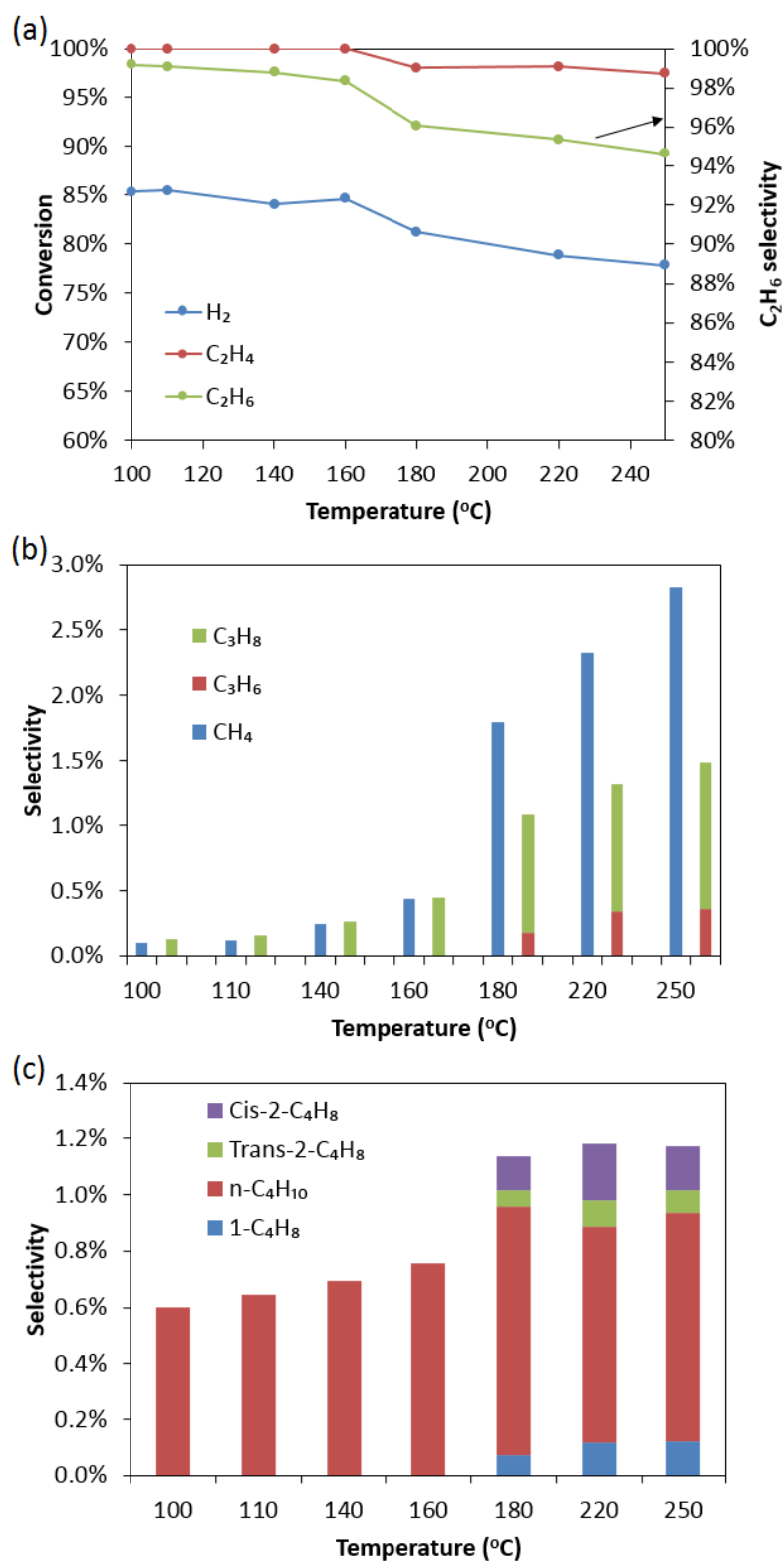
**Figure 4.3:** The effect of C<sub>2</sub>H<sub>4</sub> : H<sub>2</sub> molar ratio on the C<sub>2</sub>H<sub>4</sub> reaction at 180 °C and 20 bar gauge):  
 (a) conversion of reactants and the selectivity of C<sub>2</sub>H<sub>6</sub>; (b) selectivity of CH<sub>4</sub> and C<sub>3</sub> products;  
 (c) selectivity of C<sub>4</sub> products.

#### 4.3.4.2. Influence of reaction temperature when $C_2H_4/H_2 < 1$ in the feed gas ( $H_2$ in excess)

As described earlier, the product distribution changes with  $C_2H_4/H_2$  ratio. To investigate the effect of temperature on the reaction of  $C_2H_4$  with  $H_2$ , two groups of experiments were carried out: one using the feed gas with a molar ratio of  $C_2H_4/H_2=0.8$  (excess  $H_2$ ); the other with  $C_2H_4/H_2=4.8$  ( $H_2$  limiting- see next section). The term “excess” or “limiting” refers to the hydrogenation reaction, where a ratio  $C_2H_4/H_2=1$  would be the correct ratio if all the  $C_2H_4$  reacted to ethane. Figure 4 shows the conversions of reactants and the selectivity of  $C_1$  to  $C_4$  products, at 20 bar gauge, a total inlet flow rate of 52.5 ml/min,  $C_2H_4/H_2=0.8$  and with the reaction temperature varying from 100 to 250 °C ( $H_2$  excess).

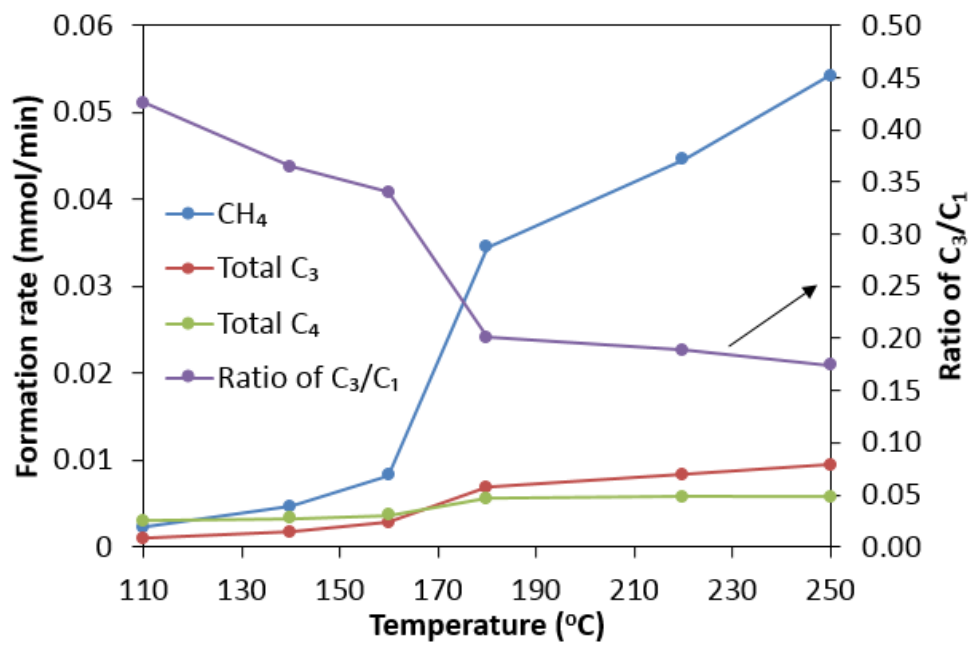
The  $C_2H_4$  was completely converted when there was  $H_2$  in the feed gas for all operating temperatures between 100 to 160 °C. As temperature increased above 160 °C,  $C_2H_4$  conversion decreased to reach 97% at 250 °C. A similar trend in  $H_2$  conversion was observed. This might be caused by acceleration of  $C_2H_4$  adsorption/ desorption with the increase in temperature.

Figure 4.4 (a) also shows the variation of the ethane selectivity with operating temperature, and it can be seen that the higher the temperature, the lower the ethane selectivity. The dominant reaction at all temperatures is  $C_2H_4$  hydrogenation, as the ethane selectivity is always higher than 94% as shown in Figure 4.4; however, the ethane selectivity drops with increase in temperature, which implies that the more  $C_2H_4$  is consumed in competing reactions, such as dimerization and hydrocracking.



**Figure 4.4:** Effect of temperature on C<sub>2</sub>H<sub>4</sub> reaction when H<sub>2</sub> is in excess (C<sub>2</sub>H<sub>4</sub>/H<sub>2</sub> = 0.8, total flow rate: 52.5 ml/min; reaction pressure: 20 bars). (a) Conversion of reactants and selectivity of C<sub>2</sub>H<sub>6</sub>. (b) Selectivity of CH<sub>4</sub> and C<sub>3</sub>. (c) Selectivity of C<sub>4</sub>.

The selectivity of CH<sub>4</sub> and C<sub>3</sub> and C<sub>4</sub> products (paraffins and olefins) are shown in Figure 4.4 (b) and (c). The selectivity of CH<sub>4</sub> and total C<sub>3</sub> and C<sub>4</sub> products all increased with increasing temperature. As seen in Figure 4.4, there was an obvious increase in selectivity between 160 °C and 180 °C. At temperature lower than this critical temperature range, only paraffins were produced and no olefins were formed. At very low temperatures (less than 120 °C), the C<sub>2</sub>H<sub>4</sub> dimer (butane) had a higher selectivity than either CH<sub>4</sub> or C<sub>3</sub> (odd number hydrocarbons). This indicates that the reaction of C<sub>2</sub>H<sub>4</sub> oligomerization was faster than that of hydrogenolysis or demethylation at the low reaction temperatures. When the reaction temperature was increased to 180 °C, there was a marked increase in the selectivity of CH<sub>4</sub>, total C<sub>3</sub> and total C<sub>4</sub> hydrocarbon products, with CH<sub>4</sub> selectivity increasing the most. The CH<sub>4</sub> selectivity increased from 1.80% to 2.83%, while the total C<sub>3</sub> selectivity only increased from 1.1% to approximately 1.5%; however, the selectivity of C<sub>2</sub>H<sub>4</sub> dimer (C<sub>4</sub>) was fairly constant (~1.2%) as the temperature was increased from 180 to 250 °C. (See Figure 4.4.) It is worth noting that the olefin products were only produced when the temperature was higher than 180 °C.



**Figure 4.5:** Effect of reaction temperature on CH<sub>4</sub> yield, total C<sub>3</sub> and total C<sub>4</sub>, when H<sub>2</sub> is in excess.

The product distribution for the reaction of C<sub>2</sub>H<sub>4</sub> in the presence of H<sub>2</sub> appears to occur via reactions that are different from those indicated in the theory on carbon chain growth in FTS. Liu et al. [38] suggested two pathways to explain these product distributions. One is the oligomerization (dimerization) of the α-olefins in the feed and the subsequent cracking with H<sub>2</sub> assistance. Another is attributed to the addition of methylene species, which are formed via the demethylation reaction [39]. To investigate the different reactions, the yields of CH<sub>4</sub>, total C<sub>3</sub> and C<sub>4</sub> products were calculated and the results are shown in Figure 4.5. In comparison to odd carbon number hydrocarbons, the yield of the C<sub>4</sub> products did not change much with temperatures over the range tested (100 °C to 250 °C). This suggests that the C<sub>2</sub>H<sub>4</sub> dimerization reaction is not sensitive to the reaction temperature. However, for the demethylation products, the yield of CH<sub>4</sub> and C<sub>3</sub> increased more than twenty and tenfold respectively. The formation of CH<sub>4</sub> and C<sub>3</sub> can be described by the following two equations:



Equation (4.5) represents direct C<sub>2</sub>H<sub>4</sub> hydrogenolysis to produced CH<sub>4</sub>. Equation (4.6) shows the methylene species formed by demethylation in carbon chain growth, which produces CH<sub>4</sub> and propene with a mole ratio of CH<sub>4</sub>/C<sub>3</sub> equal to 1:1. Equation (4.6) could be considered an analogical disproportionation. The results in Figure 4.5 indicate that the CH<sub>4</sub> yield was much higher than that of the C<sub>3</sub> products in the case of H<sub>2</sub> rich feeds. This phenomenon could indicate that a high coverage of chemisorbed H<sub>2</sub> on the surface of catalysts inhibits the methylene species that take part in chain growth reaction.

#### 4.3.4.3. Influence of reaction temperature with a H<sub>2</sub> limited feed gas

In another group of experiments, a mixture of C<sub>2</sub>H<sub>4</sub>/H<sub>2</sub> where C<sub>2</sub>H<sub>4</sub>:H<sub>2</sub>= 4.8 corresponding a H<sub>2</sub> limited feed gas, was fed to the reactor. The experiments were conducted at 20 bar, a flow rate of 40 ml/min, and the reaction temperature was varied from 100 °C to 250 °C. Figure 4.6 (a) shows that the conversion of both H<sub>2</sub> and C<sub>2</sub>H<sub>4</sub> were fairly constant at all the temperatures. H<sub>2</sub> reacted to completion and the reaction rates of both H<sub>2</sub> and C<sub>2</sub>H<sub>4</sub> were essentially the same, which is in agreement with the observed high selectivity of ethane. Thus, even in this H<sub>2</sub> limited situation, the dominant reaction was still C<sub>2</sub>H<sub>4</sub> hydrogenation. The experimental results in Figure 6 show that with a H<sub>2</sub> limited feed, the selectivity of ethane decreased from 98% (at 110 °C) to 95% (at 250 °C). (See Figure 4.6 (a).) This suggests that demethylation and oligomerization reactions are more likely to occur at a higher reaction temperature, which is the same as the result obtained for H<sub>2</sub> rich feeds.

For H<sub>2</sub> limited feeds (or correspondingly excess C<sub>2</sub>H<sub>4</sub>) we see from Figure 4.6 (b) and (c) that olefins are the main product, even at a very low temperatures and that the selectivity of C<sub>4</sub> is much higher than that of C<sub>3</sub>, which indicates that high partial pressure of C<sub>2</sub>H<sub>4</sub> promotes the dimerization reaction. The selectivity of CH<sub>4</sub>, C<sub>3</sub>H<sub>6</sub> and C<sub>3</sub>H<sub>8</sub> all increase with increasing temperature. These results indicate that a high temperature is better for the production of odd carbon number hydrocarbons. However, in comparison to the results of the previous experiment (Figure 4.4 (b) for a feed with excess H<sub>2</sub>), the product distribution of CH<sub>4</sub> and C<sub>3</sub> are different (see Figure 4.6 (b).) In this case, the selectivity to C<sub>3</sub> product is higher than that of CH<sub>4</sub>, and the selectivity of C<sub>3</sub> increases more rapidly with increasing temperature than the selectivity of CH<sub>4</sub>. This indicates that the formation of CH<sub>4</sub> could be limited by the availability of chemisorbed hydrogen. The methylene species formed by demethylation participate in chain growth more easily when C<sub>2</sub>H<sub>4</sub> in the feed is in excess, especially at high temperatures.

Moreover, the paraffin to olefin ratio decreased with increasing temperature for C<sub>3</sub> also indicating that the availability of H<sub>2</sub> may be limiting.

The change in the selectivity of C<sub>4</sub> products with temperature is shown in Figure 4.6 (c) and it can be seen that the selectivity of n-butane did not change much with temperature, while the total olefin selectivity increased initially, reached a maximum, and then decreased. The maximum selectivity of cis-2-butene was achieved at about 180 °C; for trans-2-butene, the maximum occurred at about 200 °C while for 1-butene it occurred at around 220 °C. The decrease in the selectivity of C<sub>4</sub> products at a high temperature suggests that the intermediates from C<sub>2</sub>H<sub>4</sub> dimerization on the catalyst surface may react to form other hydrocarbons. Similar to the product distribution of propene/ propane, the selectivity of butene was significantly higher than butane. The selectivity of both cis-2-butene and trans-2-butene are higher than that of 1-butene.

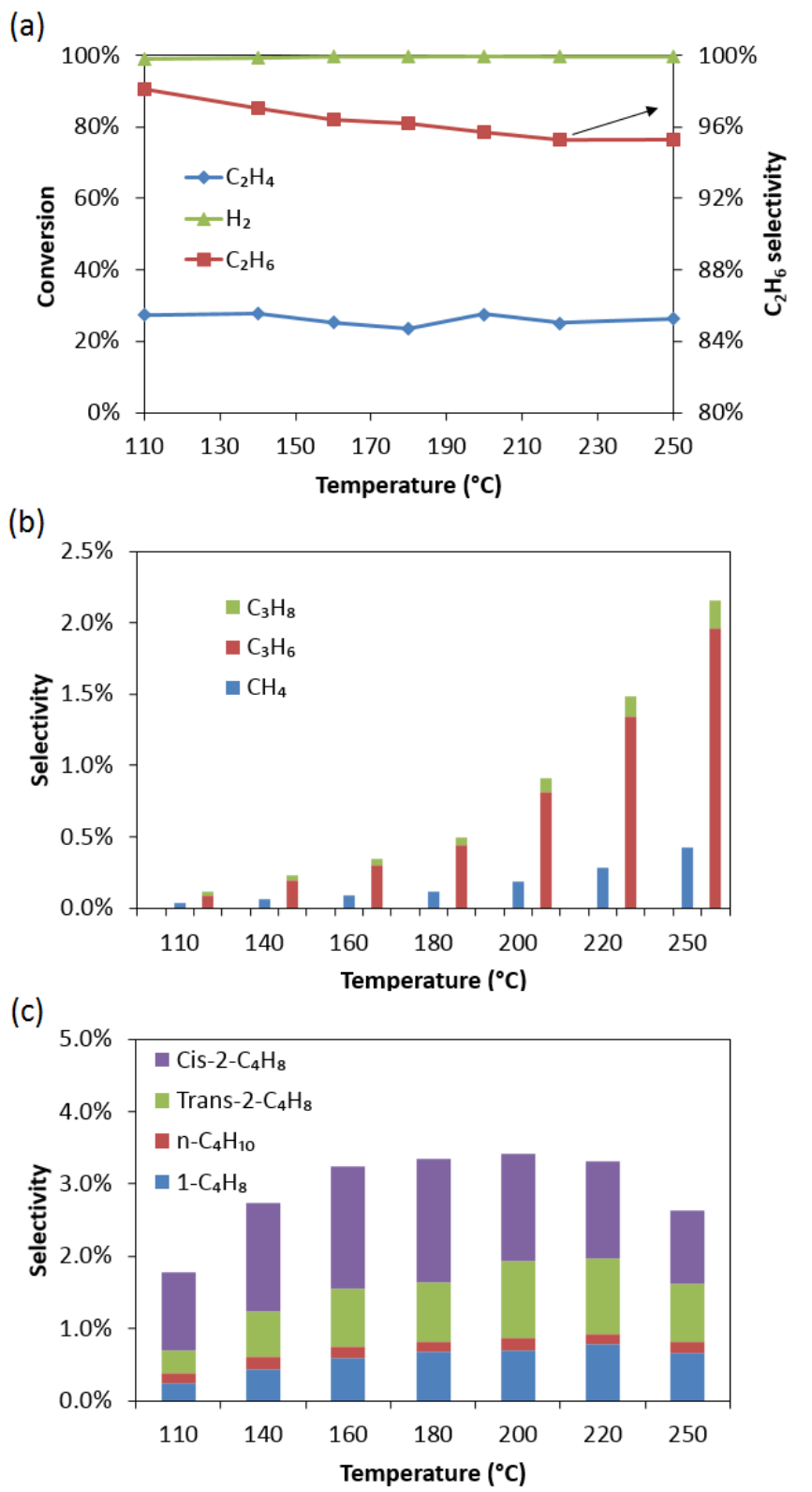


**Figure 4.6:** Effect of temperature on the C<sub>2</sub>H<sub>4</sub> reaction when H<sub>2</sub> is limiting (C<sub>2</sub>H<sub>4</sub>/H<sub>2</sub> = 4.8, total flow rate: 50 ml/min; reaction pressure: 20 bar gauge). (a) Conversion of reactants and the selectivity of C<sub>2</sub>H<sub>6</sub>. (b) Selectivity of CH<sub>4</sub> and C<sub>3</sub>. (c) Selectivity of C<sub>4</sub>.

Figure 4.7 shows the effect of temperature on the molar formation rate of the C<sub>1</sub>, C<sub>3</sub> and C<sub>4</sub> products. These are different from the results seen with excess H<sub>2</sub> in the feed (Figure 4.5), as the total yield of C<sub>4</sub> product is much higher than that of CH<sub>4</sub> and C<sub>3</sub>. This provides strong evidence that chemisorbed H<sub>2</sub> limits C<sub>2</sub>H<sub>4</sub> dimerization. In addition, the formation rates of CH<sub>4</sub> and the total C<sub>3</sub> product were different to those found for feeds with excess H<sub>2</sub>. At a low temperature (less than 180 °C), the mole ratio of CH<sub>4</sub>/C<sub>3</sub> was almost 1:1, which corresponds with Eq. 4.6. Under these conditions, some of the C<sub>2</sub>H<sub>4</sub> “disproportionates” with H<sub>2</sub> assistance to form a 1:1 mole ratio of CH<sub>4</sub> and C<sub>3</sub> product. At temperature is equal to or above 180 °C, the increase in the yield of C<sub>3</sub> is significantly higher than that of CH<sub>4</sub>. This finding implies that another reaction occurs to produce C<sub>3</sub>. Combined with the decrease in yield of C<sub>4</sub> products, an analogical comproportionation could explain this phenomenon, i.e.:



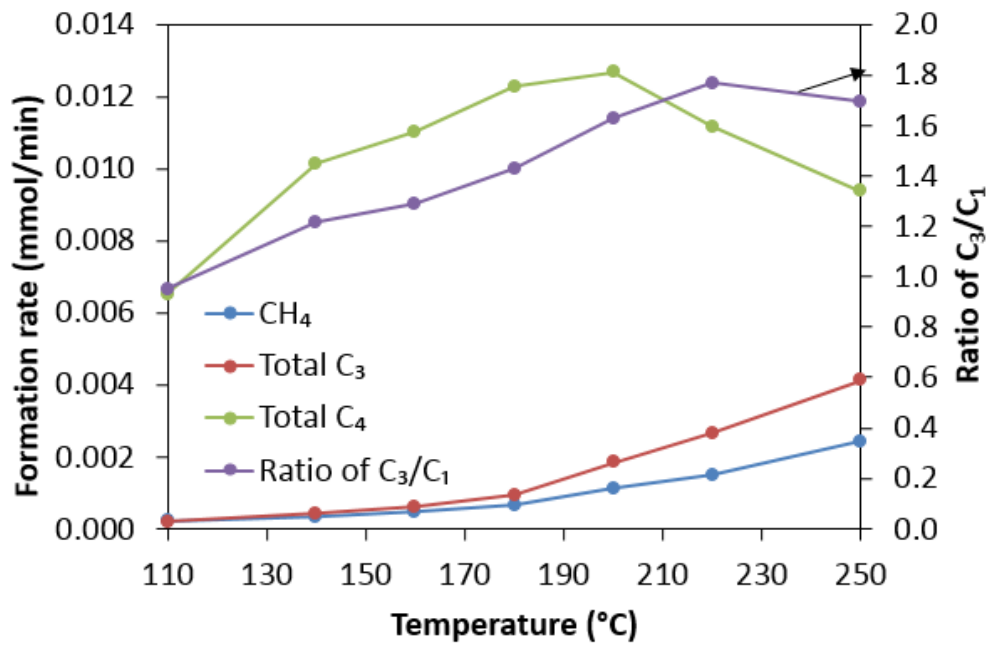


**Figure 4.7:** Effect of reaction temperature on the CH<sub>4</sub> yield, total C<sub>3</sub> and total C<sub>4</sub>, for a H<sub>2</sub> limited feed.

## 4.4. Discussion

### 4.4.1. Carbon chain growth

Figure 4.8 shows the product distribution plotted in an ASF plot for light hydrocarbons produced by (a) a feed of syngas, (b) feeds of  $C_2H_4/H_2$  with excess  $H_2$  and (c)  $H_2$  limited for different operating temperatures. When the reaction temperature is low, as shown in Figure 4.8 (b) and (c), the online GC cannot detect  $C_{5+}$  products. However, the product distribution for feeds of  $C_2H_4/H_2$  is similar to that of normal FTS at reaction temperature higher than 160 °C for feeds with  $H_2$  in excess and higher than 200 °C, when the feed is  $H_2$  limited. When the carbon number  $n$  is greater than 2, the product distribution of light hydrocarbons approaches a straight line, which is consistent with the typical FTS product distribution, as shown in Figure 4.8 (a). However, when compared to typical FTS product distribution, several differences can be seen:

- (1) Compared to the positive deviation of  $CH_4$  from the ideal ASF distribution in FTS, the  $CH_4$  in the  $C_2H_4$  hydrogenation reaction product, does not deviate from an ASF distribution in a  $H_2$  rich feed (Figure 4.8 (b)) and even has a negative deviation for  $H_2$  deficient ( $C_2H_4$  rich) feed (Figure 4.8 (c)).
- (2) Due to the dominant reaction of  $C_2H_4$  hydrogenation, the  $C_2$  product distribution deviated positively from the ideal ASF distribution for  $n=2$ .
- (3) The  $C_4$  product distribution deviates slightly from the ASF distribution. This can be attributed to  $C_2H_4$  dimerization, which would enhance  $C_4$  production.

Figure 8 indicates, in the absence of CO, the reaction of  $C_2H_4$  and  $H_2$  produce the monomers required for chain growth. Moreover, products with both even and odd carbon numbers

follow the ASF product distribution. This indicates the chain growth monomer is not only C<sub>2</sub> and that some adsorbed intermediate CH<sub>x</sub> might be produced by hydrocracking of C<sub>2</sub>H<sub>4</sub>.

Studies are still being done to determine whether the C<sub>2</sub> intermediate formed on the surface of a Co-based catalyst under FTS reaction conditions is ethyl, ethylidene or vinyl. In addition, it has not been determined whether the carbon chain-growth monomer of the C<sub>1</sub> intermediate is CH, CH<sub>2</sub> or CH<sub>3</sub> in the FTS reaction. However, the large amount of 2-butene obtained from these experiments indicates that adsorbed ethylidene (CH<sub>3</sub>-CH-\*) probably formed on the catalyst surface. Kokes [31] reported that the 2-butene dimer monomer is ethylidene.

In order to understand the carbon chain growth of C<sub>2</sub>H<sub>4</sub> and H<sub>2</sub> reaction under typical FTS operating conditions the chain growth probability ( $\alpha$ -value) was calculated using Eq. 4.8.

$$\ln\left(\frac{W_n}{n}\right) = 2\ln(1 - \alpha) + (n - 1)\ln\alpha \quad \text{Eq. 4.8}$$

Where: W<sub>n</sub> is the weight fraction of hydrocarbon product containing n atoms; n is the carbon number. The results are summarised in Table 4.4.

Under conditions of excess H<sub>2</sub> in the feed, the product is almost entirely paraffinic, and as the temperature increases, the  $\alpha$ -value decreases. Similarly, the  $\alpha$ -value of the total product (including  $\alpha$ -olefins and n-paraffins) decreases with increasing temperature for H<sub>2</sub> limited feeds. The trend in the  $\alpha$ -value of the individual n-paraffins and  $\alpha$ -olefins with temperature is also consistent. This indicates that high temperature is more conducive to the formation of low carbon chain products. In addition, the  $\alpha$ -value of the alkane higher for H<sub>2</sub> limited feeds than for feeds with excess H<sub>2</sub>. This indicates that adsorbed H<sub>2</sub> limits the chain growth, as if the

chain-growth intermediate is hydrogenated by the surface adsorbed  $H_2$  it forms a paraffin and results in the termination of the carbon chain.

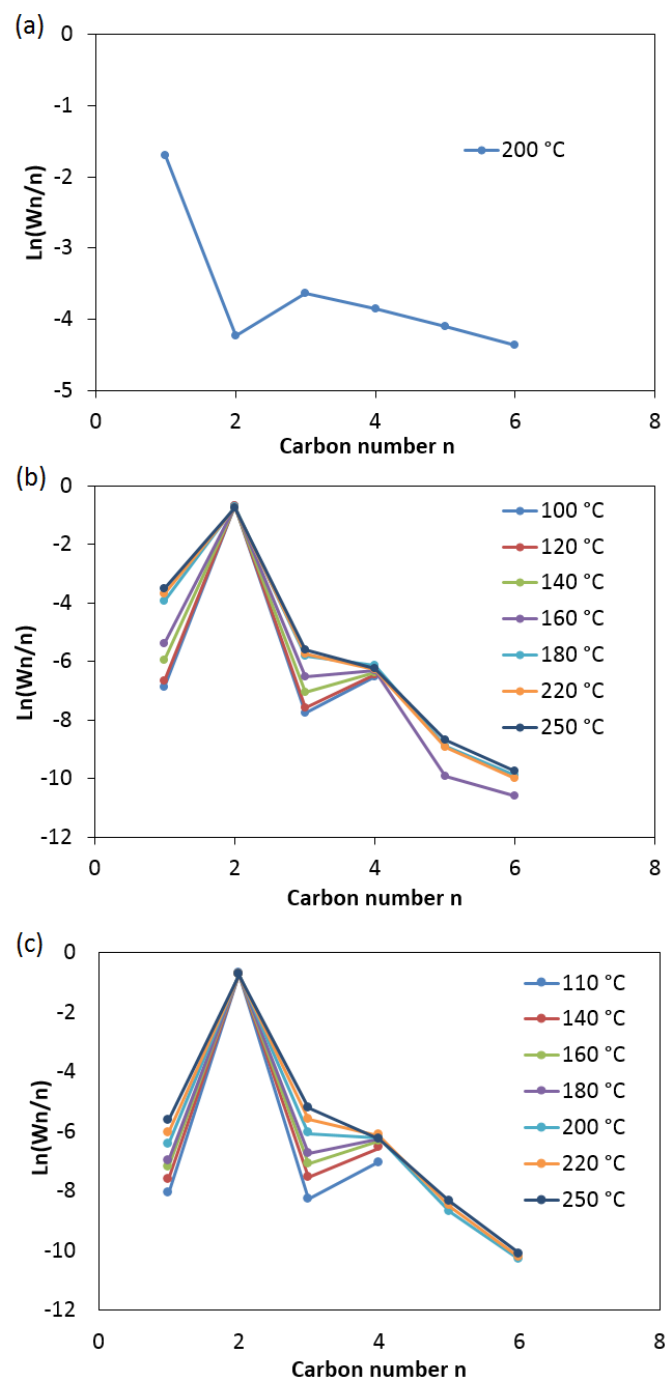


**Figure 4.8:** Logarithmic product distribution ( $\alpha$ -olefins +  $n$ -paraffins), as a function of the carbon number (ASF plot). (a) Normal FTS feed ( $H_2/CO/N_2 = 6:3:1$ , total flow rate: 30 ml/min; reaction pressure: 20 bar (on gauge)). (b)  $H_2$  rich feed ( $C_2H_4/H_2 = 0.8$ , total flow rate: 60 ml/min; reaction pressure: 20 bar (on gauge)). (c)  $H_2$  limited feed ( $C_2H_4/H_2 = 4.8$ , total flow rate: 60 ml/min; reaction pressure: 20 bar (on gauge)).

**Table 4.4:**  $\alpha$ -value of normal FTS result and  $C_2H_4$  reacted with  $H_2$ .

Temperature (°C)	$\alpha$ -value		
	<i><math>\alpha</math>-olefins + n-paraffins</i>	<i>n-paraffins</i>	<i><math>\alpha</math>-olefins</i>
<b>Feed: <math>H_2/CO/N_2=6:3:1</math></b>			
200	0.78	0.82	0.76
<b>Feed: <math>C_2H_4/H_2=0.8:1</math></b>			
160	0.32		
180	0.29		
220	0.27		
250	0.27		
<b>Feed: <math>C_2H_4/H_2=4.8:1</math></b>			
200	0.25	0.39	0.22
220	0.22	0.38	0.17
250	0.2	0.35	0.17

The  $\alpha$ -value of total n-paraffins +  $\alpha$ -olefins, individual paraffins and olefins under FTS with a syngas feed were calculated and are shown in Table 4.4. The  $\alpha$ -value of total n-paraffins +  $\alpha$ -olefins is 0.78, while the  $\alpha$ -value of the paraffin is 0.82 and olefins is 0.76. A comparison of  $\alpha$ -values of the two feed gases (CO/H<sub>2</sub> and C<sub>2</sub>H<sub>4</sub>:H<sub>2</sub>) shows that a typical FTS has a much higher carbon chain growth factor than that of C<sub>2</sub>H<sub>4</sub> hydrogenation. This result indicates that: either less chain-growth monomer is formed by the reaction of C<sub>2</sub>H<sub>4</sub> and H<sub>2</sub> than the reaction of CO with H<sub>2</sub> or that the monomer is less reactive and that the presence of CO probably has a strong inhibitory effect on hydrogenation of the chain-growth precursor and monomer (chain termination reaction). The CO essentially competes with H<sub>2</sub> for adsorption sites on the catalyst surface; thus, the presence of CO reduces the amount of H<sub>2</sub> adsorbed on the catalyst surface. As this H<sub>2</sub> reacts with chain-growth precursor and monomer (chain termination reaction). It has a significant limiting effect on the chain growth reaction. Based on this idea, the question arises: is it possible to control the  $\alpha$ -value of the hydrogenation-type chain growth product by controlling the amount of H<sub>2</sub> in the adsorbed state?

#### 4.4.2. Possible C<sub>2</sub>H<sub>4</sub> reactions

When combining our research results with the theories in the literature, the reactions of C<sub>2</sub>H<sub>4</sub> with H<sub>2</sub> could be classified as follows:

- (1) C<sub>2</sub>H<sub>4</sub> hydrogenation to ethane ( $C_2H_4 + H_2 \rightarrow C_2H_6$ ).
- (2) C<sub>2</sub>H<sub>4</sub> oligomerization, especially dimerization to C<sub>4</sub> products ( $2C_2H_4 \rightarrow C_4H_8$ ).
- (3) C<sub>2</sub>H<sub>4</sub> hydrogenolysis to methane ( $C_2H_4 + 2 H_2 \rightarrow 2 CH_4$ ).
- (4) Analogical disproportionation ( $2 C_2H_4 + 2 H_2 \rightarrow CH_4 + C_3H_8$ ).

(5) Analogical comproportionation ( $C_2H_4 + C_4H_8 \rightarrow 2 C_3H_6$ ).

(6) Methylene species formed from  $C_2H_4$  demethylation participate in carbon chain growth.

(7)  $C_2H_4$  reacts as a monomer in carbon chain growth.

In order to compare the effect of the different experimental conditions on the product distribution, Table 4.5 lists the product selectivity for  $C_1$  to  $C_4$ .

In this study,  $C_2H_4$  was the sole source of carbon. Thus all products, both odd and even carbon number hydrocarbons, all form from  $C_2H_4$ , which makes it relatively simple to recognise the possible pathways or secondary reactions of  $C_2H_4$  in FTS; these reactions may be limited by CO and/or the products of classical FTS, however these effects do not occur in this study. As the experimental results show, the selectivity of ethane was more than 94% under all the reaction conditions, thus confirming that  $C_2H_4$  hydrogenation is the dominant reaction.

When  $C_2H_4$  hydrogenates to produce ethane in FTS, it changes the ratio of paraffin to olefin, but has no direct impact on the chain growth probability. As shown, high reaction temperatures and a high ratio of  $C_2H_4/H_2$  could inhibit  $C_2H_4$  hydrogenation to some extent, which may be attributed to activation of the C-C bond at a high temperature. However, this change in the reaction kinetics was small and had no significant effect on the product distribution.

**Table 4.5:** The selectivity of products C<sub>1</sub> to C<sub>4</sub> on ethylene hydrogenation condition.

	Temperature (°C)	Selectivity							
		CH <sub>4</sub>	C <sub>2</sub> H <sub>6</sub>	C <sub>3</sub> H <sub>6</sub>	C <sub>3</sub> H <sub>8</sub>	1-C <sub>4</sub> H <sub>8</sub>	C <sub>4</sub> H <sub>10</sub>	Trans-2-C <sub>4</sub> H <sub>8</sub>	Cis-2-C <sub>4</sub> H <sub>8</sub>
Run 5	180	0.5%	98.98%	0%	0.17%	0%	0.35%	0%	0%
Run 6		0.92%	97.34%	0%	0.79%	0%	0.93%	0%	0%
Run 7		0.58%	95.75%	1.01%	0.49%	0.39%	0.30%	0.57%	0.91%
Run 8		0.12%	96.86%	0.34%	0.08%	0.43%	0.18%	0.80%	1.20%
Run 9		0.09%	96.80%	0.29%	0.05%	0.55%	0.16%	0.64%	1.42%
Run 10	100	0.10%	99.18%	0.00%	0.13%	0.00%	0.60%	0.00%	0.00%
	110	0.12%	99.08%	0.00%	0.15%	0.00%	0.64%	0.00%	0.00%
	140	0.24%	98.79%	0.00%	0.27%	0.00%	0.70%	0.00%	0.00%
	160	0.43%	98.36%	0.00%	0.44%	0.00%	0.76%	0.00%	0.00%
	180	1.80%	96.08%	0.18%	0.91%	0.07%	0.89%	0.06%	0.12%
	220	2.33%	95.35%	0.34%	0.98%	0.12%	0.77%	0.09%	0.20%
	250	2.83%	94.64%	0.36%	1.12%	0.12%	0.81%	0.08%	0.15%
Run 11	110	0.03%	98.11%	0.07%	0.02%	0.24%	0.14%	0.33%	1.08%
	140	0.05%	97.04%	0.14%	0.03%	0.44%	0.16%	0.63%	1.51%
	160	0.07%	96.41%	0.23%	0.04%	0.59%	0.16%	0.80%	1.69%
	180	0.09%	96.19%	0.34%	0.04%	0.67%	0.15%	0.82%	1.70%
	200	0.15%	95.69%	0.67%	0.08%	0.70%	0.16%	1.07%	1.48%
	220	0.22%	95.29%	1.08%	0.11%	0.78%	0.15%	1.05%	1.33%
	250	0.34%	95.28%	1.59%	0.15%	0.66%	0.16%	0.79%	1.03%

The  $C_2H_4$  dimerization is a very interesting reaction, since only a small amount of the main dimer (2-butene) is generated when in FTS over a Co catalyst. The generation of 2-olefins is routinely attributed to bond-shift isomerization of the corresponding  $\alpha$ -olefins in FTS [9]. Based on this theory, it is surmised that 2- $\sigma$ -alkyl species generated from partial hydrogenation of  $\alpha$ -olefins, and then dehydrogenated to form 2-olefins. However, Kokes established a model of  $C_2H_4$  dimerization based on the results of a study that used hydrogenation of  $C_2H_4$  over bulk Co [31]. In this model  $C_2H_4$  was reversibly bridge adsorbed on the surface of Co, and transformed to the surface intermediate 1,1- $\sigma$ -ethylidene with the assistance of the dissociated hydrogen atoms. Two molecules of this intermediate encountered head-to-head to generate cis-2-butene, while 1-butene was produced by a head-to-tail encounter. As  $C_2H_4$  could react both as an initiator and monomer under FTS conditions, it could be proposed that  $C_2H_4$  partially hydrogenates to form an ethyl surface species as the chain initiator, and another adsorbed  $C_2H_4$  inserts to generate 1-butene. In our view, 1-butene might form from both  $C_2H_4$  direct dimerization and  $H_2$  assistant carbon chain growth. We also believe that these results support that trans-2-butene is a secondary product isomerized by cis-2-butene and that cis-butene, trans-butene and that 1-butene could be interconverted through internal hydrogen transformation.

$C_2H_4$  hydrogenolysis used to form  $CH_4$  is sensitive to reaction temperature and the quantities of chemisorbed hydrogen. Shi and Davis argue that co-fed  $C_2H_4$  could decrease  $CH_4$  selectivity to some extent [26]. The current experiments show extremely low selectivity to  $CH_4$  for  $H_2$  limited feeds and is in agreement with this conclusion. This might be because  $C_2H_4$  reacts as a monomer in carbon chain growth rather than producing  $CH_4$  from hydrogenolysis.

$C_2H_4$  either reacted directly as a monomer, or demethylated to form methylene, which participated in the chain growth reaction and could be expressed to analogical comproportionation and disproportionation. These reactions generated odd carbon number products, which affected the product distribution. As the results show, the comproportionation and disproportionation were favoured in  $H_2$  limited feeds where there is less dissociated  $H_2$  on the catalyst surface, which is in agreement with the accepted FTS models on Co catalysts. In previous work done by the researchers, Lu et al. reported an olefin quasi-equilibrium reaction existed in FTS when using the same catalyst [13]. This proposed quasi-equilibrium equation is similar to the analogical comproportionation and disproportionation reaction proposed in this work.

In brief, we attempt to isolate the  $C_2H_4$  reaction system in this work, and find various  $C_2H_4$  reaction occurs. This is the first step in investigating and understanding the  $C_2H_4$  reactions in normal FTS. In normal FTS, the strong adsorption of CO on the catalyst surface results in competitive adsorption between CO and olefins ( $C_2H_4$  in this work). This competition directly suppresses some  $C_2H_4$  reaction (like dimerization). Moreover, because of the presence of CO, some important phenomenon is easy to be ignored. As we find in this work, in the absence of CO, the ethylene reacted with  $H_2$  to produce products of  $C_3$ ,  $C_5$  and  $C_6$ , which fitted the typical FTS product distribution. This phenomenon means FTS-type chain growth is not necessarily only derived from the hydrogenation of CO. The chain growth initiators and monomers required for the FTS reaction can also be formed by olefin hydrocracking, although the chain growth probability in these reactions is much lower than in normal FTS. It may give us a new understanding about the FTS mechanism when viewed from this different angle.

#### 4.5. Conclusion

With the aim of investigating the feasible reactions paths of  $C_2H_4$  and their product distribution in Fischer-Tropsch synthesis (FTS), a series of experiments were designed over a  $Co/TiO_2$  catalyst in the absence of  $CO$ . When using  $C_2H_4/N_2$  as the feed gas, no products could be detected under any of the reaction conditions tested. However, when co-feeding  $H_2$  with  $C_2H_4$  over a range of operating temperatures,  $C_2H_4$  reacted, even at  $100\text{ }^\circ C$ . Short chain hydrocarbons (including  $CH_4$ ,  $C_3H_6$ ,  $C_3H_8$ ,  $1-C_4H_8$ ,  $cis-2-C_4H_8$ ,  $trans-2-C_4H_8$ ,  $n-C_4H_{10}$ , etc.) were formed.

In the presence of hydrogen, although the dominant product was ethane, varying the temperature and partial pressure of the reactants could lead to the other reaction pathways being enhanced, resulting in varying product selectivity to  $CH_4$  and  $C_{3-6}$  olefins and paraffins.  $C_2H_4$  hydrogenated to form ethane was slightly inhibited by higher reaction temperatures. The main  $C_4$  product produced from  $C_2H_4/H_2$  feeds was 2-butene, from  $C_2H_4$  dimerization.  $C_2H_4$  hydrogenolysis and demethylation reaction rates were affected by the  $H_2$  partial pressure and therefore the quantity of chemisorbed hydrogen. The selectivity of the products of  $CH_4$ ,  $C_3$  and  $C_5$  with odd carbon numbers increased with increasing temperature. These results indicated that a high temperature preferred the production of odd carbon number hydrocarbons.

In the absence of  $CO$ , the products obtained from the  $C_2H_4$  reacted with  $H_2$  fitted a typical ASF product distribution. This indicated that both the chain-growth monomers and initiators were not necessarily only derived from  $CO$  hydrogenation, but also from  $C_2H_4$  reactions. In FTS,  $C_1$  normally lay above the ideal ASF distribution, while when using  $C_2H_4/H_2$  feeds, the  $C_1$  selectively lay on or even slightly below the ideal ASF plot. The  $\alpha$ -values for the  $C_2H_4$

hydrogenation products was lower (0.32) than that obtained for FTS (0.82) indicating that the rate of termination of the chain growth was higher. Although the feeds used in this work were not the same as that used in normal FTS, the results obtained suggested that  $C_2H_4$  followed various reaction pathways to form different products, and that it acted as a monomer and as an initiator in the chain growth reactions, thus might affect the product distributions during FTS. These results could have implications for the reaction mechanisms of FTS.

## REFERENCES:

1. Qiu, B., Yang, C., Guo, W., Xu, Y., Liang, Z., Ma, D., & Zou, R. (2017). Highly dispersed Co-based Fischer–Tropsch synthesis catalysts from metal–organic frameworks. *Journal of Materials Chemistry A*, 5(17), 8081-8086.
2. Savost'yanov, A. P., Yakovenko, R. E., Sulima, S. I., Bakun, V. G., Narochnyi, G. B., Chernyshev, V. M., & Mitchenko, S. A. (2017). The impact of Al<sub>2</sub>O<sub>3</sub> promoter on an efficiency of C<sub>5+</sub> hydrocarbons formation over Co/SiO<sub>2</sub> catalysts via Fischer-Tropsch synthesis. *Catalysis Today*, 279, 107-114.
3. Liu, C., He, Y., Wei, L., Zhang, Y., Zhao, Y., Hong, J., ... & Li, J. (2018). Hydrothermal carbon-coated TiO<sub>2</sub> as support for Co-based catalyst in Fischer–Tropsch synthesis. *ACS Catalysis*, 8(2), 1591-1600.
4. Cheng, Q., Tian, Y., Lyu, S., Zhao, N., Ma, K., Ding, T., ... & Gao, F. (2018). Confined small-sized cobalt catalysts stimulate carbon-chain growth reversely by modifying ASF law of Fischer–Tropsch synthesis. *Nature communications*, 9(1), 1-9.
5. Lyu, S., Wang, L., Zhang, J., Liu, C., Sun, J., Peng, B., ... & Nie, L. (2018). Role of active phase in Fischer–Tropsch synthesis: Experimental evidence of CO activation over single-phase cobalt catalysts. *ACS Catalysis*, 8(9), 7787-7798.
6. Sun, B., Tan, H., Liu, S., Lyu, S., Zhang, X., Zhang, Y., ... & Wang, L. (2019). Novel Cobalt Catalysts Supported on Metal–Organic Frameworks MIL-53 (Al) for the Fischer–Tropsch Synthesis. *Energy Technology*, 7(4), 1800802.
7. Dry, M. E. (1990). The Fischer-Tropsch process-commercial aspects. *Catalysis today*, 6(3), 183-206.

8. Dry, M. E. (2002). The Fischer–Tropsch process: 1950–2000. *Catalysis today*, 71(3-4), 227-241.
9. Sarup, B., & Wojciechowski, B. W. (1988). Studies of the Fischer-Tropsch synthesis on a cobalt catalyst i. evaluation of product distribution parameters from experimental data. *The Canadian Journal of Chemical Engineering*, 66(5), 831-842.
10. Pichler, H., Schulz, H., & Elstner, M. (1967). Gesetzmässigkeiten bei der synthese von kohlenwasserstoffen aus kohlenoxid und wasserstoff. *BRENNSTOFF-CHEMIE*, 48(3), 78.
11. Soled, S., Iglesia, E., & Fiato, R. A. (1990). Activity and selectivity control in iron catalyzed Fischer-Tropsch synthesis. *Catalysis Letters*, 7(1-4), 271-280.
12. Schulz, H., & Claeys, M. (1999). Reactions of  $\alpha$ -olefins of different chain length added during Fischer–Tropsch synthesis on a cobalt catalyst in a slurry reactor. *Applied Catalysis A: General*, 186(1-2), 71-90.
13. Lu, X., Hildebrandt, D., Liu, X., & Glasser, D. (2012). A Thermodynamic Approach to Olefin Product Distribution in Fischer–Tropsch Synthesis. *Industrial & engineering chemistry research*, 51(51), 16544-16551.
14. Iglesia, E., Soled, S. L., Fiato, R. A., & Via, G. H. (1993). Bimetallic synergy in cobalt ruthenium Fischer-Tropsch synthesis catalysts. *Journal of Catalysis*, 143(2), 345-368.
15. Tau, L. M., Dabbagh, H. A., & Davis, B. H. (1990). Fischer-Tropsch synthesis: carbon-14 tracer study of alkene incorporation. *Energy & fuels*, 4(1), 94-99.
16. Herzog, K., & Gaube, J. (1989). Kinetic studies for elucidation of the promoter effect of alkali in Fischer-Tropsch iron catalysts. *Journal of Catalysis*, 115(2), 337-346.

17. Liu, X., Li, X., & Fujimoto, K. (2007). Effective control of carbon number distribution during Fischer–Tropsch synthesis over supported cobalt catalyst. *Catalysis Communications*, 8(9), 1329-1335.
18. Shi, B., & Davis, B. H. (2003). Fischer–Tropsch synthesis: evidence for chain initiation by ethene and ethanol for an iron catalyst. *Topics in catalysis*, 26(1-4), 157-161.
19. Jacobs, G., & Davis, B. H. (2014). Applications of isotopic tracers in Fischer–Tropsch synthesis. *Catalysis Science & Technology*, 4(11), 3927-3944.
20. Jordan, D. S., & Bell, A. T. (1986). Influence of ethylene on the hydrogenation of carbon monoxide over ruthenium. *The Journal of Physical Chemistry*, 90(20), 4797-4805.
21. Hall, W. K., Kokes, R. J., & Emmett, P. H. (1960). Mechanism studies of the Fischer-Tropsch synthesis: the incorporation of radioactive ethylene, propionaldehyde and propanol. *Journal of the American Chemical Society*, 82(5), 1027-1037.
22. Craxford, S. R. (1939). The Fischer-Tropsch synthesis of hydrocarbons, and some related reactions. *Transactions of the Faraday Society*, 35, 946-958..
23. Eidus, Y. T., Zelinskii, N. D., & Ershov, N. I. (1948). O Kondensiruyushchem Deistvii Metilenovykh Radikalov Na Etilen. *Doklady Akademii Nauk SSSR*, 60(4), 599-601.
24. Schulz, H., Ramananda, R., & Elstner, M. (1970). Carbon-14 studies for the evaluation of the reaction mechanism of the Fischer--Tropsch synthesis. *Erdoel Kohle, Erdgas, Petrochem. Brennst.-Chem.*, 23(10).
25. Kibby, C. L., Pannell, R. B., & Kobylinski, T. P. (1984). Hydrogenation of olefins in the presence of carbon monoxide on supported cobalt catalysts. *Preprints-American Chemical Society. Division of Petroleum Chemistry*, 29(4), 1113-1119.

26. Snel, R., & Espinoza, R. L. (1987). Secondary reactions of primary products of the Fischer-Tropsch synthesis: Part 1. The role of ethene. *Journal of molecular catalysis*, 43(2), 237-247.
27. Fujimoto, K., Fan, L., & Yoshii, K. (1995). New controlling method for product distribution in Fischer-Tropsch synthesis reaction. *Topics in Catalysis*, 2(1-4), 259-266.
28. Eidus, Y. T., & Nefedov, B. K. (1960). Polymerisation of isobutene. *Russian Chemical Reviews*, 29(7), 394.
29. Eidus, Y. T. (1967). The mechanism of the Fischer-Tropsch reaction and the initiated hydropolymerisation of alkenes, from radiochemical and kinetic data. *Russian Chemical Reviews*, 36(5), 338.
30. Éidus, Y. T., Ershov, N. I., & Hoang, C. Y. (1974). Activity of Co catalysts, deposited on zeolites, in the hydropolymerization of ethylene, initiated by carbon monoxide at ~200°. *Bulletin of the Academy of Sciences of the USSR, Division of chemical science*, 23(8), 1798-1800.
31. Kokes, R. J. (1969). Formation of dimeric products during steady state hydrogenation of ethylene over cobalt. *Journal of Catalysis*, 14(1), 83-92.
32. Cant, N. W., Liu, I. O., & Scott, J. A. (2013). Ethylene oligomerisation over Co/SiO<sub>2</sub> in the presence of trace carbon monoxide: the Eidus reaction revisited. *Catalysis today*, 215, 267-275.
33. McNab, A. I., McCue, A. J., Dionisi, D., & Anderson, J. A. (2017). Quantification and qualification by in-situ FTIR of species formed on supported-cobalt catalysts during the Fischer-Tropsch reaction. *Journal of Catalysis*, 353, 286-294.

34. McNab, A. I., McCue, A. J., Dionisi, D., & Anderson, J. A. (2018). Combined quantitative FTIR and online GC study of Fischer-Tropsch synthesis involving co-fed ethylene. *Journal of Catalysis*, 362, 10-17.
35. Yao, Y., Hildebrandt, D., Glasser, D., & Liu, X. (2010). Fischer– Tropsch synthesis using H<sub>2</sub>/CO/CO<sub>2</sub> syngas mixtures over a cobalt catalyst. *Industrial & engineering chemistry research*, 49(21), 11061-11066.
36. Feyzi, M., Khodaei, M. M., & Shahmoradi, J. (2012). Effect of preparation and operation conditions on the catalytic performance of cobalt-based catalysts for light olefins production. *Fuel processing technology*, 93(1), 90-98.
37. Jalama, K., Coville, N. J., Xiong, H., Hildebrandt, D., Glasser, D., Taylor, S., ... & Hutchings, G. J. (2011). A comparison of Au/Co/Al<sub>2</sub>O<sub>3</sub> and Au/Co/SiO<sub>2</sub> catalysts in the Fischer–Tropsch reaction. *Applied Catalysis A: General*, 395(1-2), 1-9.
38. Liu, X., Li, X., Suehiro, Y., & Fujimoto, K. (2007). Elucidation of reaction network and effective control of carbon number distribution in the three phase Fischer–Tropsch synthesis. *Applied Catalysis A: General*, 333(2), 211-218.
39. Zhuo, M., Borgna, A., & Saeys, M. (2013). Effect of the CO coverage on the Fischer–Tropsch synthesis mechanism on cobalt catalysts. *Journal of catalysis*, 297, 217-226.

## Chapter 5

### **Fischer-Tropsch synthesis with ethylene co-feeding: experimental evidence of the CO-insertion mechanism at low temperature**

This work had been published in the AIChE Journal, 2020, e17029.

Part of this work was presented at Syngas Conversion 2018 and CATSA 2018.

---

#### **ABSTRACT**

Experiments were performed at both normal and rather extreme Fischer-Tropsch Synthesis (FTS) operating conditions over a typical cobalt-based catalyst, with the aim of exploring if aspects of the reaction mechanism could be elucidated. The results show that CO reacted when co-feeding  $C_2H_4$  with syngas, while CO did not react with  $H_2$  in absence of  $C_2H_4$ , under extremely low-temperature conditions (140 °C). The adsorbed CO and  $C_2H_4$  may behave as monomers and initiators, respectively, and react with each other to form long chain hydrocarbons. It suggest that the C-C bond coupling precedes the C-O bond dissociation, which is consistent with the CO-insertion mechanism.  $C_{3-6}$  product distribution with a feed of  $H_2/CO/C_2H_4$  at low temperature followed the same trends in terms of normal FTS product distribution. The observed FTS-type chain growth reaction that occurs at low temperatures (140 °C) when co-feeding  $C_2H_4$  may provide new insights into the chemistry of FTS.

## 5.1. Introduction

The Fischer Tropsch Synthesis (FTS) reaction converts syngas (a mixture of CO and H<sub>2</sub>) to liquid fuels and other base chemicals using Co and Fe based catalysts [1-3]. Syngas used for industrial FTS processes is currently derived from either natural gas or coal, but could be produced from renewable sources such as municipal waste and biomass. This offers a possible method to reduce global dependence on fossil fuels. The products of FTS are mainly paraffins, olefins, aromatic hydrocarbons and oxygenates with carbon numbers ranging from 1 to more than 50 [4-5]. Over the past 90 years, scientists have proposed various reaction mechanisms for the FTS reaction in an attempt to describe the observed product distribution and reaction kinetics [6]. However, there is still no general agreement about the details of the mechanism, due to the complex product spectrum and the behaviour of FTS systems [7].

It is widely accepted that the FTS reaction is a step-wise carbon chain growth polymerization process [8]. The reactants of FTS are first converted to initiators and monomers, and the monomers then polymerise to longer chain hydrocarbon products [2, 9]. Many researchers have focused on the chemical structure of the initiators and monomers and have proposed several mechanisms [9-14, 18]. The mechanisms differ in terms of the suggested molecular structure of both the initiator and monomer species. Among these mechanisms, we would like to highlight two distinct classes of mechanism, namely: the CO-dissociation type mechanism, where CO is dissociated to form monomers and/or initiators; and the CO-insertion mechanism, where adsorbed CO is incorporated into the chain structure.

(1) CO-dissociation type mechanism (Monomer: CH<sub>x</sub>\*; Initiator: CH<sub>x</sub>\*)

Fischer and Tropsch discovered FTS nearly 100 years ago, and proposed the carbide mechanism, whereby CH<sub>2</sub>\* is both a chain-growth monomer and an initiator [10]. With this mechanism, the adsorbed CO directly dissociates to form a surface metal carbide C\*.

Subsequently,  $C^*$  partially hydrogenates to  $CH_2^*$ , which reacts in a step-wise chain growth reaction to form long chain hydrocarbons. Experimental evidence has shown that the proposed intermediate  $CH_2^*$  state does not undergo self-polymerization, and alternative carbon chain monomers and initiators have been proposed [9]. Thus, the initial carbide mechanism has been modified using various assumptions, such as:

a) Alkyl mechanism: proposed by Brady and Pettit, based on their experimental results [9], in which the chain growth monomer is still  $CH_2^*$ , but the carbon chain initiator is  $CH_3^*$ , rather than  $CH_2^*$ .

b) Alkenyl mechanism: proposed by Maitlis et al., [11] who also proposed  $CH_2^*$  as the chain-growth monomer. However, an adsorbed vinyl ( $CH_2=CH^*$ ) is regarded as the initiator of carbon chain growth. In this model, the hydrocarbon surface species  $CH_2^*$  and  $CH^*$  are intermediates in forming the initiator.

c) Alkylidene–hydride–methylidyne mechanism: proposed by Ciobîcă et al. [12] It suggests that the chain-growth monomer is not  $CH_2^*$ , but rather  $CH^*+H^*$ . The carbon chain initiator is isomeric vinyl ( $CH-CH_2^*$ ).

d) More recently, Weststrate et al. proposed a chain growth mechanism in which alkylidyne reacts as the chain initiator and the monomer is  $CH^*$  [13].

The mechanisms, mentioned above, are all based on CO directly dissociating to form the monomers and initiators. However, in the 1950s, Storch et al. suggested that the C-C bond coupling is based on an oxygen-containing intermediate hydroxycarbene (HCOH), which is also a CO-dissociation mechanism, but it is different to the carbide mechanism [14]. Moreover, some recent studies that used density functional theory (DFT) found that the direct dissociation of CO requires a high intrinsic activation barrier on the surface of FTS catalysts [7, 15-16], which limits the rate of monomer formation. Furthermore, theoretical results have

shown that the adsorbed CO is more easily dissociated in the presence of H\* on a flat Co (0001) surface [16], which leads to the proposed H-assisted CO-dissociation mechanism.<sup>7</sup> With this mechanism, the adsorbed H\* adds to CO\* before the C-O bond breaks. Further calculations indicate that while H-assisted CO-dissociation is preferred for the Co-fcc phase, direct CO-dissociation is more important for the Co-hcp phase [17]. Therefore, the CO-dissociation type mechanism is involved in both direct and indirect dissociation paths [7, 10-14, 18]. (See Figure 5.1 (a).)

(2) The CO-insertion mechanism, (Monomer: CO\*; Initiator: CHx\*.)

Pichler et al. [19] proposed the CO-insertion mechanism, which considers the adsorbed CO as the FTS monomer. Similar to the CO-dissociation mechanism, with this mechanism, the carbon chain initiator is a surface intermediate hydrocarbon species CHx\* formed by the dissociation and hydrogenation of the adsorbed CO. (See Figure 5.1 (b).) The carbon chain occurs by repeated insertion and hydrogenation of CO\* in metal-hydrogen bonds or metal-alkyl bonds to form C-C bonds. Since the formation of the carbon chain initiator still requires CO-dissociation with this mechanism, it is difficult to identify from experiments whether the monomer is the adsorbed CO or a hydrocarbon intermediate species CHx\* from the CO-dissociation type mechanism.

Temperature-programmed X-ray photoelectron spectroscopy studies of ethanol decomposition have shown that C-O bonds in RCH<sub>2</sub>CO\* can cleave strongly onto the surface of Co (0001) under FTS reaction conditions [16]. In addition, Chakrabarti et al. used the isotope-labelling method to investigate the role of alcohols and CO<sub>2</sub> in FTS, and found that the carbon chain growth conformed to the CO-insertion mechanism [20]. Moreover, in a transient kinetic study of CO hydrogenation over Co-based model catalysts, Schweicher et al. found that the time response in transient and reverse transient experiments of gaseous

reactants and products was consistent with the CO-insertion mechanism [21]. However, direct experimental evidence is still to be provided [7].

There are three basic reactions involving carbon when converting syngas to hydrocarbon products in FTS, namely: C-O bond dissociation; C-H bond formation; and C-C bond coupling. The biggest difference between the CO-insertion mechanism and the CO-dissociation mechanism is that the C-O bond dissociation occurs before the C-C band coupling in the CO dissociation mechanism; conversely, the C-C band coupling occurs before the C-O bond dissociation in the CO-insertion mechanism.

Most of the current mechanistic FTS investigations focus on the nature of the monomer species  $\text{CH}_x^*$ , including both experimental and DFT research [22-26]. It worth noting that Zhuo et al. studied the effect of CO coverage on FTS pathways by means of DFT, and concluded that the CO-insertion mechanism is preferable to other mechanisms [27-28]. However, there is a lack of solid experimental evidence to support this.

In order to distinguish between possible FTS reaction mechanisms, a group of experiments were conducted over a typical Co-based catalyst using three different feed mixtures (namely:  $\text{H}_2/\text{CO}/\text{N}_2$ ,  $\text{H}_2/\text{CO}/\text{C}_2\text{H}_4/\text{N}_2$ (or Ar) and  $\text{H}_2/\text{C}_2\text{H}_4$ ) at reaction temperatures between 100 °C and 220 °C. These rather extreme operating conditions were used to clarify the potential initiators and monomers of the chain growth reaction. In the meantime, the role of  $\text{C}_2\text{H}_4$  in FTS was identified and discussed.

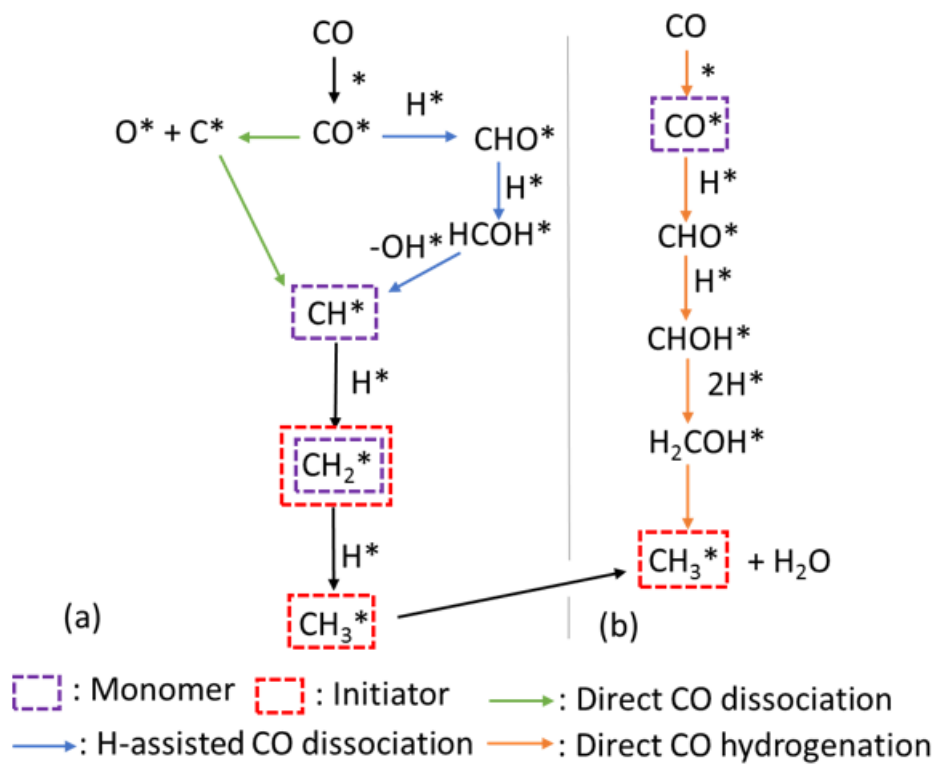


**Figure 5.1:** Examples of the possible CO activation pathways: (a) CO-dissociation mechanism, [7, 10-14]; (b) CO-insertion mechanism [18]

## **5.2. Experimental**

### **5.2.1. Preparation and characterization of catalysts**

A typical Co-based FTS catalyst (15 wt. % Co/TiO<sub>2</sub>) was used in this research. It was prepared using the traditional incipient wetness method [29]. TiO<sub>2</sub> (Degussa P-25) was used as the catalyst support precursor. A series of pre-treatments were required, before the support was loaded with cobalt. The paste was made by mixing distilled water and P-25 TiO<sub>2</sub> in a mass ratio of 1: 1. It was dried in a vacuum drying oven at 120 °C for 2 hours and then: calcined in a muffle oven, heated from room temperature to 400 °C at a rate of 5 °C/min; and maintained at 400 °C for 6 hours. It was then cooled to room temperature, and the paste was then crushed and sieved to particles with a size of 0.5-1 mm. After the water saturation experiment, the TiO<sub>2</sub> support was added to the Co(NO<sub>3</sub>)<sub>3</sub> aqueous solution (calculated using the weight amount of support), and allowed to absorb into it uniformly by impregnation. The catalyst was then dried and calcined using the same process as used for the support pre-treatment.

The results of the catalyst characterization (including XRD, BET, TEM and TPR) were reported in our previous paper [30]. It can be seen that the catalyst used in this experiment was a typical supported Co-based Fischer-Tropsch catalyst.

### **5.2.2. Experimental design**

1 g of catalyst was loaded into a stainless steel tubular fixed bed reactor with a total length of 203.7 mm and an inner diameter of 8 mm. Three sets of experiments were conducted in this work.

- (1) (Set 1) The syngas feed was switched between a mixture of (CO/H<sub>2</sub>/C<sub>2</sub>H<sub>4</sub>/N<sub>2</sub>) and a mixture of (CO/H<sub>2</sub>/N<sub>2</sub>), and a range of reaction temperatures were tested. Mass flow controllers were used to control the flow rate of the four gases (CO, H<sub>2</sub>, C<sub>2</sub>H<sub>4</sub>, N<sub>2</sub>). Firstly, a feed mixture of CO/H<sub>2</sub>/C<sub>2</sub>H<sub>4</sub>/N<sub>2</sub> was introduced into the reactor. The flow rate of C<sub>2</sub>H<sub>4</sub> was then stopped, while keeping the flow rates of CO, H<sub>2</sub> and N<sub>2</sub> constant. After the reactor stabilised, feeding of C<sub>2</sub>H<sub>4</sub> was resumed, while still keeping the flow rates of CO, H<sub>2</sub> and N<sub>2</sub> constant. The catalyst activity and product selectivity were monitored. The molar amount of H<sub>2</sub> in the C<sub>2</sub>H<sub>4</sub> co-feeding experiments was set so that there was sufficient H<sub>2</sub> to hydrogenate all the C<sub>2</sub>H<sub>4</sub> to ethane, as well as convert all the CO to -CH<sub>2</sub>- units, as occurs in FTS. Hence we labelled this set of experiments "H<sub>2</sub>-rich". The molar flow rates of CO and H<sub>2</sub> in the feed were the same for both feeds.
- (2) (Set 2) A syngas mixture (CO/H<sub>2</sub>/C<sub>2</sub>H<sub>4</sub>/Ar) with varying partial pressure of C<sub>2</sub>H<sub>4</sub> and constant partial pressures of H<sub>2</sub> and CO was used. In this experiment, the mole fraction of CO and H<sub>2</sub> was kept constant at 1:2, while the mole fraction of C<sub>2</sub>H<sub>4</sub> was varied from 0 to 30% by changing the relative flow rates of Ar and C<sub>2</sub>H<sub>4</sub>.
- (3) (Set 3) For comparison purposes, another group of experiments (C<sub>2</sub>H<sub>4</sub> hydrogenation in the absence of CO) were conducted. Detailed information on the feed gas used in the various experiments is provided in Table 5.1.

The operating temperature was controlled using a temperature regulator. The reaction temperature was varied between 100 °C and 220 °C. A backpressure regulator was used to maintain the reaction pressure at 20 bar (gauge). In order to prevent condensation of the long chain hydrocarbons in the downstream piping and fittings, and to ensure that all the products entering the online gas chromatograph (GC) were in the gas phase, a hot trap between the backpressure regulator and the online GC was heated to 120 °C, to condense the long chain

hydrocarbons in the tailgas before they entered the GC. All the pipes, fittings (apart from the hot trap) and valves from the reactor to the online GC were heated and maintained at 170 °C to prevent condensation of the products. Experiments were run at each of the reaction conditions for more than 24 hours to ensure a steady state. An online GC - Agilent 7890A with two FID and one TCD detector - was used to analyse the tailgas.

**Table 5.1:** Reaction condition for the various experiments

<i>Experiment</i>	<i>TOS</i>	<i>Temperature</i>	<i>Total Pressure</i>	<i>Total flow rate</i>	<i>Feed partial pressure (Bar)</i>			
	<i>When run started</i>	<i>°C</i>	<i>Bar (gauge)</i>	<i>ml/min</i>	<i>CO</i>	<i>H<sub>2</sub></i>	<i>C<sub>2</sub>H<sub>4</sub></i>	<i>N<sub>2</sub>/Ar</i>
Set 1 H <sub>2</sub> Rich Feed	0	100	20	80	1.6	11.0	7.9	0.5
	24	120	20	80	1.6	11.0	7.9	0.5
	48	140	20	80	1.6	11.0	7.9	0.5
	96	140	20	50	2.5	17.6	0	0.9
	144	140	20	80	1.6	11.0	7.9	0.5
	168	160	20	80	1.6	11.0	7.9	0.5
	192	160	20	50	2.5	17.6	0	0.9
	216	160	20	80	1.6	11.0	7.9	0.5
	240	180	20	80	1.6	11.0	7.9	0.5
	264	180	20	50	2.5	17.6	0	0.9
	312	180	20	80	1.6	11.0	7.9	0.5
	336	200	20	80	1.6	11.0	7.9	0.5
	360	200	20	50	2.5	17.6	0	0.9
	384	220	20	80	1.6	11.0	7.9	0.5
432	220	20	50	2.5	17.6	0	0.9	
Set 2		160 to 220	20	50	4.2	8.4	0	8.4
	Each experiment	160 to 220	20	50	4.2	8.4	2.1	6.3
	ran for 24 hours	160 to 220	20	50	4.2	8.4	4.2	4.2
		160 to 220	20	50	4.2	8.4	6.3	2.1
Set 3: C <sub>2</sub> H <sub>4</sub> hydrogenation	Each experiment	100	20	50	0	11.7	9.3	0
	ran for 24 hours	120	20	50	0	11.7	9.3	0
		140	20	50	0	11.7	9.3	0

### 5.3. Results and discussion

#### 5.3.1. Set 1: H<sub>2</sub> rich conditions

A significant increase in the activity of CO, H<sub>2</sub> and C<sub>2</sub>H<sub>4</sub> was observed with an increasing reaction temperature, as expected. However, the CO conversion depended strongly on the presence (or absence) of C<sub>2</sub>H<sub>4</sub> in the feed. The CO conversion is shown in Figure 5.2, which reveals four regions:

- (1) At very low reaction temperatures (from 100 to 120 °C), the CO conversion is very low (less than 5%), even when C<sub>2</sub>H<sub>4</sub> is co-fed into the reactor. The GC is not very accurate when the reaction conversion is lower than 5%. However, no other products could be detected at these low temperatures, except for very small amounts of ethane measured at 120 °C. This indicates that CO was almost non-reactive and only a small amount of C<sub>2</sub>H<sub>4</sub> was hydrogenated to ethane at these low temperatures.
- (2) When the reaction temperature was increased [140 °C, 160 °C], the CO conversion increased significantly when C<sub>2</sub>H<sub>4</sub> was co-fed to the reactor, to: around 20% at 140 °C; and close to 40% at 160 °C. When the feed was switched to syngas only, the CO conversion dropped to 0%. This indicates that there is no CO hydrogenation reaction at these low temperatures when using syngas as a feed. When the feed was switched back to C<sub>2</sub>H<sub>4</sub> co-feeding with syngas, the CO conversion increased back to the original value. This verifies that the lack of observed CO conversion when using a syngas (only) feed is not due to catalyst deactivation. It also proves that C<sub>2</sub>H<sub>4</sub> promotes the reactivity of CO at these temperatures.
- (3) When the reaction temperature was further increased [180 °C, 200 °C], CO reacted with H<sub>2</sub> in the absence of C<sub>2</sub>H<sub>4</sub>, but the activity was relatively low (less than 5% at 180 °C and less than 30% at 200 °C). However, when C<sub>2</sub>H<sub>4</sub> was co-fed with syngas, the

CO conversion increased, (to around 40%), which is similar to what was observed at 160 °C. This indicates that the presence of C<sub>2</sub>H<sub>4</sub> still promotes the reactivity of CO at these temperatures. However, when co-feeding C<sub>2</sub>H<sub>4</sub>, increasing the temperature from 160 to 200 °C did not significantly increase the CO conversion. This implies that there is a limit to the degree that C<sub>2</sub>H<sub>4</sub> can promote CO hydrogenation in these experiments.

- (4) When the temperature was increased to 220 °C, the CO conversion increased slightly to around 48% when co-feeding C<sub>2</sub>H<sub>4</sub>. At this temperature, when using the (hydrogen rich) syngas feed, the CO was almost completely converted. Thus, at this temperature, the addition of C<sub>2</sub>H<sub>4</sub> inhibits the CO reactivity, rather than promoting it, as is observed at lower temperatures. This could be due to a number of factors, including competitive adsorption between CO and C<sub>2</sub>H<sub>4</sub> on the catalyst surface or low H<sub>2</sub> partial pressure, due to the hydrogen being consumed by the C<sub>2</sub>H<sub>4</sub> hydrogenation reaction. (See Figure 5.2.)

As the reaction temperature is increased, the C<sub>2</sub>H<sub>4</sub> conversion increases to 100% at temperatures of 180 °C or higher, which indicates that C<sub>2</sub>H<sub>4</sub> is either used as an initiator for the chain growth reaction or completely hydrogenated to form mainly ethane. (See Supplementary Material in Figure S1 (b).) As mentioned by Schulz et al., the main reaction of the co-fed C<sub>2</sub>H<sub>4</sub> is hydrogenation to ethane [31], while Hall et al. and Eidus et al. reported that C<sub>2</sub>H<sub>4</sub> could react as the chain initiator under Co-FTS [32-33]. In addition, Hutchings et al. reported that co-fed C<sub>2</sub>H<sub>4</sub> could either form a C<sub>1</sub> species that can react further to produce CH<sub>4</sub> and higher hydrocarbons or molecularly incorporate to form other species [34].

In brief, when co-feeding C<sub>2</sub>H<sub>4</sub>, although the partial pressures of CO and H<sub>2</sub> were much lower than those without C<sub>2</sub>H<sub>4</sub> co-feeding (Table 5.2), much higher CO and H<sub>2</sub> conversions were

obtained when co-feeding  $C_2H_4$ . This indicates that adding  $C_2H_4$  strongly promotes the reactivity of CO at reaction temperatures equal to or less than 200 °C. It also indicates that the reaction of CO is dependent on the presence of  $C_2H_4$  at low reaction temperatures. At higher temperatures (220 °C), it was difficult to conclude that the increase in CO conversion was due to the  $C_2H_4$  added to the feed. For this reason, we conducted another set of experiments (Set 2 in Table 5.1), in which: the total flowrates, as well as the partial pressure of CO and  $H_2$  were fixed; while the partial pressure of  $C_2H_4$  was varied by adjusting the partial pressure of the inert gas of Ar in the feed. (See the section 5.3.2 “Set 2: Constant Partial Pressure of  $H_2$  and CO and Varying Partial Pressure  $C_2H_4$ ”)

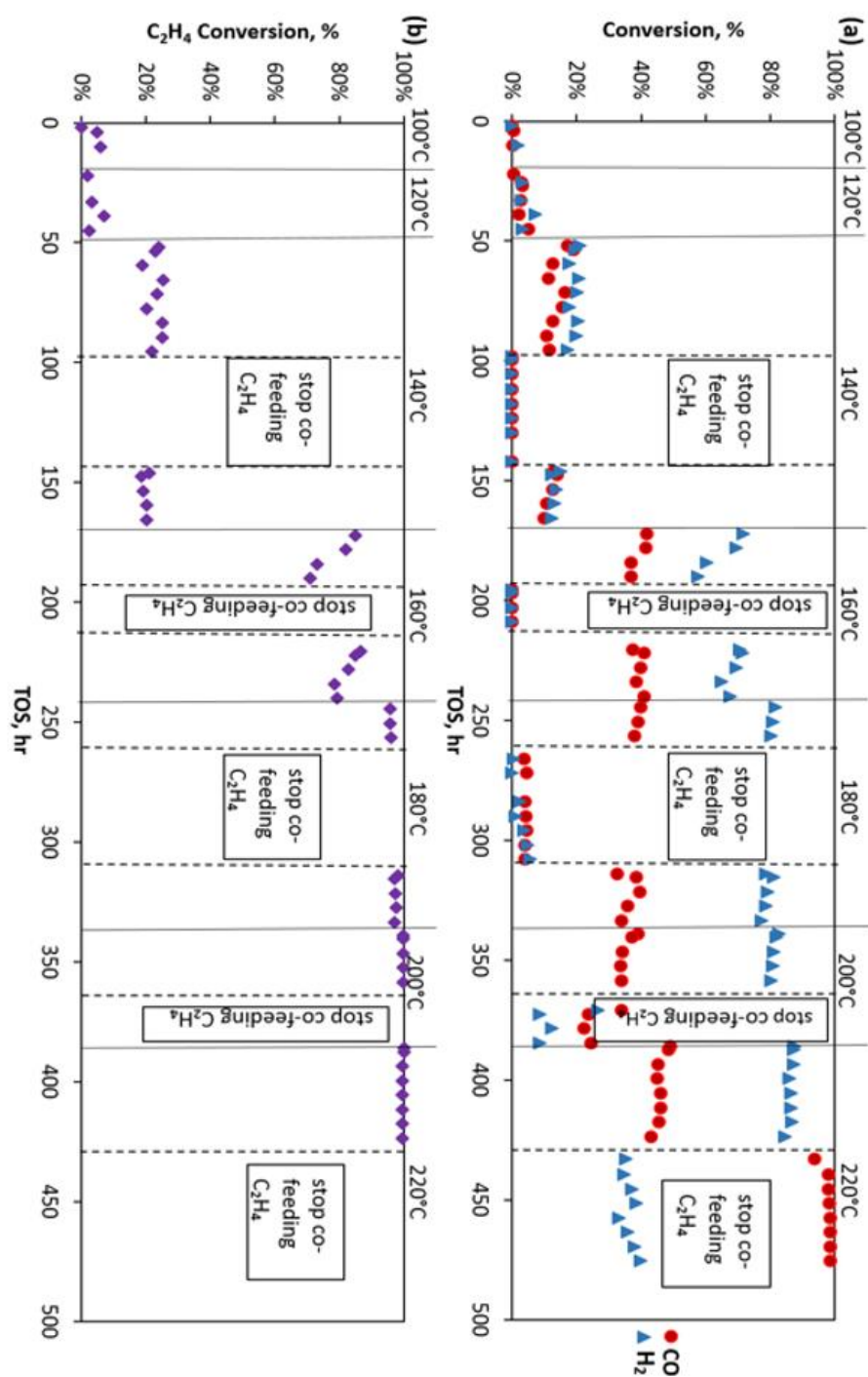


**Figure 5.2:** Conversion of reactants for reaction temperatures between 100 and 220 °C, over a catalyst of 15% Co/TiO<sub>2</sub>: (a) CO and H<sub>2</sub> conversion; (b) C<sub>2</sub>H<sub>4</sub> conversion. (Reaction conditions: 20 bar: (i) feed with C<sub>2</sub>H<sub>4</sub>: 80 ml/min with molar composition 52.5% H<sub>2</sub>/ 7.5% CO/ 37.5% C<sub>2</sub>H<sub>4</sub>/ 2.5% N<sub>2</sub>; and (ii) feed without C<sub>2</sub>H<sub>4</sub> 50 ml/min with composition 84% H<sub>2</sub>/ 12% CO / 4% N<sub>2</sub>.)

**Table 5.2:** Reactant activity, product selectivity and formation rate over a FT catalyst of 15% Co/TiO<sub>2</sub> during low temperature reaction.

Feed	55.5%H <sub>2</sub> / 45.5%C <sub>2</sub> H <sub>4</sub>			52.5%H <sub>2</sub> / 37.5%C <sub>2</sub> H <sub>4</sub> / 2.5%N <sub>2</sub> / 7.5%CO		
	100 °C	120 °C	140 °C	100 °C	120 °C	140 °C
Temperature (°C)	100 °C	120 °C	140 °C	100 °C	120 °C	140 °C
H <sub>2</sub> conversion (%)	84.05%	84.56%	84.32%	0.00%	4.41%	17.29%
C <sub>2</sub> H <sub>4</sub> conversion (%)	100.00%	100.00%	100.00%	0.00%	4.23%	21.85%
CO conversion (%)	/	/	/	0.00%	3.13%	11.66%
CH <sub>4</sub> selectivity (%)	0.08%	0.11%	0.23%	0.00%	0.33%	0.38%
CH <sub>4</sub> formation rate (mmol/min)	1.59E-03	2.01E-03	4.35E-03	0.00E+00	1.00E-05	8.73E-05
C <sub>2</sub> H <sub>6</sub> selectivity (%)	99.24%	99.18%	98.84%	0.00%	78.83%	65.75%
C <sub>2</sub> H <sub>6</sub> formation rate (mmol/min)	9.70E-01	9.70E-01	9.66E-01	0.00E+00	2.42E-02	1.76E-01

Before we consider the results for Set 2, we would like to compare the experimental results obtained with a feed of CO/H<sub>2</sub>/C<sub>2</sub>H<sub>4</sub>/N<sub>2</sub> (Set 1) to the results when using a feed of C<sub>2</sub>H<sub>4</sub>/H<sub>2</sub> (Set 3). C<sub>2</sub>H<sub>4</sub> hydrogenation experiments were run using the same catalyst and with feeds containing different proportions of C<sub>2</sub>H<sub>4</sub>/H<sub>2</sub> (no CO), as described in Table 5.1. When the ratio of C<sub>2</sub>H<sub>4</sub> to H<sub>2</sub> was above 1, C<sub>2</sub>H<sub>4</sub> converted completely to mainly ethane (selectivity greater than 98%), even at a very low temperature (100 °C). (See Table 5.2.) In addition, in the absence of CO, the formation of methane can only come from hydrocracking of C<sub>2</sub>H<sub>4</sub>. As demonstrated by the extremely low methane selectivity (less than 0.25%), this indicates that hydrocracking reaction of C<sub>2</sub>H<sub>4</sub> is slow under these conditions. We might therefore infer that, under these conditions, there is a limited amount of CH<sub>x</sub>\* on the surface, as we would have expected this species to hydrogenate to form methane if it had been present in any significant quantity.

The results shown in both Table 5.2 and Figure 5.2 indicate that even relatively small levels of CO (7.5%) disrupt the hydrogenation of C<sub>2</sub>H<sub>4</sub> at 100 °C, which indicates that CO must competitively adsorb on the surface at these temperatures, even at low concentrations in the feed gas. However, even though CO must be adsorbed onto the surface of the catalyst, the hydrogenation of CO only occurs at: 140 °C or higher when C<sub>2</sub>H<sub>4</sub> is co-fed with syngas; and 180 °C or higher for a feed of syngas only. This would seem to imply that C<sub>2</sub>H<sub>4</sub> is acting as an initiator, as there is no FT activity at 140 °C when using a syngas feed.

It has previously been reported that C<sub>2</sub>H<sub>4</sub> can initiate the FTS reaction [32-33], although this effect was observed at much higher temperatures than reported in this research. Recently, it has been reported that C<sub>2</sub>H<sub>4</sub> can act as an initiator of chain growth, as well as form C<sub>1</sub> monomers by C<sub>2</sub>H<sub>4</sub> decomposition at a relatively high temperature and a low pressure (1.85 bar) [35]. However, in this work, the lower temperatures and higher pressures resulted in

slower rates of  $C_2H_4$  decomposition, as evidenced by the extremely low selectivity to methane observed at 140 °C when  $C_2H_4$  is co-fed with syngas. (See Table 5.2.) This phenomenon indicates that the route to form the chain growth monomer is not mainly from  $C_2H_4$  hydrocracking. Moreover, the results further seem to imply that the rate limiting step at this temperature (140 °C) is the formation of the initiator and not the monomer, as once an initiator ( $C_2H_4$ ) is present, the FTS reaction occurs, even at 140 °C. This indicates that a monomer is present and formed at a rate sufficient to sustain the FTS reaction. In addition, based on the low methane selectivity, we might infer that, at these temperatures, the monomer must be  $CO^*$  instead of  $CH_x^*$ , as we know that CO adsorbs strongly onto the surface - even at these low concentrations in the feed - and is thus available for the FTS reaction.

The distribution of light hydrocarbon product at different temperatures was plotted (Figure 3) and the following can be observed:

(1) Figure 5.3 (a): When using a (hydrogen rich) syngas and no  $C_2H_4$  in the feed (at temperatures of 200 and 220 °C), the product distribution is consistent with a typical Anderson-Schulz-Flory (ASF) distribution [36], with a relatively high yield of methane, a low yield of  $C_2$  and a linear distribution of  $C_{3-6}$  product.

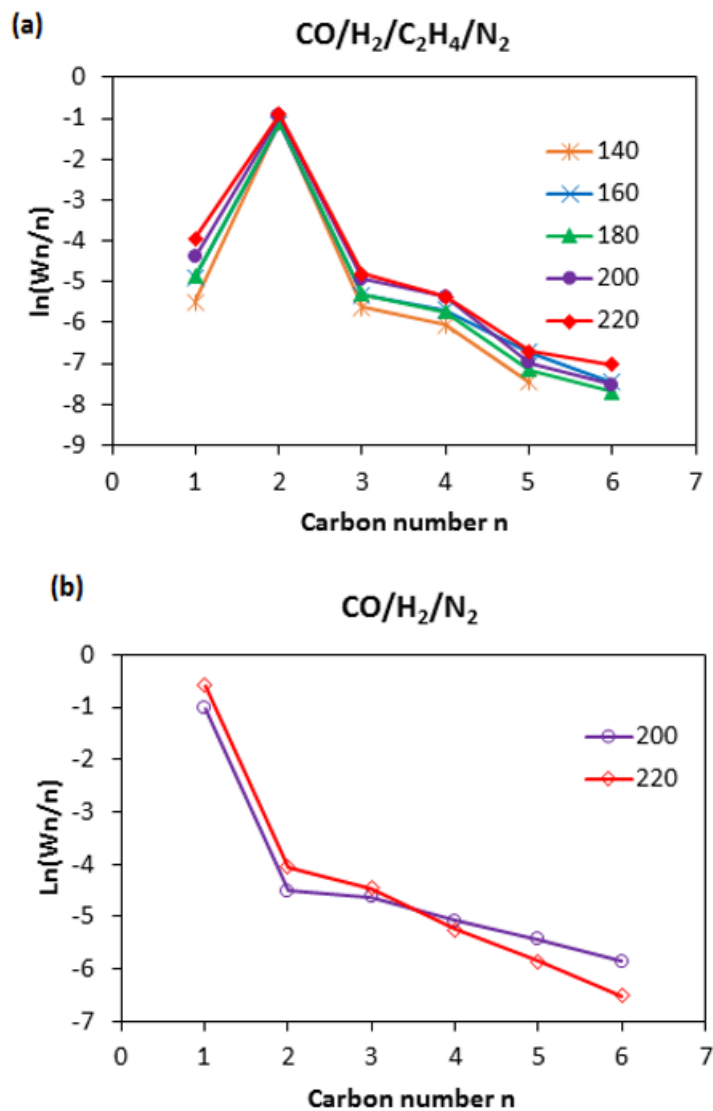


**Figure 5.3:** An ASF plot of the light hydrocarbon products formed over a 15% Co/TiO<sub>2</sub> catalyst: (a) with co-feeding ethylene; and (b) without co-feeding ethylene. Reaction conditions: (a) 20 bar, 140 – 220 °C, 80ml/min, feed gas composition: 52.5% H<sub>2</sub> / 7.5% CO / 37.5% C<sub>2</sub>H<sub>4</sub> / 2.5% N<sub>2</sub>; and (b) 20 bar, 200 – 220 °C, 50 ml/min, feed gas composition: 84% H<sub>2</sub> / 12% CO / 4% N<sub>2</sub>.

(2) Figure 5.3 (b): When using a feed of  $C_2H_4$  co-fed with syngas (at temperatures of 140 to 220 °C), the product distribution shows some differences from the typical ASF plot, namely:

i. Low methane selectivity. This inhibition of methane formation when co-feeding  $C_2H_4$  has been reported previously [37].

ii. An extremely high  $C_2$  selectivity, caused by the hydrogenation of the co-fed  $C_2H_4$  to ethane.

iii. The selectivity of  $C_4$  is slightly higher than when using syngas only. This might be attributed to  $C_2H_4$  dimerization, which would enhance the production of  $C_4$ .

Apart from the differences in the  $C_1$  and  $C_2$  selectivity, the trend in the  $C_{3+}$  product distribution seen in Figure 5.3 (b) is similar to a typical FTS product distribution - as seen in Figure 3 (a) - even at temperatures much lower than that normally used for FTS. Thus, we have FTS occurring at temperatures as low as 140 °C, and being initiated by  $C_2H_4$ , while the monomer is most likely  $CO^*$ .

The implication of the observed difference in methane selectivity is worth considering. We notice that there is no (or very little) methane formed when co-feeding  $C_2H_4$  at all temperatures. In contrast, at temperatures of 180 °C or higher, the methane selectivity with a hydrogen-rich syngas feed is 45% and increases to 85% at 220 °C. (This is shown in Figure S1 (a) in the Supplementary Material). When co-feeding  $C_2H_4$  at temperatures below 180 °C, the  $C_2H_4$  acts as an initiator, forming some  $C_2^*$  species that react with the monomer to form  $C_{3+}$  products. In this situation, the reaction rate would be higher than that for a syngas feed (as the  $C_2H_4$  is acting as an initiator), and the methane selectivity would be lower.

When using a syngas feed, increasing the temperature allows some  $CH_x^*$  to form, resulting in FTS occurring with a relatively low rate and high methane selectivity (as the  $CH_x^*$  can hydrogenate to methane). As the reaction temperature increases, it becomes easier to cleave

the CO\* bond, which allows more CH<sub>x</sub>\* species to form, thus simultaneously increasing the FTS reaction rate for this reaction pathway, as well as the methane selectivity. Therefore, it could be that as the temperature increases, the rate limiting mechanism changes from CO-insertion to a CO-dissociation mechanism. In addition, at normal FTS reaction temperatures [180 °C, 220 °C], oxygenates (propanal and propanol) were detected when using a feed mixture of 52.5% H<sub>2</sub>/ 7.5% CO/ 37.5% C<sub>2</sub>H<sub>4</sub>/ 2.5% N<sub>2</sub>. (Please refer to Figure S3 in the Supplementary Material for more details). The formation of these C<sub>3</sub> oxygenates may be attributed to C<sub>2</sub>H<sub>4</sub> hydroformylation (where the C<sub>2</sub>H<sub>4</sub> could either be co-fed or produced in the reaction), which follows the CO-insertion mechanism. These results indicate that the CO-dissociation mechanism does not completely dominate the chain growth mechanism during FTS. Combined with the experimental results obtained at lower temperatures [140 °C - 160 °C], we conclude that both the CO-insertion mechanism and CO-dissociation mechanism may exist and compete at normal FTS reaction temperatures.

### **5.3.2. Set 2: Constant Partial Pressure of H<sub>2</sub> and CO and Varying Partial Pressure C<sub>2</sub>H<sub>4</sub>**

The experiments reported in Figure 5.2 were run in a H<sub>2</sub> rich environment, which is according to the conditions at which FTS is usually run. In order to understand if the observed results would still be observed under more standard FTS conditions, another set of experiments were performed. In these experiments, a feed consisting of a mixture of H<sub>2</sub>/CO/C<sub>2</sub>H<sub>4</sub>/Ar, was used. The mole fraction of CO and H<sub>2</sub> was kept constant at 1:2, while the mole fraction of C<sub>2</sub>H<sub>4</sub> was varied from 0 to 30%. This gas was again fed to a fixed bed reactor operating at 20 bar, using the same catalyst as in the previous experiments.

The CO conversion at different temperatures and with different percentages of C<sub>2</sub>H<sub>4</sub> in the feed is shown in Figure 5.4. The CO conversion increases with the increasing reaction temperature, as would be expected. Similar to the results shown in Figure 5.2, the CO activity is much higher when co-feeding C<sub>2</sub>H<sub>4</sub> than when there is no C<sub>2</sub>H<sub>4</sub> in the syngas fed to the reactor. At 160 °C: there is no FTS reaction detected when there is no C<sub>2</sub>H<sub>4</sub> in the feed; as the amount of C<sub>2</sub>H<sub>4</sub> in the feed increases, the CO conversion increases to over 5%, even at this low temperature. These results verify that C<sub>2</sub>H<sub>4</sub> acts as an initiator in FTS and it thus has a positive effect on CO reactivity, even at typical FTS gas compositions. Furthermore, at temperatures between 160 °C – 200 °C, CO conversion increases with increasing C<sub>2</sub>H<sub>4</sub> content, while at 220 °C, a maximum in the CO conversion is observed at an (intermediate) level of 10% C<sub>2</sub>H<sub>4</sub> in the feed. For experiments run with a higher C<sub>2</sub>H<sub>4</sub> content at 220 °C, the reaction becomes hydrogen-limited and this is probably why the observed conversion of CO drops.

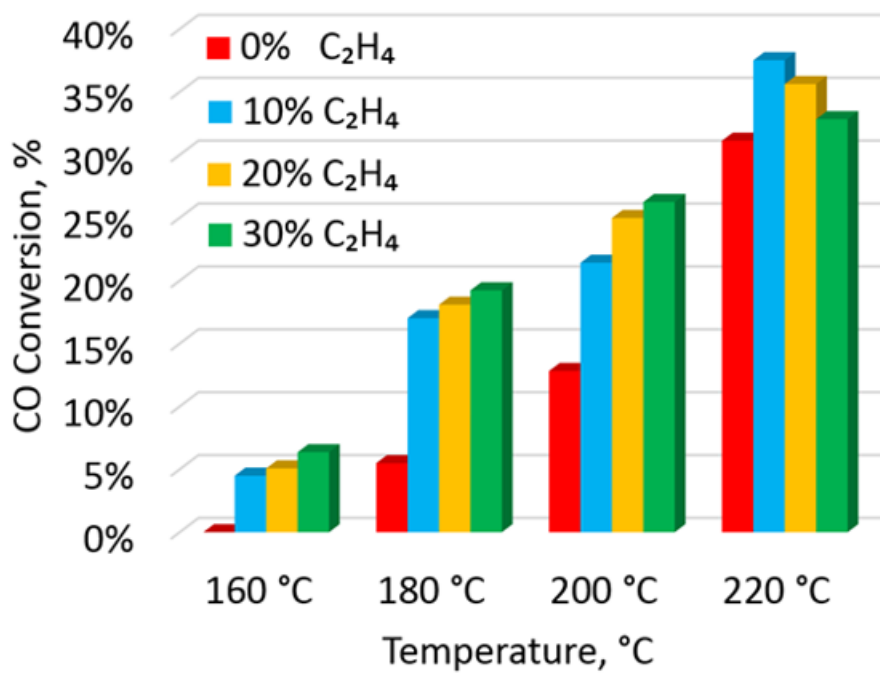


**Figure 5.4:** CO conversion at different reaction temperatures, with different percentages of C<sub>2</sub>H<sub>4</sub> in the syngas feed, over a 15% Co/TiO<sub>2</sub> catalyst. (Reaction conditions: total reaction pressure: 20 bar; total flow rate: 50 ml/min; feed gas composition: 40% H<sub>2</sub>/ 20% CO / X% C<sub>2</sub>H<sub>4</sub>/ (40-X) % Ar, X=0%, 10%, 20% or 30%).

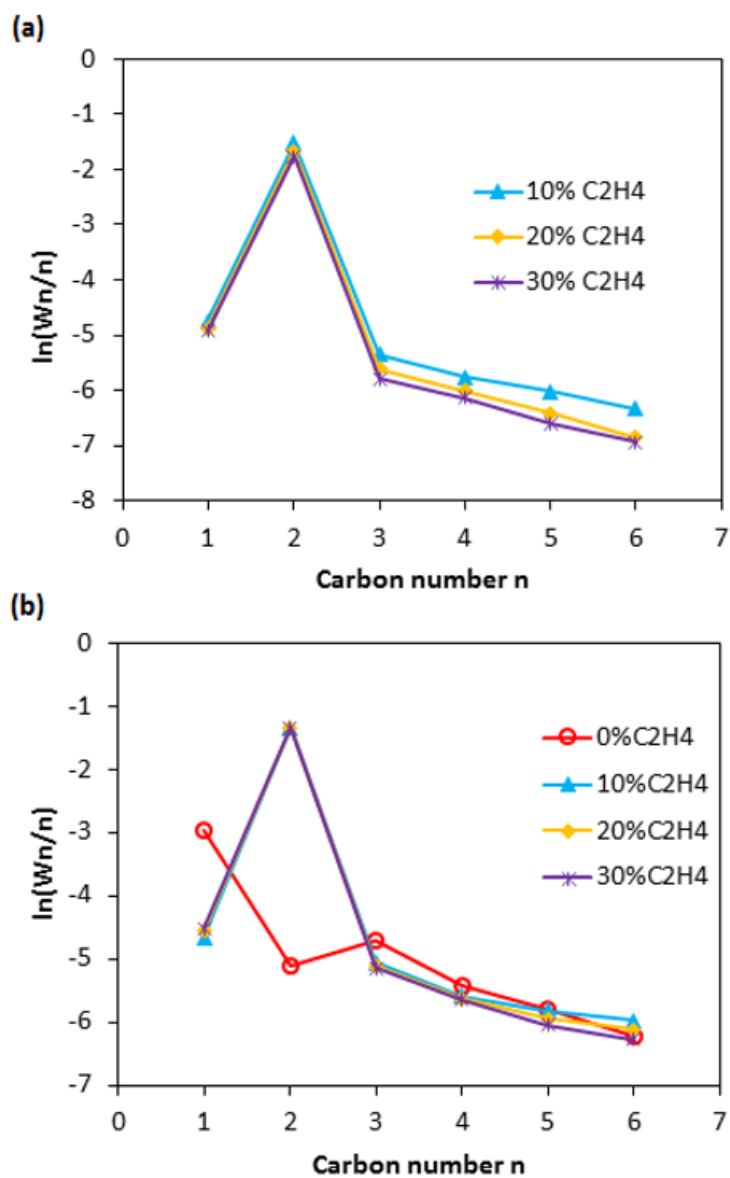


**Figure 5.5:** ASF plot of the experimental hydrocarbon data with varying proportions of C<sub>2</sub>H<sub>4</sub> in the feed: (a) at 160 °C; (b) at 180 °C. (Reaction conditions: total reaction pressure: 20 bars; total flow rate: 50 ml/min; and feed gas composition: 40% H<sub>2</sub>/ 20% CO / X% C<sub>2</sub>H<sub>4</sub>/ (40-X) % Ar, X=0%, 10%, 20% or 30%).

The light hydrocarbon product distribution for Set 2 is plotted in Figure 5.5. Figure 5.5 shows that the trend in the product distribution is quite similar to that shown in Figure 5.3. As shown in Figure 5.5 (b), a typical ASF plot is obtained with high methane selectivity when the feed contains no  $C_2H_4$ . When  $C_2H_4$  is co-fed, a significantly higher  $C_2$  selectivity is observed, which is due to the hydrogenation of  $C_2H_4$  in the feed. However, the  $C_3$  to  $C_6$  product distribution is similar to a typical ASF distribution, even at a reaction temperature of 160 °C, which is lower than the normal FTS reaction temperature. Furthermore, as seen previously, the  $C_1$  selectivity is low when  $C_2H_4$  is co-fed to the reactor.

Based on the results of these two groups of experiments, we can conclude that: CO reacts at a temperature of 160 °C or lower in the presence of  $C_2H_4$ ; and that the  $C_3$  to  $C_6$  product follows the ASF distribution. As discussed earlier, there are currently two main groups of mechanisms used to describe FTS [7, 10-14, 18]. (See Figure 5.1.) In the first group of mechanisms, the CO bond dissociates before the C-C bond forms, resulting in chain growth. The CO-dissociation mechanism (including direct dissociation and H-assisted dissociation) falls in this category [7, 10-14]. The second group of mechanisms propose that the CO bond breaks after the C-C bond is formed; these are known as CO-insertion mechanisms [18]. For CO-dissociation type mechanisms, both monomers and initiators are intermediates with a chemical structure  $CH_x^*$ . (See Figure 5.1.) In the case of the CO-insertion mechanism, the initiator has the form  $CH_x^*$  and the monomer has the form  $CO^*$  [18].

$C_2H_4$  hydrogenation occurs on FTS catalysts at temperatures as low as 100 °C, and the predominate product is ethane (more than 98% selectivity). CO was observed to stop the  $C_2H_4$  hydrogenation reaction, even at temperatures as low as 100 °C. This indicates that, even at these low temperatures and relatively low concentrations, CO adsorbs competitively on the catalyst surface.

According to our experimental results, there is no CO activity in the absence of C<sub>2</sub>H<sub>4</sub>, either at or below a temperature of 160 °C. In the syngas-fed system, the initiator for either mechanism is a species of the form CH<sub>x</sub>\*; and as the observed reaction rates are low, this must imply that CH<sub>x</sub>\* is hard to form by either direct CO-dissociation or H-assisted CO-dissociation pathways. This implies that the CO-dissociation mechanism may not occur or may occur very slowly at these reaction conditions.

C<sub>2</sub>H<sub>4</sub>-syngas mixtures react at temperatures as low as 140 °C, and both the (high) CO conversion and the observed ASF type product distribution for C<sub>3-6</sub> indicates that CO\* undergoes a carbon chain growth reaction. In contrast, syngas does not react at these temperatures. C<sub>2</sub>H<sub>4</sub> has previously been reported to initiate the FTS reaction [32-33]. Therefore, the C<sub>2</sub>H<sub>4</sub> that was added in these experiments acts as an initiator and reacts with the adsorbed CO\*, resulting in the step-wise chain growth reaction, and resulting in the product distributions shown in Figures 5.3 and 5.5. It has been reported that various possible chain initiators can be formed from C<sub>2</sub>H<sub>4</sub>, including CH<sub>3</sub>-CH<sub>2</sub>\*, [12] CH<sub>2</sub>=CH\*, [17] \*CH<sub>2</sub>-CH= [18] and CH<sub>3</sub>-C\* [38]. Although it is hard to identify the exact chemical structure of the C<sub>2</sub> initiator formed by C<sub>2</sub>H<sub>4</sub>, the experimental results shown in Figures 5.2-5.5 indicate that C-C coupling happens preferentially to C-O bond dissociation at reaction temperatures below 160 °C. The observed low methane selectivity for C<sub>2</sub>H<sub>4</sub>-syngas feeds supports this inference, as, if methane is formed by hydrogenating a CH<sub>x</sub>\* species, the low selectivity of methane implies that there are low concentrations of this intermediate, which is formed by CO\*-dissociation. As the CO reaction rates are low in the syngas systems at low temperatures, this would also imply that the reaction rate is limited by the formation of the CH<sub>x</sub>\* initiator species. At normal FTS temperatures [180 °C, 220 °C], the syngas systems begin to react without C<sub>2</sub>H<sub>4</sub> initiation; this implies that CH<sub>x</sub>\* species are formed, which act as initiators and which could

be monomers as well, depending on the reaction mechanism.  $C_2H_4$  still promotes the reactivity of CO at these temperatures, which indicates that both the CO-insertion mechanism and the CO-dissociation mechanism could exist simultaneously, with the CO-insertion mechanism dominating at lower temperatures.

Figure 5.6 plots the ratio of the CO conversion with co-feeding 10%, 20% or 30%  $C_2H_4$  to CO conversion without  $C_2H_4$  co-feeding. The ratio is always higher than 1 and decreases with increasing reaction temperature; this indicates that the CO-insertion mechanism dominates at lower reaction temperatures.

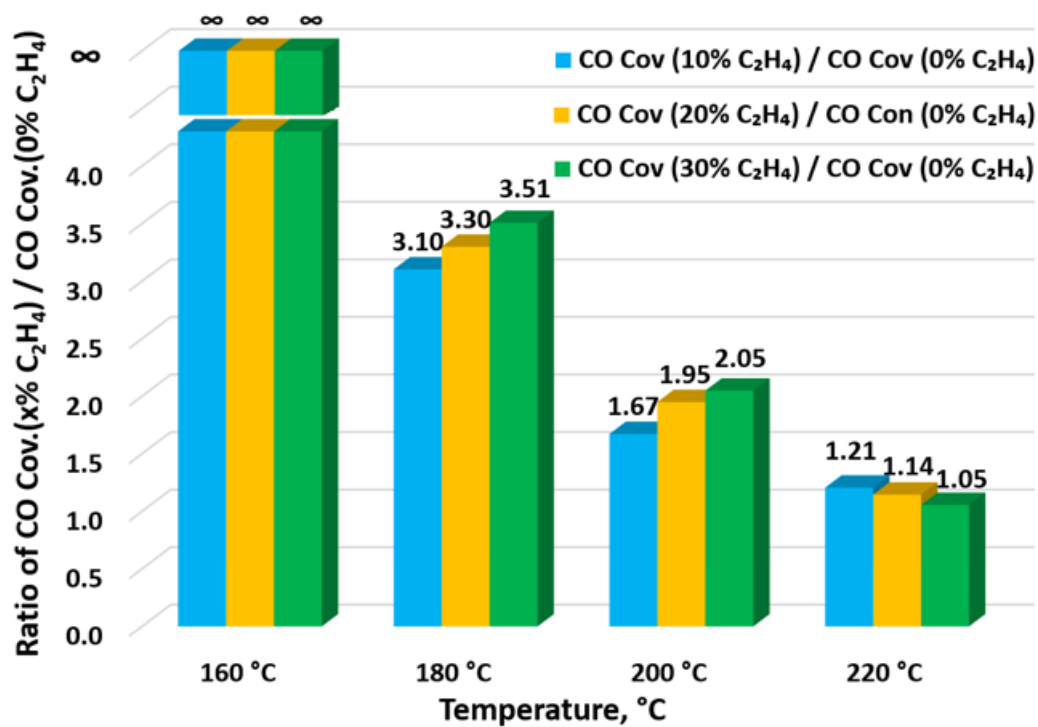


**Figure 5.6:** Ratio of CO conversion with syngas to the CO conversion with X % C<sub>2</sub>H<sub>4</sub> co-feeding (X=10%, 20% or 30%). (Reaction conditions: total reaction pressure: 20 bars; total flow rate: 50 ml (NTP)/min; and feed gas composition: 40% H<sub>2</sub>/ 20% CO / X% C<sub>2</sub>H<sub>4</sub>/ (40-X)% Ar, X=0%, 10%, 20% or 30%).

#### 5.4. Conclusion

In summary, at lower temperatures [140 °C – 160 °C], CO exhibits relatively high reactivity when C<sub>2</sub>H<sub>4</sub> is co-fed with syngas, while CO in syngas-fed systems show no reactivity at these temperatures. In addition, the C<sub>3+</sub> product distribution observed at these low temperatures with C<sub>2</sub>H<sub>4</sub> co-fed systems is consistent with a typical FTS product distribution. The experimental data indicates that it is hard to form the chain-growth monomer CH<sub>x</sub>\* via direct CO- or H-assisted CO-dissociation at low temperatures. However, the adsorbed C<sub>2</sub>H<sub>4</sub> acts as an initiator and could react with adsorbed CO\* via the CO-insertion mechanism to form long chain hydrocarbons. The results imply that the C-C bond coupling occurs prior to C-O bond cleavage at lower reaction temperatures. At higher temperatures [180 °C – 220 °C], oxygenates are detected in the product, which supports the assumption of the existence of the CO-insertion mechanism. Thus, both the CO-insertion mechanism and the CO-dissociation mechanism may exist and compete at normal FTS reaction temperatures.

## REFERENCES:

1. Yan, B., Ma, L., Gao, X., Zhang, J., Ma, Q., & Zhao, T. S. (2019). Amphiphobic surface fabrication of iron catalyst and effect on product distribution of Fischer–Tropsch synthesis. *Applied Catalysis A: General*, 585, 117184.
2. dos Santos, R. G., & Alencar, A. C. (2020). Biomass-derived syngas production via gasification process and its catalytic conversion into fuels by Fischer Tropsch synthesis: A review. *International Journal of Hydrogen Energy*, 45(36), 18114-18132.
3. Peng, X., Cheng, K., Kang, J., Gu, B., Yu, X., Zhang, Q., & Wang, Y. (2015). Impact of Hydrogenolysis on the Selectivity of the Fischer–Tropsch Synthesis: Diesel Fuel Production over Mesoporous Zeolite-Y-Supported Cobalt Nanoparticles. *Angewandte Chemie International Edition*, 54(15), 4553-4556.
4. Qian, W., Zhang, H., Ying, W., & Fang, D. (2011). Product distributions of Fischer-Tropsch synthesis over Co/AC catalyst. *Journal of natural gas chemistry*, 20(4), 389-396.
5. Price, S. W., Martin, D. J., Parsons, A. D., Sławiński, W. A., Vamvakeros, A., Keylock, S. J., ... & Mosselmans, J. F. W. (2017). Chemical imaging of Fischer-Tropsch catalysts under operating conditions. *Science advances*, 3(3), e1602838.
6. Khodakov, A. Y., Chu, W., & Fongarland, P. (2007). Advances in the development of novel cobalt Fischer–Tropsch catalysts for synthesis of long-chain hydrocarbons and clean fuels. *Chemical reviews*, 107(5), 1692-1744.
7. Mousavi, S., Zamaniyan, A., Irani, M., & Rashidzadeh, M. (2015). Generalized kinetic model for iron and cobalt based Fischer–Tropsch synthesis catalysts: review and model evaluation. *Applied Catalysis A: General*, 506, 57-66.

8. Anderson, R. B., Kölbl, H., & Ralek, M. (1984). *The Fischer-Tropsch Synthesis (Vol. 16)*. New York: Academic Press.
9. Brady III, R. C., & Pettit, R. (1980). Reactions of diazomethane on transition-metal surfaces and their relationship to the mechanism of the Fischer-Tropsch reaction. *Journal of the American Chemical Society*, 102(19), 6181-6182.
10. Fischer, F., & Tropsch, H. (1923). The preparation of synthetic oil mixtures (synthol) from carbon monoxide and hydrogen. *Brennstoff-Chem*, 4, 276-285.
11. Maitlis, P. M. (2004). Fischer–Tropsch, organometallics, and other friends. *Journal of organometallic chemistry*, 689(24), 4366-4374.
12. Ciobîcă, I. M., Kramer, G. J., Ge, Q., Neurock, M., & Van Santen, R. A. (2002). Mechanisms for chain growth in Fischer–Tropsch synthesis over Ru (0001). *Journal of Catalysis*, 212(2), 136-144.
13. Weststrate, C. J., Ciobîcă, I. M., Saib, A. M., Moodley, D. J., & Niemantsverdriet, J. W. (2014). Fundamental issues on practical Fischer–Tropsch catalysts: how surface science can help. *Catalysis Today*, 228, 106-112.
14. Storch, H. H. (1951). *The Fischer-Tropsch and Related Syntheses: Including A Summary Of Theoretical And Applied Contact Catalysis*. Wiley.
15. Ojeda, M., Nabar, R., Nilekar, A. U., Ishikawa, A., Mavrikakis, M., & Iglesia, E. (2010). CO activation pathways and the mechanism of Fischer–Tropsch synthesis. *Journal of Catalysis*, 272(2), 287-297.
16. Weststrate, C. J., Gericke, H. J., Verhoeven, M. W., Ciobica, I. M., Saib, A. M., & Niemantsverdriet, J. W. (2010). Ethanol decomposition on Co (0001): C–O bond scission

- on a close-packed cobalt surface. *The Journal of Physical Chemistry Letters*, 1(12), 1767-1770.
17. Liu, J. X., Wang, P., Xu, W., & Hensen, E. J. (2017). Particle size and crystal phase effects in Fischer-Tropsch catalysts. *Engineering*, 3(4), 467-476.
  18. Todic, B., Ma, W., Jacobs, G., Davis, B. H., & Bukur, D. B. (2014). CO-insertion mechanism based kinetic model of the Fischer-Tropsch synthesis reaction over Re-promoted Co catalyst. *Catalysis Today*, 228, 32-39.
  19. Pichler, V. H., & Schulz, H. (1970). Neuere Erkenntnisse auf dem Gebiet der Synthese von Kohlenwasserstoffen aus CO und H<sub>2</sub>. *Chemie Ingenieur Technik*, 42(18), 1162-1174.
  20. Chakrabarti, D., Gnanamani, M. K., Shafer, W. D., Ribeiro, M. C., Sparks, D. E., Prasad, V., ... & Davis, B. H. (2015). Fischer-Tropsch Mechanism: <sup>13</sup>C<sup>18</sup>O Tracer Studies on a Ceria-Silica Supported Cobalt Catalyst and a Doubly Promoted Iron Catalyst. *Industrial & Engineering Chemistry Research*, 54(25), 6438-6453.
  21. Schweicher, J., Bundhoo, A., & Kruse, N. (2012). Hydrocarbon chain lengthening in catalytic CO hydrogenation: evidence for a CO-insertion mechanism. *Journal of the American Chemical Society*, 134(39), 16135-16138.
  22. Visconti, C. G., Tronconi, E., Lietti, L., Forzatti, P., Rossini, S., & Zennaro, R. (2011). Detailed kinetics of the Fischer-Tropsch synthesis on cobalt catalysts based on H-assisted CO activation. *Topics in Catalysis*, 54(13-15), 786-800.
  23. Zijlstra, B., Broos, R. J., Chen, W., Oosterbeek, H., Filot, I. A., & Hensen, E. J. (2019). Coverage effects in CO dissociation on metallic cobalt nanoparticles. *ACS Catalysis*, 9(8), 7365-7372..

24. Filot, I. A., Fariduddin, F., Broos, R. J., Zijlstra, B., & Hensen, E. J. (2016). A quantum-chemical DFT study of CO dissociation on Fe-promoted stepped Rh surfaces. *Catalysis Today*, 275, 111-118.
25. Zha, H., Dong, X., Yu, Y., & Zhang, M. (2018). Hydrogen-assisted versus hydroxyl-assisted CO dissociation over Co-doped Cu (111): A DFT study. *Surface Science*, 669, 114-120.
26. Keyvanloo, K., Lanham, S. J., & Hecker, W. C. (2016). Kinetics of Fischer-Tropsch synthesis on supported cobalt: Effect of temperature on CO and H<sub>2</sub> partial pressure dependencies. *Catalysis Today*, 270, 9-18.
27. Zhuo, M., Tan, K. F., Borgna, A., & Saeys, M. (2009). Density functional theory study of the CO insertion mechanism for Fischer-Tropsch synthesis over Co catalysts. *The Journal of Physical Chemistry C*, 113(19), 8357-8365.
28. Zhuo, M., Borgna, A., & Saeys, M. (2013). Effect of the CO coverage on the Fischer-Tropsch synthesis mechanism on cobalt catalysts. *Journal of catalysis*, 297, 217-226.
29. Lu, X., Hildebrandt, D., Liu, X., & Glasser, D. (2010). Making Sense of the Fischer-Tropsch Synthesis Reaction: Start-up. *Industrial & engineering chemistry research*, 49(20), 9753-9758.
30. Zhang, Y., Tshwaku, M., Yao, Y., Chang, J., Lu, X., Liu, X., & Hildebrandt, D. (2020). Reaction of ethylene over a typical Fischer-Tropsch synthesis Co/TiO<sub>2</sub> catalyst. *Engineering Reports*, 2(9), e12232.
31. Schulz, H., & Claeys, M. (1999). Reactions of  $\alpha$ -olefins of different chain length added during Fischer-Tropsch synthesis on a cobalt catalyst in a slurry reactor. *Applied Catalysis A: General*, 186(1-2), 71-90.

32. Hall, W. K., Kokes, R. J., & Emmett, P. H. (1960). Mechanism studies of the Fischer-Tropsch synthesis: the incorporation of radioactive ethylene, propionaldehyde and propanol. *Journal of the American Chemical Society*, 82(5), 1027-1037.
33. Eidus, Y. T., Zelinskii, N. D., & Ershov, N. I. (1948). O Kondensiruyushchem Deistvii Metilenovykh Radikalov Na Etilen. *Doklady Akademii Nauk SSSR*, 60(4), 599-601..
34. Hutchings, G. J., Copperthwaite, R. G., & van der Riet, M. (1995). Low methane selectivity using Co/MnO catalysts for the Fischer-Tropsch reaction: Effect of increasing pressure and Co-feeding ethene. *Topics in Catalysis*, 2(1-4), 163-172.
35. Yang, J., Rodriguez, C. L., Qi, Y., Ma, H., Holmen, A., & Chen, D. (2020). The effect of Co-feeding ethene on Fischer Tropsch Synthesis to Olefins over Co-based catalysts. *Applied Catalysis A: General*, 117564.
36. Dry, M. E. (1990). The Fischer-Tropsch process-commercial aspects. *Catalysis today*, 6(3), 183-206.
37. Kibby, C. L., Pannell, R. B., & Kobylinski, T. P. (1984). Hydrogenation of olefins in the presence of carbon monoxide on supported cobalt catalysts. *Preprints-American Chemical Society. Division of Petroleum Chemistry*, 29(4), 1113-1119.
38. Weststrate, C. J., Van Helden, P., & Niemantsverdriet, J. W. (2016). Reflections on the Fischer-Tropsch synthesis: Mechanistic issues from a surface science perspective. *Catalysis Today*, 275, 100-110.

## Supplementary Material for Chapter 5

### Table of contents:

#### 1. Calculation of conversion and selectivity

The C<sub>2</sub>H<sub>4</sub> and the CO conversions and hydrocarbon selectivity S<sub>C<sub>n</sub></sub> (based on carbon) are estimated by means of the following equations:

$$X_{\text{C}_2\text{H}_4}(\%) = (F_{\text{C}_2\text{H}_4,\text{in}} - F_{\text{C}_2\text{H}_4,\text{out}}) / F_{\text{C}_2\text{H}_4,\text{in}} \times 100\% \quad \text{Eq. S5.1}$$

$$X_{\text{CO}}(\%) = (F_{\text{CO},\text{in}} - F_{\text{CO},\text{out}}) / F_{\text{CO},\text{in}} \times 100\% \quad \text{Eq. S5.2}$$

$$S_{\text{C}_n}(\%) = n \times F_{\text{C}_n,\text{out}} / [(F_{\text{CO},\text{in}} - F_{\text{CO},\text{out}}) + 2 \times (F_{\text{C}_2\text{H}_4,\text{in}} - F_{\text{C}_2\text{H}_4,\text{out}})] \times 100\% \quad \text{Eq. S5.3}$$

Where: X<sub>C<sub>2</sub>H<sub>4</sub></sub> is C<sub>2</sub>H<sub>4</sub> conversion, %; X<sub>CO</sub> is the CO conversion, %; S<sub>C<sub>n</sub></sub> is the selectivity of hydrocarbon product C<sub>n</sub>, %. F<sub>CO,in</sub> and F<sub>CO,out</sub> are the CO molar flow rates of the feed gas and the tailgas, respectively (mmol/min). F<sub>C<sub>2</sub>H<sub>4</sub>,in</sub> and F<sub>C<sub>2</sub>H<sub>4</sub>,out</sub> are the ethylene molar flow rates of the feed gas and the tailgas, respectively (mmol/min). *n* is the carbon number of product C<sub>n</sub> and F<sub>C<sub>n</sub>,out</sub> is the molar flow rate of hydrocarbon product with carbon number *n* in tailgas (mmol/min).

## 2. Selectivity of the C<sub>1</sub>-C<sub>4</sub> products

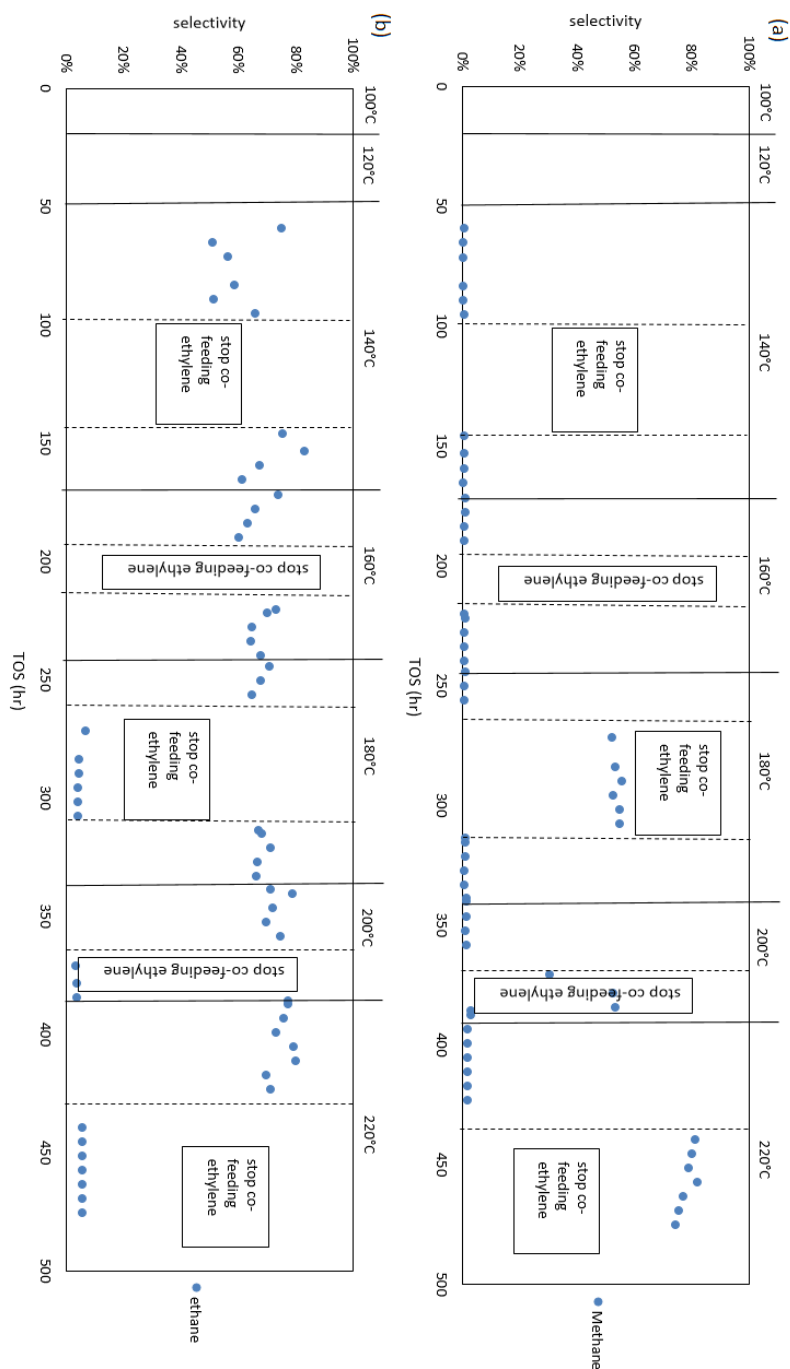


**Figure 5.S1:** Product selectivity under different reaction temperatures over a 15% Co/TiO<sub>2</sub> catalyst: (a) methane selectivity; (b) ethane selectivity. Reaction conditions: 20 bar, 80 ml/min for the feed of syngas with ethylene (52.5% H<sub>2</sub>/ 7.5% CO/ 37.5% C<sub>2</sub>H<sub>4</sub>/ 2.5% N<sub>2</sub>), and 50 ml/min for the feed of syngas without ethylene (84% H<sub>2</sub>/ 12% CO / 4% N<sub>2</sub>).

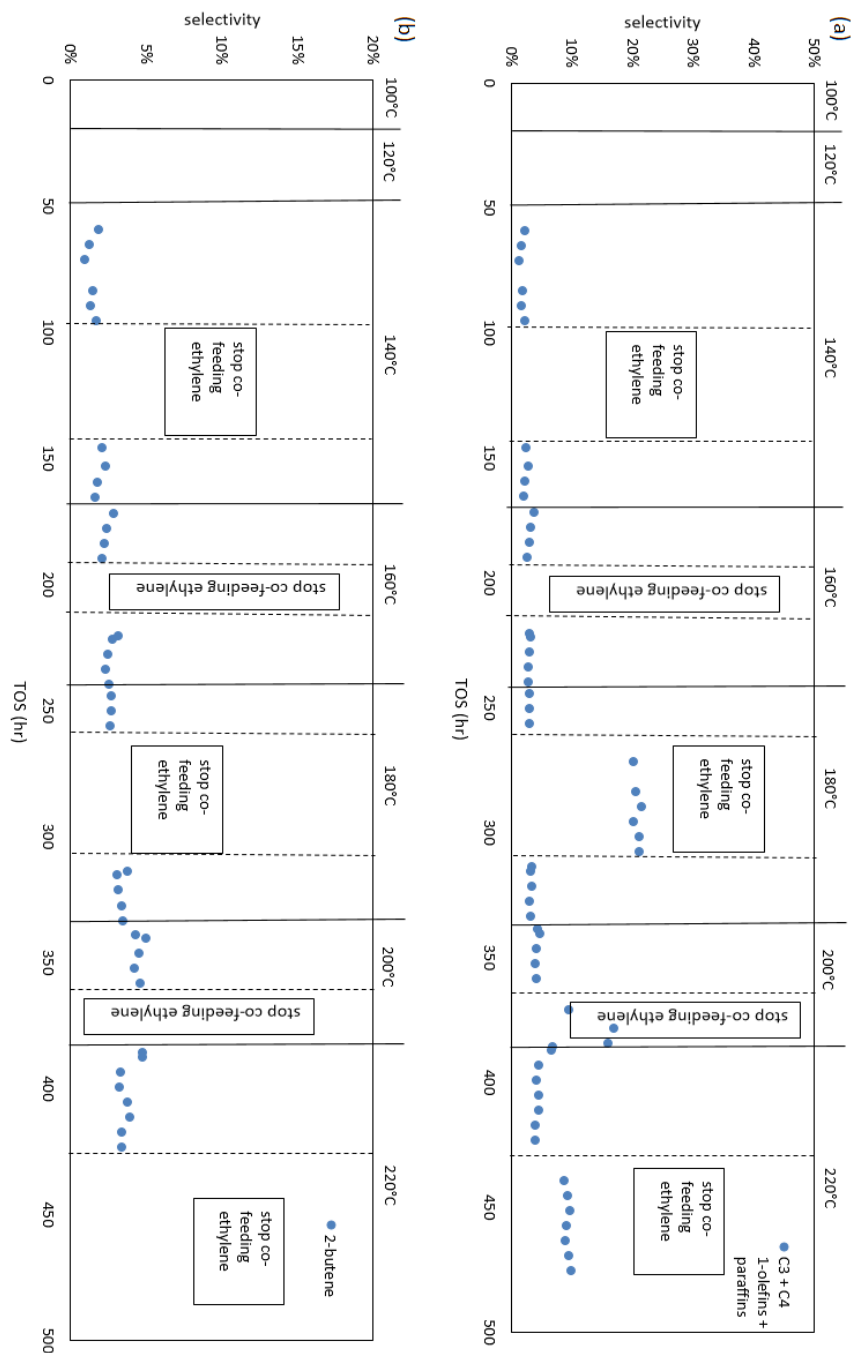


**Figure 5.S2:** Product selectivity under different reaction temperatures over a 15% Co/TiO<sub>2</sub> catalyst: (a) 1-olefin + n-paraffin selectivity of (C<sub>3</sub> + C<sub>4</sub>); (b) 2-butene (including cis- and trans-) selectivity. Reaction conditions: 20 bar, 80 ml/min for the feed of syngas with ethylene (52.5% H<sub>2</sub>/ 7.5% CO/ 37.5% C<sub>2</sub>H<sub>4</sub>/ 2.5% N<sub>2</sub>); and 50 ml/min for the feed of syngas without ethylene (84% H<sub>2</sub>/ 12% CO / 4% N<sub>2</sub>).

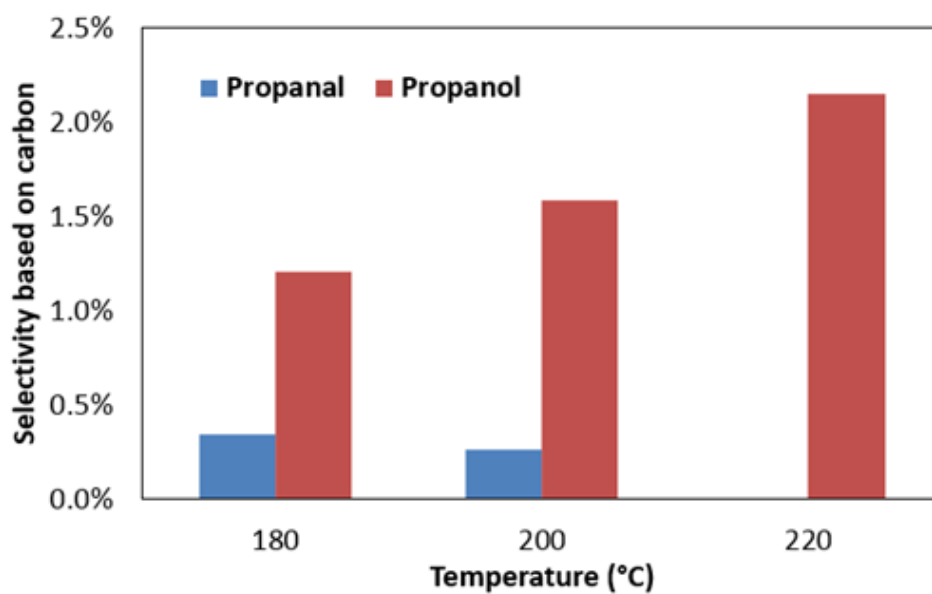


**Figure 5.S3:** Oxygenate product selectivity at different reaction temperatures over a 15% Co/TiO<sub>2</sub> catalyst. Reaction conditions: 20 bar, 80 ml/min for a feed of syngas with ethylene (52.5% H<sub>2</sub>/ 7.5% CO/ 37.5% C<sub>2</sub>H<sub>4</sub>/ 2.5% N<sub>2</sub>).

## Chapter 6

### Effect of co-feeding ethylene on the light hydrocarbon product distribution during cobalt catalysed Fischer Tropsch synthesis

This work has been prepared in the form of a paper for future publication.

Part of this work was presented at Syngas Conversion 2018 and CATSA 2018.

---

#### ABSTRACT

The effect of co-feeding ethylene on the performance of a cobalt-based catalyst during Fischer-Tropsch Synthesis (FTS) was investigated. The feed used was syngas mixed with different proportions of ethylene, ranging from 0 to 30 mol % , denoted in moles % as: ( 40% H<sub>2</sub>; 20% CO; X% C<sub>2</sub>H<sub>4</sub>; (40-X)%; Ar (X)) where (X=0, 10, 20, 30)). Syngas (X=0) did not react at 160°C. However, the following was observed with the addition of ethylene to the feed gas: CO reactivity increased significantly, especially at relatively low reaction temperatures (160°C – 190°C); a lower methane selectivity and a higher ethane selectivity; propanal and trans- and cis-2-butenes were formed, which are not typical products of Co catalysed FTS. The observed activity and selectivity of the light hydrocarbons indicates that CO and ethylene mainly react by the CO insertion mechanism to form long chain hydrocarbons and that only small amounts of oxygenates are formed as by-products. The dominant ethylene reaction is hydrogenation to ethane although other side reactions, such as dimerization to form 2-butene, also occur. The light products (C<sub>3</sub>-C<sub>6</sub>) follow the ASF product distribution over the temperature range tested (160 °C -220°C) for all values of X. It was also observed the addition of ethylene to the feed increases the chain growth probability of the product.

## 6.1. Introduction

Fischer-Tropsch synthesis (FTS) has been used in commercial coal-to-liquid (CTL) and gas-to-liquid (GTL) processes, and is an established route for converting syngas to predominately linear paraffins and olefins ( $C_1$  to  $C_{50+}$ ) [1-2]. Among these products, the reaction of linear  $\alpha$ -olefins have received considerable attention since they may reabsorb on the catalyst surface and take part in secondary reactions, thereby influencing the overall product distribution [3]. As reported in the literature, the secondary reactions of  $\alpha$ -olefins could include: hydrogenation to corresponding n-paraffins [4-5]; isomerization (bond-shift) to internal olefins [6-7]; hydrocracking and hydrogenolysis (demethylation) to short chain hydrocarbons and/or methane [8]; reinsertion into growing chains (predominately occurring with  $C_2H_4$ ) [9-10]; reabsorption and initiation of hydrocarbon chains [11]; other reactions (such as hydroformylation to produce oxygenates) [12].

In the past few decades, researchers have studied the secondary reactions of  $\alpha$ -olefins by varying the residence time of the reactants in the catalyst bed and/or by co-feeding of  $\alpha$ -olefins. In 1967, Pichler et al. reported that the  $\alpha$ -olefins could undergo a bond-shift reaction to form internal olefins and that they could be hydrogenated to the corresponding alkanes [13]. Later, Schulz and co-workers reported that [14-15]: (1) relatively short residence times suppressed the secondary reactions; (2) around 70-90 mol % of the product produced over an Fe/Mn catalyst was olefinic; and (3) more than 95% of the olefin products were  $\alpha$ -olefins, indicating that  $\alpha$ -olefins are the primary products of FTS [15].

A considerable amount of research on the secondary reactions of olefins has been conducted on cobalt-based [14, 16-27], iron-based [28-32] and ruthenium-based [12, 24, 33-34] catalysts. Snel and Espinoza studied the performance of co-fed ethylene over Fe–CaO in a

fixed bed [29], and found that when 10% ethylene is added to the syngas feed, both the CO conversion and olefin selectivity increases significantly. However, Botes found that light olefins (excluding ethylene) did not have a significant tendency to incorporate or hydrogenate during low temperature FTS (LTFT) over an iron-based catalyst [30].

Jordan and Bell looked at co-feeding  $\alpha$ -olefins ( $C_2$  to  $C_4$ ) over a Ru/SiO<sub>2</sub> catalyst at near atmospheric pressure, and they found that the selectivity to long chain hydrocarbons increased [12, 33-34]. Ethylene has been found to be very active and shows high hydrogenation reactivity [12, 33-34].

The majority of  $\alpha$ -olefin co-feeding experiments have been carried out on cobalt-based catalysts. As early as the 1930s, Smith found that the addition of ethylene to the feed increased the yield of olefin and alcohol products [16]. In the 1940s, Eidus and his collaborators conducted the first of many experiments on co-feeding low molecular weight  $\alpha$ -olefins and H<sub>2</sub>, CO [17-22]. There was a resurgence in research on the effect of co-feeding olefins over cobalt-based catalyst from the 1970s to the 1990s. Schulz added a small amount of isotope-labelled ethylene-C<sup>14</sup> to synthesis gas, and found that more than 90% of the co-fed ethylene hydrogenated to ethane [14]. Another group of experiments conducted by Schulz showed that the partial pressure of carbon monoxide affected the ethylene hydrocracking reaction [23]. Iglesia showed that long-chain  $\alpha$ -olefins were more easily re-adsorbed on the catalyst surface, and this was used to explain the positive deviation from ideal ASF product distribution for C<sub>10+</sub> [24].

Recently, Chen et al. added isotopically labelled propylene to the FTS reaction system and found that propylene decomposition is more dependent on the free sites on the catalyst than on CO dissociation [25]. McNab et al. investigated the effect of co-feeding ethylene on cobalt

catalysts by *in-situ* Fourier transform infrared (FTIR) and online gas chromatography (GC) [26-27]. They found that the product selectivity and chain length of the adsorbed species on the catalyst were different from that observed in the absence of ethylene, where the selectivity was constant, but the chain length of the adsorbed species changed.

In summary, some important phenomena have been observed by researchers, but the conclusions drawn are not consistent, most likely due to the complexity of the Fischer-Tropsch (FT) reaction. Researchers have found it difficult to investigate individual aspects of the reactions, because of the complexity reaction system.

This work investigates aspects of the FTS reaction (ethylene secondary reaction) separately. As mentioned in the previous chapters, to avoid interference of the strongly suppressing effect of CO and other products from FTS, Chapter 4 discusses ethylene reactivity and product distribution with H<sub>2</sub> only. To avoid the interference of CO hydrogenation, Chapter 5 discusses the reactants reactivity and products distribution under non-typical low temperature. Based on the results obtained before, the current chapter tries to discuss the effect of co-feeding ethylene on typical FTS condition.

This work investigates aspects of the FTS reaction with co-feeding different amount of ethylene. Initially, experiments using a mixture of syngas and a diluent gas as the feed were performed; the reaction temperature was varied and the effect on CO conversion and selectivity of the FT product was observed. This information described the base line FT behaviour of the catalyst. Thereafter, volume of the diluent gas in the feed was replaced by ethylene while maintaining the space velocity and the partial pressure of carbon monoxide and hydrogen constant. The effect varying the ethylene concentration in the feed and the

operating temperature on the conversion of the reactants (CO, ethylene) and the product selectivity were observed.

## 6.2. Experiments

A supported cobalt catalyst (15% Co/85% TiO<sub>2</sub>, BET area 42.9 m<sup>2</sup>/g, with an average pore diameter of 16.7 nm) was used in the experiments. The catalysts used in this study were prepared using the traditional incipient wetness method. Co(NO<sub>3</sub>)<sub>3</sub>·6H<sub>2</sub>O (Sigma Aldrich) was used as the metal precursor salt, and TiO<sub>2</sub> (Degussa P-25) was used as the catalyst support precursor. Hydrogen (99.999%), carbon monoxide (99.999%), argon (99.999%) and ethylene (99.95%) were used as the feed gases.

1 gram of catalyst was loaded into a stainless tube reactor (length: 230 mm; ID: 8 mm). Temperature regulators were used to control the temperature of the reactor system. The pipelines between the reactor and gas chromatograph (GC) were maintained at 170 °C. A backpressure regulator was used to control the pressure in the reactor. A liquid knock out pot was placed between the reactor and the backpressure regulator and the temperature of this pot was maintained at 120 °C to separate the wax and heavy oil from the tailgas. The feed and tail gases were analysed using an online Agilent 7890A GC, which had two FIDs and one TCD. The total space velocity was maintained constant at 3000 h<sup>-1</sup> for all runs. A feed mixture of 40% H<sub>2</sub> / 20% CO/ X% C<sub>2</sub>H<sub>4</sub>/ (40-X)% Ar was used in this study ( where X= 0, 10, 20, 30 %). The partial pressure of H<sub>2</sub> and CO were maintained constant, while the partial pressure of ethylene was changed by adjusting the partial pressure of the inert gas Ar as needed. The details of the feed conditions used in the various experiments are summarised Table 6.1. The operating pressure set at 21 bars in all experiments and the reaction temperature was varied

between 160 to 220 °C. The reactor system was flushed using A before changing any reactor operating conditions.

**Table 6.1:** Feed conditions for the various experiments. The feed composition is denoted (40% H<sub>2</sub>; 20% CO; X% C<sub>2</sub>H<sub>4</sub>; (40-X)% Ar) where X= (0, 10, 20, 30).

Feed gas	Total flow rate	Total pressure	Partial pressure (bar)			
	ml/min	bar	P <sub>H<sub>2</sub></sub>	P <sub>CO</sub>	P <sub>C<sub>2</sub>H<sub>4</sub></sub>	P <sub>Ar</sub>
X=0%	50	21	8.4	4.2	0	8.4
X=10%	50	21	8.4	4.2	2.1	6.3
X=20%	50	21	8.4	4.2	4.2	4.2
X=30%	50	21	8.4	4.2	6.3	2.1

For comparison, experiments were also performed using a feed of H<sub>2</sub> and ethylene only. In this part experiment, the operation pressure was 20 bars (on gauge) as well, and total flow rate of hydrogen and ethylene was 52.5 ml/min. The ratio of H<sub>2</sub> to ethylene was 55.5: 45.5. The reaction temperature range was 100 to 140 °C.

As there are two carbon containing components in the feed, the conversion and selectivity must be clearly defined. The C<sub>2</sub>H<sub>4</sub> and CO conversion ( $X_{CO}$  and  $X_{C_2H_4}$  respectively) and the carbon based selectivity of product C<sub>n</sub> based on total carbon ( $S_{C_n}$ ) were calculated using equations 6.1 and 6.2:

$$X_{CO/C_2H_4}(\%) = (F_{CO/C_2H_4,in} - F_{CO/C_2H_4,out})/F_{CO/C_2H_4,in} \times 100\% \quad \text{Eq. 6.1}$$

$$S_{C_n}(\%) = n \times F_{C_n,out}/[(F_{CO,in} - F_{CO,out}) + 2 \times (F_{C_2H_4,in} - F_{C_2H_4,out})] \times 100\% \quad \text{Eq. 6.2}$$

Where,  $F_{CO/C_2H_4,in}$  and  $F_{CO/C_2H_4,out}$  were the flow rate of inlet and outlet of CO and ethylene, respectively; n was carbon number of product C<sub>n</sub>;  $F_{C_n,out}$  was outlet flow rate of product C<sub>n</sub>.

Equations 6.3 to 6.6 were used to calculate the selectivity of: methane, based on CO consumption  $S_{CH_4\_CO}(\%)$ ; ethane, based on C<sub>2</sub>H<sub>4</sub> consumption  $S_{C_2H_6\_C_2H_4}(\%)$ ; and propanal, based on either CO  $S_{C_2H_5CHO\_CO}(\%)$  or ethylene  $S_{C_2H_5CHO\_C_2H_4}(\%)$ ; consumption.

$$S_{CH_4\_CO}(\%) = F_{CH_4\_CO,out}/(F_{CO,in} - F_{CO,out}) \times 100\% \quad \text{Eq. 6.3}$$

$$S_{C_2H_6\_C_2H_4}(\%) = F_{C_2H_6\_C_2H_4,out}/(F_{C_2H_4,in} - F_{C_2H_4,out}) \times 100\% \quad \text{Eq. 6.4}$$

$$S_{C_2H_5CHO\_CO}(\%) = F_{C_2H_5CHO\_CO,out}/(F_{CO,in} - F_{CO,out}) \times 100\% \quad \text{Eq. 6.5}$$

$$S_{C_2H_5CHO\_C_2H_4}(\%) = F_{C_2H_5CHO\_C_2H_4,out}/(F_{C_2H_4,in} - F_{C_2H_4,out}) \times 100\% \quad \text{Eq. 6.6}$$

## 6.3. Results

### 6.3.1. CO conversion $X_{CO}$

Figure 6.1 shows  $X_{CO}$  for different amounts of ethylene in the feed ( $X= 0 - 30\%$ ) and at different reaction temperatures. We see the when there is no ethylene in the feed ( $X=0\%$ ) (1) no product was detected in the tail gas at a reaction temperature of 160 °C which indicates that CO/H<sub>2</sub> does not react at such a low temperature; (2)  $X_{CO}$  increased from 5.48% to 31.12% when the reaction temperature was increased from 180 to 220 °C. These results are consistent with typical cobalt-based FTS performance [35].

The reactivity of CO changed significantly when ethylene was added to the reactor feed. With  $X=10\%$ , the CO reacted, even at 160 °C. In comparison, CO did not react at this temperature when there was no ethylene in the feed ( $X=0\%$ ). In other words, at this low temperature, CO cannot dissociate either directly or via a hydrogen-assisted dissociation carbide-type mechanism to form either the initiators and/or the monomer CH<sub>x</sub>\* required for FTS chain growth. The reaction of CO in the presence of ethylene at low temperature might occur because the ethylene weakens the C-O bond via a CO insertion mechanism, which would promote the subsequent hydrogenation of CO. Under these conditions, ethylene may work as an initiator and react with CO, which is consistent with reports in the literature [17-36].

Comparing a feed of syngas ( $X=0\%$ ) to a feed with  $X=10\%$ , it is observed that  $X_{CO}$ : increased from about 5.5% to 17% at 180 °C; increased from 12.8% to 21.5% at 200 °C; and increased from 31% to 37.5% at 220 °C. This result demonstrates that co-feeding ethylene has a significant effect on the reactivity of CO. However, this promoting effect is attenuated as the reaction temperature increases. This phenomenon may be due to competition between the CO dissociation and the CO insertion mechanisms.

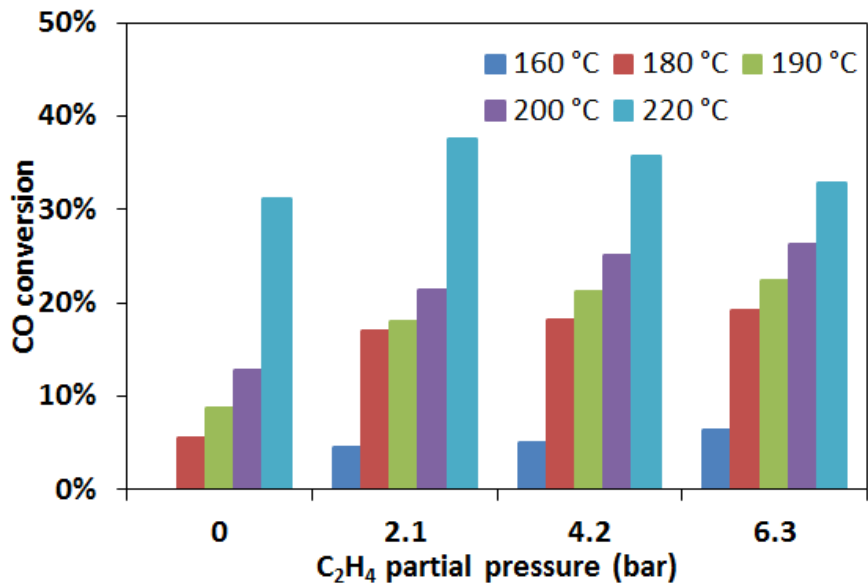


**Figure 6.1:** CO conversion  $X_{CO}$  at different reaction temperatures and different ethylene partial pressure over 15% Co/TiO<sub>2</sub>. (Reaction conditions: total reaction pressure - 21 bars; total flow rate - 50 ml (NTP)/min; feed gas composition – (40% H<sub>2</sub>; 20% CO ; X% C<sub>2</sub>H<sub>4</sub>; (40-X)% Ar) where X=0%, 10%, 20% or 30%.

In a recent DFT computation report, the direct CO dissociation at the “step-edge” facets is considered the main reaction mechanism for CO hydrogenation chain growth [37]. At typical FTS reaction temperatures, the syngas reacts without the assistance of ethylene. The initiators and monomers are formed by CO dissociation via a carbide-type mechanism. As the reaction temperature increases, more CO undergoes direct dissociative hydrogenation. The observed promotional effect of ethylene therefore implies that the CO insertion mechanism exist simultaneously with the carbide-type mechanism. However, the effect of ethylene weakens as reaction temperature increases, which indicates that a carbide-type mechanism dominates at higher temperatures.

As X increased, the reactivity of carbon monoxide increased for temperatures between 160 to 200 °C. For example, when X was increased from 10% to 30%,  $X_{CO}$  increases as follows: from 4.5% to 6.4% at 160 °C; from 17% to 19.2% at 180 °C; from 21.4% to 26.3% at 200 °C. However, at 220 °C,  $X_{CO}$  decreased from 37.5% to 32.8% when X increased from 10% to 30%. Therefore, at high temperatures, a high ethylene partial pressure leads to a decrease in CO reactivity, which may be due to the increased competitive adsorption of ethylene relative to CO on active sites on the surface of the catalyst.

### **6.3.2. Ethylene reactivity**

The ethylene conversion  $X_{C_2H_4}$  and reaction rate for different X and varying reaction temperatures is shown in Figure 6.2. Figure 6.2(a) shows that, as the temperature increases,  $X_{C_2H_4}$  increases from 13.13% to 96.62% for X= 10%. It is worth noting that when there is no CO in the feed to the reactor (i.e. the feed gas is a mixture of ethylene and H<sub>2</sub>), the conversion of ethylene can reach 100%, under conditions of excess H<sub>2</sub>, even at low reaction temperatures

(100 °C), as shown in Table 6.2. The relatively  $X_{C_2H_4}$  that is observed in the presence of CO would support that there is a competitive adsorption between ethylene and CO on the catalyst surface and that this is a key factor in determining the ethylene reaction rate.

Under FTS conditions, CO occupies most of the active sites, which makes it difficult for the ethylene molecules to adsorb on the catalyst surface. As the reaction temperature increases, the adsorption and desorption rate of CO increases and more ethylene can adsorb on the surface, resulting in an increase in  $X_{C_2H_4}$  with increasing temperature. In addition, it is observed increasing  $X$  does not cause a significant increase in  $X_{C_2H_4}$ . This indicates that when the ethylene content exceeds 10% of the feed gas, the partial pressure of ethylene has little effect on the reactivity of ethylene over the cobalt-based catalyst. Schultz et al. obtained similar results [38] and reported that the selectivity of the ethylene hydrogenation reaction and the ethylene incorporation reaction was roughly constant.

The reaction rate of ethylene is shown in Figure 6.2(b). The reaction rate increases with increasing temperature. As the partial pressure of ethylene increases, the reaction rate of ethylene also increases. Moreover, a linear relationship between the reaction rate and the concentration of ethylene is observed, which indicates a first-order reaction (See Figure 6.2(b).)

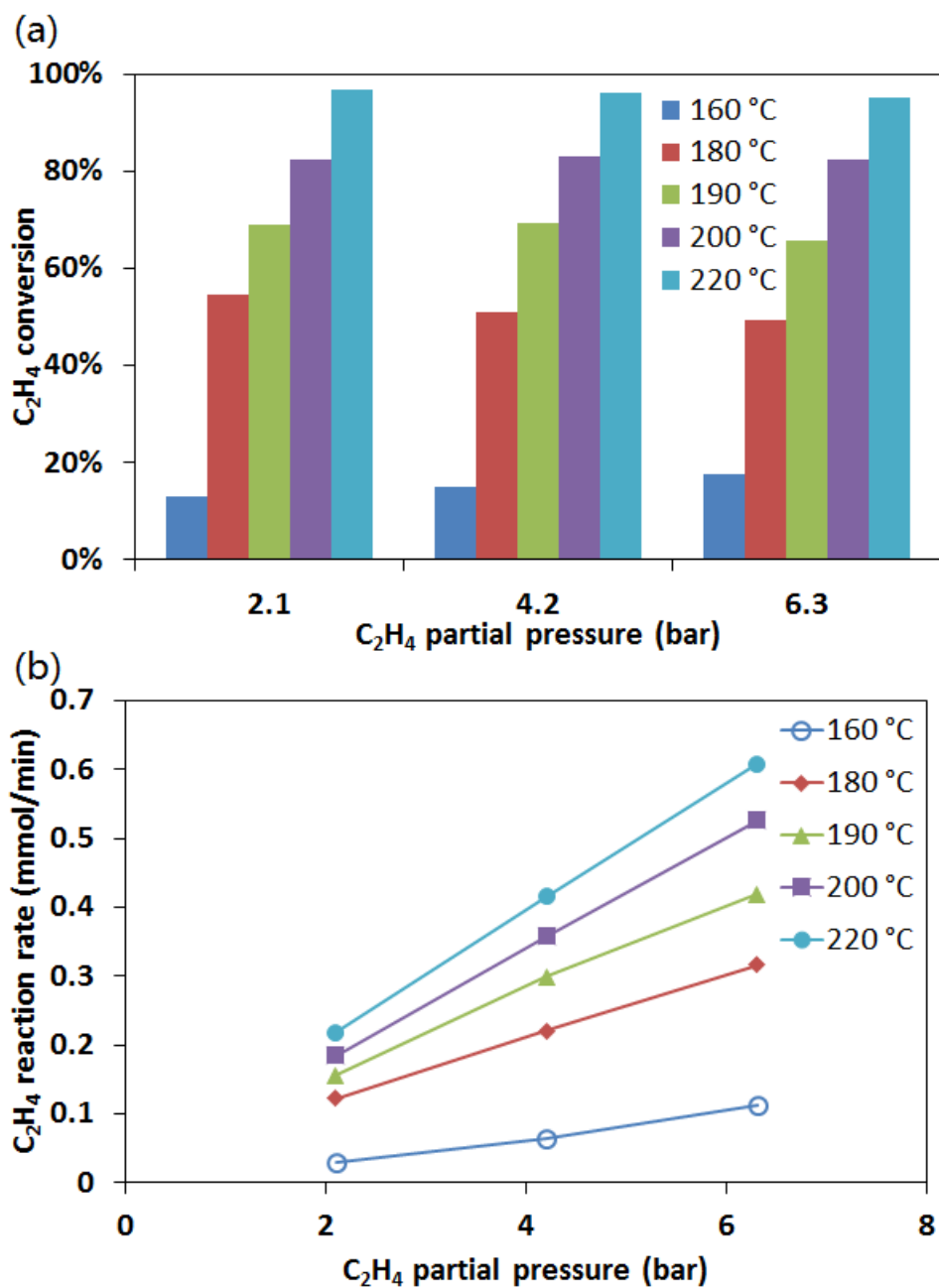


**Figure 6.2:** Ethylene conversion  $X_{C_2H_4}$  (a) and ethylene reaction rate (b) under different reaction temperatures and different ethylene partial pressure, over 15% Co/TiO<sub>2</sub> ( Reaction conditions: total reaction pressure - 21 bars; total flow rate - 50 ml (NTP)/min; feed gas composition – (40% H<sub>2</sub>; 20% CO; X% C<sub>2</sub>H<sub>4</sub>; (40-X)% Ar) , for X=0%, 10%, 20% or 30%).

**Table 6.2:** The conversion of ethylene in  $X_{C_2H_4}$  when using a feed of ethylene and  $H_2$ , ( $C_2H_4:H_2 = 55.5:45.5$ ) at low temperatures over the Co-based FTS catalyst.

Feed	55.5% $H_2$ / 45.5% $C_2H_4$		
	100°C	120°C	140°C
Temperature (°C)	100°C	120°C	140°C
$H_2$ conversion (%)	84.05%	84.56%	84.32%
$C_2H_4$ conversion $X_{C_2H_4}$ (%)	100.00%	100.00%	100.00%
$C_2H_6$ selectivity $S_{C_2H_6}$ (%)	99.18%	99.08%	98.79%

### 6.3.3. Side reactions

In order to investigate the effect of co-feeding ethylene on the product distribution of FTS, the selectivity and formation rates of various products are discussed in this section. The products considered include methane, ethane, propanal and C<sub>4</sub>. The reactions involved in forming these products include CO methanation to produce methane; ethylene hydrogenation to produce ethane; ethylene hydroformylation to produce propanal and ethylene dimerization to produce C<sub>4</sub>.

#### 6.3.3.1. Methanation

As the simplest hydrogenation product in FTS, methane plays an important role in understanding the CO hydrogenation reaction. However, there is still no definitive conclusion about the methane formation mechanism under FTS conditions, and the details of this mechanism still attracts interest [39]. In cobalt-based FTS, the challenge is to increase the selectivity of long chain products while simultaneously reducing the methane selectivity. Figure 6.3 shows: methane selectivity based on total carbon source  $S_{CH_4}$ ; the methane formation rate; and methane selectivity based on CO consumption  $S_{CH_4\_CO}$  for different X and reaction temperatures.

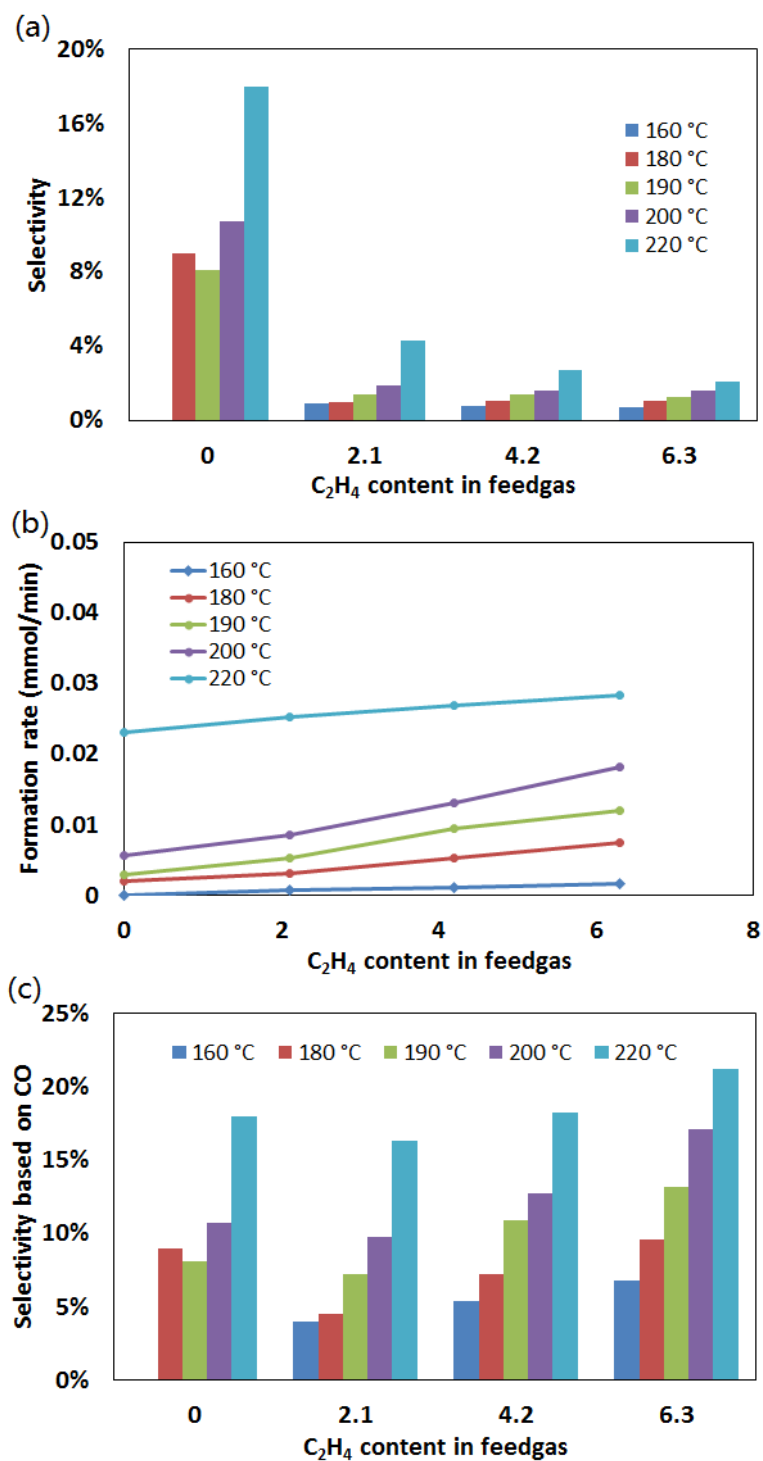


**Figure 6.3:** CH<sub>4</sub> selectivity based on total carbon source (a), CH<sub>4</sub> formation rate (b) and CH<sub>4</sub> selectivity based on CO (c) at different reaction temperatures, with different ethylene partial pressures in the feed over a 15% Co/TiO<sub>2</sub> catalyst. (Reaction conditions: total reaction pressure - 21 bars; total flow rate - 50 ml (NTP)/min; feed gas composition - 40% H<sub>2</sub>/ 20% CO / X% C<sub>2</sub>H<sub>4</sub>/ (40-X)% Ar, X=0%, 10%, 20% or 30%).

As shown in Figure 6.3(a), for  $X=0$  the methane selectivity  $S_{CH_4}$  is about 10% and does not change much as the temperature is increased from 180°C – 200 °C. (Under these conditions, the CO conversion is less than 15% as shown in Figure 6.1.) However, the  $S_{CH_4}$  increased to about 18% at 220 °C (corresponding to a CO conversion of 30% - see Figure 6.1.) This result is in line with other published results [39]. When the feed was changed to  $X= 10 \%$ , the  $S_{CH_4}$  decreased significantly and at 160 °C,  $S_{CH_4}$  dropped to less than 2% while it increased to around 4.3% at 220 °C.  $S_{CH_4}$  decreased with increasing partial pressure of ethylene (corresponding to increasing  $X$ ).

Figure 6.3(b) shows that the methane formation rate increases with increasing reaction temperature; this indicates that higher temperatures favours the formation of methane. In addition, as  $X$  increases, the rate of formation of methane increases as well. There is a linear relationship between the formation rate of methane and the partial pressure of ethylene. This result indicates that a portion of the methane may be produced from the demethylation reaction of ethylene, and that this reaction is first order in ethylene partial pressure.

Because there are two carbon sources in the reactor feed - CO and ethylene - it is hard to identify whether the methane was produced from the reaction of CO (Eq.6.7), ethylene (Eq. 6.8), or both.



If we define the methane selectivity based on CO consumption,  $S_{CH_4\_CO}$ , (see Figure 6.3(c)), we see that when  $X=10$ ,  $S_{CH_4\_CO}$  decreases compared to  $S_{CH_4\_CO}$  when  $X=0$ . This result indicates that ethylene has a negative effect on CO methanation. We speculate that there are two

possible causes for this inhibition. One is that when a certain amount of ethylene adsorbs on the surface of the catalyst, more CO reacts with ethylene via the CO insertion mechanism, rather than hydrogenating with H<sub>2</sub> via the carbide mechanism (CO direct dissociation to CH<sub>x</sub>). Another possibility is that CH<sub>x</sub>, which is a precursor of methane that is formed by CO dissociation and partial hydrogenation, reacts directly with the ethylene molecules or transient intermediates of ethylene adsorbed on the surface of the catalyst. Thus far, we do not have enough evidence to prove the mechanism of methane formation and it is likely to be the result of a combination of the two mechanisms.

Furthermore, Figure 6.3(c) shows that as the partial pressure of ethylene increases,  $S_{CH_4\_CO}$  rises sharply for temperatures less than 220 °C. This is obviously not caused by CO methanation, but as previously described is due to the demethylation reaction of ethylene.

### 6.3.3.2. Ethylene hydrogenation

Many studies indicate that the main reaction when co-feeding 1-olefins is hydrogenation, which forms the corresponding alkanes [38]. In the absence of CO, more than 90% of the ethylene is hydrogenated to ethane under typical Co-based catalyst FTS condition, as shown in Table 6.2. Figure 6.4(a) and 6.4(c) show ethane selectivity based on total carbon source  $S_{C_2H_6}$  and ethane selectivity based on ethylene consumption  $S_{C_2H_6\_C_2H_4}$ , respectively for varying X. The formation rate of ethane under different reaction conditions is shown in Figure 6.4(b).

As shown in Figure 6.4(a), for X=0 (no ethylene in the feed),  $S_{C_2H_6}$  is between 1% to 2.5%, for reaction temperatures between 180 to 220 °C. This is consistent with the low C<sub>2</sub> selectivity normally observed in cobalt-based FTS [40]. In addition, at a relatively high reaction temperature (220 °C),  $S_{C_2H_6}$  is significantly higher than at the low reaction temperatures (less

than 200 °C). This is consistent with results that show that a higher temperature favours the production of light hydrocarbons [41]. However, when co-feeding ethylene,  $S_{C_2H_6}$  increases sharply to nearly 60%, indicating that ethylene undergoes a hydrogenation reaction. An increase in the partial pressure of ethylene leads to a decrease in  $S_{C_2H_6}$  at lower reaction temperatures (160 and 180 °C). However,  $S_{C_2H_6}$  does not change much when the reaction temperature increases (from 200 – 220 °C) and/or the partial pressure of ethylene increases (X increases from 10% to 30%).

Figure 6.4(b) shows that the formation rate of ethane is low when  $X=0$  over the whole temperature range tested (160 to 220 °C) even though  $X_{CO}$  increased from 0 to more than 30%. (See Figure 6.1.) This indicates that the amount of ethane formed in the FTS reaction is very low. As X increases, the formation rate of ethane increases significantly and the formation rate of ethane is approximately linear with respect to partial pressure of ethylene. This strongly suggests that ethane is mainly derived from ethylene hydrogenation.

Since only a small amount of the reacted CO is hydrogenated to ethane in typical cobalt-based FTS, we assume that the observed ethane (for  $X>0$ ) is produced almost entirely from the hydrogenation of ethylene in the feed. As shown in Figure 6.4(c), when  $X= 10\%$ , more than 70% of the reacted ethylene hydrogenates to form ethane.  $S_{C_2H_6\_C_2H_4}$  is not sensitive to reaction temperature (except at 160 °C), and decreases with increasing ethylene partial pressure. It can be seen in Figure 6.4(c) that there is a decreasing relationship between  $S_{C_2H_6\_C_2H_4}$  and ethylene partial pressure for temperatures greater than 160 °C. This indicates that the more ethylene that is added, the more ethylene participates in other reactions other than hydrogenation.

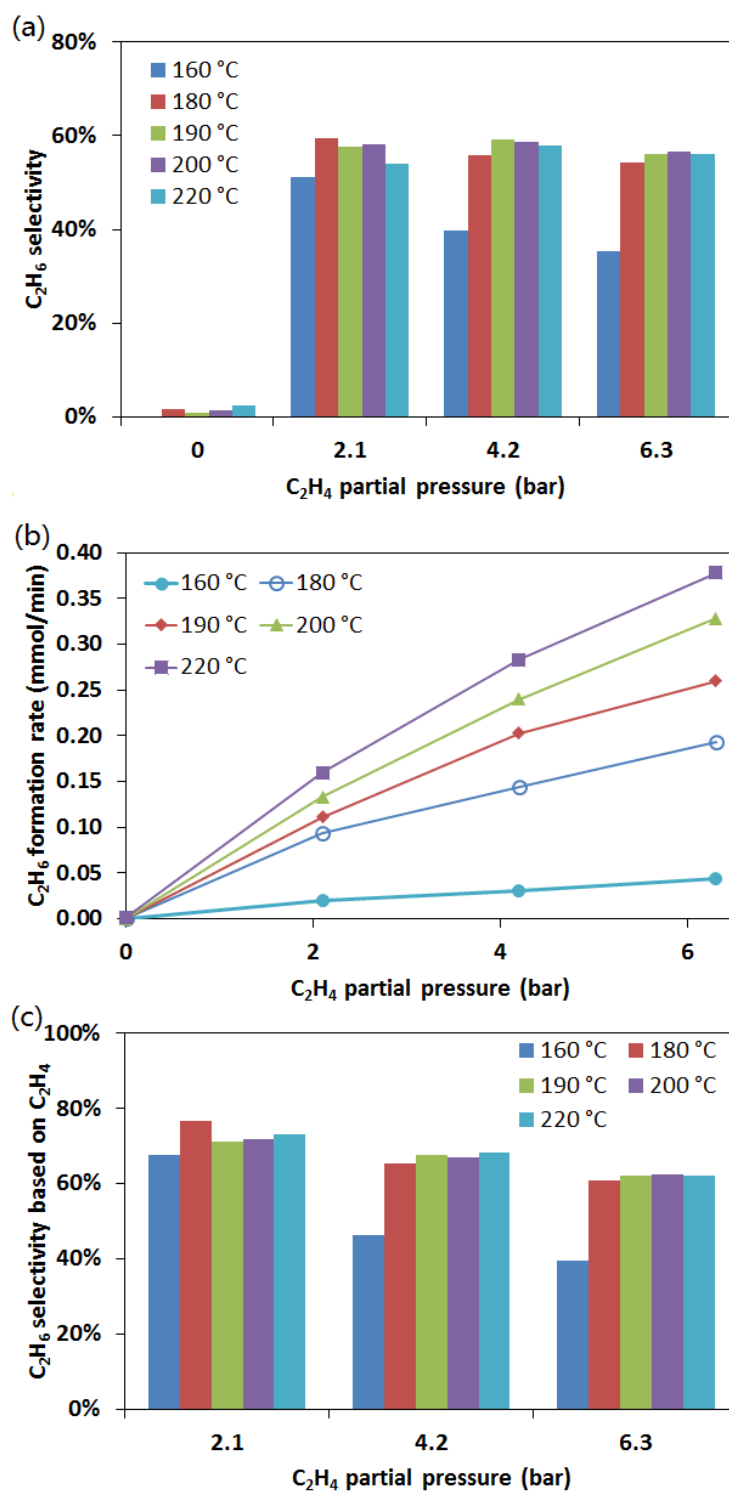


**Figure 6.4:** C<sub>2</sub>H<sub>6</sub> selectivity based on total carbon source (a), C<sub>2</sub>H<sub>6</sub> formation rate (b) and C<sub>2</sub>H<sub>6</sub> selectivity, based on C<sub>2</sub>H<sub>4</sub> (c) at different reaction temperatures, with different ethylene partial pressure levels over 15% Co/TiO<sub>2</sub>. (Reaction conditions: total reaction pressure - 21 bars; total flow rate - 50 ml (NTP)/min; feed gas composition (40% H<sub>2</sub>; 20% CO ; X% C<sub>2</sub>H<sub>4</sub>; (40-X)% Ar) where X=0%, 10%, 20% or 30%).

### 6.3.3.3. Hydroformylation

Hydroformylation is a very special side reaction in FTS. In the CO insertion mechanism in FTS, aldehyde - the hydroformylation product - is an intermediate or precursor, which can undergo further hydrogenation to form alcohols and hydrocarbons.

The selectivity of propanal - a product of ethylene hydroformylation - based on total carbon source  $S_{C_2H_5CHO}$  is shown in Figure 6.5(a). Figure 6.5(a) indicates that propanal was detected in the product when  $X=0$  (no ethylene in the feed) which indicates that the rate of the hydroformylation reaction is very low for all reaction temperatures between 160 to 220 °C. For a feed of  $X= 10\%$ , propanal was formed at temperatures above 160 °C; however for  $X= 30\%$ , propanal was detected even at 160 °C. The production of propanal in the presence of ethylene is experimental evidence of the CO insertion mechanism, as CO insertion must occur to make the aldehyde. When compared to the normal FTS product formed from a feed of syngas, this indicates that the reaction precursor (chain growth initiator) which is formed from ethylene on the catalyst surface and into which the CO insertion occurs might be different from the chain growth initiator for FTS.

As shown in Figure 6.5(a),  $S_{C_2H_5CHO}$  increased from 4.5% to 6.1% for  $X=0\%$  when the temperature was increased from 180 to 220 °C. Furthermore,  $S_{C_2H_5CHO}$  decreases with increasing  $X$ . As will be seen from Figure 6.5(b) this occurs because, although the rate of propanol formation increases with increasing ethylene in the feed, the amount of carbon participate into reaction increases faster. On one hand, with  $X$  increasing, more ethylene converts to ethane and other products. On another hand, the increasing added ethylene promote CO hydrogenated-chain growth reaction.  $S_{C_2H_5CHO}$  decreases with increasing temperature (corresponding to increasing CO conversion). This phenomenon can be

attributed to the higher FTS reaction activity at higher temperatures. This result also suggests that there is competition between the CO insertion mechanism and the CO dissociation mechanism occurring in cobalt-based catalytic FTS.

Figure 6.5(b) shows the formation rate of propanal at different reaction conditions. The formation rate of the ethylene hydroformylation product at constant X increases with temperature. In addition, at the same reaction temperature, the formation rate of propanal increases linearly with X for temperatures between 180 to 220 °C. Furthermore, the slope of the trend line increases from 180 to 200 °C, but decreases at 220 °C.

The hydroformylation reaction between ethylene and CO can be described as per Eq. 6.9:



Thus for each molecule of propanal one molecule of CO and one molecule of ethylene are consumed. In order to investigate the reactivity of CO and ethylene in hydroformylation, the propanal selectivity based on CO consumption,  $S_{C_2H_5CHO\_CO}$ , and on  $C_2H_4$  consumption,  $S_{C_2H_5CHO\_C_2H_4}$ , are shown in Figure 6.5(c) and 6.5(d), respectively.

As shown in Figure 6.5(c), with a feed of X = 10%,  $S_{C_2H_5CHO\_CO}$  increases from 6.75% to 10% as temperature increases from 180 to 200 °C. This result indicates that a higher reaction temperature promotes the CO hydroformylation reaction.  $S_{C_2H_5CHO\_CO}$  drops to 7.76% as the temperature is further increased to 220 °C. This suggests competition between the CO insertion mechanism and the CO dissociation hydrogenation mechanism on the catalyst surface.  $S_{C_2H_5CHO\_CO}$  increases linearly with increasing X, even when the ethylene: CO ratio in the feed is greater than 1 (X=30%).

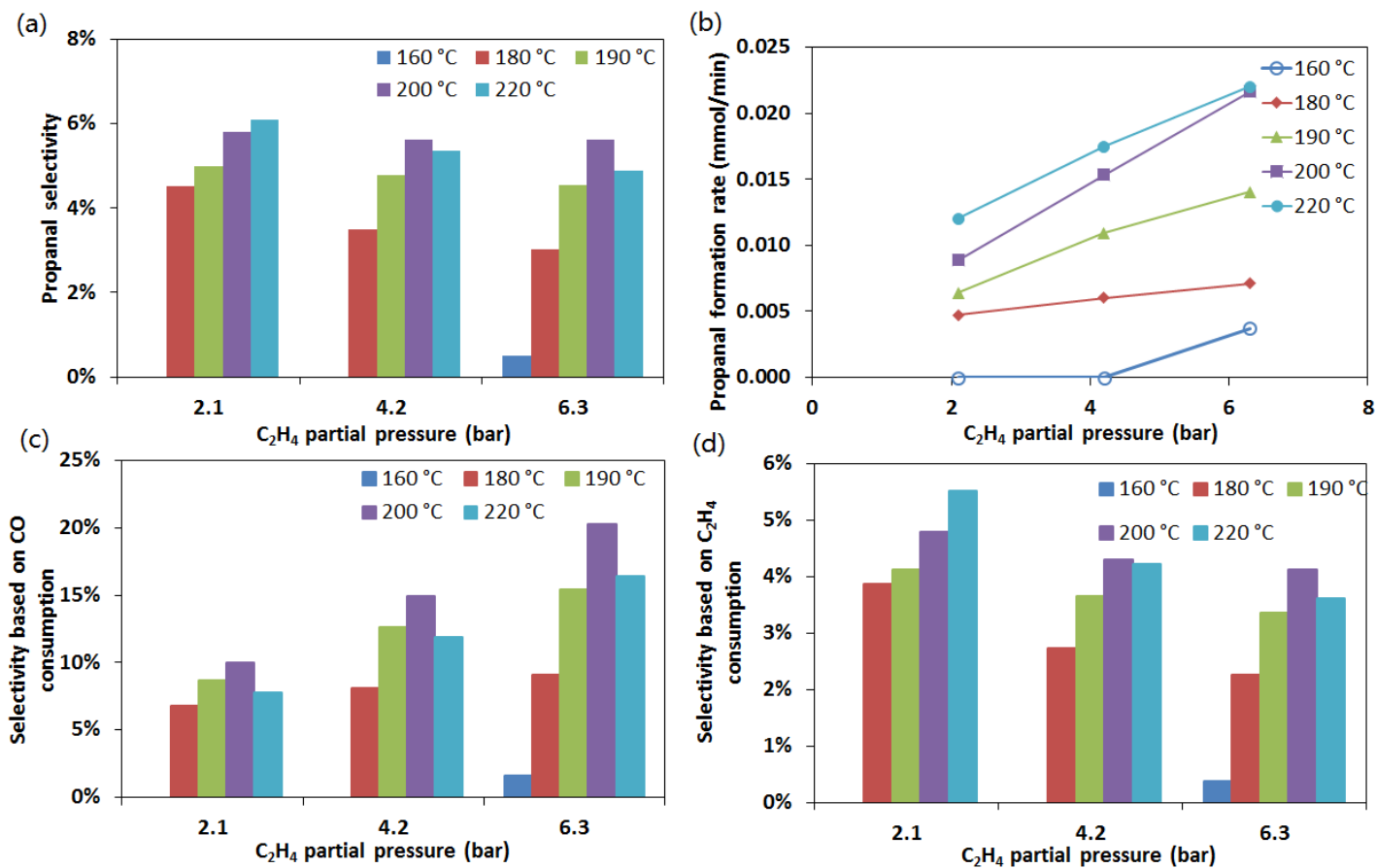


**Figure 6.5:** Propanal selectivity  $S_{C_2H_5CHO}$  (a), the formation rate of propanal (b), propanal selectivity based on CO consumption  $S_{C_2H_5CHO\_CO}$  (c) and propanal selectivity based on C<sub>2</sub>H<sub>4</sub> consumption  $S_{C_2H_5CHO\_C_2H_4}$  (d), under different reaction temperatures with different ethylene partial pressure levels over 15% Co/TiO<sub>2</sub>. (Reaction conditions: total reaction pressure - 21 bars; total flow rate - 50 ml (NTP)/min; feed gas composition - 40% H<sub>2</sub>/ 20% CO / X% C<sub>2</sub>H<sub>4</sub>/ (40-X)% Ar, X=0%, 10%, 20% or 30%).

It is worth mentioning that at reaction temperatures between 180 to 200 °C,  $S_{C_2H_5CHO\_CO}$  increases with X. However, as temperature is increased to 220 °C,  $S_{C_2H_5CHO\_CO}$ . When X=10%,  $S_{C_2H_5CHO\_C_2H_4}$  increases from 3.8% (at 180 °C) to 5.5% (at 220 °C) as shown in See Figure 6.5(d). However, as X increases,  $S_{C_2H_5CHO\_C_2H_4}$  decreases for temperatures of 180 °C or higher. This implies that as the partial pressure of ethylene increases, more ethylene participates in other reactions than hydroformylation.

#### 6.3.3.4. Dimerization

The  $C_4$  products are of special interest due to the large number different reaction that lead to the formation of these products. They may be derived solely from the CO hydrogenation chain growth of FTS, the dimerization of co-fed ethylene, or even combinations of the FT chain growth reaction and ethylene insertion.

The on-line GC detected four kinds of  $C_4$  products: 1-butene, n-butane, trans-2-butene and cis-2-butene. The selectivity and formation rates of the various  $C_4$  products are shown in Figure 6.6.

For a syngas feed (X=0) it is observed that:

- (1) The highest 1-butene selectivity occurs the 180 °C. It was approximately constant at higher temperatures.
- (2) The n-butane selectivity has a minimum at 190 °C.
- (3) No trans- and cis- 2-butene were produced.

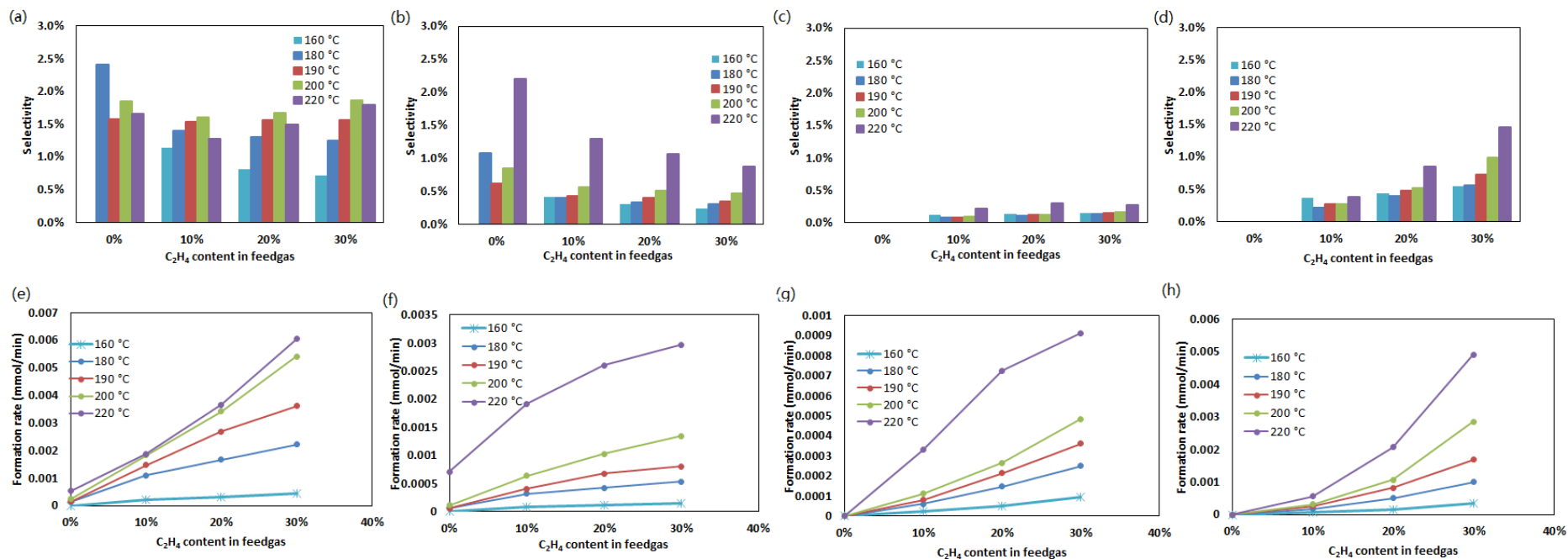


**Figure 6.6:** The selectivity and formation rate of C<sub>4</sub> products, i.e. the selectivity of 1-butene (a), n-butane (b), trans-2-butene (c), cis-2-butene (d) and the formation rate of 1-butene (e), n-butane (f), trans-2-butene (g), cis-2-butene (h) under different reaction temperatures, with different ethylene partial pressure levels, over 15% Co/TiO<sub>2</sub>. (Reaction conditions: total reaction pressure - 21 bars; total flow rate - 50 ml (NTP)/min; feed gas composition - 40% H<sub>2</sub>/ 20% CO / X% C<sub>2</sub>H<sub>4</sub>/ (40-X)% Ar, X=0%, 10%, 20% or 30%).

When co-feeding ethylene, it is observed that:

- (1) There was a maximum in the n-butane selectivity at 200 °C.
- (2) The n-butane selectivity increased with increasing temperature.
- (3) Some amount of trans- and cis 2-butene were produced. The selectivity of cis-2-butene was higher than that of trans-2-butene. This is consistent with Kokes' report [42]. Cis-2-butene is considered a primary product of dimerization and trans-2-butene an isomeric product of cis-2-butene. Moreover, the highest selectivity of trans- and cis 2-butene was obtained as 220 °C.
- (4) Increasing X from 10% to 30% did not change the C<sub>4</sub> selectivity much.

In addition, the reaction rate of these four kinds of C<sub>4</sub> products increased with an increase in both the partial pressure of ethylene and the reaction temperature. Both trans- and cis 2-butene were only detected when co-feeding ethylene, which indicates that the production of 2-butene may result from ethylene dimerization rather than isomerization of 1-butene.

#### **6.3.4. Product distribution**

In order to investigate the effect of co-feeding ethylene on the product distribution, the chain growth probability ( $\alpha$ -values) of the light hydrocarbons C<sub>3</sub>-C<sub>6</sub> were calculated and compared. Figure 6.7 is an example of an ASF plot fitted to the experimental, and it can be seen that both the light olefin and the light paraffin products follow a typical ASF plot. It is important to note that the overall product distribution also fits the ASF model, even when co-feeding a large amount of ethylene.

The  $\alpha$ -values of the olefins, paraffins and hydrocarbons (olefins + paraffins) were calculated, based on the slope of the ASF plot ( $C_3$  to  $C_6$ ) and are listed in Table 6.3.

Table 6.3 shows that the  $\alpha$ -values of olefins are lower than those of paraffins and that they follow the order (1-olefins) < (hydrocarbons) < (n-paraffins) for each run, even when co-feeding large amounts of ethylene. The  $\alpha$ -values at 220 °C are lower than those observed at lower temperatures in almost all cases, which indicates that a higher temperature favours the formation of small molecular hydrocarbons.

The  $\alpha$  of the hydrocarbon product for a feed of  $X=10$  is higher than that from a feed of  $X=0$  at temperatures between 180 °C – 190 °C. However, the  $\alpha$ -value of the hydrocarbon product with feed  $X=10$  is lower than that produced from a syngas feed at 220 °C (See Table 6.3.) In addition, increasing  $X$  from 10% to 30% seems to result in a slight decrease in the  $\alpha$ -values. For the co-feeding experiments, the highest  $\alpha$  value is obtained at 180 °C with  $X=10\%$  while the lowest  $\alpha$  value occurs at 220 °C with a feed of  $X=30\%$  ethylene. (See Table 6.3).

The results indicate that adding a certain amount of ethylene at low reaction temperatures has the potential to increase the chain growth probability, and consequently to improve the selectivity to long chain hydrocarbons. When a large amount of ethylene are added to the feed, it inhibits chain growth at higher reaction temperatures.

At a lower reaction temperature (< 200 °C): the added ethylene could absorb and participate in the ethylene-assisted chain growth reaction, which promoted the conversion of CO to longer chain hydrocarbons. Thus, both the CO conversion and chain-growth factor ( $\alpha$ ) were increased by adding 10% ethylene to the FTS reaction system. However, further increasing the partial pressure of ethylene enhanced the ethylene reaction rate via the "ethylene hydrocracking chain growth mechanism (as mentioned in Chapter 4), which led to the

production of short-chain products with a low alpha value. Therefore, co-feeding 20% or 30% of ethylene decreased the chain growth probability (Table 6.3).

At a higher reaction temperature (220 °C), both CO hydrogenation via the CO dissociation mechanism and ethylene hydrogenation with ethylene hydrocracking occurred competitively, resulting in chain growth. The promotional effect of ethylene on the FTS system weakened. When adding 10% of ethylene, CO conversion only increased slightly. Increasing the concentration of ethylene in the feed resulted in more H<sub>2</sub> being consumed by the ethylene hydrogenation reaction, and the production of short-chain hydrocarbons. The more that is ethylene added, the lower the CO conversion and the lower the chain growth factor ( $\alpha$ -value).

**Table 6.3:** The  $\alpha$ -values of olefins, paraffins and hydrocarbons (paraffins + olefins) at different reaction temperatures and with different ethylene partial pressure levels over 15% Co/TiO<sub>2</sub> (Reaction conditions: total reaction pressure - 20 bars; total flow rate - 50 ml (NTP)/min; feed gas composition - 40% H<sub>2</sub>/ 20% CO / X% C<sub>2</sub>H<sub>4</sub>/ (40-X)% Ar= X)

<b>Chain growth probability (<math>\alpha</math>-values)</b>					
<b>Feed</b>	<b>160 °C</b>	<b>180 °C</b>	<b>190 °C</b>	<b>200 °C</b>	<b>220 °C</b>
Hydrocarbons (olefins + paraffins, C <sub>3</sub> -C <sub>6</sub> )					
X=0%	/	0.61	0.68	0.7	0.75
X=10%	0.73	0.74	0.72	0.7	0.7
X=20%	0.66	0.72	0.7	0.69	0.64
X=30%	0.68	0.69	0.71	0.7	0.59
Olefins (C <sub>3</sub> -C <sub>6</sub> )					
X=0%	/	0.56	0.66	0.67	0.64
X=10%	0.72	0.73	0.7	0.67	0.61
X=20%	0.66	0.71	0.69	0.66	0.58
X=30%	0.67	0.69	0.7	0.68	0.56
Paraffins (C <sub>3</sub> -C <sub>6</sub> )					
X=0%	/	0.74	0.74	0.81	0.83
X=10%	0.74	0.8	0.8	0.81	0.77
X=20%	0.67	0.76	0.77	0.79	0.73
X=30%	0.7	0.72	0.77	0.8	0.67

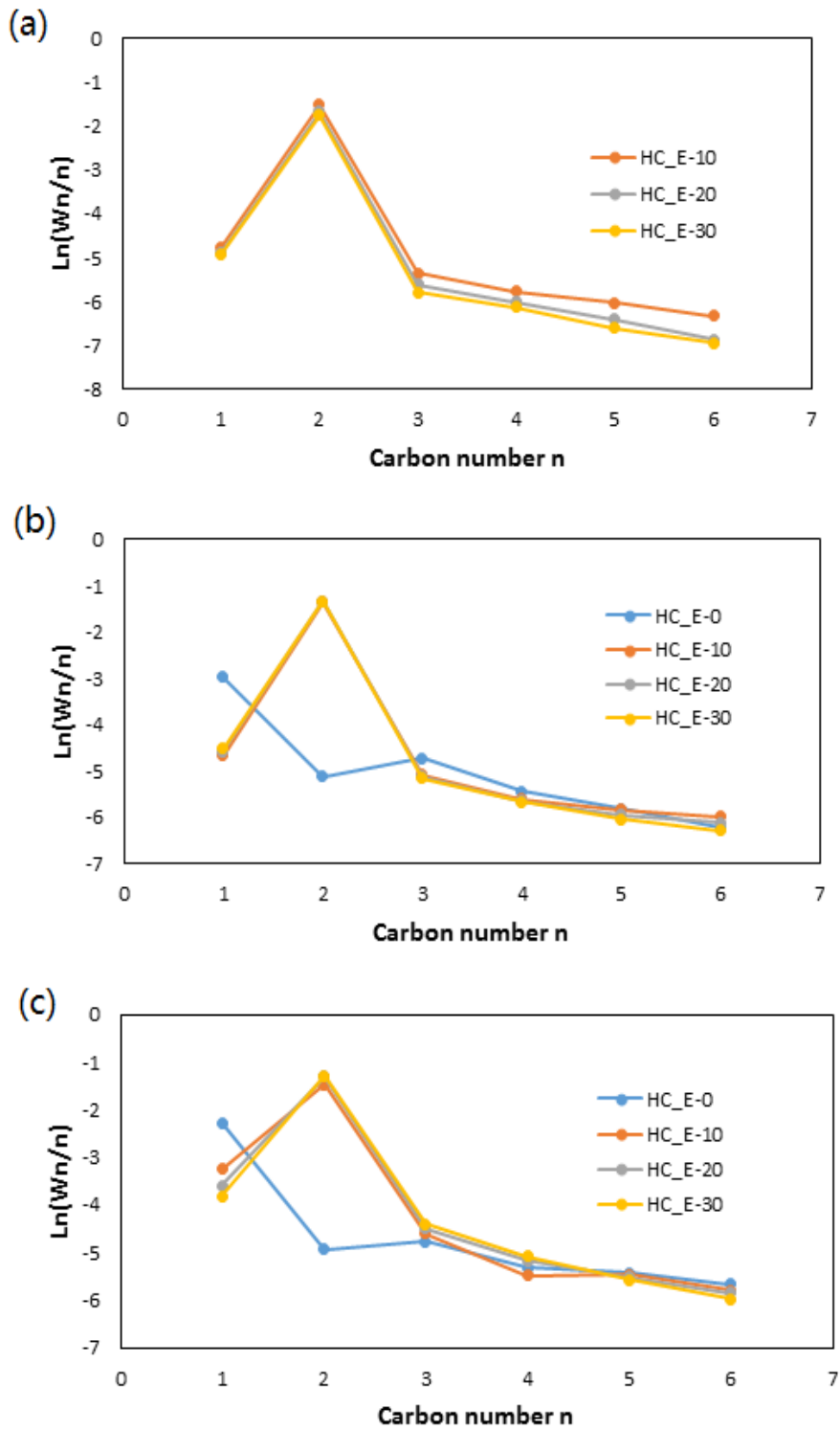


**Figure 6.7:** Examples of the experimental data fitted to an ASF plot: (a) 160 °C; (b) 180 °C; (c) 220 °C.

#### 6.4. Discussion

The previous section considered the effect of co-feeding ethylene on catalyst activity and selectivity. Table 6.4 lists the results for two different feed gases namely,  $X=0\%$  and  $X=10\%$ , at low temperatures (160 °C and 180 °C). The results for a feed gas of  $H_2:C_2H_4$  are shown in Table 6.2, where it can be seen that the  $X_{C_2H_4}$  can be 100%, even at the very low temperatures of 100 to 140 °C. However, when both CO and ethylene are fed to the reactor, the  $X_{C_2H_4}$  drops to 13.1% at 160 °C, which suggests that there is the competitive adsorption between ethylene and CO on the catalyst surface.

Some literature proposed that there is competitive adsorption between CO and olefins during FTS [31, 32]. Boelee et al. found that reducing the partial pressure of CO increased the reaction rate of  $\alpha$ -olefins [31]. They attributed this to the competitive adsorption of  $\alpha$ -olefins and CO. A similar conclusion was reached by Hanlon and Satterfield [32], who reported that the conversion of olefins increased at high CO conversion (low CO partial pressure in the reactor). The results of this study indicate that CO inhibits the reactivity of ethylene. However, a CO conversion increased when co-feeding small amounts of ethylene, which suggests that ethylene promotes the reactivity of CO during FTS.

When large amount of ethylene is co-fed into FTS system at high temperature, the co-feeding ethylene caused insufficient  $H_2$  for CO hydrogenation. Yang et al. considered the "H-scavenging effect" of ethylene as a reasonable explanation for the reduced CO conversion when co-feeding more ethylene into a reactor [43]. Our research results (Figure 6.1) show that CO conversion increases when co-feeding 10% ethylene, and then decreases when co-feeding 30% ethylene in syngas at 220 °C. At this high temperature, a large amount of ethylene reacted with  $H_2$ , which suppressed CO conversion, due to insufficient  $H_2$ .

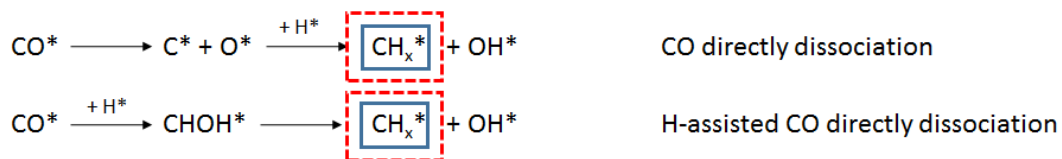
**Table 6.4:** Reactant activity and product selectivity over FTS catalyst of 15% Co/TiO<sub>2</sub> for low temperature reaction.

	<b>H<sub>2</sub>/CO/Ar =</b>		<b>H<sub>2</sub>/CO/C<sub>2</sub>H<sub>4</sub>/Ar =</b>	
<b>Feed</b>	<b>40%:20%:40%</b>		<b>40%:20%:10%:30%</b>	
<b>Temperature, °C</b>	160	180	160	180
<b>CO conversion, %</b>	0.00%	5.48%	4.49%	17.01%
<b>C<sub>2</sub>H<sub>4</sub> conversion, %</b>	/	/	13.13%	54.48%
<b>Selectivity based on total carbon</b>				
<b>CH<sub>4</sub></b>	/	9.02%	0.94%	1.01%
<b>C<sub>2</sub>H<sub>6</sub></b>	/	1.71%	51.10%	59.59%
<b>C<sub>3</sub>H<sub>6</sub></b>	/	4.18%	1.39%	1.93%
<b>C<sub>3</sub>H<sub>8</sub></b>	/	1.14%	0.35%	0.36%
<b>C<sub>3</sub>H<sub>8</sub>O</b>	/	0.00%	0.00%	4.50%
<b>1-C<sub>4</sub>H<sub>8</sub></b>	/	2.41%	1.14%	1.40%
<b>trans-2-C<sub>4</sub>H<sub>8</sub></b>	/	0.00%	0.12%	0.08%
<b>cis-2-C<sub>4</sub>H<sub>8</sub></b>	/	0.00%	0.37%	0.21%
<b>n-C<sub>4</sub>H<sub>10</sub></b>	/	1.07%	0.41%	0.40%

Various reaction mechanisms have been proposed to describe the initiation, chain growth and termination steps of the FTS reaction [44-45]. Among these are two popular mechanisms: namely the CO dissociation-type mechanism, which was originally proposed by Fischer and Tropsch [44]; the other is the CO insertion mechanism that was initially developed by Pichler and Schulz [45]. There are two CO dissociation pathways that form CH<sub>x</sub> in CO dissociation-type mechanism, which are referred to as CO direct dissociation and hydrogen-assisted CO dissociation. Scheme 6.1 shows the scheme of both these routes, where CH<sub>x</sub> is a monomer for carbon chain growth in the CO dissociation-type mechanism. Researchers have developed various kinetic models based on these two reaction mechanisms [23, 46-48]. In recent years, with the development of computational chemistry, density functional theory (DFT) calculations have focussed on FTS, using these two mechanisms [49-53].

No propanal was detected in the product when using syngas as the feed (X=0%) at any reaction temperatures. However, when co-feeding ethylene, propanal was produced temperatures of 180 °C or higher, which indicate that CO and ethylene could react even at relatively low temperatures (See Table 6.3 and Figure 6.5). Although there is no reaction at 160 °C for a feed of syngas (X=0%), CO reacts to form hydrocarbons when ethylene is added to the feed, and the product distribution followed an ASF distribution (See Figure 6.7). These results illustrate that both ethylene and CO participate in the chain growth reactions that produce the hydrocarbon products. Therefore, we propose that CO reacts with ethylene via the CO insertion mechanism and the absorbed CO\* can act as a chain growth monomer while ethylene can act as initiator.

(a) CO dissociation type mechanism



(b) Ethylene-assisted CO insertion mechanism



  Chain growth initiator      Chain growth monomer

**Scheme 6.1:** Pathways of the CO dissociation-type mechanism [44] and CO insertion mechanism [45].

## 6.5. Conclusions

The effect of ethylene on catalyst activity and selectivity was investigated using a Co/TiO<sub>2</sub> catalyst. Different amount ( $X=0, 10, 20$  and  $30\%$ ) of ethylene was introduced into FTS reaction system.

When using a feed of syngas ( $X=0\%$ ), it was observed that:

1. No reactions occurs at  $160\text{ }^{\circ}\text{C}$
2. A very low CO conversion ( $5.5\%$ ) was obtained at  $180\text{ }^{\circ}\text{C}$ .
3. The CO conversion increased with an increase in reaction temperature.
4. No propanal was detect in the product.

When co-feeding ethylene ( $X>0$ ) it was found that:

1. CO reacted at  $160\text{ }^{\circ}\text{C}$ ;
2. The CO conversion increased with the addition of ethylene when  $X<30\%$ ; this indicates a positive effect of ethylene on the catalyst activity at low concentrations of ethylene;
3. The CO conversion increased with temperature;
4. The methane selectivity decreased ( $<4.1\%$ ) and the ethane selectivity increased ( $>50\%$ ). This indicates that the CO methanation reaction was suppressed by adding ethylene. The dominant reaction of ethylene was hydrogenation reaction to form ethane;
5. A relatively high propanal selectivity was obtained, which indicates that CO and ethylene reacted via the hydroformylation reaction;
6. Trans- and cis-2 butene were produced via ethylene dimerization.

In addition, the light products ( $C_3$ - $C_6$ ) followed the ASF distribution for both the syngas feed ( $X=0\%$ ) as well as the experiments with ethylene co-feeding ( $X=10$  to  $30\%$ ). The effect of ethylene on chain growth probability was complex, as a positive effect was obtained at lower reaction temperatures ( $<200$  °C); while there was a negative influence was observed at the highest reaction temperature ( $220$  °C).

Comparing the activity and selectivity measured when using a feed of syngas only or feeds of syngas and ethylene, we suggest that CO, ethylene and  $H_2$  may react via the CO-insertion mechanism, especially at low reaction temperatures.

## REFERENCES:

1. Qian, W., Zhang, H., Ying, W., & Fang, D. (2011). Product distributions of Fischer-Tropsch synthesis over Co/AC catalyst. *Journal of Natural Gas Chemistry*, 20(4), 389-396.
2. Price, S. W., Martin, D. J., Parsons, A. D., Sławiński, W. A., Vamvakeros, A., Keylock, S. J. ... & Mosselmanns, J. F. W. (2017). Chemical imaging of Fischer-Tropsch catalysts under operating conditions. *Science Advances*, 3(3), e1602838.
3. Lu, X., Hildebrandt, D., Liu, X., & Glasser, D. (2012). A thermodynamic approach to olefin product distribution in Fischer–Tropsch Synthesis. *Industrial & Engineering Chemistry Research*, 51(51), 16544-16551.
4. Hanlon, R. T., & Satterfield, C. N. (1988). Reactions of selected 1-olefins and ethanol added during the Fischer-Tropsch synthesis. *Energy & Fuels*, 2(2), 196-204.
5. Tau, L. M., Dabbagh, H. A., & Davis, B. H. (1990). Fischer-Tropsch synthesis: Carbon-14 tracer study of alkene incorporation. *Energy & Fuels*, 4(1), 94-99.
6. Soled, S., Iglesia, E., & Fiato, R. A. (1990). Activity and selectivity control in iron catalyzed Fischer-Tropsch synthesis. *Catalysis Letters*, 7(1-4), 271-280.
7. Herzog, K., & Gaube, J. (1989). Kinetic studies for elucidation of the promoter effect of alkali in Fischer-Tropsch iron catalysts. *Journal of Catalysis*, 115(2), 337-346.
8. Liu, X., Li, X., & Fujimoto, K. (2007). Effective control of carbon number distribution during Fischer–Tropsch synthesis over supported cobalt catalyst. *Catalysis Communications*, 8(9), 1329-1335.
9. Shi, B., & Davis, B. H. (2003). Fischer–Tropsch synthesis: evidence for chain initiation by ethene and ethanol for an iron catalyst. *Topics in Catalysis*, 26(1-4), 157-161.
10. Zhang, R., Hao, X., & Li, Y. (2011). Investigation of acetylene addition to Fischer–Tropsch Synthesis. *Catalysis Communications*, 12(12), 1146-1148.

11. Jacobs, G., & Davis, B. H. (2014). Applications of isotopic tracers in Fischer–Tropsch synthesis. *Catalysis Science & Technology*, 4(11), 3927-3944.
12. Jordan, D. S., & Bell, A. T. (1986). Influence of ethylene on the hydrogenation of carbon monoxide over ruthenium. *The Journal of Physical Chemistry*, 90(20), 4797-4805.
13. Pichler, H. M. Z. K., Schulz, H., & Elstner, M. (1967). Gesetzmässigkeiten bei der synthese von kohlenwasserstoffen aus kohlenoxid und wasserstoff. *Brennstoff-Chemie*, 48(3), 78.
14. Schulz, H., Ramananda, R., & Elstner, M. (1970). Carbon-14 studies for the evaluation of the reaction mechanism of the Fischer-Tropsch synthesis. *Erdoel Kohle, Erdgas, Petrochem. Brennst.-Chem.*, 23(10).
15. Schulz, H., Gökcebay, H., Prepr. Ninth Conf. on Catal. and Organic Reactions, Charleston, S.C., USA (1982), in: J.R. Kosak, (Eds.), *Catalysis of Organic Reactions*, Marcel Dekker, New York, 1984.
16. Smith, D. F., Hawk, C. O., & Golden, P. L. (1930). The mechanism of the formation of higher hydrocarbons from water gas. *Journal of the American Chemical Society*, 52(8), 3221-3232.
17. Eidus, Y. T., Zelinskii, N. D., & Ershov, N. I. (1948). o kondensiruyushchem deistvii metilenovykh radikalov na etilen. *doklady akademii nauk sssr*, 60(4), 599-601.
18. Eidus, Y. T. (1950). ND 7. Elinskii, and KV Puzitskii. *Izvest. Akad. Nauk SSSR, Otdel. Khim, Nauk*, 98.
19. Eidus, Y. T., Zelinskii, n. D., puzitskii, k. V., & ershov, n. I. (1952). \* o kataliticheskoi gidrokondensatsii okisi ugleroda s olefinami. 7. Vliyanie kontsentratsii okisi ugleroda na protsess ee gidrokondensatsii s propilenom i n-butilenom. *Izvestiya akademii nauk sssr-seriya khimicheskaya*, (1), 145-151.

20. Eidus, Y. T., & Ordyan, M. B. (1957). Methylation of cyclopentene by methylene radicals that form when carbon monoxide is reduced by contact with hydrogen. In *Doklady Akademii Nauk* (Vol. 116, No. 1, pp. 101-104). Russian Academy of Sciences.
21. Puzitskii, K. V. E., Eidus, Y. T., & Ryabova, K. G. (1961). Production of carboxylic acids and their esters by acid catalysis from carbon monoxide and alcohols. In *Doklady Akademii Nauk* (Vol. 141, No. 3, pp. 636-637). Russian Academy of Sciences.
22. Eidus, Y. T. (1967). The mechanism of the Fischer–Tropsch reaction and the initiated hydropolymerisation of alkenes, from radiochemical and kinetic data. *Russian Chemical Reviews*, 36(5), 338.
23. Schulz, H., & Achtsnit, H. D. (1977). Olefin reactions during the Fischer-Tropsch Synthesis. *Revista Portuguesa de Quimica, Lisboa*, 19(1-4), 317-322.
24. Iglesia, E., Soled, S. L., Fiato, R. A., & Via, G. H. (1993). Bimetallic synergy in cobalt ruthenium Fischer-Tropsch synthesis catalysts. *Journal of Catalysis*, 143(2), 345-368.
25. Chen, W., Filot, I. A., Pestman, R., & Hensen, E. J. (2017). Mechanism of cobalt-catalyzed CO hydrogenation: 2. Fischer–Tropsch Synthesis. *ACS catalysis*, 7(12), 8061-8071.
26. McNab, A. I., McCue, A. J., Dionisi, D., & Anderson, J. A. (2017). Quantification and qualification by in-situ FTIR of species formed on supported-cobalt catalysts during the Fischer-Tropsch reaction. *Journal of Catalysis*, 353, 286-294.
27. McNab, A. I., McCue, A. J., Dionisi, D., & Anderson, J. A. (2018). Combined quantitative FTIR and online GC study of Fischer-Tropsch synthesis involving co-fed ethylene. *Journal of Catalysis*, 362, 10-17.
28. Kummer, J. T., & Emmett, P. H. (1953). Fischer—Tropsch synthesis mechanism studies. The addition of radioactive alcohols to the synthesis gas. *Journal of the American Chemical Society*, 75(21), 5177-5183.

29. Snel, R., & Espinoza, R. L. (1987). Secondary reactions of primary products of the Fischer-Tropsch synthesis: Part 1. The role of ethene. *Journal of Molecular Catalysis*, 43(2), 237-247.
30. Botes, F. G. (2007). Proposal of a new product characterization model for the iron-based low-temperature Fischer-Tropsch Synthesis. *Energy & Fuels*, 21(3), 1379-1389.
31. Boelee, J. H., Cüsters, J. M. G., & Van Der Wiele, K. (1989). Influence of reaction conditions on the effect of Co-feeding ethene in the Fischer-Tropsch synthesis on a fused-iron catalyst in the liquid phase. *Applied Catalysis*, 53(1), 1-13.
32. Hanlon, R. T., & Satterfield, C. N. (1988). Reactions of selected 1-olefins and ethanol added during the Fischer-Tropsch synthesis. *Energy & Fuels*, 2(2), 196-204.
33. Jordan, D. S., & Bell, A. T. (1987). The influence of propylene on CO hydrogenation over silica-supported ruthenium. *Journal of Catalysis*, 107(2), 338-350.
34. Jordan, D. S., & Bell, A. T. (1987). The influence of butene on CO hydrogenation over ruthenium. *Journal of Catalysis*, 108(1), 63-76.
35. Anderson, R. B. (1984). *The Fischer-Tropsch Synthesis*. Academic Press. New York.
36. Hall, W. K., Kokes, R. J., & Emmett, P. H. (1960). Mechanism studies of the Fischer-Tropsch synthesis: The incorporation of radioactive ethylene, propionaldehyde and propanol. *Journal of the American Chemical Society*, 82(5), 1027-1037.
37. Tan, K. F., Xu, J., Chang, J., Borgna, A., & Saeys, M. (2010). Carbon deposition on Co catalysts during Fischer-Tropsch synthesis: A computational and experimental study. *Journal of Catalysis*, 274(2), 121-129.
38. Schulz, H., & Claeys, M. (1999). Reactions of  $\alpha$ -olefins of different chain length added during Fischer-Tropsch synthesis on a cobalt catalyst in a slurry reactor. *Applied Catalysis A: General*, 186(1-2), 71-90.

39. Chen, W., Pestman, R., Zijlstra, B., Filot, I. A., & Hensen, E. J. (2017). Mechanism of cobalt-catalyzed CO hydrogenation: 1. Methanation. *ACS Catalysis*, 7(12), 8050-8060.
40. Schulz, H., Van Steen, E., & Claeys, M. (1993). Olefin formation, hydrogenation and isomerization in the kinetic regime of Fischer-Tropsch synthesis. *Selective hydrogenation and dehydrogenation*, DGMK, Kassel, Germany.
41. Rytter, E., Tsakoumis, N. E., & Holmen, A. (2016). On the selectivity to higher hydrocarbons in Co-based Fischer–Tropsch synthesis. *Catalysis Today*, 261, 3-16.
42. Kokes, R. J. (1969). Formation of dimeric products during steady state hydrogenation of ethylene over cobalt. *Journal of Catalysis*, 14(1), 83-92.
43. Yang, J., Rodriguez, C. L., Qi, Y., Ma, H., Holmen, A., & Chen D. (2020). The effect of co-feeding ethene on Fischer-Tropsch Synthesis to olefins over Co-based catalysts. *Appl. Catal. A: General*. **598**, 117564.
44. Fischer, F., & Tropsch, H. (1926). The synthesis of petroleum at atmospheric pressures from gasification products of coal. *Brennstoff-Chemie*, 7, 97-104.
45. Pichler, V. H., & Schulz, H. (1970). Neuere Erkenntnisse auf dem Gebiet der Synthese von Kohlenwasserstoffen aus CO und H<sub>2</sub>. *Chemie Ingenieur Technik*, 42(18), 1162-1174.
46. Govini Thantrige, K., & Saeys, M. (2017). Reaction Mechanism and Microkinetics of the Cobalt Catalyzed Fischer–Tropsch Synthesis. In 2017 AIChE Annual Meeting (AIChE).
47. Mousavi, S., Zamaniyan, A., Irani, M., & Rashidzadeh, M. (2015). Generalized kinetic model for iron and cobalt based Fischer–Tropsch synthesis catalysts: Review and model evaluation. *Applied Catalysis A: General*, 506, 57-66.
48. Kamyar, K., Lanham, S., and Hecker, W. Kinetics of Fischer-Tropsch synthesis on supported cobalt: Effect of temperature on CO and H<sub>2</sub> partial pressure dependencies. *Catalysis Today* 270 (2016): 9-18.

49. Zhuo, M., Tan, K. F., Borgna, A., & Saeys, M. (2009). Density functional theory study of the CO insertion mechanism for Fischer–Tropsch synthesis over Co catalysts. *The Journal of Physical Chemistry C*, 113(19), 8357-8365.
50. Cheng, J., Hu, P., Ellis, P., French, S., Kelly, G., & Lok, C. M. (2009). Density functional theory study of iron and cobalt carbides for Fischer–Tropsch synthesis. *The Journal of Physical Chemistry C*, 114(2), 1085-1093.
51. Liu, H., Zhang, R., Ling, L., Wang, Q., Wang, B., & Li, D. (2017). Insight into the preferred formation mechanism of long-chain hydrocarbons in Fischer–Tropsch synthesis on Hcp Co (10– 11) surfaces from DFT and microkinetic modeling. *Catalysis Science & Technology*, 7(17), 3758-3776.
52. Inderwildi, O. R., Jenkins, S. J., & King, D. A. (2008). Fischer–Tropsch mechanism revisited: alternative pathways for the production of higher hydrocarbons from synthesis gas. *The Journal of Physical Chemistry C*, 112(5), 1305-1307.
53. Ojeda, M., Nabar, R., Nilekar, A. U., Ishikawa, A., Mavrikakis, M., & Iglesia, E. (2010). CO activation pathways and the mechanism of Fischer–Tropsch synthesis. *Journal of Catalysis*, 272(2), 287-297.

## Chapter 7

### **The influence of CO partial pressure on the ethylene reaction with hydrogen under typical Co-based Fischer-Tropsch Synthesis catalysts**

This work has been prepared in the form of a paper for future publication.

Part of this work was presented at Syngas Conversion 2018 and CATSA 2018.

---

#### **ABSTRACT**

To investigate the effect of added CO on ethylene hydrogenation and understand Fischer-Tropsch Synthesis (FTS) from a different perspective, a group of experiment about different amounts of co-fed CO in ethylene hydrogenation over Co/TiO<sub>2</sub> catalysts was conducted at a wide range of temperatures. The introduced CO exhibited a strong limiting effect on both the ethylene reactivity and the its own reactivity as well. This suppression was attributed by the “occupancy effect” of CO on surface of catalysts, and weaken by the increasing temperature.

The added CO suppressed all hydrogenation reactions, resulting the decrease on the selectivity of paraffins. Ethylene hydroformylation reaction took place with CO co-feeding. At different temperature, the presence of CO strengthened the probability of carbon chain growth via different mechanisms: at low temperature (140 °C), the occupancy effect of CO led to insufficient surface hydrogen, resulting in a decrease in chain termination rate; at normal FTS temperature (220 °C), CO dissociation (directly or H-assisted) occurred, which enhanced the formation of long chain products. It indicated FTS-type chain growth reaction was the result of combined influence of different mechanisms.

## 7.1. Introduction

Fischer-Tropsch Synthesis (FTS) is an important industrial-scale heterogeneously catalysed reaction process that converts syngas to chemicals and fuels [1-4]. The  $\alpha$ -olefins are not only products of FTS, but can also re-adsorb and react with the reactants, which is named as  $\alpha$ -olefins secondary reactions. These  $\alpha$ -olefins secondary reactions have attracted the attention of many researchers, since they offer a reasonable explanation for the deviation of FTS products from the ideal Anderson–Schulz–Flory (ASF) kinetic model [5-8]. Via changing residence time and  $\alpha$ -olefins co-feeding experiments, several different types of  $\alpha$ -olefins secondary reactions are reported in publications [9-17]. Table 7.1 lists the possible secondary reaction of  $\alpha$ -olefins. Primary linear olefins produced from FTS reactions can resorb and insert into the carbon chain process. Iglesia et al. [18] reported that the reinsertion rate increased exponentially with an increase in the carbon chain, which resulted in a passive deviation from the ASF kinetic model.

As a special  $\alpha$ -olefin (two  $\alpha$ -carbon and special symmetry), ethylene has the highest activity among the  $\alpha$ -olefins. To understand the performance of ethylene in FTS, a large number of FTS experiments with co-feeding of ethylene were conducted over Co-based [19-27], Fe-based [28-30] and Ru-based catalysts [18, 30]. The researchers found that most of the co-feed ethylene is converted to ethane by hydrogenation [23, 28-29]. In chain growth reaction, ethylene reacted not only as the chain initiative, to participate in chain growth; and also inserted into the carbon chain directly as a monomer [14, 15]. As be reported by Yang et al., at low operation pressure (1.85 bar) and normal FTS temperature (210 °C), ethylene reacted as chain growth starter, as well as formed  $C_1^*$  species by decomposition [31]. Moreover, ethylene hydrocracked to form  $C_1^*$  species that can further hydrogenate to form methane or

generate higher hydrocarbons by reinserting to carbon chain [32]. This special reactivity of ethylene leads to a special lower C<sub>2</sub> selectivity compared to standard ASF product distribution. In our previous work, more than 90% converted ethylene hydrogenated to ethane over a typical Co-based catalyst by feeding different proportion of ethylene and H<sub>2</sub> in absence of CO [33]. In that work, C<sub>3</sub> to C<sub>6</sub> hydrocarbon products distribution was consisted with typical FTS products distribution. This phenomenon indicated chain growth monomer formed by ethylene hydrocracking without CO. However, Schulz et al. showed that ethylene hydrogenolysis was directly related to the partial pressure of CO [34].

In addition, several scientists have investigated the performance of CO poisoning in ethylene hydrogenation [35-41]. Chen et al. found that: there is competitive adsorption of ethylene and CO on the Pt (111) surface; and CO could poison the ethylene hydrogenation reaction, even when the reaction temperature is higher than the desorption temperature of CO (400 K). This indicates that the adsorbed CO, which is in equilibrium with the gas phase CO, occupies the adsorption site of ethylene [36-37]. Rioux et al. reported on the effect of Pt particle size on CO poisoning of the ethylene hydrogenation reaction, and concluded that the ethylene hydrogenation reaction is structurally insensitive in the presence of CO [38]. As indicated by Hwang et al. [39] and Grunes et al. [40], CO poisons the ethylene hydrogenation, and the activation energy of this reaction increases from 10.8 to 20.2 kcal/mol on Pt (111). These researchers reported the reaction activation energy after poisoning used the CO approach to the desorption energy of CO. Hwang et al. further concluded that ethylene hydrogenation can occur only after CO desorption [39].

**Table 7.1:** Various  $\alpha$ -olefins secondary reactions in FTS

<b><i>Reaction type</i></b>	<b><i>Products</i></b>
<b>Hydrogenation</b>	Corresponding n-paraffins [9-10]
<b>Isomerization (bond-shift reaction)</b>	Internal olefins [11-12]
<b>Hydrocracked and hydrogenolysis (demethylation)</b>	Short carbon chain products [13]
<b>Reinserted into growing chains (mostly effective for C<sub>2</sub>H<sub>4</sub>)</b>	Long carbon chain products [14-15]
<b>Reabsorbed and initiation of hydrocarbon chains</b>	Long carbon chain products [16]
<b>Other reactions (like hydroformylation)</b>	Oxygenates [17]

Recently, a group of experiments was done by Cant et al. on the ethylene reaction with hydrogen, by introducing trace CO (25 to 500 ppm) [42]. They listed three types of reactions starting from adsorbed ethylene: hydrogenation, dimerization, and further surface reactions to carbonaceous deposits. The added CO promoted the selectivity of higher hydrocarbons by inhibiting surface adsorption of hydrogen.

To date, most studies on the secondary reaction of ethylene on FTS, which are detailed in the literature studied the CO-Ethylene-H<sub>2</sub> system using fixed partial pressure for CO while changing the co-feed amount of ethylene. However, due to the great influence of CO partial pressure on the reactivity of ethylene, those experiments are not sufficient to fully study the reaction of ethylene and its effect on FTS. In this study, different amounts of CO were introduced into the ethylene hydrogenation reaction system as co-feeding gas, while the total gas hourly space velocity (GHSV) and the partial pressure of both hydrogen and ethylene were maintained and kept equal. (Both ethylene and hydrogen were 40 vol. % in the feed gas.) The experiments used a typical Co-based FTS catalyst (15% Co/TiO<sub>2</sub>). The possible reactions and the contribution of these reactions to the product distribution were investigated at different reaction temperatures: 140 °C (a typical temperature at which FTS does not normally take place); 180 °C (the initiation temperature of Co catalytic FTS); 220 °C (the typical operating temperature for Co catalytic FTS).

## **7.2. Experiment**

The 15 wt. % Co/TiO<sub>2</sub> catalysts used in this research were prepared using the traditional incipient wetness method. Co(NO<sub>3</sub>)<sub>3</sub>·6H<sub>2</sub>O (Sigma Aldrich) was used as a cobalt precursor. TiO<sub>2</sub> (Degussa P-25) was used as a catalyst support precursor. The paste was made by mixing distilled water and P-25 TiO<sub>2</sub> in a mass ratio of 1: 1. It was: dried in a vacuum drying oven at

120 °C for 2 hours; and then calcined in a Muffle oven, which was heated from room temperature to 400 °C at a ramping rate of 5 °C/min, and maintained at 400 °C for 6 hours. It was then cooled to room temperature. The paste was crushed and sieved to particles with a size of 0.5-1 mm. After the water saturation experiment, the TiO<sub>2</sub> support was added to the Co(NO<sub>3</sub>)<sub>3</sub> aqueous solution (calculated using the weight amount of support), and allowed to absorb into it uniformly by impregnation. The catalysts were then dried and calcined used the same process as with the support pre-treatment. Table 7.2 listed the physical properties of the catalyst used in the study.

In the catalytic performance experiment, 1 g of catalyst was loaded in a stainless tubular fixed bed reactor (length: 230 mm, ID: 8 mm). All the pipes, connectors and valves from the reactor to the gas chromatogram (GC) were heated and maintained at 170 °C. A hot trap was connected between the reactor and the backpressure regulator, and this was heated to 120 °C, in order to condense the long chain hydrocarbons from the tailgas. A mixture of 40% H<sub>2</sub> / 40% C<sub>2</sub>H<sub>4</sub>/ x% CO/ (20-x)% Ar was introduced into the reactor.

**Table 7.2:** Physical properties of 15 % Co/TiO<sub>2</sub>

<b>Catalyst</b>	<b>15% Co/TiO<sub>2</sub></b>
<b>Particle size (mm)</b>	0.5-1
<b>BET surface area (m<sup>2</sup>/g)</b>	42.92
<b>Pore volume (cm<sup>3</sup>/g)</b>	0.29
<b>Average pore diameter (nm)</b>	16.7

The total flow rate of the feed was maintained at 50 ml/min for all the runs. The flow rates of CO and Ar were adjusted accordingly, in order to change the partial pressure of CO, while the flow rates of both H<sub>2</sub> and C<sub>2</sub>H<sub>4</sub> were maintained equal. The reaction conditions used in this research are listed in Table 7.3. The operating pressure for all the experimental runs was kept at 20 bars (gauge), and the experimental temperature was changed from 140 to 220 °C. Each reaction condition was run for more than 24 hrs, after steady state achieved. Ar was used to flush the whole reactor system for more than 2 hrs before changing the reaction conditions to the next design point, while using the same temperature.

The C<sub>2</sub>H<sub>4</sub> and CO conversions ( $X_{CO/C_2H_4}$ ), and hydrocarbon selectivity with carbon number  $n$  ( $S_{Cn}$ ), were estimated using the following equations:

$$X_{CO/C_2H_4}(\%) = (F_{CO/C_2H_4,in} - F_{CO/C_2H_4,out})/F_{CO/C_2H_4,in} \times 100\% \quad \text{Eq. 7.1}$$

$$S_{Cn}(\%) = n \times F_{Cn,out}/[(F_{CO,in} - F_{CO,out}) + 2 \times (F_{C_2H_4,in} - F_{C_2H_4,out})] \times 100\% \quad \text{Eq. 7.2}$$

The selectivity of propanal, based on CO and C<sub>2</sub>H<sub>4</sub> consumption, was calculated using the following equations:

$$S_{C_2H_5CHO\_CO}(\%) = F_{C_2H_5CHO\_CO,out}/(F_{CO,in} - F_{CO,out}) \times 100\% \quad \text{Eq. 7.3}$$

$$S_{C_2H_5CHO\_C_2H_4}(\%) = F_{C_2H_5CHO\_C_2H_4,out}/(F_{C_2H_4,in} - F_{C_2H_4,out}) \times 100\% \quad \text{Eq. 7.4}$$

The chain growth probability ( $\alpha$  value) was obtained using the following equation:

$$\ln\left(\frac{W_n}{n}\right) = 2\ln(1 - \alpha) + (n - 1)\ln\alpha \quad \text{Eq. 7.5}$$

Where:  $W_n$  was the weight fraction of the hydrocarbon product containing  $n$  atoms;  $n$  was the carbon number.

**Table 7.3:** The components of the feed gas used for this experiment

<b>Feed gas</b>	<b>Total flow rate (ml/min)</b>	<b>Total pressure bar</b>	<b>P<sub>H2</sub> bar</b>	<b>P<sub>CO</sub> bar</b>	<b>P<sub>C2H4</sub> bar</b>	<b>P<sub>Ar</sub> bar</b>
HE_C-0	50	21	8.4	0	8.4	4.2
HE_C-1.3	50	21	8.4	1.3	8.4	2.9
HE_C-2.9	50	21	8.4	2.9	8.4	1.3

## **7.3. Results**

### **7.3.1. Ethylene reactivity**

As shown in Figure 7.1, at an ethylene-hydrogen ratio of 1:1, ethylene reacted completely in the absence of CO, at a temperature of 140 °C to 220 °C. Thereafter, the conversion of ethylene was drastically changed in the presence of CO. As the CO partial pressure increased, the conversion rate of ethylene decreased from 100% (with no CO) to 13% (2.9 bar CO added) at 140 °C, 73% at 180 °C and 97% at 220 °C. This phenomenon could be related to the competitive adsorption between ethylene and CO at the active sites of the catalyst surface. It was known that CO had a lower adsorption energy on the surface of the metal catalyst compared to ethylene, and it was more easily adsorbed to the active site, thereby occupying the adsorption site of ethylene [36]. In other words, the co-feed of CO poisoned the hydrogenation of ethylene over a cobalt-based catalyst.

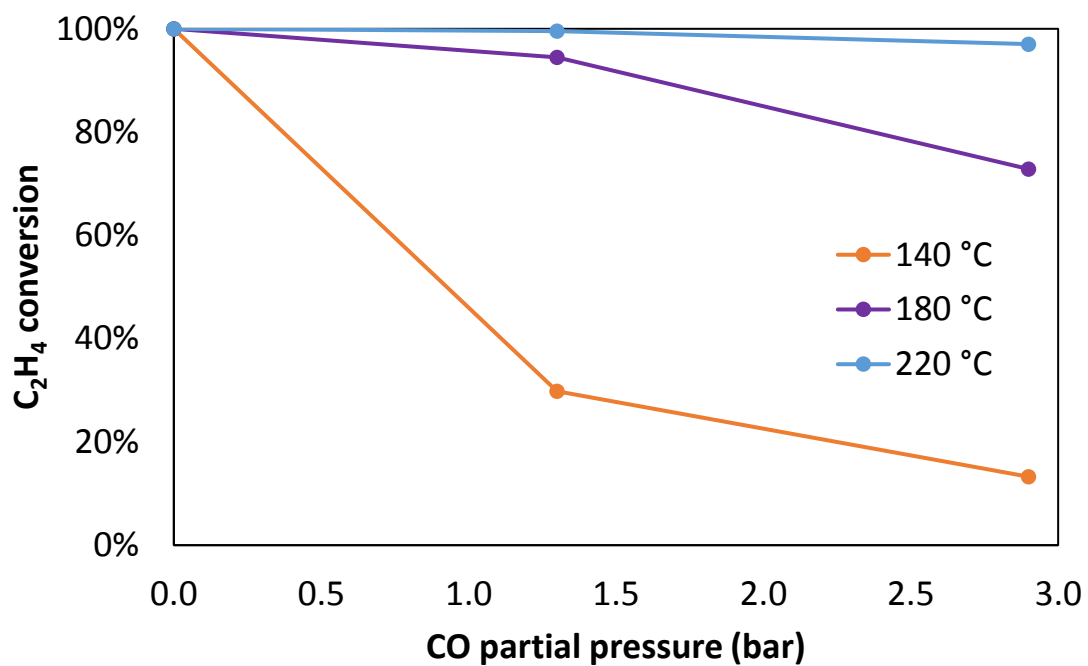


**Figure 7.1:** C<sub>2</sub>H<sub>4</sub> conversion. (Reaction conditions: 20 bar (gauge), total flow rate of 50 ml/min, 40% H<sub>2</sub> / 40% C<sub>2</sub>H<sub>4</sub> / x % CO/ (20-x) % Ar)

Reaction temperature also played an important role in the effect of CO partial pressure on ethylene reactivity. Figure 7.1 showed that ethylene conversion increased with an increase in the reaction temperature, with the same amount of CO co-fed. When 1.3 bar CO was introduced into the reaction system, the ethylene conversion dropped sharply from 100% to 30% at 140 °C; however, it showed only a slight decrease to 95% at 180 °C, and remained above 99% at 220 °C. The increase in ethylene reactivity with an increase in temperature was attributed to adsorption competition between CO and ethylene. [31]

When increasing the CO partial pressure in the feed gas from 0 up to 2.9 bar, the ethylene reactivity varied at different reaction temperatures. At 140 °C, CO showed no reactivity with typical heterogeneous cobalt catalytic FTS, but it occupied a large number of active sites, resulting in a sharp drop in ethylene conversion. As the CO partial pressure increased, the suppressing effect on the ethylene activity further strengthened. At Co-catalytic FTS starting temperature (180 °C), the change in the ethylene conversion first slightly decreased (1.3 bar CO introduced) and then dropped sharply with an increase in CO partial pressure (2.9 bar). Ethylene conversion did not decrease significantly at normal FTS reaction temperature (220 °C).

### **7.3.2. CO reactivity**

The occupancy of CO at the catalyst active site had a significant inhibitory effect on the ethylene reactivity, as well as a significant influence on the reactivity of CO itself. The conversion (Figure 7.2 (a)) and reaction rate (Figure 7.2(b)) were shown in Figure 7.2.

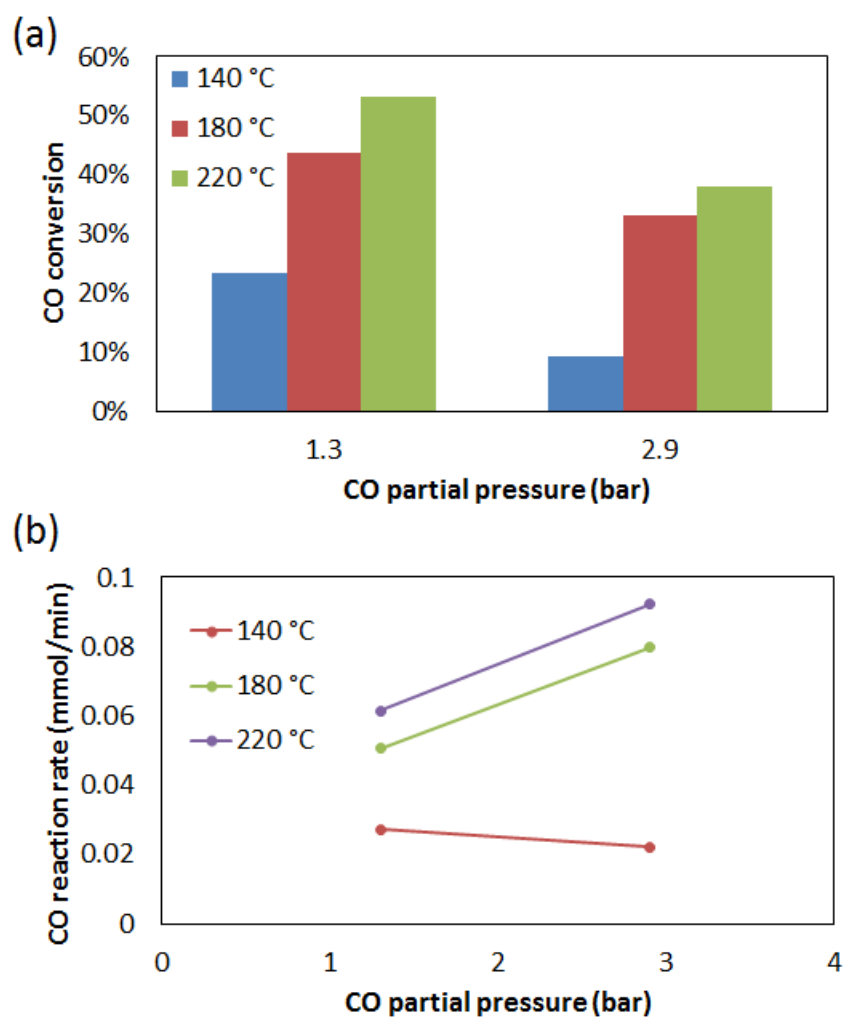


**Figure 7.2:** Rate of CO: (a) conversion; (b) reaction rate. (Reaction conditions: 20 bar (gauge), total flow rate of 50 ml/min, 40% H<sub>2</sub> / 40% C<sub>2</sub>H<sub>4</sub> / x % CO / (20-x) % Ar)

It was known that CO did not react with hydrogen at 140 °C on the Co-based FTS catalyst. However, CO participated in the reaction at 140 °C in the presence of ethylene. (See Figure 7.2 (a).) The figure showed that as the reaction temperature increased from 140 to 220 °C, the CO conversion rate increased: from 23.5% to over 53% in the presence of 1.3 bar CO; and from 9% to 38% in presence of 2.9 bar CO. Therefore, it was no doubt that the reaction temperature had a significant influence on the reactivity of CO.

As CO partial pressure increased, the CO reaction rates showed different changes in the low temperature (140 °C) and normal FTS reaction temperature (180 and 220 °C). As seen in Figure 7.2 (b), at 140 °C, the reaction rate of CO decreased with increasing CO partial pressure, which showed a negative reaction order of CO. This result indicated self-inhibition of CO, which meant that CO poisons the catalyst and the poisoning reacted not only to other reactants (ethylene or hydrogen), but also the CO reaction itself.

We believed that this CO self-inhibition was mainly due to strong adsorption of CO at the active site of the catalyst. Under typical cobalt-catalysed FTS conditions, CO and hydrogen had no reactivity at a reaction temperature of 140 °C. This indicated that the low-temperature reaction of CO required ethylene to assist with the CO dissociation process. However, when more CO was fed into the reaction system, more CO was occupied on the active sites on the catalyst surface, which stopped ethylene adsorbing and further reaction. In addition, when increasing the reaction temperature, the poisoning effect of CO on the catalytic hydrogenation of ethylene was weakened.

At normal FTS reaction temperatures (180 °C and 220 °C), the reaction rate of CO increased with an increase in its partial pressure. This phenomenon could be attributed to two reasons. First, at this condition, the competitive adsorption of ethylene and CO was weakened, which

meant that more ethylene was adsorbed on the surface of the catalyst and assisted with the CO reaction [31]. Second, based on the CO dissociation mechanism of FTS, as the reaction temperature increased, CO underwent C-O bond cleavage (with or without H-assistance) at the active site of the catalyst, and the FTS reaction occurred. [43-44]

### **7.3.3. Ethylene hydrogenation**

Ethylene hydrogenation to ethane was the dominant reaction without CO. Figure 7.3 showed that the ethane selectivity was higher than 80% for the feed without CO co-feeding, and the selectivity did not change much with an increase in the reaction temperature.

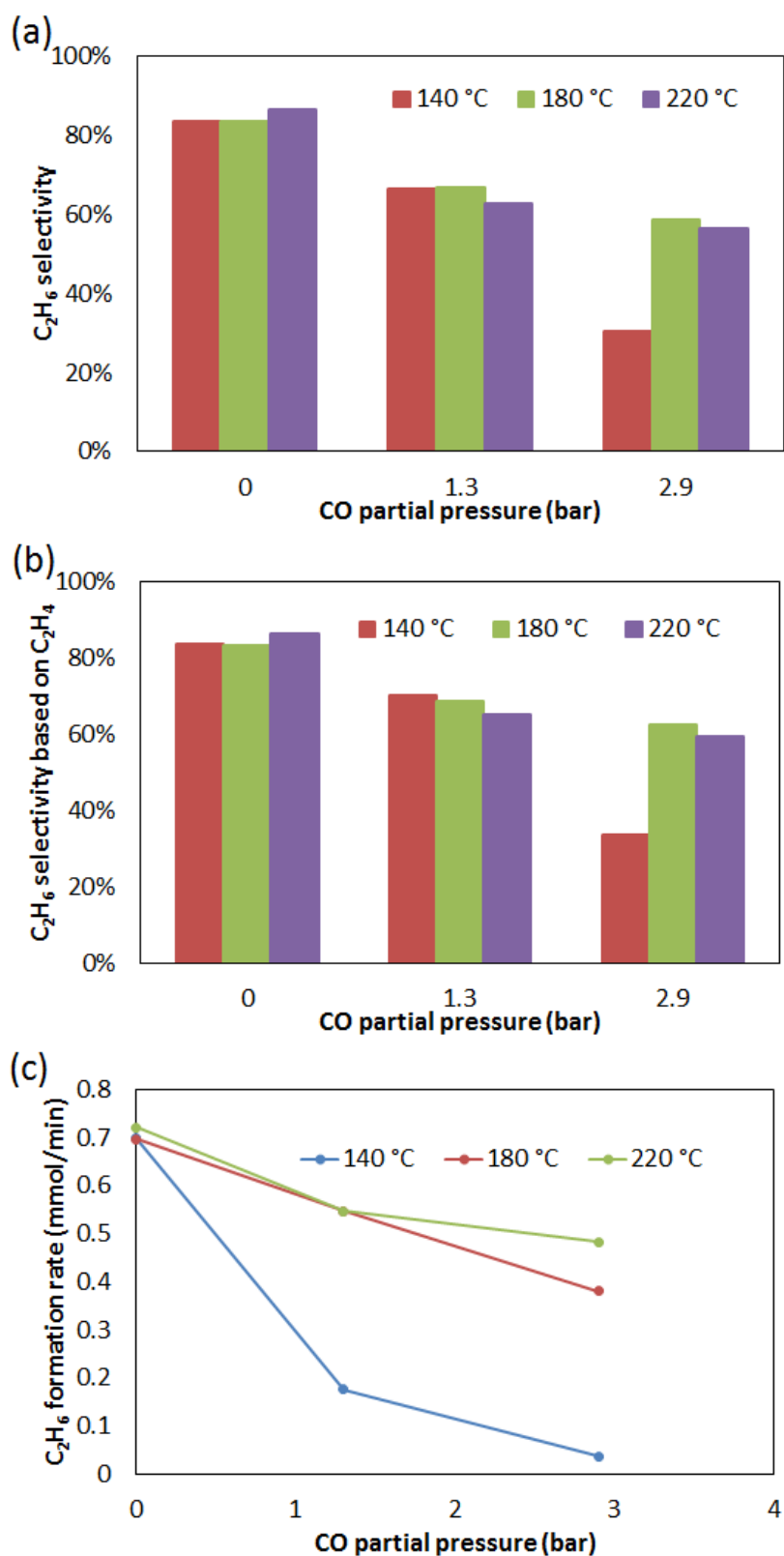


**Figure 7.3:** Selectivity and formation rate of  $C_2H_6$ . (a) Selectivity based on all carbon sources; (b) selectivity based on ethylene; (c) formation rate. (Reaction conditions: 20 bar (gauge), total flow rate of 50 ml/min, 40%  $H_2$  / 40%  $C_2H_4$  / x % CO / (20-x) % Ar)

When CO partial pressure increased from 0 to 1.3 bar, the ethane selectivity dropped significantly, i.e. from 85% to around 65%, at all reaction temperature range. Since the formation of ethane was mainly derived from the ethylene hydrogenation reaction, a plot was drawn of the ethane selectivity, based on ethylene hydrogenation. Figure 7.3(b) showed that less than 70% of the reacted ethylene converted into ethane in the presence of 1.3 bar CO. It indicated that the addition of CO inhibited the ethylene hydrogenation reaction. As the reaction temperature increased from 140 to 220 °C, the selectivity of ethane decreased, based on ethylene hydrogenation from 70% to 65%. The result was similar to the change seen in ethane selectivity in the absence of CO. However, when more CO (2.9 bar) was added to the feed gas, the ethane selectivity underwent a greater change. First, as more CO was added to the reaction system, the hydrogenation of ethylene was further inhibited, as the ethane selectivity was based on ethylene decreased with increasing CO partial pressure (seen in Figure 7.3(b)). Second, the ethane selectivity varied greatly between the 140 °C and normal CO-catalytic FTS reaction temperatures (180 to 220 °C). It was very different to when there was less CO or no CO present. The ethane selectivity based on ethylene was less than 34% at 140 °C, while it was around 60% at a temperature range of 180 to 220 °C. These results showed that the “site occupancy effect” of CO inhibited the adsorption of ethylene on the catalyst surface. The unusually low ethane selectivity might indicate that the CO “site occupancy effect” that was seen with a low temperature and a high CO content affected the adsorption of hydrogen on the catalyst surface.

Figure 7.3(c) showed the change in the ethane formation rate at different reaction temperatures and with different CO partial pressure levels. The ethane formation rate decreased with an increase in CO partial pressure at all the reaction temperature ranges. In the absence of CO, the ethane formation rate did not change much at various temperature

levels. When 1.3 bar CO was added to the feed gas, the ethane formation rate was reduced sharply from 0.7 to 0.18 mmol/min at 140 °C, while at 180 and 220 °C, both ethane formation rates dropped from 0.7 mmol/min to about 0.55 mmol/min. When more CO (2.9 bar) was in the feed gas, the ethane formation rate dropped further. However, a comparison of the ethane formation rates at different temperatures showed that it increased with an increase in the reaction temperature.

#### 7.3.4. Ethylene hydroformylation

We also observed the hydroformylation reactions in this study, where propanol was formed. As per Equation 7.6, the stoichiometric ratio of reactant ethylene, CO and hydrogen was 1:1:1 in ethylene hydroformylation was:



The propanol selectivity and formation rate were shown in Figure 7.4. The propanal selectivity based on CO consumption and ethylene consumption were shown in Figure 7.4(b) and 7.4(c), respectively.

The results showed that: both the reaction temperature and the CO partial pressure affected the ethylene hydroformylation reaction. As shown in Figure 7.4(a), when the reaction temperature increased, the total carbon source based propanal selectivity first raised and then dropped; when the CO partial pressure increased, the total carbon source based propanal selectivity changed at different reaction temperatures. At a low temperature (140 °C), more CO inhibited the occurrence of ethylene hydroformylation in the reaction system. At a higher reaction temperature (180 °C and 220 °C), as the amount of CO that was added increases, the selectivity of the ethylene hydroformylation to propanal increased. It

was mainly caused by the difference in the reactivity of CO at different reaction temperatures and the competitive adsorption between ethylene and CO, as indicated below.

(1) At 140 °C

In the previous chapter (Chapter 5), we found that the CO itself did not undergo C-O bond cleavage or H-assistance dissociation under typical FTS reaction conditions at 140 °C. Under this condition, the adsorbed ethylene that acted as an initiator could react with adsorbed CO\*, via the CO insertion mechanism, to form propanal. However, due to the strong adsorption of CO on the surface of the catalyst, the amount of ethylene adsorbed on the catalyst surface decreased, as the CO partial pressure increased. The limitation of the amount of adsorbed ethylene resulted in the low hydroformylation activity. (See Figure 7.4 (b-c) at 140° C.)

(2) At 180 °C

180 °C was considered the starting temperature for most typical cobalt-based heterogeneous catalytic FTS reactions (low temperature FTS: 180 to 250 °C). [45] Compared with the results obtained at 140 °C, the proportion of reacted CO and ethylene that participated in the ethylene hydroformylation reaction increased significantly. It might be due to an increase in the ethylene adsorbed on the catalyst surface. A similar decrease in the proportion of CO participating in the hydroformylation reaction was seen with CO partial pressure increasing, as shown by the results obtained at 140 °C. (See Figure 7.4 (b).) However, the proportion of ethylene attended into hydroformylation increased as CO partial pressure increased. This could be because, as the CO partial pressure increased, the amount of CO adsorption on the surface of the catalyst increased, while the amount of ethylene adsorption decreased.

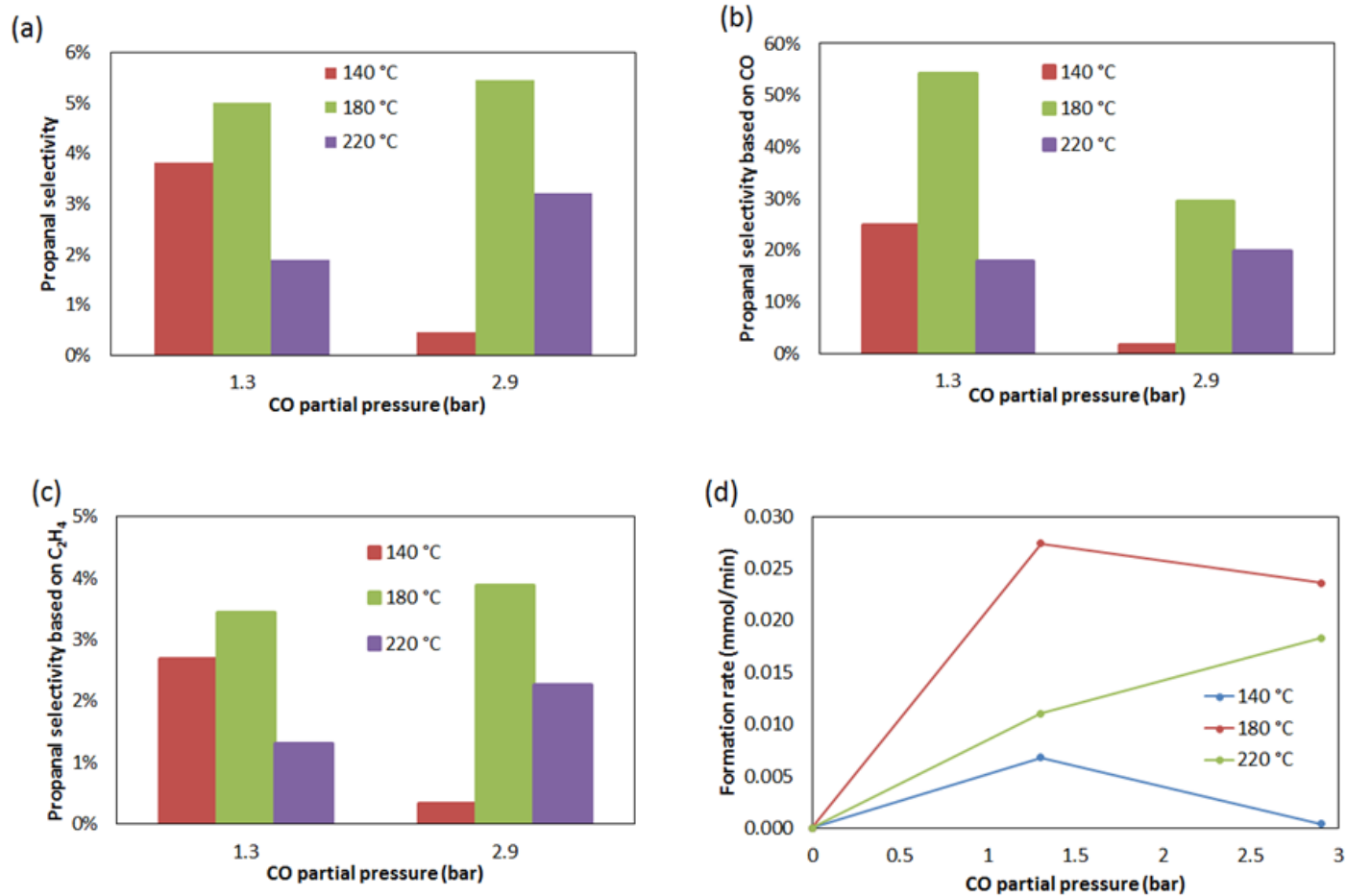


**Figure 7.4:** Selectivity and formation rate of propanal: (a) propanal selectivity based on total carbon consumption; (b) propanal selectivity based on CO consumption; (c) propanal selectivity based on ethylene consumption; (d) propanal formation rate. (Reaction conditions: 20 bar (gauge), total flow rate of 50 ml/min, 40% H<sub>2</sub> / 40% C<sub>2</sub>H<sub>4</sub> / x % CO / (20-x) % Ar)

(3) At 220 °C

When the reaction temperature increased to 220 °C, the FTS reactivity of CO increased. In addition, the adsorption and desorption rates of both ethylene and CO increased, and the reaction rates also accelerated compared to the results at a lower temperature. With this temperature, CO preferred to follow the self-dissociation or hydrogen-assisted dissociation mechanism to generate the FTS products, instead of the CO insertion mechanism for ethylene hydroformylation. Compared with the results obtained at 180 °C, the proportion of CO participating in ethylene hydroformylation was reduced, and the proportion of ethylene participating in the hydroformylation reaction was reduced. (See Figure 7.4 (b) and (c).)

Figure 7.4 (d) showed the propanal formation rate. When the CO partial pressure increased from 1.3 to 2.9 bar in the feed, the propanal formation rate decreased at a low reaction temperature (140 °C and 180 °C). However, when the reaction temperature increased to 220 °C, the propanal formation rate raised with an increase in CO in the system. Moreover, as the reaction temperature increased, the propanal formation rate first increased and then decreased under the same partial pressure of CO.

### **7.3.5. Ethylene dimerization**

Dimerization of ethylene is one of the major side reactions of ethylene hydrogenation over a Co-based FTS catalyst. About 50 years ago, Kokes et al. reported that excess ethylene reacted with hydrogen with unsupported Co catalysts at room temperature and produced approximately 8% total C<sub>4</sub> products. Among these, trans-2-butene was the main product [46]. In addition, Schulz et al. reported that a double bond shift reaction (one of the  $\alpha$ -olefins secondary reactions) would isomerize the primary 1-olefins products to produce corresponding inner C-C double bond olefins under typical FTS reaction conditions [47]. It

meant that 2-butene - the ethylene dimerization product - could also be derived from CO hydrogenation and isomerization, if CO was introduced in feed gas. Figure 7.5 showed the selectivity and formation rate of different C<sub>4</sub> products with different reaction temperatures and different levels of CO partial pressure.

Figure 7.5 (a) indicated that, in the absence of CO, the only ethylene dimerization product was n-butane between 140 to 220 °C. This indicated that when using C<sub>2</sub>H<sub>4</sub>/H<sub>2</sub> (1:1 ratio) without CO co-feeding, the amount of hydrogen was sufficient, and all the butene produced by ethylene dimerization was hydrogenated into butane. With co-fed CO in the feed, the dominant C<sub>4</sub> products were olefins, rather than butane. It demonstrates the hydrogenation of C<sub>4</sub> olefins was inhibited by CO. Among the C<sub>4</sub> olefin products produced, cis-2-butene was one of the main products produced under all the reaction conditions. It was consistent with the distribution of ethylene dimerization products reported in some literatures [42, 46]; however, in typical Co-catalytic FTS, the internal olefins were not the main products. As mentioned, Schulz et al. considered internal double bond olefins obtained from isomerization of corresponding terminal double bond olefins [47]. It implied that the C<sub>4</sub> product came mainly from ethylene dimerization.

The selectivity and formation rate of the C<sub>4</sub> products were shown in Figure 7.5. In the absence of CO, as the reaction temperature increased, the n-butane selectivity decreased. This indicated that a high reaction temperature was more conducive to ethylene hydrogenation and ethylene hydrogenated cracking, but not to ethylene dimerization, when sufficient hydrogen was available. However, in the presence of CO, the selectivity and formation rate of total C<sub>4</sub> products increased when the reaction temperature raised, which was consistent with the trend in ethylene reactivity. As the temperature increased, more ethylene adsorbed onto the active sites on the surface of the catalyst, and then more ethylene dimerized into

the C<sub>4</sub> product. However, the increase in the selectivity of the total C<sub>4</sub> product could not be explained by competitive adsorption. As already indicated, when hydrogen was sufficient and CO was not present, the high temperature suppressed ethylene dimerization. After co-feeding CO, the amount of adsorped hydrogen on the catalyst surface was limited by the “occupancy effect” of CO. It inhibited ethylene hydrogenation, which caused ethylene to be more prone to the dimerization reaction. This was the main reason why ethylene dimerization selectivity increased with an increase in the reaction temperature.

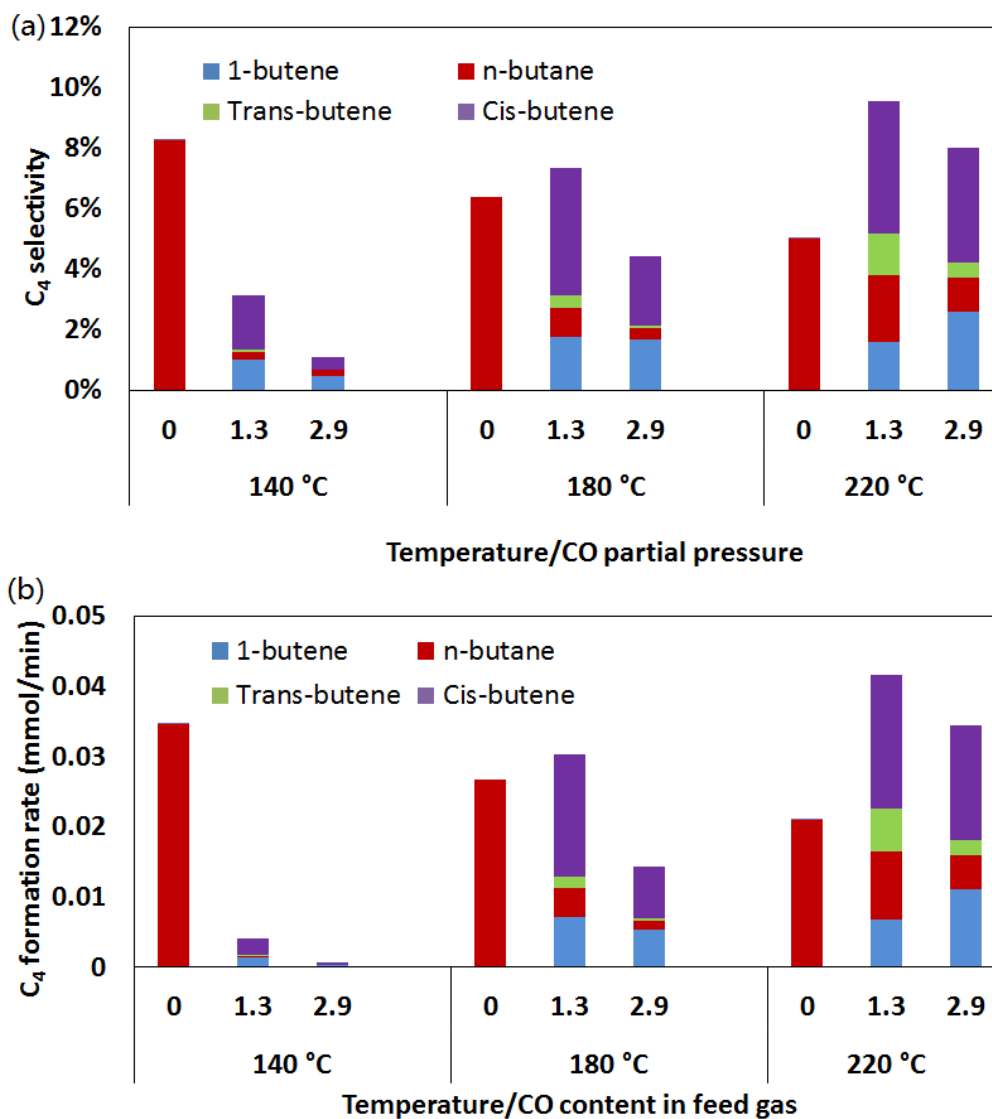


**Figure 7.5:** Selectivity and formation rate of various C<sub>4</sub> products: (a) selectivity, and; (b) formation rate. (Reaction conditions: 20 bar (gauge), total flow rate of 50 ml/min, 40% H<sub>2</sub> / 40% C<sub>2</sub>H<sub>4</sub> / x % CO/ (20-x) % Ar).

Above 180 °C, when the direct CO hydrogenation reaction (CO dissociation with or without H-assistance) could occur, the introduction of CO could boost the selectivity of the ethylene dimer (C<sub>4</sub>). It indicated that the partial pressure of H<sub>2</sub> affected whether ethylene promoted the hydrogenation reaction or the dimerization reaction. In this condition, CO consumed part of the adsorbed H<sub>2</sub>, which suppressed ethylene hydrogenation. (See Figure 7.3.) Conversely, ethylene dimerization could be promoted by reducing the amount of hydrogen adsorbed on the surface of the catalyst.

As seen in Figure 7.5, there were four kinds of C<sub>4</sub> products: 1-butene, n-butane, trans-butane and cis-2-butene. Their selectivity and rate of formation varied with a change in the reaction temperature and CO partial pressure. The changes in the selectivity and formation rate of n-butane, trans-butane and cis-2-butene were consistent with the changing in the total C<sub>4</sub> product for all the reaction conditions. However, 1-butene was different. At 140 °C, the selectivity change of 1-butene was consistent with other C<sub>4</sub> products. Under this condition, 1-butene was from the isomerization of 2-butene (ethylene dimerization products). When the reaction temperature reached 220 °C and the FTS reaction was dominant, the 1-butene selectivity increased with the CO partial pressure. It implied that a portion of the C<sub>4</sub> product is derived from CO hydrogenation, or FTS.

#### **7.3.6. Odd carbon number products**

Odd carbon number products were observed from ethylene hydrogenation condition in the absence of CO. It might be the result of a number of reactions, such as: the ethylene hydrocracking (Equation 7.7); ethylene disproportionation (Equation 7.8); ethylene comproportionation with its dimerization product C<sub>4</sub> (Equation 7.9); the disproportionation

reaction of the ethylene oligomerization products (especially dimerization products  $C_4$ ) (Equation 7.10).



When CO was present in the reaction system, methane could be derived from the methanation of CO, while other carbon number products could be derived from the carbon chain growth of FTS. The selectivity of methane,  $C_3$  products and  $C_5$  products at different reaction temperatures and different CO partial pressure levels were shown in Figure 7.6.

In absence of CO, no  $C_3$  or  $C_5$  olefins products were formed at all reaction temperatures in the range. This was consistent with the results of the  $C_4$  product distribution, which again illustrated that when there was sufficient hydrogen in the reaction system, all olefin products were saturated hydrogenation. The selectivity of all the odd carbon number products increased as the reaction temperature increased in the absence of CO. Because ethylene was the only carbon source in the absence of the CO condition, the generation of odd carbon number products must be via the C-C bond cleave of ethylene or its dimerization products. The high temperature was of benefit for C-C bond rupture.

With the addition of CO, propylene and pentene were formed and their selectivity was higher than that of the corresponding alkane. It implied that the introduced CO caused insufficient hydrogen on the catalyst surface, which was consistent with  $C_4$  products, as discussed in the previous section. It was worth noting that the selectivity of the  $C_3$  product was significantly higher than that of the methane and  $C_5$  products. This may indicate that a portion of the  $C_3$  product was derived from the hydrodehydration of the ethylene hydroformylation product.

Figure 7.6 showed that the total selectivity of methane, and the C<sub>3</sub> and C<sub>5</sub> products increased with temperature at the same CO partial pressure. The paraffin to olefin ratio of the C<sub>3</sub> and C<sub>5</sub> products also increased with temperature. It could be attributed to competitive adsorption between CO and H<sub>2</sub>. At higher temperatures, the “occupancy effect” of CO on activated sites was weakened, so more hydrogen could be adsorbed. These adsorbed hydrogens facilitated the hydrogenolysis of the reactant ethylene, and reacted with the surface intermediate CH<sub>x</sub>\*, which was produced from CO partial hydrogenation, to form the corresponding paraffins via the FTS reaction. When the reaction temperature was lower than 180 °C, the selectivity of all odd carbon number hydrocarbons first increased and then decreased as the CO partial pressure increased.

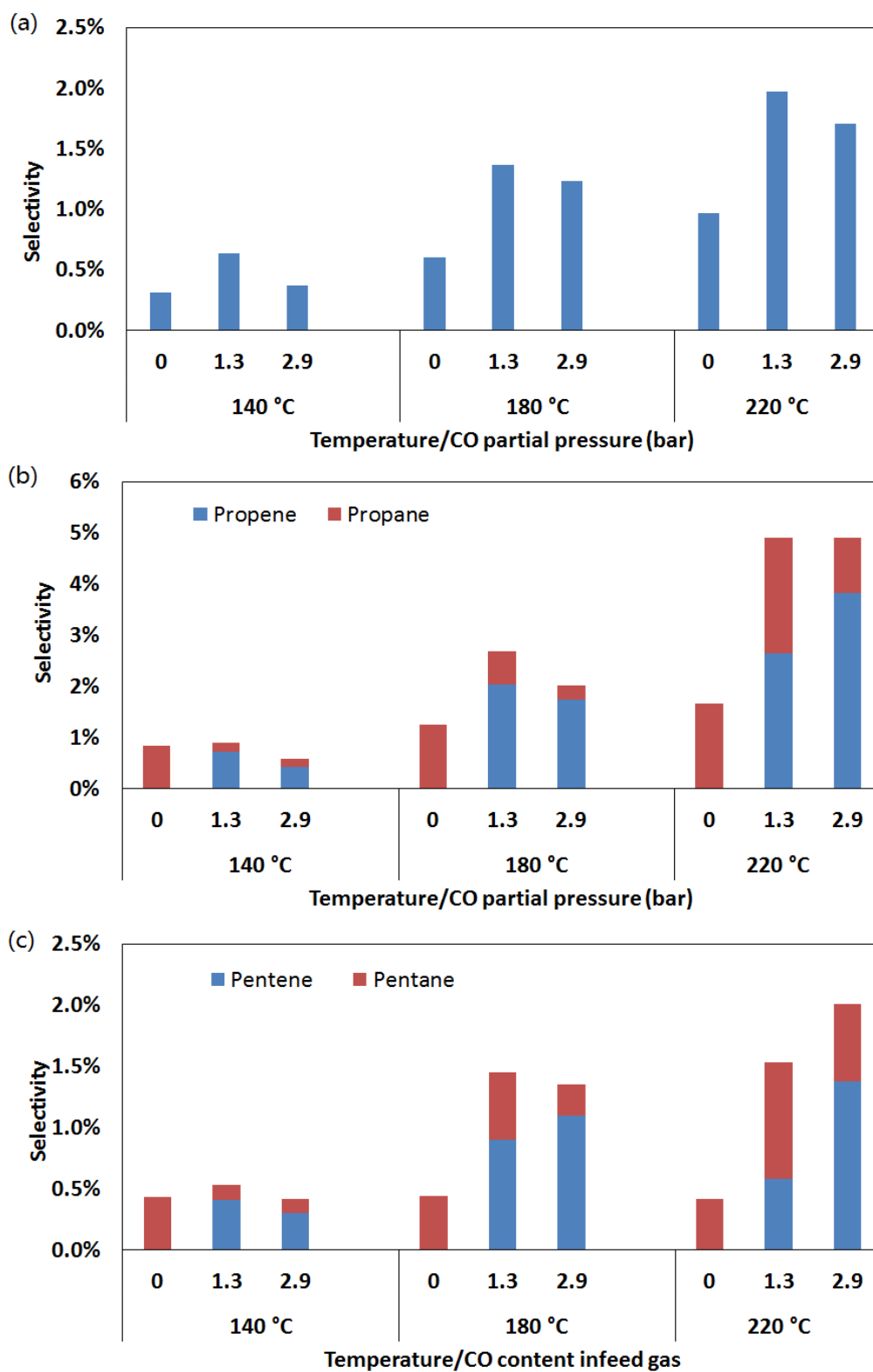


**Figure 7.6:** Selectivity of: (a) methane; (b) C<sub>3</sub> products, and; (c) C<sub>5</sub> products. (Reaction conditions: 20 bar (gauge), total flow rate of 50 ml/min, 40% H<sub>2</sub> / 40% C<sub>2</sub>H<sub>4</sub> / x % CO/ (20-x) % Ar).

## 7.4. Discussion

### 7.4.1. The inhibiting effect of CO

Figure 7.7 (b) indicated that CO inhibited the reactivity of ethylene, especially at a lower temperature. As mentioned, this was mainly due to the competitive adsorption between ethylene and CO. This conclusion had been suggested in other literature on the hydrogenation reaction of CO poisoning ethylene [36-40].

Hwang et al. reported that with ethylene hydrogenation on platinum catalysts, the activation energy of ethylene hydrogenation was almost same as the CO desorption energy, which indicates that ethylene hydrogenation can only take place when CO molecules desorb from the active sites [39]. As the reaction temperature raised, the competitive adsorption between ethylene and CO gradually decreased. That was, when the reaction temperature was sufficiently high, the CO occupancy on the catalyst surface was insufficient to suppress the reactivity of ethylene. As shown in Figure 7.1, the ethylene conversion increased from 13% at 140 °C to 97% at 220 °C, when 2.9 bar CO was co-fed.

The CO poisoning effect over the ethylene reactions could be explained as follows. First, CO occupied the activate sites and thus inhibited ethylene adsorption. Second, CO also inhibited hydrogen adsorption on the catalyst surface, and thus limited the hydrogenation reaction. It was reason why the products of the ethylene hydrogenation reaction and the side reaction were all alkanes in the absence of CO, but once CO was introduced, the main products were olefins.

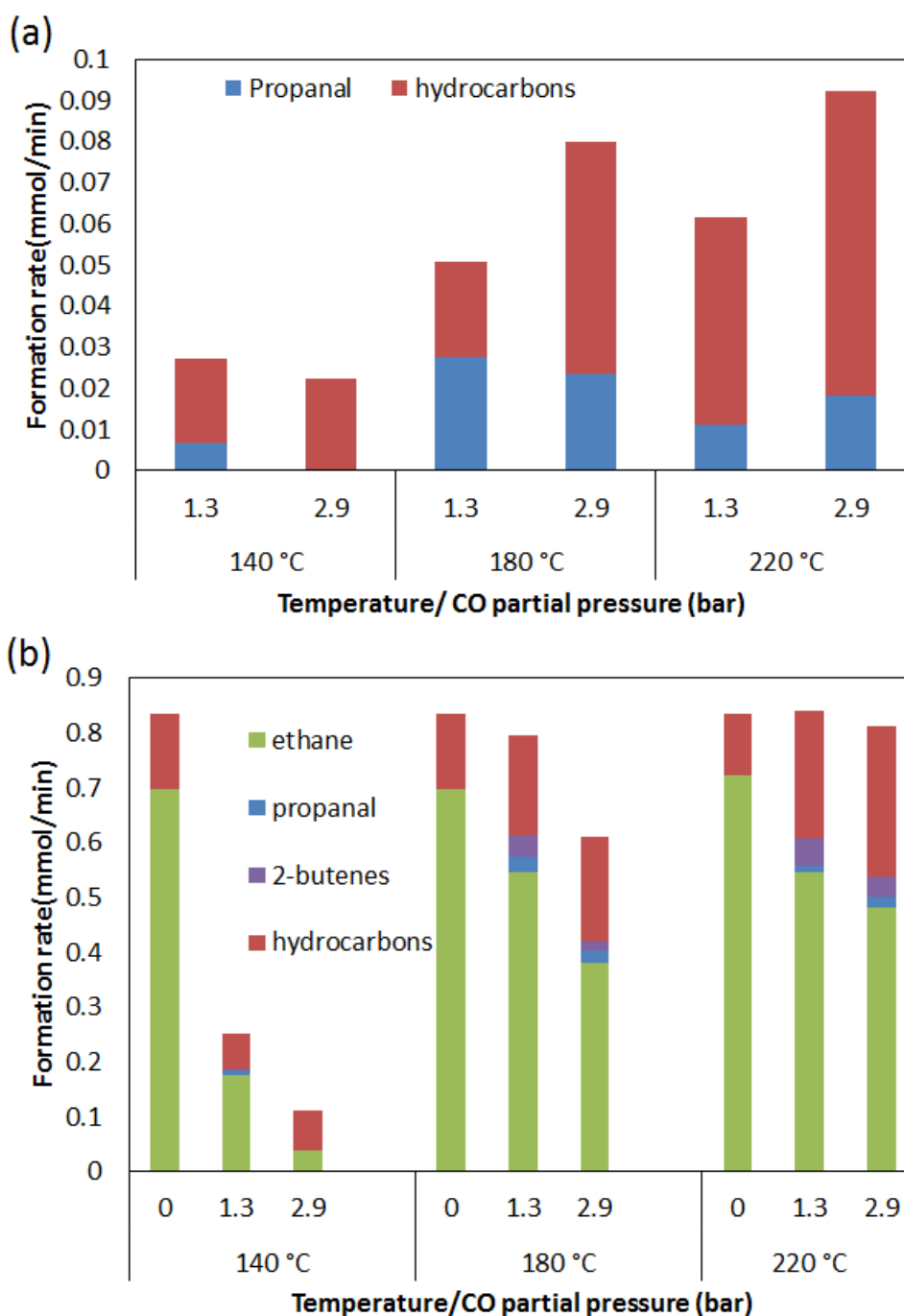


**Figure 7.7:** Product distribution spectrum of: (a) CO, and; (b) ethylene under different reaction temperatures at different CO partial pressure levels. (Reaction conditions: 20 bar (gauge), total flow rate of 50 ml/min, 40% H<sub>2</sub> / 40% C<sub>2</sub>H<sub>4</sub> / x % CO/ (20-x) % Ar) In this figure, hydrocarbons represent all the C<sub>x</sub>H<sub>y</sub>, except C<sub>2</sub>H<sub>6</sub> and 2-butene.)

#### 7.4.2. Effect of CO on product distribution

The chain growth probability ( $\alpha$ -value) was calculated, as shown in Table 4. It was obvious in our study that, due to ethylene hydrogenation and ethylene dimerization, the  $C_2$  and  $C_4$  products deviated significantly from the ideal ASF kinetic model. The  $\alpha$ -value was then calculated using only methane,  $C_3$ , and  $C_5$  to  $C_6$ . The  $\alpha$ -olefins and n-paraffins product distributions were calculated using the same methods and the  $\alpha$ -value of olefins and paraffins were listed in Table 7.4. Figure 7.8 showed the experiment results as an ASF plot.

In the absence of CO, there were only paraffin products. Therefore, the chain growth probability of total carbon and the chain growth probability of n-paraffins was the same. Interestingly, in the absence of CO, the  $C_{3+}$  products also showed carbon chain growth, which was consistent with the product distribution of FTS. Chen et al. reported similar conclusions, when they co-fed propylene and hydrogen into a typical FTS reaction [48]. It implied that the olefin could form a carbon chain-growth monomer  $CH_x^*$  under FTS conditions. The chain growth probability of ethylene hydrogenation (0.38 at 220 °C) was much less than that of the typical FTS product (around 0.75, as shown in previous chapter). (See Table 7.4.)

As shown in Table 7.4, when the reaction temperature increased, the  $\alpha$ -value decreased for all the runs, for both the overall hydrocarbon products and the individual olefins or paraffins, when no CO or 1.3 bar CO was co-fed into reaction system. It indicated that a high temperature favoured the formation of short chain products at low CO partial pressure conditions. However, when 2.9 bar CO was co-fed, the  $\alpha$ -value increased from 0.65 to 0.69, with the reaction temperature rising from 140 °C to 180 °C, and then decreases to 0.53 at 220 °C. At this point, the overall chain growth probability and the individual chain growth probability of olefins and paraffins had the same change trend. As indicated in the previous

section, CO could not directly dissociate or H-assisted dissociate at 140 °C, therefore the chain growth monomer was adsorbed CO\* and C<sub>1</sub>\* species formed by ethylene hydrogenolysis. In this condition, the chain initiator came from ethylene, which was consistent with publications by co-feeding ethylene in FTS [31, 49]. However, there was a strong suppression effect of CO on ethylene adsorption at a relatively high CO partial pressure condition. Moreover, a low temperature inhibited ethylene hydrogenolysis. At 180 °C, normal FTS started to occur. CO hydrogenation to form the chain growth initiators and monomers at this temperature. Furthermore, the CO “occupancy effect” on ethylene was weaker than it is at 140 °C. More initiator and monomer was formed by ethylene. The  $\alpha$ -value increased can be attributed to a combination of two factors. First, when temperature increased to 220 °C, competitive adsorption was further weakened. Second, with this condition, a large amount of H<sub>2</sub> was consumed by ethylene hydrogenation reaction, which caused an “H scavenging effect” [31]. It resulted in an  $\alpha$ -value decrease.

At the same reaction temperature, the addition of CO had a considerable promotion effect on the chain growth reaction. The amount of CO that was added (from 1.3 bar to 2.9 bar), had little effect on the probability of carbon chain growth at 140 °C. In other words, the quantity of CO attended into the chain growth reaction under 1.3 bar CO in the feed gas was almost same as with 2.9 bar CO in the feed gas at 140 °C. Therefore, the promotion of this carbon to the chain growth reaction was due to its presence inhibiting the adsorption of hydrogen on the surface of the catalyst. Because the hydrogen in the adsorbed state was reduced, the probability of chain termination, hydrogenation of the adsorbed intermediates (chain growth monomers) was lowered, thereby increasing the probability of chain growth.

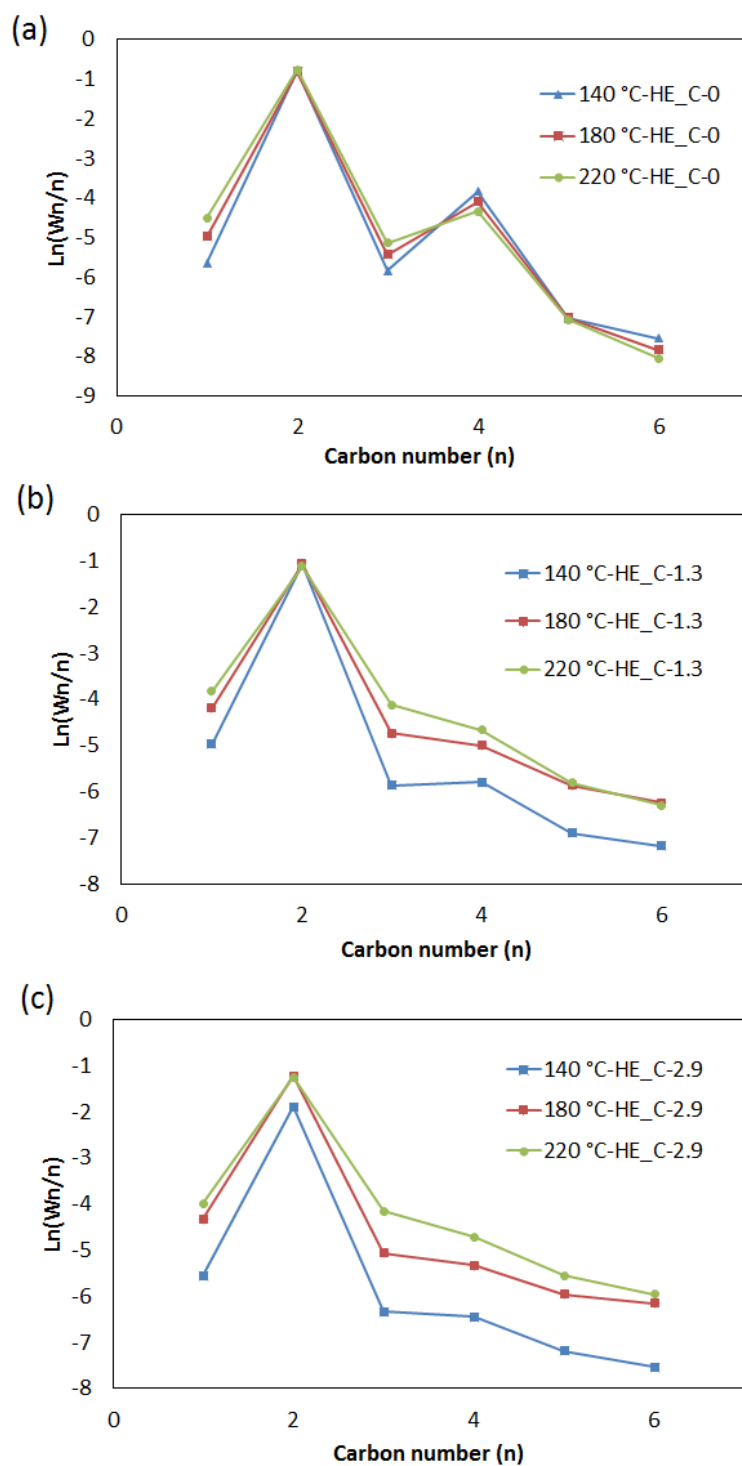


**Figure 7.8:** Experimental results plotted into an ASF product distribution model of the results seen when using different feed gas compositions.

**Table 7.4:** The a-value of total hydrocarbons,  $\alpha$ -olefins and n-paraffins under different reaction temperatures with CO partial pressure over 15% Co/TiO<sub>2</sub>. (Pressure: 20 bars; Total flow rate: 50 ml/min, H<sub>2</sub>: 40%, C<sub>2</sub>H<sub>4</sub>: 40%.)

CHAIN GROWTH PROBABILITY	140 °C	180 °C	220 °C
<b>TOTAL (OLEFIN+PARAFFIN)</b>			
HE_C-0	0.57	0.45	0.38
HE_C-1.3	0.64	0.60	0.47
HE_C-2.9	0.65	0.69	0.53
<b>OLEFINS</b>			
HE_C-0	--	--	--
HE_C-1.3	0.63	0.54	0.41
HE_C-2.9	0.64	0.67	0.51
<b>PARAFFINS</b>			
HE_C-0	0.57	0.45	0.38
HE_C-1.3	0.66	0.73	0.52
HE_C-2.9	0.67	0.78	0.61

## 7.5. Conclusion

The effect of co-fed CO on ethylene hydrogenation under typical Co catalytic FTS conditions was investigated. In the absence of CO, the dominant reaction of ethylene was hydrogenation. The main side reaction was ethylene dimerization. In addition, there were some odd-number carbon hydrocarbons in the product, which could be formed by an ethylene C-C double bond cleavage. Under these conditions, all products were paraffins and the product distribution was in accordance with the ASF kinetic model, except for the C<sub>2</sub> and C<sub>4</sub> products.

When CO was introduced into the reaction system, the reactivity of ethylene and all hydrogenation reactions were suppressed. The inhibition of the reactivity of ethylene was due to the competitive adsorption between ethylene and CO at the activated sites of the catalysts. The mechanism by which the hydrogenation reaction was inhibited at different reaction temperatures was different: at a low temperature, hydrogenation was suppressed by the CO occupancy effect, which resulted in insufficient hydrogen adsorption on the catalyst surface; at a high temperature, this limitation was because some of the adsorbed hydrogen was consumed by the CO hydrogenation reaction. Moreover, CO was self-poisoning in the low reaction temperature range, because the CO occupancy effect caused other reactants to be adsorbed insufficiently, which affected the reaction rate of CO adversely. In addition, CO had a certain promoting effect on the chain growth reaction. This promotion was achieved by inhibiting the hydrogenation chain termination reaction under low temperature reaction conditions. Under high temperature conditions, CO was involved in self-hydrogenation to enhance the chain growth probability.

## REFERENCES:

1. Dry, M. E. (1982). Catalytic aspects of industrial Fischer-Tropsch Synthesis. *Journal of Molecular Catalysis*, 17(2-3), 133-144.
2. Savost'yanov, A. P., Yakovenko, R. E., Narochnyi, G. B., Bakun, V. G., Sulima, S. I., Yakuba, E. S., & Mitchenko, S. A. (2017). Industrial catalyst for the selective Fischer–Tropsch Synthesis of long-chain hydrocarbons. *Kinetics and Catalysis*, 58(1), 81-91.
3. Rytter, E., & Holmen, A. (2017). Perspectives on the effect of water in cobalt Fischer–Tropsch Synthesis. *ACS Catalysis*, 7(8), 5321-5328.
4. Davidson, A. L., Webb, P. B., Parker, S. F., & Lennon, D. (2019). Hydrogen partitioning as a function of time-on-stream for an unpromoted iron-based Fischer–Tropsch Synthesis catalyst applied to CO hydrogenation. *Industrial & Engineering Chemistry Research*, 59(1), 52-60.
5. Schulz, H. (1999). Short history and present trends of Fischer–Tropsch Synthesis. *Applied Catalysis A: General*, 186(1-2), 3-12.
6. Li, J., Yang, G., Yoneyama, Y., Vitidsant, T., & Tsubaki, N. (2016). Jet fuel synthesis via Fischer–Tropsch Synthesis with varied 1-olefins as additives using Co/ZrO<sub>2</sub>–SiO<sub>2</sub> bimodal catalyst. *Fuel*, 171, 159-166.
7. Schulz, H. (2014). Self-organization in Fischer–Tropsch Synthesis with iron-and cobalt catalysts. *Catalysis Today*, 228, 113-122.
8. Liu, X., & Tokunaga, M. (2010). Controllable Fischer–Tropsch Synthesis by in situ-produced 1-Olefins. *ChemCatChem*, 2(12), 1569-1572.
9. Hanlon, R. T., & Satterfield, C. N. (1988). Reactions of selected 1-olefins and ethanol added during the Fischer-Tropsch Synthesis. *Energy & Fuels*, 2(2), 196-204.

10. Tau, L. M., Dabbagh, H. A., & Davis, B. H. (1990). Fischer-Tropsch Synthesis: carbon-14 tracer study of alkene incorporation. *Energy & Fuels*, 4(1), 94-99.
11. Soled, S., Iglesia, E., & Fiato, R. A. (1990). Activity and selectivity control in iron catalyzed Fischer-Tropsch Synthesis. *Catalysis Letters*, 7(1-4), 271-280.
12. Herzog, K., & Gaube, J. (1989). Kinetic studies for elucidation of the promoter effect of alkali in Fischer-Tropsch iron catalysts. *Journal of Catalysis*, 115(2), 337-346.
13. Liu, X., Li, X., & Fujimoto, K. (2007). Effective control of carbon number distribution during Fischer-Tropsch Synthesis over supported cobalt catalyst. *Catalysis Communications*, 8(9), 1329-1335.
14. Shi, B., & Davis, B. H. (2003). Fischer-Tropsch Synthesis: evidence for chain initiation by ethene and ethanol for an iron catalyst. *Topics in Catalysis*, 26(1-4), 157-161.
15. Zhang, R., Hao, X., & Li, Y. (2011). Investigation of acetylene addition to Fischer-Tropsch Synthesis. *Catalysis Communications*, 12(12), 1146-1148.
16. Jacobs, G., & Davis, B. H. (2014). Applications of isotopic tracers in Fischer-Tropsch Synthesis. *Catalysis Science & Technology*, 4(11), 3927-3944.
17. Jordan, D. S., & Bell, A. T. (1986). Influence of ethylene on the hydrogenation of carbon monoxide over ruthenium. *The Journal of Physical Chemistry*, 90(20), 4797-4805.
18. Iglesia, E., Soled, S. L., Fiato, R. A., & Via, G. H. (1993). Bimetallic synergy in cobalt ruthenium Fischer-Tropsch Synthesis catalysts. *Journal of Catalysis*, 143(2), 345-368.
19. Eidus, Y. T., Zelinskii, N. D., & Ershov, N. I. (1948). O Kondensiruyushchem Deistvii Metilenovykh Radikalov Na Etilen. *Doklady Akademii Nauk Ssr*, 60(4), 599-601.
20. Eidus, Y. T. (1950). ND 7. Elinskii, and KV Puzitskii. *Izvest. Akad. Nauk SSSR, Otdel. Khim, Nauk*, 98.

21. Eidus, Y. T., Zelinskii, N. D., Puzitskii, K. V., & Ershov, N. I. (1952). \* O Kataliticheskoi Hidrokondensatsii Okisi Ugleroda S Olefinami. 7. Vliyanie Kontsentratsii Okisi Ugleroda Na Protsess Ee Hidrokondensatsii S Propilenom I N-Butilenom. *Izvestiya Akademii Nauk Sssr-Seriya Khimicheskaya*, (1), 145-151.
22. Eidus, Y. T., & Ordyan, M. B. (1957). Methylation of cyclopentene by methylene radicals that form when carbon monoxide is reduced by contact with hydrogen. In *Doklady Akademii Nauk* (Vol. 116, No. 1, pp. 101-104). Russian Academy of Sciences.
23. Schulz, H., Ramananda, R., & Elstner, M. (1970). Carbon-14 studies for the evaluation of the reaction mechanism of the Fischer-Tropsch Synthesis. *Erdoel Kohle, Erdgas, Petrochem. Brennst.-Chem.*, 23(10).
24. Tau, L. M., Dabbagh, H. A., & Davis, B. H. (1990). Fischer-Tropsch Synthesis: carbon-14 tracer study of alkene incorporation. *Energy & Fuels*, 4(1), 94-99.
25. Herzog, K., & Gaube, J. (1989). Kinetic studies for elucidation of the promoter effect of alkali in Fischer-Tropsch iron catalysts. *Journal of Catalysis*, 115(2), 337-346.
26. McNab, A. I., McCue, A. J., Dionisi, D., & Anderson, J. A. (2017). Quantification and qualification by in-situ FTIR of species formed on supported-cobalt catalysts during the Fischer-Tropsch reaction. *Journal of Catalysis*, 353, 286-294.
27. McNab, A. I., McCue, A. J., Dionisi, D., & Anderson, J. A. (2018). Combined quantitative FTIR and online GC study of Fischer-Tropsch Synthesis involving co-fed ethylene. *Journal of Catalysis*, 362, 10-17.
28. Botes, F. G. (2007). Proposal of a new product characterization model for the iron-based low-temperature Fischer-Tropsch Synthesis. *Energy & Fuels*, 21(3), 1379-1389.

29. Boelee, J. H., Cüsters, J. M. G., & Van der Wiele, K. (1989). Influence of reaction conditions on the effect of Co-feeding ethene in the Fischer-Tropsch Synthesis on a fused-iron catalyst in the liquid phase. *Applied Catalysis*, 53(1), 1-13.
30. Tau, L. M., Dabbagh, H. A., & Davis, B. H. (1990). Fischer-Tropsch Synthesis: carbon-14 tracer study of alkene incorporation. *Energy & Fuels*, 4(1), 94-99.
31. Yang, J., Rodriguez, C. L., Qi, Y., Ma, H., Holmen, A., & Chen D. (2020). The effect of co-feeding ethene on Fischer-Tropsch Synthesis to olefins over Co-based catalysts. *Appl. Catal. A: General*. **598**, 117564.
32. Hutchings, G. J., Copperthwaite, R. G., & Riet M. V. D. (1995). Low methane selectivity using Co/MnO catalysts for the Fischer-Tropsch reaction: effect of increasing pressure and co-feeding ethene. *Top. Catal.* 1995; **2**(1-4): 163-172.
33. Zhang, Y., Tshwaku, M., Yao, Y., Chang, J., Lu, X., Liu, X., & Hildebrandt D. (2020). Reaction of Ethylene over a typical Fischer-Tropsch Synthesis Co/TiO<sub>2</sub> Catalyst. *Engineering Reports*. DOI: 10.1002/eng2.12232
34. Schulz, H., & Achtsnit, H. D. (1977). Olefin reactions during the Fischer-Tropsch Synthesis. *Revista Portuguesa de Quimica, Lisboa*, 19(1-4), 317-322.
35. Crampton, A. S., Rötzer, M. D., Schweinberger, F. F., Yoon, B., Landman, U., & Heiz, U. (2016). Ethylene hydrogenation on supported Ni, Pd and Pt nanoparticles: Catalyst activity, deactivation and the d-band model. *Journal of Catalysis*, 333, 51-58.
36. Chen, P., Westerberg, S., Kung, K. Y., Zhu, J., Grunes, J., & Somorjai, G. A. (2002). CO poisoning of catalytic ethylene hydrogenation on the Pt (1 1 1) surface studied by surface sum frequency generation. *Applied Catalysis A: General*, 229(1-2), 147-154.

37. Chen, P., Kung, K. Y., Shen, Y. R., & Somorjai, G. A. (2001). Sum frequency generation spectroscopic study of CO/ethylene coadsorption on the Pt (111) surface and CO poisoning of catalytic ethylene hydrogenation. *Surface Science*, 494(3), 289-297
38. Rioux, R. M., Komor, R., Song, H., Hoefelmeyer, J. D., Grass, M., Niesz, K. ... & Somorjai, G. A. (2008). Kinetics and mechanism of ethylene hydrogenation poisoned by CO on silica-supported monodisperse Pt nanoparticles. *Journal of Catalysis*, 254(1), 1-11.
39. Hwang, K. S., Yang, M., Zhu, J., Grunes, J., & Somorjai, G. A. (2003). The molecular mechanism of the poisoning of platinum and rhodium catalyzed ethylene hydrogenation by carbon monoxide. *Journal of Molecular Catalysis A: Chemical*, 204, 499-507.
40. Grunes, J., Zhu, J., Yang, M., & Somorjai, G. A. (2003). CO poisoning of ethylene hydrogenation over Pt catalysts: a comparison of Pt (111) single crystal and Pt nanoparticle activities. *Catalysis Letters*, 86(4), 157-161.
41. Tang, D. C., Hwang, K. S., Salmeron, M., & Somorjai, G. A. (2004). High pressure scanning tunneling microscopy study of CO poisoning of ethylene hydrogenation on Pt (111) and Rh (111) single crystals. *The Journal of Physical Chemistry B*, 108(35), 13300-13306.
42. Cant, N. W., Liu, I. O., & Scott, J. A. (2013). Ethylene oligomerisation over Co/SiO<sub>2</sub> in the presence of trace carbon monoxide: The Eidus reaction revisited. *Catalysis Today*, 215, 267-275.
43. Mousavi, S., Zamaniyan, A., Irani, M., & Rashidzadeh, M. (2015). Generalized kinetic model for iron and cobalt based Fischer–Tropsch synthesis catalysts: Review and model evaluation. *Applied Catalysis A: General*, 506, 57-66.
44. Todic, B., Ma, W., Jacobs, G., Davis, B. H., & Bukur, D. B. (2014). CO-insertion mechanism based kinetic model of the Fischer–Tropsch Synthesis reaction over Re-promoted Co catalyst. *Catalysis Today*, 228, 32-39.

45. James, O. O., Chowdhury, B., Mesubi, M. A., & Maity, S. (2012) Reflections on the chemistry of the Fischer-Tropsch Synthesis. *RSC Adv*, 2, 7347-66.
46. Kokes, R. J. (1969). Formation of dimeric products during steady state hydrogenation of ethylene over cobalt. *Journal of Catalysis*, 14(1), 83-92.
47. Schulz, H., & Claeys, M. (1999). Reactions of  $\alpha$ -olefins of different chain length added during Fischer-Tropsch synthesis on a cobalt catalyst in a slurry reactor. *Applied Catalysis A: General*, 186(1-2), 71-90.
48. Chen, W., Pilot, I. A., Pestman, R., & Hensen, E. J. (2017). Mechanism of cobalt-catalyzed CO hydrogenation: 2. Fischer-Tropsch Synthesis. *ACS Catalysis*, 7(12), 8061-8071.
49. Hall, W. K., Kokes, R. J., & Emmett, P. H. (1960). Mechanism studies of the Fischer-Tropsch Synthesis: the incorporation of radioactive ethylene, propionaldehyde and propanol. *Journal of the American Chemical Society*, 82(5), 1027-1037.

## Chapter 8

### Effect of ethylene co-feeding in Fischer-Tropsch synthesis: A study of reaction equilibrium and competition

This work has been prepared in the form of a paper for future publication.

---

#### ABSTRACT

The effect of the partial pressures of both  $C_2H_4$  and  $CO$  on the paraffin to olefin (P/O) ratio of the products was investigated over a typical cobalt-based Fischer-Tropsch (FT) catalyst. Both the catalyst activity and P/O ratio were strongly dependent on the operating conditions: Co-feeding  $C_2H_4$  into the  $CO/H_2$  feed increased the  $CO$  conversion while decreased the P/O ratio; Co-feeding  $CO$  into the  $C_2H_4/H_2$  feed decreased both the ethylene activity and the P/O ratio. The effect of reaction temperature ( $140\text{ }^\circ\text{C} - 220\text{ }^\circ\text{C}$ ) was complicated, which may due to the interaction between different chain-growth mechanisms. The study group used a “Yao-plot” graph to re-plot the data obtained. Although the P/O ratio was a function of the operating conditions, a linear relationship between  $P_{n+1}/O_{n+1}$  and  $P_n/O_n$  ( $n>2$ ) was obtained with a slightly different gradient for all the reaction conditions used in this work. Some attempt was made to explain the research results, based on competitive reaction equilibrium. As large amount of ethylene in feed, the added ethylene significant enhanced some elementary reaction, which caused the gradient of  $P_3/O_3$  vs.  $P_2/O_2$  changed. However, it would not to continue to affect the gradient of  $P_{n+1}/O_{n+1}$  vs.  $P_n/O_n$  ( $n>2$ ).

## 8.1. Introduction

Fischer-Tropsch synthesis (FTS) reaction can be viewed as a carbon chain growth reaction, whereby the monomer is the adsorbed intermediates  $C_1$  species formed by CO dissociation with or without hydrogen assistance [1]. Linear olefins and paraffins formed from syngas are the most important products of FTS. Other products include gas phase light hydrocarbons, liquid oils and solid waxes. In addition, small amounts of isomeric hydrocarbon products, and partially-oxygenated organics, such as alcohols and aldehydes are also formed in FTS.

Due to the complexity of FTS products, it is important to predict the distribution of FTS products. At present, the Anderson–Shultz–Flory (ASF) kinetic model is widely used to describe the distribution of FTS products [2-3]. In this model, the probability of carbon chain growth - called  $\alpha$ -value in FTS - is defined as the ratio of the rate of chain growth to the sum of the rate of chain growth and termination. In addition, in an ideal ASF distribution, there is a linear relationship between the logarithms of the mole fraction of component  $n$ , when plotted versus chain length  $n$ . The following equations are used to calculate  $\alpha$  value:

$$\frac{W_n}{n} = (1 - \alpha)^2 \alpha^{n-1} \quad \text{Eq. 8.1}$$

$$\ln\left(\frac{W_n}{n}\right) = 2\ln(1 - \alpha) + (n - 1)\ln(\alpha) \quad \text{Eq. 8.2}$$

Where:  $W_n$  is the weight fraction of the hydrocarbon product containing  $n$  atoms;  $n$  is the carbon number. By plotting  $\ln(W_n/n)$  versus  $n$ , the slope is indicated as  $\ln(\alpha)$ .

The  $\alpha$ -value is independent of carbon number  $n$ .

However, both negative [4-5] and positive [6-8] deviations from the ideal ASF product distribution model were reported in various research studies [7-13], and several theories and mechanisms were developed to explain these phenomena from various viewpoints, e.g. [14]:

- (i) Two chain-growth active sites on the catalyst.
- (ii) Vapour–liquid equilibrium (VLE) of the products under reaction conditions.
- (iii) Accumulation of the long-chain products.
- (iv) Enhanced secondary reaction of the primary products ( $\alpha$ -olefins).

Due to the deficiencies of the ASF model, other models that are based on diffusion, solubility, physical adsorption or chemisorption, have been proposed by researchers to explain the distribution of FTS products and the variation in the paraffin to olefin (P/O) ratio with different carbon numbers [8, 13, 15-17]. A few researchers have also found some potential equilibrium points in the FTS reaction [14, 19-20]. Masuku's report [19] indicates that the FT product distribution could be the result of a system at partial equilibrium, in which only some species equilibrate. The results show that the olefin product distribution is determined by equilibrium, and paraffins are formed by secondary reactions, which are determined kinetically [19]. Lu et al. [14] introduced a triangular plot similar to a residue curve map, which is used for reactive distillation, to display the relationships among adjacent products of  $O_n$  (olefin with carbon number  $n$ ),  $P_n$  (paraffin with carbon number  $n$ ) and  $O_{n+1}$  (olefin with carbon number  $n+1$ ). Their experimental results suggested that the olefin product distribution may be determined by thermodynamics [14].

Yao et al. [20] reported a linear relationship between  $(P_{(n+1)} / P_{(n+1)})$  and  $P_n / O_n$ , which holds for many experiments using different kinds of catalyst, types of reactor and variation in syngas composition. This graphical plot is called the "Yao plot" and Yao developed two simple models to explain the phenomenon [20]. One is based on vapour-liquid equilibrium (VLE); the other is based on quasi-reaction equilibrium. Following the Yao study, Muleja et al. [21] re-plotted

their data using the Yao plot, and then obtained a similar linear relationship between  $P_{n+1}/O_{n+1}$  and  $P_n/O_n$  [21].

The P/O ratio is an important factor that is used to present the selectivity of paraffin products and olefin products during FTS. This depends on the reactor type, type of catalyst (including structure, support and activation method) and operation conditions, such as temperature, reaction pressure and composition of gas feeding [22]. The literature shows that the P/O ratio increases exponentially with the carbon number (n) of products and is attributed to chain-length-dependent  $\alpha$ -olefins re-absorption and secondary reaction [15, 17, 23-25].

Olefins are the primary product of the FTS reaction and may participate in the secondary reaction to either form corresponding paraffins or participate in the chain growth reaction to form long-chain hydrocarbons. The latter plays an important role in explaining the deviation of the product distribution from the ideal ASF model. Scientists have done many experiments on the co-feed of olefins, to study the reactivity of alpha-olefins on cobalt-based [26-30], iron-based [16, 31, 32] and ruthenium-based catalysts under FTS conditions [27, 33,34]. They found that several types of  $\alpha$ -olefins secondary reactions would take place under typical FTS reaction conditions, including hydrogenation, hydrogenolysis, hydroformylation, re-absorption and reinsert into chain growth, and isomerization [33, 35-39].

However, little attention has been paid to the effect of co-feeding  $\alpha$ -olefins on the P/O ratio, and the potential equilibrium in FTS. In this paper, the effect of ethylene on the P/O ratio was investigated using a feed mixture of  $H_2/CO/C_2H_4/Ar$  with various proportions. The relationship between P/O ratios of neighbouring carbon numbers was compared by applying the Yao plot. Current work being done will provide valuable information to further understand the reaction mechanism and product distribution of FTS.

## 8.2. Experiment

In this study, a typical FTS 15 wt. % Co/TiO<sub>2</sub> catalyst was used, which was prepared using the traditional incipient wetness method. Co(NO<sub>3</sub>)<sub>3</sub>·6H<sub>2</sub>O (*Sigma Aldrich*) was used as the metal precursor salt, and the catalyst support precursor was prepared using TiO<sub>2</sub> (Degussa P-25). TiO<sub>2</sub> was mixed with an equal weight of distilled water to form a paste, which was then dried at 120 °C for 2 hours. After drying, the TiO<sub>2</sub> paste was calcined in a muffle oven at 400 °C for 6 hours. The support was then crushed and sieved and particles in the size range of 0.5-1 mm were selected for the (next) impregnation step. A Co(NO<sub>3</sub>)<sub>3</sub> aqueous solution with a cobalt metal loading of 15% by mass was used for impregnation. After impregnation, the catalyst was treated with the same drying and calcination procedure as used for the support pre-treatment process.

1 g of catalyst was loaded into a stainless tubular reactor with a length of 230 mm and an ID of 8 mm. To prevent liquid condensation, all pipes, fittings and valves from the outlet of the reactor to the GC were heated to 170 °C. A hot trap, which was heated to 120 °C, was designed for separating the long-chain hydrocarbon products from the tailgas stream, to ensure that liquid products did not affect the analytical results. After the hot trap, the tailgas was introduced into an online GC (Agilent 7890A), which had two flame ionization detectors (FID) and one thermal conductivity detector (TCD). The two FID detectors were used to analyse: the hydrocarbon products from C<sub>1</sub> to C<sub>4</sub>; the hydrocarbon products of C<sub>4+</sub>.

Before FTS reaction, the catalyst was activated with H<sub>2</sub> at 30 mL/min, 1bar (gauge) and 350 °C for 8 hours. After catalyst reduction, the reactor was cooled down to room temperature, and a series of FTS experiments were then conducted under different reaction conditions.

Eight kinds of feed mixtures -  $\text{H}_2/\text{CO}/\text{C}_2\text{H}_4/\text{Ar}$  with different proportions - were introduced into the reactor at: a constant total flow rate of 50 NTP mL/min; and a constant total pressure of 20 bar (gauge). The feed gas composition results and the reaction conditions are summarized in the inserts, as follows: Table 8.1 - S1 is a typical syngas mixture; S2-S4 are syngas with co-feeding different amount of ethylene; S5 is a mixture of  $\text{H}_2/\text{C}_2\text{H}_4$  with a ratio of 1:1; S6-S7 are co-feeding different amount of CO into  $\text{H}_2/\text{C}_2\text{H}_4$ ; and S8 is a mixture of  $\text{H}_2/\text{C}_2\text{H}_4$  with a ratio of 1:5 (ethylene-rich feed). The reaction temperature was set in a wide range, [140 °C, 220 °C], during the reaction.

**Table 8.1:** The different operating conditions during FTS

Sample name	Total flow rate (mL/min)	Temperature (°C)	Total pressure on gauge (bar)	FR of H <sub>2</sub> (mL/min)	FR of CO (mL/min)	FR of C <sub>2</sub> H <sub>4</sub> (mL/min)	FR of Ar (mL/min)
<b>S1</b>	50	180-220	20	20	10	0	20
<b>S2</b>	50	180-220	20	20	10	5	15
<b>S3</b>	50	180-220	20	20	10	10	10
<b>S4</b>	50	180-220	20	20	10	15	5
<b>S5</b>	50	140-220	20	20	0	20	10
<b>S6</b>	50	140-220	20	20	3	20	7
<b>S7</b>	50	140-220	20	20	6	20	4
<b>S8</b>	50	180-220	20	8.5	0	41.5	0

### 8.3. Results and discussion

#### 8.3.1. Reactant conversion

Either introducing ethylene into a typical syngas of FTS system or adding CO into an ethylene hydrogenation system would cause obvious changes to all the reactants conversion and product selectivity. Table 8.2 lists the conversion of all the reactants with the different feed gas mixtures and the operating temperatures shown in Table 8.1.

- For feed S1-S4 and co-feeding ethylene into syngas, both the CO and ethylene conversion increased with an increase in the reaction temperature. Co-feeding ethylene into the feed gas enhanced the CO conversion significantly (see S1 and S2 in Table 8.2), especially at a lower reaction temperature, which indicates that ethylene may associate CO bond dissociation (via carbide type mechanism of FTS) or follow with the CO insertion mechanism. However, as the amount of ethylene added increases, there is no significant change in ethylene conversion with the same reaction temperature. The hydrogen conversion increases with an increase in the amount of ethylene added.
- For feed S5-S7 and co-feeding CO into the H<sub>2</sub>/C<sub>2</sub>H<sub>4</sub> mixture, in the absence of CO, ethylene conversion maintains at 100% with a reaction temperature change from 140 to 220 °C. However, ethylene conversion decreased when CO was added to the feed, and as the amount of CO added increased, the conversion of both hydrogen and ethylene decreased significantly. This may be due to competitive adsorption among CO, H<sub>2</sub> and ethylene on the catalyst surface. Another interesting finding was that as the amount of added CO increased, CO conversion decreased when using the same reaction temperature. The strong adsorption of CO on the catalyst surface and its self-inhibition contribute to the low CO reactivity.

- For feed S8 and 17% $H_2$ /83%  $C_2H_4$  with no CO in the feed,  $H_2$  converted completely with a temperature change from 180 to 220 °C. The ethylene conversion maintained at around 25% at different reaction temperatures, but this was limited by the amount of  $H_2$  fed into the reaction system.

**Table 8.2:** Reactant conversion using different reaction temperatures with different ethylene/CO partial pressure over 15% Co/TiO<sub>2</sub>. (Reaction pressure: 20 bars (gauge); for S1 to S4, H<sub>2</sub>: 40%; CO: 20%; C<sub>2</sub>H<sub>4</sub>: x%; Ar: 40-x%. x= 0, 10, 20 and 30; for S5 to S7, H<sub>2</sub>: 40%; C<sub>2</sub>H<sub>4</sub>: 40%; CO: x%; Ar: 20-x%. x= 0, 6 and 14; for S8, H<sub>2</sub>: 17%; C<sub>2</sub>H<sub>4</sub>: 83%).

Sample	Temperature	H <sub>2</sub> Conversion	CO Conversion	C <sub>2</sub> H <sub>4</sub> Conversion
S1	180°C	5.69%	5.48%	--
	190°C	7.55%	8.75%	--
	200°C	11.08%	12.82%	--
	220°C	30.25%	31.12%	--
S2	180°C	25.03%	17.01%	54.48%
	190°C	28.27%	17.99%	69.11%
	200°C	33.41%	21.42%	82.22%
	220°C	52.09%	37.51%	96.62%
S3	180°C	31.30%	18.09%	50.96%
	190°C	42.01%	21.11%	69.35%
	200°C	50.55%	24.98%	82.90%
	220°C	64.69%	35.63%	96.09%
S4	180°C	38.36%	19.23%	49.48%
	190°C	49.97%	22.33%	65.55%
	200°C	62.02%	26.25%	82.22%
	220°C	72.84%	32.83%	95.14%
S5	140°C	78.09%	--	100.00%
	180°C	78.72%	--	100.00%
	220°C	79.27%	--	100.00%
S6	140°C	28.25%	23.50%	29.83%
	180°C	74.73%	43.73%	94.48%
	220°C	79.46%	53.18%	99.54%
S7	140°C	11.43%	9.16%	13.26%
	180°C	65.89%	33.04%	72.84%
	220°C	79.05%	38.14%	97.04%
S8	180°C	100%	--	23.46%
	200°C	100%	--	27.51%
	220°C	100%	--	25.03%

### 8.3.2. Paraffins/Olefin (P/O) ratio

Figure 8.1(a)–(e) show the P/O ratio of light hydrocarbons ( $C_2$  to  $C_6$ ) as a function of reaction temperature with varying amounts of ethylene in the feed gas (S1 to S4 in Table 8.1). As shown, under all reaction conditions, the value of  $P_2/O_2$  ratio is bigger than those with higher carbon numbers with or without ethylene co-feeding. This indicates that the precursor of the  $C_2$  product has the highest hydrogenation activity, comparing with other carbon number products. This is consistent with the results of a typical cobalt-based catalytic FTS [14]. In addition, as the carbon chain length of the product increases, the P/O ratio increase as well, except for  $C_2$  products. According to the Like Dissolves Like Theory, this may be because the longer carbon chain products has a higher solubility in the liquid layer of the catalyst surface, therefore, its residence time in the bed is longer and the hydrogenation reaction is easier. This result is similar to the finding that long carbon olefins are more susceptible to secondary reactions in FTS, as reported by Iglaisa [27].

As the co-feed ethylene was introduced into the reactor, the P/O ratio of all carbon number products was reduced by varying degrees at different temperatures, except for the  $C_2$  products. Moreover, the more ethylene that was added, the lower the P/O ratio that was obtained. This can be attributed to the large amount of adsorbed hydrogen consumed by the co-feed of ethylene (H-scavenging effect of ethylene), as the conversion of  $H_2$  increases with increasing ethylene in the feed (See Table 8.2). In addition, our previous experimental results [42] indicate that the absorbed ethylene may convert to chain growth initiators or monomers to participate in the chain growth reaction, which may affect the long-chain hydrocarbon product distribution. These two reasons together may contribute to lowering the P/O ratio.

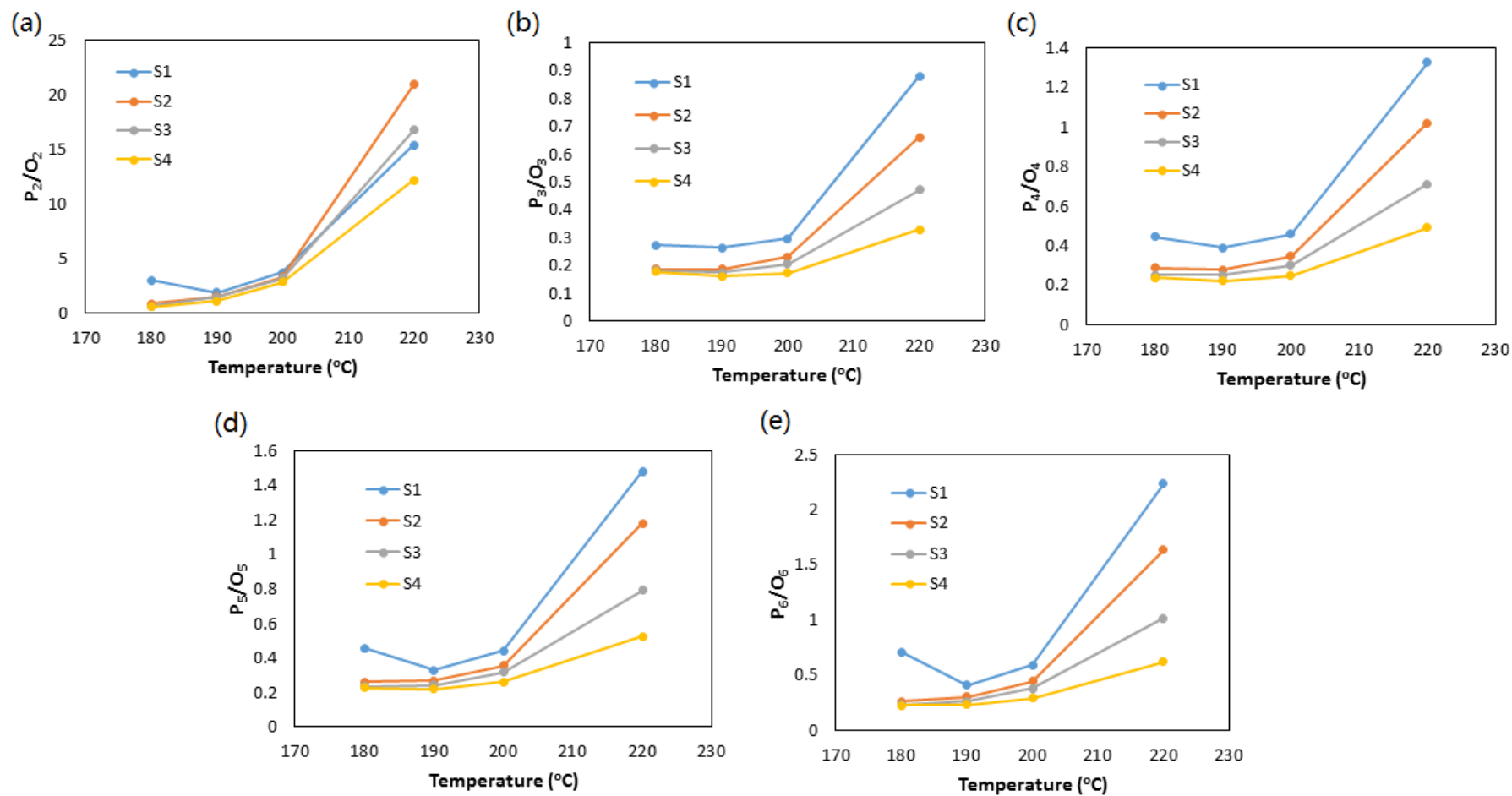


**Figure 8.1:** Mole paraffins to olefins ( $P_n/O_n$ ) ratio as a function of reaction temperature, with different amounts of ethylene in the feed gas: (a)  $n=2$ ; (b)  $n=3$ ; (c)  $n=4$ ; (d)  $n=5$ ; (e)  $n=6$ .

The change in the  $P_2/O_2$  ratios with reaction temperature were different. At a lower operating temperature ( $<200\text{ }^\circ\text{C}$ ), the  $P_2/O_2$  ratio with syngas was higher than the one with syngas co-feeding ethylene, even when the temperature was increased above  $200\text{ }^\circ\text{C}$ , and a higher  $P_2/O_2$  ratio was obtained for the added ethylene in feed gas (excluding S4 with the largest amount of ethylene co-fed). This could be due to the competitive adsorption of CO and ethylene on the catalyst surface, as an increase in temperature enhances the ethylene hydrogenation reaction.

It should also be noted that the P/O ratios for the same feed gas did not change much when the temperature increased from  $180$  to  $200\text{ }^\circ\text{C}$ , but a significant increase was observed when the operating temperature increased from  $200$  to  $220\text{ }^\circ\text{C}$ .

When  $H_2/C_2H_4$  is introduced into the reactor at a ratio of 1:1 (S5 in Table 8.1), there are no olefin products, i.e. all the products are paraffins. When a certain amount of CO was co-fed into the reactor with  $H_2/C_2H_4$  (S6 and S7 in Table 8.1), the trend in the change of the P/O ratio with the amount of CO co-fed and the temperature was plotted - see Figure 8.2. The results are very different to the experimental results obtained with syngas co-fed ethylene shown in Figure 8.1. In the presence of small amount of CO (6%), the paraffins to olefins ratio increases with an increase in the reaction temperature. However, when more CO is added into the feed gas, the P/O ratio first decreases at  $180\text{ }^\circ\text{C}$ , and then increases at  $220\text{ }^\circ\text{C}$ , except for  $C_2$ . This difference may due to the strong adsorption of CO on the catalyst surface (CO occupancy effect) and, in consequence, CO participate into normal FTS reaction over the typical FTS cobalt based catalyst.

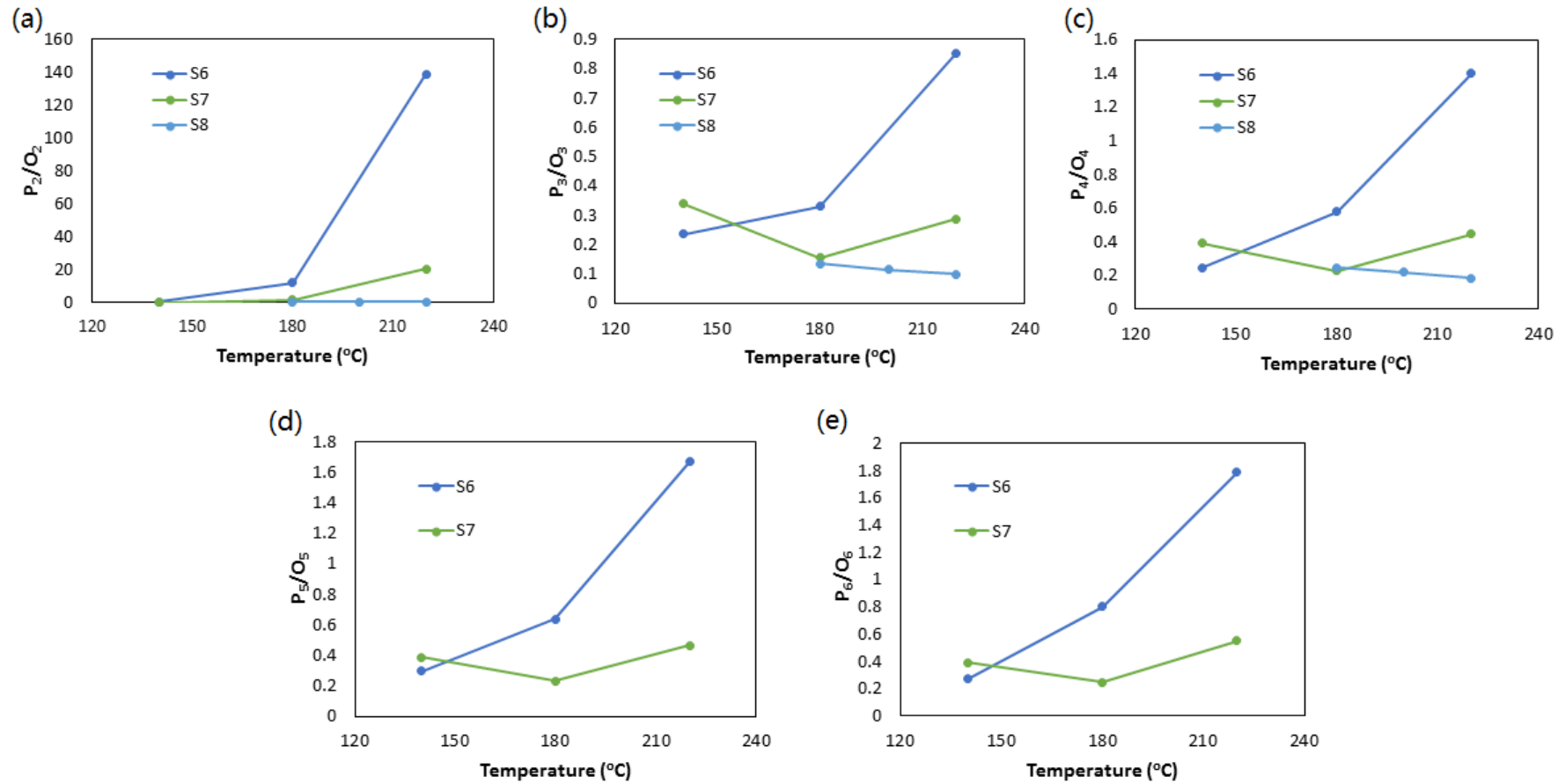


**Figure 8.2:** Mole paraffins to olefins ( $P_2/O_2$ ) ratio as a function of the reaction temperature, with different quantities of CO in the ethylene hydrogenation feed gas: (a)  $n=2$ ; (b)  $n=3$ ; (c)  $n=4$ ; (d)  $n=5$ ; (e)  $n=6$ .

With different partial pressure levels of CO added into the feeds (S6 and S7 in Table 8.1), the changes of the P/O ratio under different reaction temperatures were different. At a very low reaction temperature of 140 °C, the higher P/O ratio is obtained with a higher CO partial pressure (Figure 8.2). However, with increasing the temperature from 180 to 220 °C, the P/O ratio for the feed of S6 is much higher than the one for S7. We believe the changes of the P/O ratio is due to the different chain-growth mechanisms. Our previous study [43] experimentally proved that CO cannot dissociate with H<sub>2</sub> to attain the chain growth reaction under 140 °C, while, it can react with ethylene/H<sub>2</sub> via ethylene-assisted CO insertion mechanism to form long chain hydrocarbons. However, CO can dissociate with H<sub>2</sub> when increasing the reaction temperature to the normal FTS reaction temperatures (180 °C and 220 °C), and the dissociated species (CH<sub>x</sub>) can react to form long chain hydrocarbons via CO dissociation chain growth mechanism.

Both CO insertion mechanism and CO dissociation mechanism may co-exist under FTS reaction conditions [43]. However, CO insertion mechanism prefers a lower reaction temperature, but CO dissociation mechanism may be dominate at a higher reaction temperature. The shifting from one chain growth mechanism to another with increasing the reaction temperature may result in the different changes of P/O ratios (Figure 8.2). At 140 °C, the CO occupied the active sites of the catalyst surface and suppressed the adsorption of ethylene, so that the conversion of ethylene significantly decreased (see S6 and S7 in Table 8.2). The effect of CO occupation was not only decreasing the reactivity of the ethylene, but also suppressed the production of other olefins from ethylene, so that P/O ratio is higher with a higher CO partial pressure (Figure 8.2). At 180 and 220 °C, CO could directly be hydrogenate with H<sub>2</sub>, the more the CO added, the lower the P/O ratio obtained.

As mentioned above, when  $H_2/C_2H_4$  with a ratio of 1:1 was introduced into the feed, all the products were paraffins, which means all the product precursors were hydrogenated to alkanes. Then, a feed gas of  $H_2/C_2H_4$  with a very low ratio of around 1:5 (S8 in Table 8.1) was introduced into the reactor to check if an ethylene-rich feed could produce olefin products or not. The results from feed gas S8 were also plotted in Figure 8.2. It shows that: both olefin and paraffin products are formed; the P/O ratios are not sensitive to reaction temperature with a change from 180 to 220°C. It should be noted that some paraffin and olefin products of  $C_5$  and  $C_6$  were detected by online GC. However, the peaks from the GC were too tiny, so the ratios of  $P_5/O_5$  and  $P_6/O_6$  were not dealt with in this chapter.

### 8.3.3. Quasi-equilibrium: Yao plot

In the previous section, it was indicated that the P/O ratios depend strongly on the composition of the feed mixtures, with or without ethylene and reaction temperature, which is hard to predict. This research group created a plot, called the “Yao” plot, which is very different to the typical way of presenting experimental data, and which exposes some new types of behaviour in the product distribution [20]. The Yao plot is a graph that represents the relationship between the P/O ratio with carbon number (n+1) and the P/O ratio with carbon number n [40-41].

With the aim of investigating the relationship of P/O ratio with different carbon number, the Yao plot was used to re-plot the experimental data - see Figures 8.3 - 8.6. The P/O data was grouped into four parts: (1) data from S1\_  $H_2/CO$  (normal syngas); (2) data from S2-S4\_  $H_2/CO$  with co-feeding different partial pressure levels of ethylene; (3) data from S6-S7\_  $H_2/C_2H_4$  with

co-feeding different partial pressure levels of CO; and (4) data from S8\_H<sub>2</sub>/C<sub>2</sub>H<sub>4</sub> with an ethylene-rich environment. The feed composition details of S1-S8 are provided in Table 8.1. As shown in Figure 8.3(a), there was a linear relationship between P<sub>3</sub>/O<sub>3</sub> ratio and P<sub>2</sub>/O<sub>2</sub> ratio, when the normal syngas was fed into the reactor at different reaction temperatures. The slope of the trend line is 0.0487. Figure 8.3(b) shows three straight lines with different slopes for the feed co-feed ethylene with 3 different partial pressure levels (S2-S4 in Table 8.1). The slopes are 0.0243, 0.0191 and 0.0149 with 10%, 20% and 30% ethylene in the feed, respectively, and these figures are lower than the values seen when using only syngas (0.0487 in Figure 8.3(a)). As the amount of co-feed ethylene increases, the slope of the trend line decreases. It is worth noting that although the slope lines of the linear relationship between P<sub>3</sub>/O<sub>3</sub> vs P<sub>2</sub>/O<sub>2</sub> are different with differing amounts of ethylene added to the reactor, the intercepts of the trend lines are very close to each other: 0.137 for syngas; 0.152 for syngas with 10% ethylene; 0.154 for syngas with 20% ethylene; and 0.149 for syngas with 30% ethylene. The average value is 0.148. These data indicate that the amount of ethylene that is co-fed affects the slope line for the linear relationship of P<sub>3</sub>/O<sub>3</sub> against P<sub>2</sub>/O<sub>2</sub>, but it does not influence the intercept of the lines.

Figure 8.3(c) shows the experimental results for the feed of H<sub>2</sub>/C<sub>2</sub>H<sub>4</sub> with CO co-feeding. As can be seen, the data for P<sub>3</sub>/O<sub>3</sub> against P<sub>2</sub>/O<sub>2</sub> does not show a linear relationship for the feed S7 when a larger amount of CO was co-fed into the reactor, especially at a very low temperature of 140°C. However, with the feed of H<sub>2</sub>/C<sub>2</sub>H<sub>4</sub> without CO (S8), the distribution of the ratio of P<sub>3</sub>/O<sub>3</sub> vs P<sub>2</sub>/O<sub>2</sub> is scattered, as shown in Figure 8.3(d).

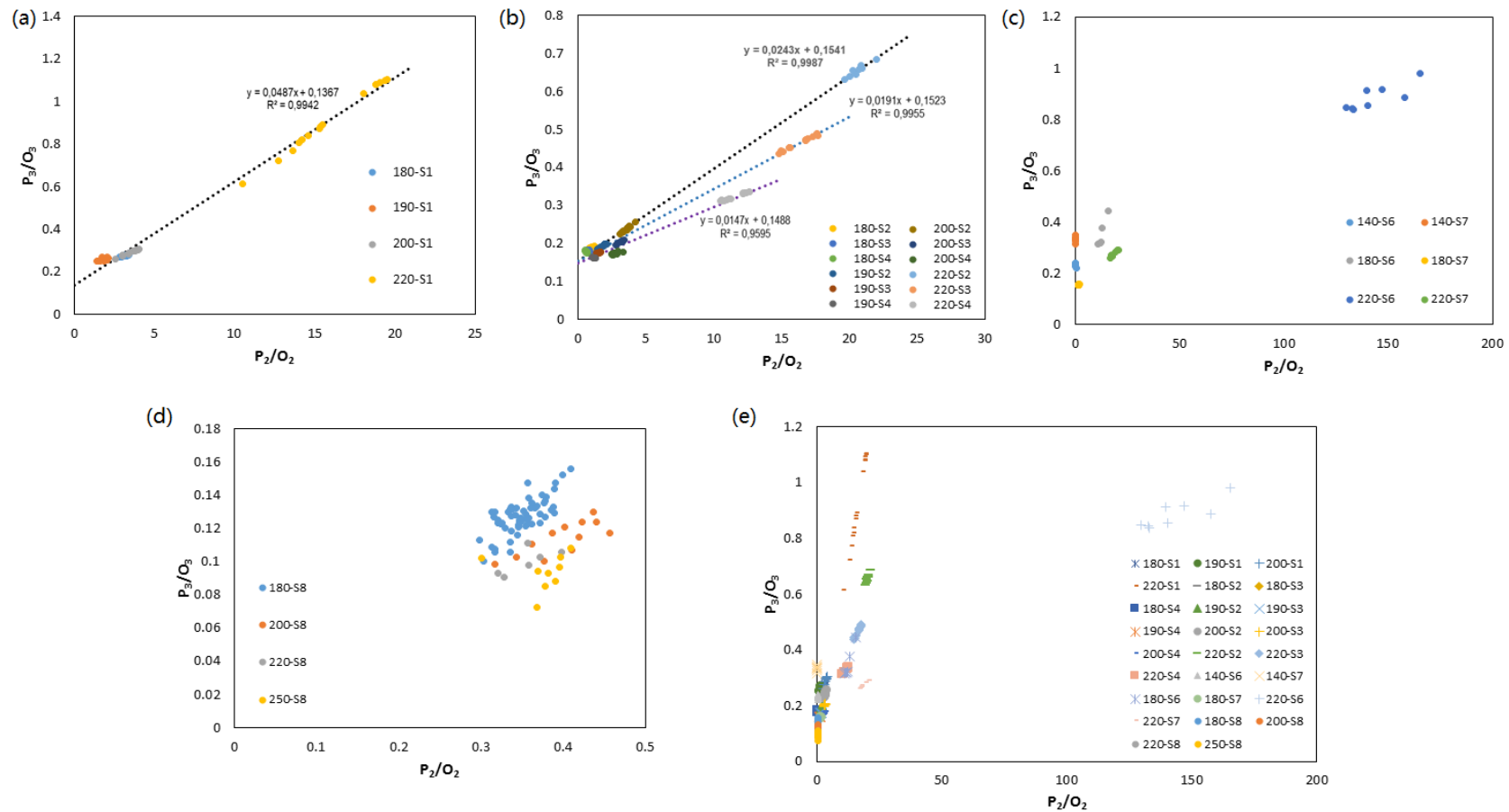


**Figure 8.3:** The Yao plot - paraffin (P) to olefin (O) ratio  $P_3/O_3$  as a function of  $P_2/O_2$  for: (a) normal FTS (S1); (b) ethylene co-feeding FTS (S2 to S4); (c) CO co-feeding ethylene hydrogenation (S6 and S7); (d) ethylene hydrogenation in ethylene rich environment; (e) summary of all the results together.

For comparison purposes, Figure 8.3(e) was produced; it is a collection of all the data from Figures 8.3(a)-(d). The linear relationship between  $P_3/O_3$  vs  $P_2/O_2$  is not easy to see, as the scattered data from Figure 8.3(c) and (d) affect the results. The different trends obtained may be due to the mechanisms of production of  $P_2$  and  $O_2$  being varied by the amount of the two carbon resources ( $CO$  and  $C_2H_4$ ) in the feed and the operating temperature.

Figures 8.4 – 8.6 are a plot of the relationship between the  $P_{n+1}/O_{n+1}$  ratio and  $P_n/O_n$  ratio with  $n$  equals 3, 4 and 5, respectively. When comparing the data from the normal FTS (S1, as shown in Figure 8.4(a), 8.5(a) and 8.6(a)), the slope of the trend lines does not change much when using the data obtained when co-feeding ethylene into syngas (S2-S4) and when co-feeding  $CO$  into ethylene hydrogenation system (S6-S7). For the ethylene hydrogenation system, with or without co-feeding  $CO$ , although the reaction conditions are far from the typical cobalt based-catalytic FTS, the linear relationship was obtained as well.

This is not the same as the relationship for  $P_3/O_3$  and  $P_2/O_2$  (Figure 8.3), as the linear relationship was observed under different reaction conditions and the slopes of the trend lines are quite close. This indicates that the linear relationship between the  $P_{n+1}/O_{n+1}$  ratio and the  $P_n/O_n$  ratio with the same carbon number is independent of the feed gas composition ( $H_2/CO$ ,  $H_2/CO/C_2H_4$ , and  $H_2/C_2H_4$ ) and the reaction temperature (140 to 220 °C). In addition, the slope gradient for different carbon numbers are quite close to each other (1.528 for  $n=3$ , 1.100 for  $n=4$  and 1.289 for  $n=5$ ). In order to compare the results for different carbon number  $n$ , all the data from Figures 8.4 – 8.6 were re-plotted. (See Figure 8.7.) The results show a linear relationship between  $P_{n+1}/O_{n+1}$  ratio and  $P_n/O_n$ , with an average slope of 1.258.

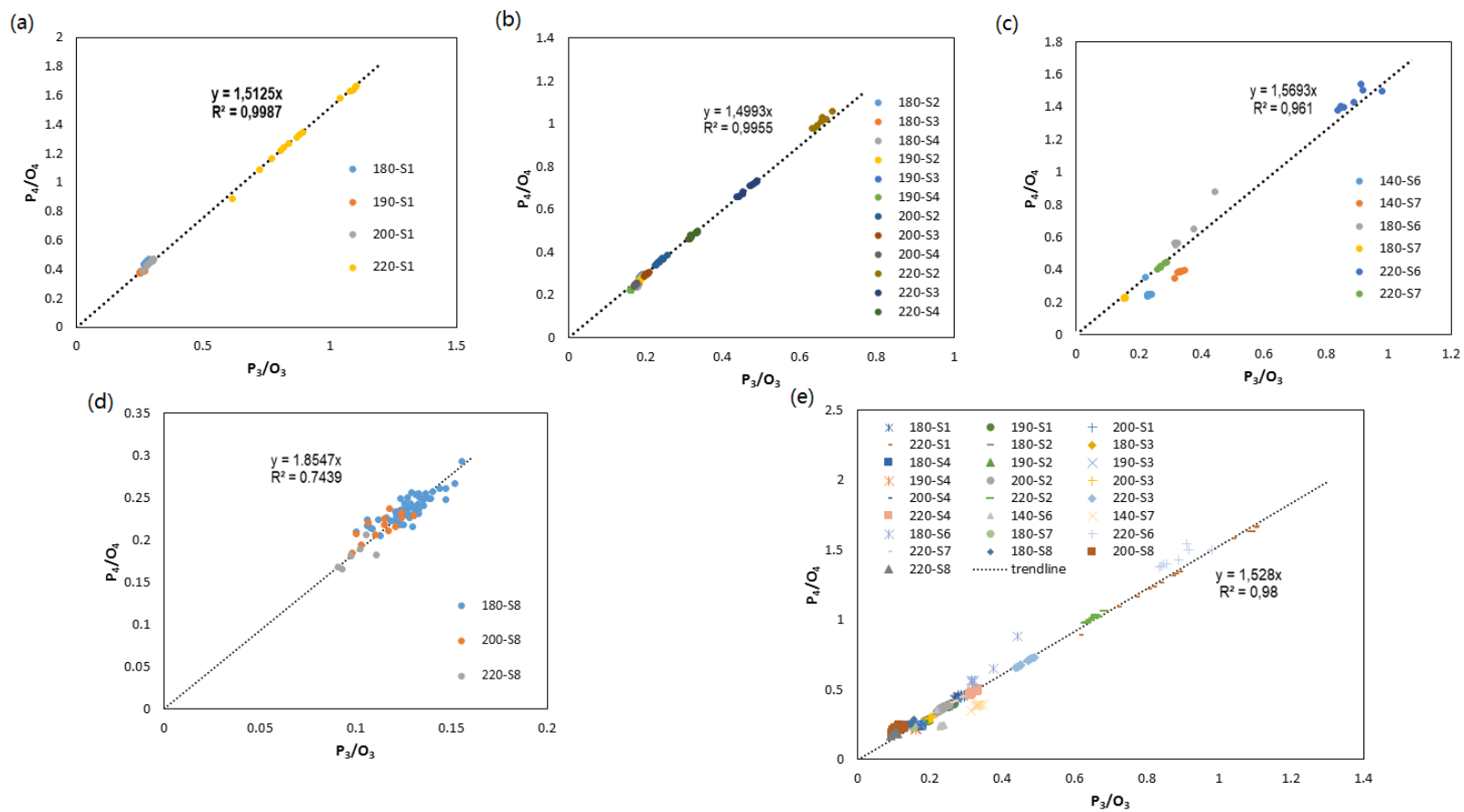


**Figure 8.4:** The Yao plot - paraffin (P) to olefin (O) ratio  $P_4/O_4$  as a function of  $P_3/O_3$  for: (a) normal FTS (S1); (b) ethylene co-feeding FTS (S2 to S4); (c) CO co-feeding ethylene hydrogenation (S6 and S7); (d) ethylene hydrogenation in an ethylene rich environment; (e) summary of all the results together.

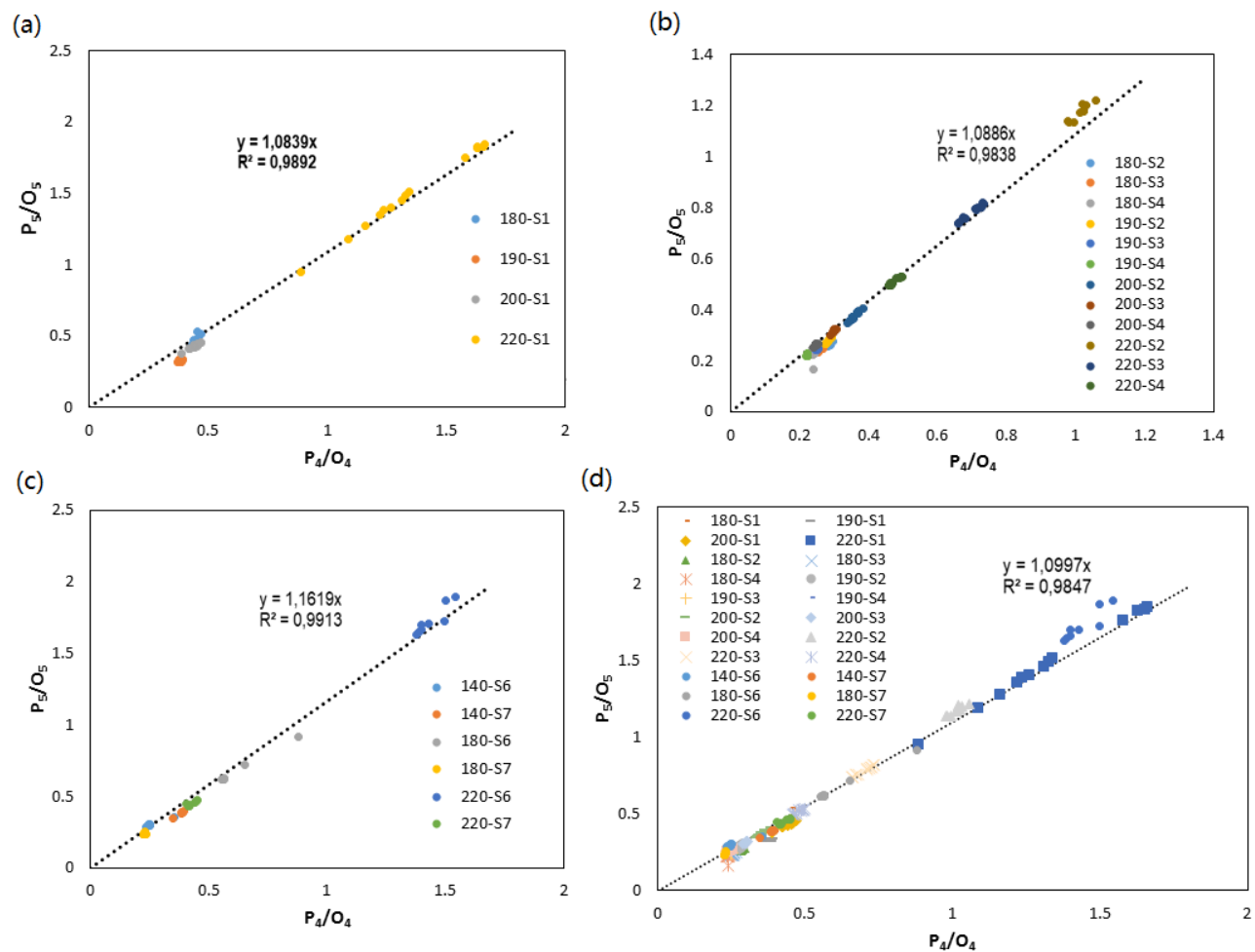


**Figure 8.5:** The Yao plot - paraffin (P) to olefin (O) ratio  $P_5/O_5$  as a function of  $P_4/O_4$  for: (a) normal FTS (S1); (b) ethylene co-feeding FTS (S2 to S4); (c) CO co-feeding ethylene hydrogenation (S6 and S7); (d) summary of all the results together.

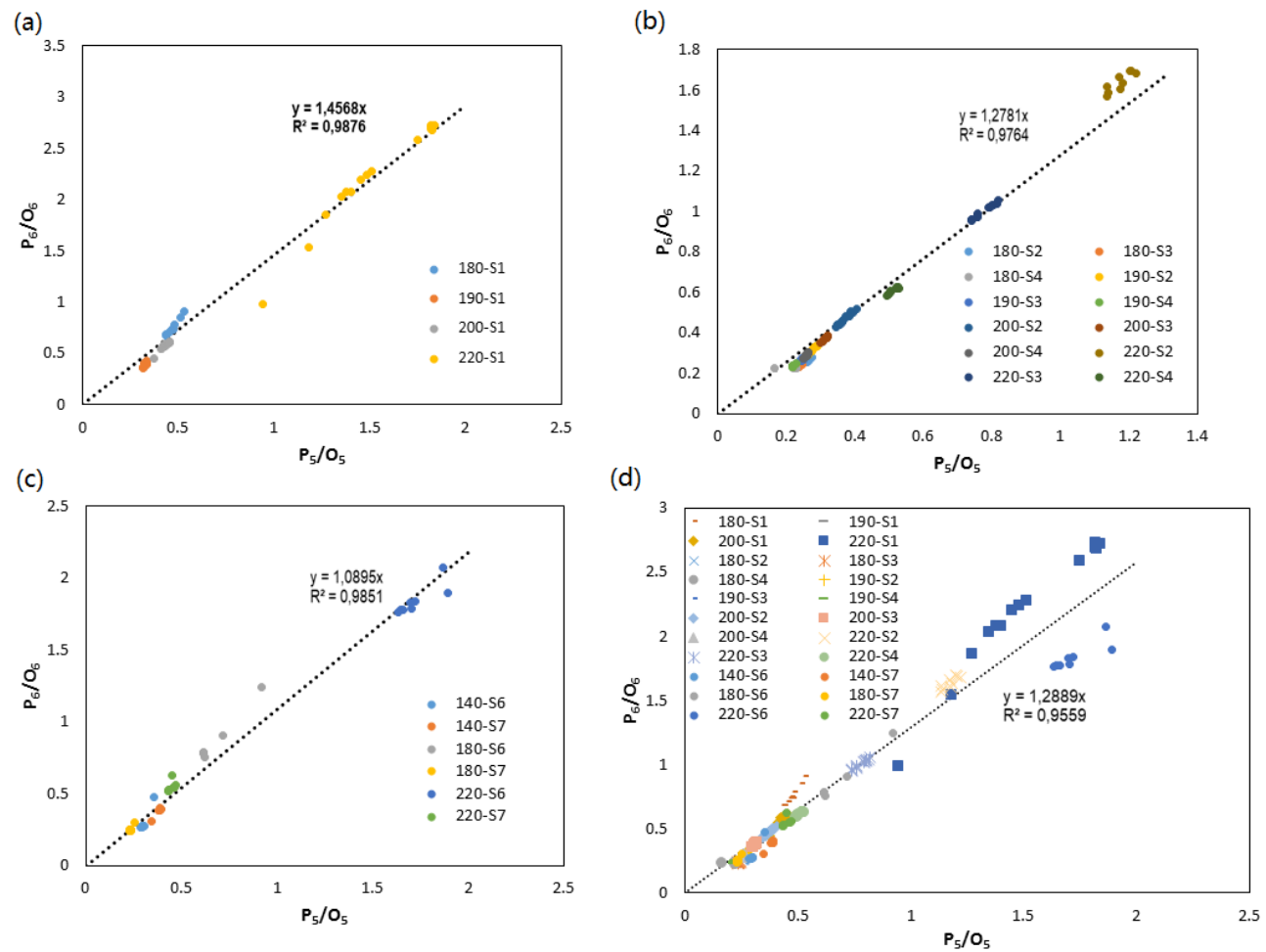


**Figure 8.6:** The Yao plot - paraffin (P) to olefin (O) ratio  $P_6/O_6$  as a function of  $P_5/O_5$  for: (a) normal FTS (S1); (b) ethylene co-feeding FTS (S2 to S4); (c) CO co-feeding ethylene hydrogenation (S6 and S7); (d) summary of all the results together.

In summary, when carbon number  $n=3, 4$  and  $5$ , the slope of the linear relationship between  $P_{n+1}/O_{n+1}$  and  $P_n/O_n$  is greater than  $1$  for all the experimental conditions conducted, and these are much higher than the values with carbon number  $n=2$ . This result is consistent with the experimental data obtained by Yao [20].

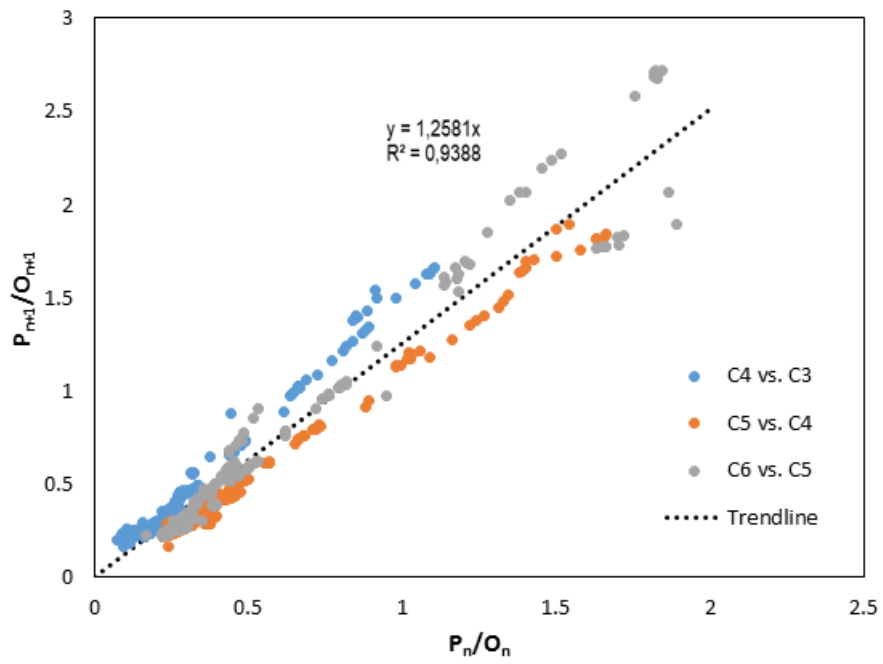


**Figure 8.7:** The Yao plot -  $P_{n+1}/O_{n+1}$  ratio as a function of  $P_n/O_n$  ratio ( $n = 3, 4$  and  $5$ ). (Summary of the data in Figures 8.4 to 8.6.)

#### 8.4. Discussion

As reported by Yao et al. [20], the slopes for  $n > 2$  are in the range of [1.244, 1.319] and is independent of the type of catalyst, type of reactor and the reaction conditions [20]. The linear relationship could be explained as follows:

$$P_{n+1}/O_{n+1} = \xi_{n>2} \times (P_n/O_n) \quad \text{Eq. 8.3}$$

$$P_{n+1}/p_n = \xi_{n>2} \times (O_{n+1}/O_n) \quad \text{Eq. 8.4}$$

Where:  $\xi_{n>2}$  is the slope of the plot for  $P_{n+1}/O_{n+1}$  against  $P_n/O_n$ , when carbon number  $n$  is bigger than 2. Since the product distribution of  $n$ -paraffins and the  $\alpha$ -olefins can be plotted separately by the ASF model, Equation 8.4 can be re-arranged as follows:

$$\alpha_{P,n} = \xi_{n>2} \times \alpha_{O,n} \quad \text{Eq. 8.5}$$

Where:  $\alpha_{P,n}$  is the chain growth probability of  $n$ -paraffins;  $\alpha_{O,n}$  represents the chain growth probability of  $\alpha$ -olefins. Equation 8.5 indicates the relationship between paraffin and olefin product distribution: the paraffin product distribution links to the olefin product distribution or vice versa. As mentioned in reference, this relationship fits for a wide range of product distribution under different FTS catalysts (including Co-based and Fe-based catalysts) and reaction conditions [20, 40-41]. In this work, we notice this relationship fits for ethylene, CO and  $H_2$  co-reaction system and even some condition of ethylene hydrogenation as well (as mentioned in figure 8.7). Therefore, we deduce this linear relationship might not only exist in products distribution of FTS process, but a certain universality (at least, exists in the process with FTS-type chain growth reaction).

Yao et al. [20] developed a model based on vapour liquid equilibrium (VLE) to explain the linear relationship of  $P_{n+1}/O_{n+1}$  and  $P_n/O_n$ . However, according to our system, about 99% of the products were light hydrocarbons with the feed  $H_2/C_2H_4$  (S8). Therefore, it is hard to form a liquid phase on the catalyst surface under the reaction conditions and VLE may not be the

reason for the phenomenon obtained when using H<sub>2</sub>/C<sub>2</sub>H<sub>4</sub> (S8) as a feed gas (Figure 8.4(d)). Yao et al. [20] also provided another explanation, i.e. that the linear relationship might be due to a quasi-reaction equilibrium, which can be explained as follows:

$$O_{n+1} + P_n = P_{n+1} + O_n \quad \text{Eq. 8.6}$$

Since paraffins show no reactivity under normal CO-based catalytic FTS condition, Equation 8.6 is a mass balance, rather than a reaction.

In addition, the P/O ratio obtained with the feed H<sub>2</sub>/C<sub>2</sub>H<sub>4</sub> without CO added also followed the Yao-plot with n>3, which indicates that the same chain growth mechanism may be followed by both CO and ethylene. In other words, CO and ethylene may transform to the same chain growth precursor. This precursor may desorb to form olefin, hydrogenate to paraffin and participate in the chain growth reaction to form another precursor.

The competitive equilibrium between the products or the precursors of products was used in an attempt to present the linear relationship between P<sub>n+1</sub>/O<sub>n+1</sub> and P<sub>n</sub>/O<sub>n</sub>, as discussed below [20].

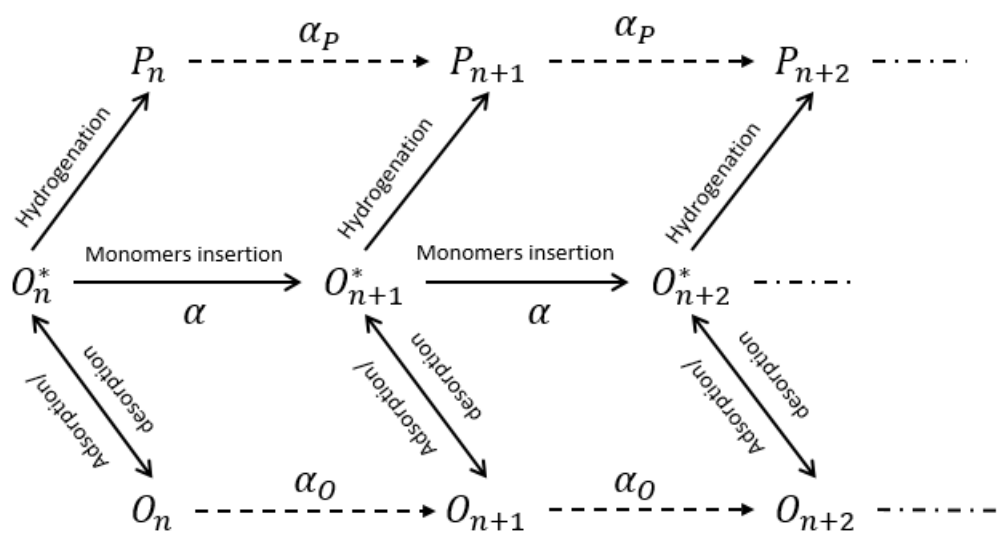
### **Competition equilibrium between hydrogenation and chain growth**

The results of the experimental data brought into the Yao plot show that there is some form of equilibrium relationship between the gas phase small molecular  $\alpha$ -olefins and paraffins. In fact, when using the reaction conditions of a typical FTS gas composition (S1), or a large amount of ethylene co-feed reaction conditions (S2 to S4), or CO co-feeding ethylene hydrogenation conditions (S6-7), or even H-insufficient ethylene hydrogenation condition (S8, P<sub>4</sub>/O<sub>4</sub> vs. P<sub>3</sub>/O<sub>3</sub>), the results obtained for the reaction equilibriums are consistent. In addition, these equilibriums were stable, both in the initial stage of the reaction and in the inactive

catalyst deactivation stage after prolonged reaction. These results indicate that the quasi-reaction equilibrium proposed by Yao may be an essential feature of the FTS reaction. In the experiments done in this study, a large amount of ethylene was present in the reaction system, which means that the reaction deviated from the typical FTS reaction, and we prefer to call it the analogous FTS reaction system. The data obtained under the incomplete FTS condition still fits these equilibriums and shows that equilibrium may be ubiquitous.

As mentioned in Yao et al [20], they assumed this equilibrium was caused by possible reactions between the reaction products and/or product precursors. However, under the conditions of FTS, the reactivity of n-paraffin was still doubtful and not widely accepted. Moreover, due to the complexity of the FTS mechanisms, it was still difficult to determine the precursors of paraffin and olefin products. This explanation is still not to be widely accepted by all researchers.

In this work, we assume a reaction competitive equilibrium to explain this linear relationship. In this equilibrium, the FTS process is simply regarded as a monomeric polymerization-type carbon chain-growth process, the carbon-chain termination reaction and the chain-growth reaction compete on the catalyst surface. Then the FTS can be described as per Scheme 8.1. In scheme 8.1,  $O_n^*$  represents the adsorbed  $\alpha$ -olefins with carbon number n, while  $O_n$  and  $P_n$  correspond to the  $\alpha$ -olefins and paraffins at the gas phase with carbon number n. In addition,  $\alpha_o$ ,  $\alpha_p$  and  $\alpha$  refer to the chain growth probability of  $\alpha$ -olefins, paraffins and the total  $\alpha$ -(olefins + paraffins), respectively. Solid arrows indicate that the pathway can take place, while dash arrows indicate that this process does not actually occur.



**Scheme 8.1:** Carbon chain growth and termination in FTS.

Scheme 8.1 shows that the reaction of carbon chain growth is the monomers insertion reaction with the precursor  $O_n^*$ . In our previous work, we found the FTS-type chain growth reaction existed in ethylene hydrogenation system in absence of CO [42]. Therefore, no matter the chain growth reaction via olefin hydrocrack mechanism, olefin-assisted CO insertion mechanism or CO dissociation type mechanism; the chain growth process can be simplified to monomeric insertion process. The carbon chain termination consists of two parts: the desorption of the adsorbed olefinic precursor into the gas phase  $\alpha$ -olefins; the hydrogenation and desorption of the adsorbed olefinic precursor to form gaseous paraffins. Then, the relationship between adjacent carbon number products can be described as the following equations:



In FTS condition, it believes that the hydrogenation reaction of  $\alpha$ -olefins is irreversible. Moreover, without considering the hydrogenolysis of long-chain products to form short-chain products, the chain growth in FTS is also considered an irreversible reaction. In other words, the FTS product paraffins cannot participate in the reaction again, and the long-chain product cannot react to form a short-chain product. Then, the quasi-reaction equilibrium can be transferred to Eq. 8.7 + Eq. 8.11 = Eq. 8.8 + Eq. 8.10. The products linear relationship may be caused by competition between these reactions. Although the individual chain termination

reaction by hydrogenation and the chain growth reaction by insertion of monomers are irreversible, there is no equilibrium. However, both reactions are based on the same reaction precursor, and there is competition between them, so the reaction equilibrium appears. Yao plot could be described using equations 8.7 to F8.11 as:

$$Eq. (8.11)/Eq. (8.10) = \xi \times (Eq. (8.8)/Eq. (8.7))$$

Returning to our experiments, after a large amount of ethylene as a reactant co-fed into the reaction system, the reaction rate of ethylene hydrogenation (Eq. 8.8) was directly enhanced. Under sufficient hydrogen, the rate of Eq. 8.8 increases with the increase in adding ethylene. This is the reason that the trend line slope of  $P_3/O_3$  vs.  $P_2/O_2$  decreases from 0.0487 (in absence of ethylene) to 0.0147 (30% ethylene added in feed gas).

However, the added ethylene could not directly affect the reactions of longer chain products (Eq. 8.10 and Eq. 8.11). Therefore, when carbon number  $n$  is greater than 2, the linear relationship from Yao plot after ethylene co-feeding is consistent with the results obtained in the absence of ethylene.

## 8.5. Conclusion

A wide range of feed gas mixtures, including syngas ( $H_2/CO$ ), ethylene hydrogenation gas ( $H_2/C_2H_4$ ), co-feeding ethylene into syngas, and co-feeding CO into ethylene hydrogenation gas, were used to investigate the effect of feed mixture on catalyst activity and P/O ratio over a typical cobalt based FT catalyst. Adding ethylene into syngas and co-feeding CO into the  $H_2/C_2H_4$  decreased the P/O ratio for all  $n > 2$ ; however, this is not the case with  $n = 2$ . Upon increasing the temperature, the P/O ratio showed a different trend that is complex to summarise. When the results from CO,  $H_2$  and ethylene co-reaction system were re-plotted to fit into Yao plot, there was a linear relationship between the  $P_{n+1}/O_{n+1}$  and  $P_n/O_n$ . These

results indicate that the olefin product distribution is linked to the paraffin product distribution. We assumed a reaction competitive equilibrium to explain this linear relationship. The adding of ethylene could directly enhance the  $O_2^*$  hydrogenation, which caused the slope of Yao plot is a function of the amount of ethylene added in the feed, when carbon number  $n=2$ . While, when carbon number  $n$  was greater than 2, the added ethylene has no direct impact on all reactions. Therefore, the gradients are quite similar, and this is independent of the composition of the feed and the operating temperature.

## REFERENCES:

1. Davis, B. H., & Occelli, M. L. (Eds.). (2016). Fischer-Tropsch synthesis, catalysts, and catalysis: advances and applications (Vol. 142). CRC Press.
2. Friedel, R. A., & Anderson, R. B. (1950). Composition of synthetic liquid fuels. Product distribution and analysis of C5—C8 paraffin isomers from cobalt catalyst. *Journal of the American Chemical Society*, 72(3), 1212-1215.
3. Flory, P. J. (1936). Molecular size distribution in linear condensation polymers. *Journal of the American Chemical Society*, 58(10), 1877-1885.
4. Satterfield, C. N., Huff Jr, G. A., & Longwell, J. P. (1982). Product distribution from iron catalysts in Fischer-Tropsch slurry reactors. *Industrial & Engineering Chemistry Process Design and Development*, 21(3), 465-470.
5. Dictor, R. A., & Bell, A. T. (1983). An explanation for deviations of Fischer-Tropsch products from a Schulz-Flory distribution. *Industrial & Engineering Chemistry Process Design and Development*, 22(4), 678-681.
6. Madon, R. J., & Taylor, W. F. (1981). Fischer-Tropsch synthesis on a precipitated iron catalyst. *Journal of Catalysis*, 69(1), 32-43.
7. Iglesia, E., Reyes, S. C., & Madon, R. J. (1991). Transport-enhanced  $\alpha$ -olefin readsorption pathways in Ru-catalyzed hydrocarbon synthesis. *Journal of Catalysis*, 129(1), 238-256.
8. Kuipers, E. W., Scheper, C., Wilson, J. H., Vinkenburg, I. H., & Oosterbeek, H. (1996). Non-ASF product distributions due to secondary reactions during Fischer–Tropsch synthesis. *Journal of Catalysis*, 158(1), 288-300.
9. Bhatelia, T., Li, C. E., Sun, Y., Hazewinkel, P., Burke, N., & Sage, V. (2014). Chain length dependent olefin re-adsorption model for Fischer–Tropsch synthesis over Co-Al<sub>2</sub>O<sub>3</sub> catalyst. *Fuel Processing Technology*, 125, 277-289.

10. Shi, B., & Davis, B. H. (2004). Fischer–Tropsch synthesis: accounting for chain-length related phenomena. *Applied Catalysis A: General*, 277(1-2), 61-69.
11. Zhan, X., & Davis, B. H. (2002). Assessment of internal diffusion limitation on Fischer–Tropsch product distribution. *Applied Catalysis A: General*, 236(1-2), 149-161.
12. Ji, Y. Y., Xiang, H. W., Yang, J. L., Xu, Y. Y., Li, Y. W., & Zhong, B. (2001). Effect of reaction conditions on the product distribution during Fischer–Tropsch synthesis over an industrial Fe-Mn catalyst. *Applied Catalysis A: General*, 214(1), 77-86.
13. Van der Laan, G. P., & Beenackers, A. A. C. M. (1999). Kinetics and selectivity of the Fischer–Tropsch synthesis: a literature review. *Catalysis Reviews*, 41(3-4), 255-318.
14. Lu, X., Hildebrandt, D., Liu, X., & Glasser, D. (2012). A thermodynamic approach to olefin product distribution in Fischer–Tropsch Synthesis. *Industrial & Engineering Chemistry Research*, 51(51), 16544-16551.
15. Cheng, J., Song, T., Hu, P., Lok, C. M., Ellis, P., & French, S. (2008). A density functional theory study of the  $\alpha$ -olefin selectivity in Fischer–Tropsch synthesis. *Journal of Catalysis*, 255(1), 20-28.
16. Botes, F. G. (2007). Proposal of a new product characterization model for the iron-based low-temperature Fischer–Tropsch Synthesis. *Energy & Fuels*, 21(3), 1379-1389.
17. Kapteijn, F., De Deugd, R. M., & Moulijn, J. A. (2005). Fischer–Tropsch synthesis using monolithic catalysts. *Catalysis Today*, 105(3-4), 350-356.
18. Masuku, C. M., Hildebrandt, D., & Glasser, D. (2011). The role of vapour–liquid equilibrium in Fischer–Tropsch product distribution. *Chemical Engineering Science*, 66(23), 6254-6263.

19. Masuku, C. M., Ma, W., Hildebrandt, D., Glasser, D., & Davis, B. H. (2012). A vapor–liquid equilibrium thermodynamic model for a Fischer–Tropsch reactor. *Fluid Phase Equilibria*, 314, 38-45.
20. Yao, Y., Liu, X., Hildebrandt, D., & Glasser, D. (2012). Fischer–Tropsch synthesis using H<sub>2</sub>/CO/CO<sub>2</sub> syngas mixtures: A comparison of paraffin to olefin ratios for iron and cobalt based catalysts. *Applied Catalysis A: General*, 433, 58-68.
21. Muleja, A. A., Yao, Y., Glasser, D., & Hildebrandt, D. (2016). A study of Fischer-Tropsch synthesis: Product distribution of the light hydrocarbons. *Applied Catalysis A: General*, 517, 217-226.
22. Pour, A. N., & Housaindokht, M. R. (2013). The olefin to paraffin ratio as a function of catalyst particle size in Fischer–Tropsch synthesis by iron catalyst. *Journal of Natural Gas Science and Engineering*, 14, 204-210.
23. Shi, B., & Davis, B. H. (2005). Fischer–Tropsch synthesis: The paraffin to olefin ratio as a function of carbon number. *Catalysis Today*, 106(1-4), 129-131.
24. Kuipers, E. W., Vinkenburg, I. H., & Oosterbeek, H. (1995). Chain length dependence of  $\alpha$ -olefin readsorption in Fischer-Tropsch synthesis. *Journal of Catalysis*, 152(1), 137-146.
25. Van der Laan, G. P., & Beenackers, A. A. (1999). Hydrocarbon selectivity model for the gas–solid Fischer–Tropsch synthesis on precipitated iron catalysts. *Industrial & Engineering Chemistry Research*, 38(4), 1277-1290.
26. Schulz, H., & Achtsnit, H. D. (1977). Olefin reactions during the Fischer-Tropsch Synthesis. *Revista Portuguesa de Quimica, Lisboa*, 19(1-4), 317-322.
27. Iglesia, E., Soled, S. L., Fiato, R. A., & Via, G. H. (1993). Bimetallic synergy in cobalt ruthenium Fischer-Tropsch synthesis catalysts. *Journal of Catalysis*, 143(2), 345-368.

28. Chen, W., Filot, I. A., Pestman, R., & Hensen, E. J. (2017). Mechanism of cobalt-catalyzed CO hydrogenation: 2. Fischer–Tropsch Synthesis. *ACS catalysis*, 7(12), 8061-8071.
29. McNab, A. I., McCue, A. J., Dionisi, D., & Anderson, J. A. (2017). Quantification and qualification by in-situ FTIR of species formed on supported-cobalt catalysts during the Fischer-Tropsch reaction. *Journal of Catalysis*, 353, 286-294.
30. McNab, A. I., McCue, A. J., Dionisi, D., & Anderson, J. A. (2018). Combined quantitative FTIR and online GC study of Fischer-Tropsch synthesis involving co-fed ethylene. *Journal of Catalysis*, 362, 10-17.
31. Boelee, J. H., Cüsters, J. M. G., & Van der Wiele, K. (1989). Influence of reaction conditions on the effect of co-feeding ethene in the Fischer-Tropsch synthesis on a fused-iron catalyst in the liquid phase. *Applied Catalysis*, 53(1), 1-13.
32. Hanlon, R. T., & Satterfield, C. N. (1988). Reactions of selected 1-olefins and ethanol added during the Fischer-Tropsch synthesis. *Energy & Fuels*, 2(2), 196-204.
33. Jordan, D. S., & Bell, A. T. (1986). Influence of ethylene on the hydrogenation of carbon monoxide over ruthenium. *The Journal of Physical Chemistry*, 90(20), 4797-4805.
34. Jordan, D. S., & Bell, A. T. (1987). The influence of propylene on CO hydrogenation over silica-supported ruthenium. *Journal of Catalysis*, 107(2), 338-350.
35. Tau, L. M., Dabbagh, H. A., & Davis, B. H. (1990). Fischer-Tropsch synthesis: carbon-14 tracer study of alkene incorporation. *Energy & Fuels*, 4(1), 94-99.
36. Herzog, K., & Gaube, J. (1989). Kinetic studies for elucidation of the promoter effect of alkali in Fischer-Tropsch iron catalysts. *Journal of Catalysis*, 115(2), 337-346.
37. Liu, X., Li, X., & Fujimoto, K. (2007). Effective control of carbon number distribution during Fischer–Tropsch synthesis over supported cobalt catalyst. *Catalysis Communications*, 8(9), 1329-1335.

38. Shi, B., & Davis, B. H. (2003). Fischer–Tropsch synthesis: evidence for chain initiation by ethene and ethanol for an iron catalyst. *Topics in Catalysis*, 26(1-4), 157-161.
39. Jacobs, G., & Davis, B. H. (2014). Applications of isotopic tracers in Fischer–Tropsch synthesis. *Catalysis Science & Technology*, 4(11), 3927-3944.
40. Gorimbo, J., Muleja, A., Lu, X., Yao, Y., Liu, X., Hildebrandt, D., & Glasser, D. (2017). Lu Plot and Yao Plot: Models to Analyze Product Distribution of Long-Term Gas-Phase Fischer–Tropsch Synthesis Experimental Data on an Iron Catalyst. *Energy & Fuels*, 31(5), 5682-5690.
41. Muleja, A. A., Yao, Y., Glasser, D., & Hildebrandt, D. (2016). A study of Fischer-Tropsch Synthesis: Product distribution of the light hydrocarbons. *Applied Catalysis A: General*, 517, 217-226.
42. Zhang, Y., Tshwaku, M., Yao, Y., Chang, J., Lu, X., Liu, X., & Hildebrandt, D. (2020). Reaction of ethylene over a typical Fischer-Tropsch synthesis Co/TiO<sub>2</sub> catalyst. *Engineering Reports*, 2(9), e12232.

## Chapter 9

### Conclusive remark and perspectives

---

The aim of this project was to investigate the reactivity of various feed gases (CO, H<sub>2</sub> and C<sub>2</sub>H<sub>4</sub>), and the effect of the interactions between these gases on the reactions, when using a Co-based FTS catalyst (15%Co/TiO<sub>2</sub>). The major objective was to identify potential reaction mechanisms by monitoring how the product distribution changed when varying the proportions of two different carbon sources, namely CO and C<sub>2</sub>H<sub>4</sub>, in the feed. Accordingly, five groups of experiments were conducted using different feed gas compositions and covering a wide range of reaction temperatures (100 °C – 220 °C). The groups of experiments were as follows:

- **Group 1:** C<sub>2</sub>H<sub>4</sub>/N<sub>2</sub> was introduced into the reactor (N<sub>2</sub> as an inert gas). The ratio of C<sub>2</sub>H<sub>4</sub>/N<sub>2</sub> and the reaction temperature were adjusted to test if C<sub>2</sub>H<sub>4</sub> reacted on the Co-based FT catalyst or not.
- **Group 2:** C<sub>2</sub>H<sub>4</sub>/H<sub>2</sub> was fed into the reactor in different proportions over a range of reaction temperatures. This was used to identify the possible reaction pathways of C<sub>2</sub>H<sub>4</sub> in the presence of H<sub>2</sub>.
- **Group 3:** The feed gas was switched between mixtures of CO/H<sub>2</sub> and CO/H<sub>2</sub>/C<sub>2</sub>H<sub>4</sub> over a (wide) range of reaction temperatures. This group of experiments was used to identify the potential reaction paths of both CO and C<sub>2</sub>H<sub>4</sub>.
- **Group 4:** Co-feeding different proportions of C<sub>2</sub>H<sub>4</sub> with syngas. Initially a feed of syngas was used to determine the base line performance of the catalyst for FTS.

Thereafter, different proportions of  $C_2H_4$  were introduced into the feed while the syngas partial pressure was kept constant. The effect of the  $C_2H_4$  concentration on activity and selectivity was observed at different reaction temperatures.

- **Group 5:** Co-feeding different proportions of CO into a  $C_2H_4/H_2$  feed. Initially a feed of  $C_2H_4/H_2$  was used to determine the base line performance of the catalyst for  $C_2H_4$  hydrogenation. Thereafter, different proportions of CO were introduced to the feed while keeping the  $C_2H_4/H_2$  partial pressures constant. The effect of the CO concentration on activity and selectivity was observed at different reaction temperatures.

## 9.1. Conclusion remarks

### 9.1.1. Reactant activity and product selectivity

No product was detected when using a feed of  $C_2H_4/N_2$ , which indicates that  $C_2H_4$  was not reactive over the temperature range of 160 °C to 250 °C. However, feeds of  $C_2H_4/H_2$  did react to produce short chain products. Even at 100 °C, the conversion of  $C_2H_4$  reached 100% when using a feed ratio of  $C_2H_4/H_2=0.8$ . Apart from ethane, the conversion of  $C_2H_4$  to other hydrocarbon products (including  $CH_4$ ,  $C_3H_6$ ,  $C_3H_8$ , 1- $C_4H_8$ , cis-2- $C_4H_8$ , trans-2- $C_4H_8$ , n- $C_4H_{10}$ , etc.), could be enhanced by decreasing the  $H_2/C_2H_4$  ratio and increasing the reaction temperature. The selectivity of the  $C_4$  product was relatively high (excluding  $C_2$ ). This indicated that some of the  $C_2H_4$  underwent a dimerization reaction.

No product could be detected when using a syngas feed ( $CO/H_2$ ) at temperatures below 160 °C. When the temperature was increased to 180 °C, CO reacted slowly and a very low CO

conversion (<5%) was observed. As the reaction temperature was further increased from 180 °C to 220 °C, the CO conversion increased and typical FT products were observed.

When switching between a CO/H<sub>2</sub> and CO/H<sub>2</sub>/C<sub>2</sub>H<sub>4</sub> feed at low temperature, the CO in the CO/H<sub>2</sub> mixture did not react while the CO in the CO/H<sub>2</sub>/C<sub>2</sub>H<sub>4</sub> mixture reacted, even 140 °C. This indicates that co-feeding a small amount of C<sub>2</sub>H<sub>4</sub> could enhance CO hydrogenation, even at temperatures below the normal FTS reaction temperatures.

When co-feeding different amounts of C<sub>2</sub>H<sub>4</sub> into the CO/H<sub>2</sub> feed, C<sub>2</sub>H<sub>4</sub> worked as a double-edged sword. Co-feeding a small amount of C<sub>2</sub>H<sub>4</sub> significantly improved the CO conversion and increased long-chain hydrocarbon selectivity at mild reaction temperatures. However, both the CO reactivity and chain growth probability decreased when co-feeding a relatively large amount of C<sub>2</sub>H<sub>4</sub> at higher reaction temperatures.

CO co-fed into the ethylene hydrogenation system significantly suppressed C<sub>2</sub>H<sub>4</sub> reactivity, which is evidence of the existence of the CO 'occupancy effect'. This effect was dominant at a low reaction temperatures and weakened at higher reaction temperatures. At low reaction temperatures, CO competitively occupied the active sites of catalyst resulting in reduced H<sub>2</sub> and C<sub>2</sub>H<sub>4</sub> adsorption on the catalyst surface.

### **9.1.2. Product distribution**

Although ethane was the main products of C<sub>2</sub>H<sub>4</sub> hydrogenation without CO in the feed, there still were some other products was produced. The product distribution of C<sub>2</sub>H<sub>4</sub> hydrogenation followed an ASF product distribution, which indicate that C<sub>2</sub>H<sub>4</sub> could converted to initiators and monomers, consequently, the initiators and monomers attended the chain growth

reaction to form other hydrocarbon products. However, the value of the chain growth probability was only around 0.32 that was much lower than that obtained for normal FTS (0.82).

When Co-feeding C<sub>2</sub>H<sub>4</sub> into syngas feed at low reaction temperature, all the products were fitted to ASF product distribution model. However, the effect of C<sub>2</sub>H<sub>4</sub> exhibited different trends: under low reaction temperature (<200 °C), add 10% of C<sub>2</sub>H<sub>4</sub> into the feed could increase the chain growth probability, while chain growth probability was decreased by either adding more C<sub>2</sub>H<sub>4</sub> into the feed or operating at high reaction temperature.

When co-feeding CO into the C<sub>2</sub>H<sub>4</sub>/H<sub>2</sub> feed, the products also followed ASF product distribution; and the more the CO added, the higher the chain growth probability was observed.

### 9.1.3. Reaction paths and mechanisms

Based on the product distribution and selectivity, the following reaction paths were discussed in the present research:

- (1) Hydrogenation of C<sub>2</sub>H<sub>4</sub> to form ethane (C<sub>2</sub>H<sub>4</sub> + H<sub>2</sub> → C<sub>2</sub>H<sub>6</sub>).
- (2) Oligomerization, including dimerization (2C<sub>2</sub>H<sub>4</sub> → C<sub>4</sub>H<sub>8</sub>).
- (3) Hydrogenolysis of C<sub>2</sub>H<sub>4</sub> to CH<sub>4</sub> (C<sub>2</sub>H<sub>4</sub> + 2H<sub>2</sub> → 2CH<sub>4</sub>).
- (4) Analogical disproportionation (2C<sub>2</sub>H<sub>4</sub> + H<sub>2</sub> → CH<sub>4</sub> + C<sub>3</sub>H<sub>8</sub>).
- (5) Analogical comproportionation (C<sub>2</sub>H<sub>4</sub> + C<sub>4</sub>H<sub>8</sub> → 2C<sub>3</sub>H<sub>6</sub>).
- (6) C<sub>2</sub>H<sub>4</sub> demethylation to form methylene, which participates in the chain growth FTS reaction (\*C<sub>2</sub>H<sub>4</sub> → \*CH<sub>x</sub>).

- (7) CO insertion: CO reacts directly with initiators to form FTS reaction intermediates, in particular, the present work shows that C<sub>2</sub>H<sub>4</sub> acts as an initiator and CO as a monomer to react with each other to form the corresponding intermediates ( $*C_2H_4 + *CO \rightarrow C_2H_4-CO*$ ). These intermediates react with H<sub>2</sub> to form another chain growth intermediate ( $C_2H_4-CO* + H* \rightarrow C_2H_5-CHx*$ ).
- (8) CO dissociation with or without H<sub>2</sub> assistance, forming FTS reaction intermediates ( $CO*+H* \rightarrow CHx$  or  $*CO \rightarrow *C+O*$ ,  $*C + H* \rightarrow *CHx$ ).
- (9) C<sub>2</sub>H<sub>4</sub> hydroformylation ( $CO+ C_2H_4 + H_2 \rightarrow C_2H_5CHO$  or  $C_2H_5CH_2OH$ ).

Reaction (6) was used to explain the chain growth reaction occurring with a feed of C<sub>2</sub>H<sub>4</sub>/H<sub>2</sub>, which showed that C<sub>1</sub>, C<sub>3</sub>, C<sub>5</sub> and C<sub>6</sub> product distributions followed a typical ASF distribution model.

The different catalytic behaviours obtained when using a feed mixture of CO/H<sub>2</sub>/C<sub>2</sub>H<sub>4</sub> at both low and high reaction temperatures were explained by the CO insertion mechanism and CO dissociation mechanism. At a low reaction temperature (such as 140 °C), CO did not react in the absence of C<sub>2</sub>H<sub>4</sub>, which indicates that it was hard for the adsorbed CO to dissociate to form the initiators of the chain growth reaction. When adding C<sub>2</sub>H<sub>4</sub> into the system, CO reacted appreciably. This data indicated that the adsorbed C<sub>2</sub>H<sub>4</sub> (acting as an initiator) reacted with the adsorbed CO (acting as a monomer) through the CO insertion mechanism to form long chain hydrocarbons (Reaction (7)).

With increasing reaction temperature, the effect of C<sub>2</sub>H<sub>4</sub> on CO reactivity decreased, which indicates that CO can dissociate to form initiators without the assistance of C<sub>2</sub>H<sub>4</sub>. We conclude that: both the CO insertion mechanism and CO dissociation mechanism may exist and compete under normal FTS reaction conditions; the CO insertion mechanism dominates at

relatively low reaction temperatures; while the CO dissociation mechanism is dominant at higher reaction temperatures.

The P/O ratio is one of the key factors used to describe the product selectivity of FTS, and it is strongly dependent on the operating conditions. Co-feeding CO or C<sub>2</sub>H<sub>4</sub> into the system decreased the P/O ratio (excluding carbon number n=2). However, it is difficult to summarise the trends observed when increasing the reaction temperature, therefore a new graphical plot, called the Yao Plot was used to plot the data. It showed a linear relationship between the P<sub>n+1</sub>/O<sub>n+1</sub> and P<sub>n</sub>/O<sub>n</sub>. These results indicate that the olefin product distribution was linked to that of the paraffin products. We proposed a new explanation to explain the linear relationship, called “reaction competitive equilibrium”.

## 9.2. Perspectives

The use of C<sub>2</sub>H<sub>4</sub> to potentially enhance CO hydrogenation to long chain hydrocarbons has been experimentally demonstrated in our present work. However, the optimal reaction conditions, such as the amount of C<sub>2</sub>H<sub>4</sub> in the feed and the reaction temperature, have not yet been determined. More research in this area is recommended.

Propanal (C<sub>3</sub> oxygenate) was also detected in the product. Its selectivity was found to depend on the composition of the feed gas and the reaction temperature. The highest selectivity to hydroformylation occurred at a relatively low temperature (180 °C for the CO co-fed ethylene hydrogenation system and 200 °C for the ethylene co-fed FTS system). Enhancing the CO insertion reaction and suppressing both the CO dissociation and olefin hydrogenation reactions may promote the production of oxygenates. We believe these results are helpful in

understanding how to increase the production of aldehydes in FTS. As these oxygenates are valuable chemicals, it could be an important route to adding value to the FTS process.